CRANFIELD UNIVERSITY

SIRIKANYA CHOKAOUYCHAI

DEVELOPMENT OF SYNTHESIS PROTOCOLS BASED ON A SINGLE ROUTE TO PRODUCE FULLERENOL WITH SPECIFIED LEVEL OF HYDROXYLATION WITHIN PRACTICAL RANGE, AND INVESTIGATION OF FULLERENOL AS SUPERCAPACITOR ELECTRODE ADDITIVES

SCHOOL OF AEROSPACE, TRANSPORT
AND MANUFACTURING
PhD in Manufacturing

PhD
Academic Year: 2014 - 2016

Supervisor: Dr Qi Zhang
September 2017

CRANFIELD UNIVERSITY

SCHOOL OF AEROSPACE, TRANSPORT
AND MANUFACTURING
PhD in Manufacturing

PhD

Academic Year 2014 - 2016

SIRIKANYA CHOKAOUYCHAI

Development of synthesis protocols based on a single route to produce fullerenol with specified level of hydroxylation within practical range, and investigation of fullerenol as supercapacitor electrode additives

Supervisor: Dr Qi Zhang
September 2017

This thesis is submitted in partial fulfilment of the requirements for the degree of Doctor of Philosophy

ABSTRACT

This research aims to develop synthesis protocols (based on a single route) to produce fullerenol with specified level of hydroxylation ($n_{(OH)}$), and to demonstrate comparison of effects from different classes of fullerenol (i.e. different $n_{(OH)}$) in an unexplored application (energy storage).

The route of fullerene hydroxylation by NaOH in presence of phase-transfer catalyst TBAH was chosen as a basis for this research. Producton consistency in terms of achieved $n_{(OH)}$ was evaluated, and effects of selected three process parameters on $n_{(OH)}$ were investigated. Non-linear relationship between amount of TBAH used and $n_{(OH)}$ showed a maximum ($n_{(OH)}$ = 14 groups) for TBAH = 24 drops, and a minimum ($n_{(OH)}$ = 8 groups) for 3 drops. Relationship between volume of NaOH solution used and $n_{(OH)}$ resembles Freundlich Adsorption Isotherm for liquid-solid adsorption. 8.0 ml NaOH solution gave the same $n_{(OH)}$ = 16 groups as 4.0 ml solution, however an increase in production capacity was more obvious. Reaction time 10-30 minutes did not cause noticeable changes to $n_{(OH)}$.

Three protocols for producing three classes of fullerenol ($n_{(OH)} < 10$; $n_{(OH)}$ = 10-14; $n_{(OH)}$ = 15-20) within practical range based on TBAH-NaOH route have been developed. Adverse effects of CO_2 and O_3 on the route have been discovered. The research also established systematic mathematical calculations for determining empirical formula of fullerenol using TGA and EDX ('TGA-EDX method'). Minimum requirements of process design for fullerenol production are provided.

Scale-up syntheses using the developed protocols were conducted and the products were used for investigation on the effect of $n_{(OH)}$ on performance of symmetric activated carbon supercapacitor containing fullerenol as electrode additives. Although lower in specific capacitance (and larger ESR), all fullerenol-containing supercapacitors offered higher maximum power, energy density and charge-transfer when compared to additive-free supercapacitor - suggesting potential and possibilities of fullerenol in energy applications.

Keywords:

Nanotechnology; Nanomaterial; Nanoparticle; Fullerene; Carbon; Energy storage

ACKNOWLEDGEMENTS

Throughout the course of this research, the journey from the first day until today when I have finally produced this thesis has been quite a unique adventure. To appropriately acknowledge the people who have given their support to me and this research, I feel that my Acknowledgements section could not be written in a conventional way.

At the end of the first year of my PhD study, there was a major organisational restructuring within the university and consequently I had to be transferred to a new department within the university.

Dr Qi Zhang, my current supervisor, has kindly agreed to supervise me from the beginning of my second year to the end. During the time under his supervision, I have always received generous support from him whenever I needed, on both academic and non-academic matters. Especially, when I encountered with crises during the course of this research, he has helped and guided me to the solution. In the latest crisis when my data storage containing important files for thesis submission were completely corrupted, he went to speak to the Registry with me, and helped me to eventually be granted with the precious extension to thesis submission. His kind consideration and understanding are always appreciated. I am deeply grateful to the generous support he has always given to me.

Dr Charles Wainwright, the Chair of my internal review committee, has always taken care of me from the start of my PhD study. He has been a very important advisor, and a very important and big moral support at the university to me for both academic and non-academic matters. During the time between the end of my first year and the beginning of my second year, he has given me an immense support in finding and arranging a new place within the university for me to continue and complete my degree. His great support continues to encourage me to overcome many obstacles and worries, and finally arrive to this point today. I strongly feel that I am very fortunate to have known and

received support from him who is truly a gentleman. I really do not know how to thank him enough for all the immense and continuous support he has given me.

There is one person whom I can never forget for his merits and gratitude to my postgraduate study. Dr Yi Ge had supported me since my MSc study when he was both the course director and the supervisor for my research project, and it was Dr Ge that provided me with the opportunity to become a PhD student at this university through the invitation to join his research group. He is the person who introduced me to the world of fullerenol. During the time under his supervision, I had always received useful advice and suggestions, as well as generous support and understanding from him. Although my PhD research and thesis are now in a completely different direction from when I was under his supervision in the first year, I am always grateful to him, who is now a senior lecturer in Pharmaceutical Science/Biotechnology at Queen's University Belfast.

Achievements in this research would not have been possible without the tremendous and continuous support by a special team at Cranfield Defence and Security (CDS) based in the Defence Academy of the United Kingdom, Shrivenham Station. The team consists of Dr Mike Williams, Dr Susan Waring, Peter Wilkinson, Beatrice Kingdon, and Niki Darcy. Throughout the course, Dr Mike Williams and Dr Susan Waring from Centre for Defence Chemistry had kindly granted me the permission to access their TGA and FTIR facilities on every request I submitted (even when it coincided with busy time at the Shrivenham site). When the work in each visit was completed, I always went to express my gratitude to them again before travelling back to Cranfield, and both of them always said "We are glad we are able to help". The scenes will always stay clear in my mind. Peter kindly and continuously provided training for operating both facilities as well as support, no matter how small my problem was, whenever I needed while working there. I am very thankful to his generosity and care. Niki also helped with general requirements on several occasions. Shrivenham is quite a distance from Cranfield (4 hours per journey by bus) and, since each of my visit to Shrivenham was extremely tight-packed with measurements to run full day on every day throughout, the person I am

especially grateful to is Beatrice who had always cooperated with the Shrivenham Station to provide an accommodation in the Officer's Mess for me to stay (as well as making arrangement with the Station Main Gate). Her great support is very meaningful to me since it allowed me to make full use of available time. She has also provided useful advices, and given me warm wishes and moral support which encourage me to overcome obstacles in my research. With all the tremendous support from the team, I always felt the most relaxed and peaceful during my every visit to Shrivenham Station (which I always looked forward to) despite the completely full and exhausting work schedule. I will cherish all the prestigious, wonderful experience and memories with me forever.

Prof Colin Webb, my Personal Tutor at the University of Manchester from when I was studying for my undergraduate degree, continues to support me in both academic and non-academic matters. For this research, he has provided many important advices on chemical engineering aspects of the work, as well as technical English language. He and his wife, Ann, have been so kind to me and always give me encouragement to carry on and achieve my ultimate goal. The two have been such a big moral support for me. I feel that now they are my dear relatives. I am the most grateful to their kindness, and their warm and continuous support.

I would like to dedicate this special acknowledgement to Prof Ken Kokubo from Osaka Univeristy in Japan. He has never known me before, but kindly and willingly answered my e-mails which were sent to ask for his help in explaining the method he and his team had developed for determination of hydrated empirical formula of fullerenol product using information from TGA and elemental analysis. It was only a couple of e-mails, but very valuable and meaningful. His thorough explanation and clarification has enabled formation of ideas to arrive at solutions. It even led to development of the 'TGA-EDX method' in this research, which is a systematic mathematical calculation modified from the iterative method by Prof Kokubo and his team. Without his support, the research would not have been able to come out from difficult

situations in the past. I would like to express my sincere gratitude to him here again.

Dr Ken Mingard at the National Physical Laboratory (NPL) in London had been very supportive with SEM/EDX services at NPL. The last portion of research budget remained could only afford limited number of hours of the service, but there was a large number of samples to run. Dr Mingard kindly understood the situation and managed to perform SEM/EDX services on all required samples. It was a tight-packed day. I am really appreciated of his kind consideration, understanding and support on this matter.

Andrew Stallard had kindly helped with transforming stainless-steel rods into ready-to-use current collector rods for supercapacitor experiments, as well as making some modification on supercapacitor housing. They were pretty, sturdy and easy to use. I am very thankful to his kind help.

I am really grateful to the kindness and understanding from Dr Glenn Leighton for agreeing to let me use his space in the fume cupboard when I was in a difficult situation from working-space crisis (caused by non-regular users) and went to ask for help. I also would like to thank Dr Quentin Lonne, my laboratory neighbour, who kindly welcomed me to use the same fume cupboard and offered many helps and advices in the laboratory. Dr Christopher Shaw had assisted with risk assessment and CoSHH approvals for this project.

I would like to thank Prof Sam Tothill who had kindly permitted access to DLS instrument in her laboratory during these past years. She also provided valuable comments for scientific writing when she was an assessor for my second-year review meeting. Dr Iva Chianella had given useful comments on analysis of results in my first- and final-year review meeting, as well as the support when I needed to access Prof Tothill's laboratory to use the DLS instrument.

The TEM images in this thesis were taken and processed by Dr Xianwei Liu, who also helped with some SEM training session. Christine Kimpton helped with SEM sessions, and had kindly provided training for SEM/EDX facilities

Rosemary Burns had greatly helped with relocation of the rotary evaporator, a very important equipment for this research, to the current laboratory. She also helped with health and safety considerations and documentation for the project.

To Noor, my previous laboratory neighbour in my first year, I am always thankful to her crucial help on several occasions, as well as wonderful friendship. Her husband, Dr Yunus, had also helped with training for DLS instrument, and given useful advice.

I would like to dedicate another special acknowledgement to Debbie Coates (Senior Registry Administrator), Anthea Fraser (Student and Academic Compliance Officer) and Meave Williamson (Student Academic Support Lead) for their kind consideration and understanding when I was in a grave crisis with corrupted storage of important files. Extension to thesis submission was granted to me and it was immensely meaningful. The precious extra time played an enormous part in completion of this thesis. I am very grateful to everyone involved in this approval. I am also very grateful to Cranfield University that it prepares such important emergency policy and procedures to help students in difficult situations.

Most importantly, my family at home has always been with me on every step I took, despite the fact that we were physically on the opposite sides of the world. In great times, we smiled together. When I faced problems, no matter how big or small, they have always been there to support me. My family is the biggest drive for me to carry on and eventually completed this thesis.

It is my honour to have won the competition for the *Royal Thai Government Scholarship for Ministry of Science and Technology* which has fully sponsored my entire study from A-Level to PhD in the United Kingdom. I would like to express my gratitude to my sponsor here again.

TABLE OF CONTENTS

LIST OF FIGURES

LIST OF TABLES

LIST OF EQUATIONS

LIST OF ABBREVIATIONS

AC	Activated carbon
CNT	Carbon nanotube
CRD	Completely randomised design
CV	Cyclic voltammetry
DLS	Dynamic light scattering
DNA	Deoxyribonucleic acid
EDX	Energy dispersive X-ray spectroscopy
EIS	Electrochemical impedance spectroscopy
ESR	Equivalent series resistance
FTIR	Fourier-Transform infrared spectroscopy
GCD	Galvanostatic chare-discharge
IG	Induced grating
KBr	Potassium bromide
NaOH	Sodium hydroxide
NMP	N-methyl-2-pyrrolidone
NMR	Nuclear magnetic resonance
PPF	Product per initial fullerene mass ratio
PTFE	Polytetrafluoroethylene
PU	Polyurethane
PVA	Polyvinyl alcohol
PVDF	Polyvinylidine fluoride
ROS	Reactive oxygen species
SEM	Scanning electron microscopy
TBAH	Tetrabutylammonium hydroxide
TEM	Tranmission electron microscopy
TGA	Thermogravimetric analysis
THF	Tetrahydrofuran
UV	Ultraviolet
UV-Vis	Ultraviolet-visible light
XPS	X-ray photoelectron spectroscopy

1 INTRODUCTION

Fullerenol (also called fullerol, or polyhydroxylated fullerene) is a class of water-soluble fullerene derivative developed to expand the applications of fullerene to hydrophilic environment, eliminating restrictions related to its hydrophobicity. It has received continuous attention from researchers across the globe, and is being explored in various fields. Most of fullerenol researches to date focus on exploring applications of fullerenol, especially in nanomedicine including the aspects of anti-oxidative capability, anti-tumour therapy, anti-inflammation, anti-aging, anti-viral/microbial agents, neuroprotective properties, and drug-delivery systems (Grebowski, Kazmierska and Krokosz, 2013; Wang et al., 2015). Other fullerenol applications are, for example, manufacturing abrasives and polymer additives for improved features (Takaya et al., 2009; Semenov et al., 2016). Several methods for the synthesis of fullerenol have been reported and each method claimed a distinct number of hydroxyl groups per fullerenol molecule it produced. This is further described in Section 2.3.

Recently, the concept of theranostic is attracting more attention from researchers. A theranostic agent contains both therapeutic and diagnostic functions within the same structure. Due to its small size, spherical shape, possibility for surface functionalisation, hydrophilic nature, and presumably low toxicity compared to many nanomaterials, fullerenol is considered a very attractive and promising nanomaterial for theranostic applications. Examples of fullerenol applications in theranostic researches include targeted anti-cancer therapy, and targeted and controlled-release drug delivery vehicle (Chen et al., 2012). If successful, it would be an enormous achievement, bringing medicine and health care to a new page, which would be extremely beneficial to human kind in such a way that its worth could not be estimated.

However, that does not seem practicable now or in the near future due to several limitations. Considering fullerenol itself, the material is not yet fully understood. It is known that fullerenol has several possible chemical formulae, depending on how many hydroxyl groups it contains. Fullerenol particles aggregate rather easily and quickly, which leads to size profiles. Furthermore,

there is a very concerning problem regarding synthesis of fullerenol for use in research and development sector.

It was found that researchers synthesised fullerenol for their research using different synthesis routes (see Section 2.3). Fullerenol contains hydroxyl ligands which can easily bond with surrounding chemical species, including the trace residues from fullerenol synthesis itself. Even if the residual components do not form chemical bonds with fullerenol molecules, their own properties may affect the performance of fullerenol applications. It is suggested that fullerenol produced from different synthesis methods should have different properties, even if they have the same number of hydroxyl groups per fullerenol molecule. This leads to concerns over comparing and integrating results from different researches based on fullerenol produced from different synthesis methods. These concerns create gaps within the knowledge of fullerenol, and are obstacles to understanding and standardisation of the material (which also affect other parts of fullerenol community, such as quality control, safety, environmental issues, etc). Nevertheless, it is unexpected that the issue is still neglected. In other words, fullerenol application is being explored and advanced on a huge pile of uncertainty regarding the material itself.

Even when the gap in fullerenol research can eventually be eliminated, as the majority of fullerenol research is geared towards medical uses, the applications which require materials of superior quality, many more processes and techniques still have to be developed and optimized in order to achieve production of fullerenol with such homogeneity, properties and grades suitable for medical research. With the currently available knowledge in the synthesis of fullerenol, the produced materials still show profiles of properties within and among batches, especially on level of hydroxylation and particle size. However, materials for medical research, and especially the real uses, are required to be of superior quality, having high homogeneity and narrow profiles for both within batch and among batches. If fullerenol produced at the current stage is to be applied to these applications, the majority of the produced materials (could even be as large as 90% of the batch) would be discarded during purification and

screening to achieve the required and acceptable quality and uniformity. Although there are some other applications in which these discarded fullerenol may be used, they somehow have not received much attention when compared to the medical applications. This could lead to a massive waste of material. At an industrial scale, this would also lead to a huge cost for waste treatment if they cannot be used for other meaningful purposes. This means that, although fullerenol is very attractive and promising, its production, as well as research and development require a high capital. This might be an important reason why the fullerenol sector is rather small when compared to those of its relatives in carbon nanomaterial family, such as graphene, carbon nanotubes, or fullerene itself.

This research sees that one way to facilitate the ultimate, ambitious and highly beneficial application of fullerenol in medical uses, as well as its other applications, is to attract more flow of cash into the fullerenol sector. To achieve this, it is of great importance to find applications that are both compatible with fullerenol of currently achievable grades, and are of great necessities for lives or are having an increasing demand. This way, the majority of producible material would not be wasted, but would be turned into more impactful benefits, increasing its worth and attracting more investors. As a result, there would be more funding to support the sector. When the sector can sustain itself with reasonable cash flow, this would eventually lead to development and advancement of the required methods and techniques, and significantly raises the quality of product and production to the aimed levels where the merits and benefits to human lives could eventually be cultivated and enjoyed. With reference to the unusual and special molecular structure as well as electronic configurations of the fullerene cage (Hirsch and Brettreich, 2005), this research sees that applications in energy sector, especially in energy storage, is a good candidate for the purpose. Among various types of energy storage devices, supercapacitor is becoming increasingly popular following the increased demand in energy consumption due to its high discharge rate. Potential uses of supercapacitors include energy storage for electrical vehicles and a more

domestic application such as power bank (Winter and Brodd, 2004; Stoller and Ruoff, 2010; Gonzalez et al., 2016).

Guided by this direction, it can be seen that both solving fullerenol synthesis issues and finding other applications that are practical and compatible with the products in the current stage are equally critical. This research therefore started from the true root of these problems – synthesis of fullerenol – and formed a question of whether it is possible to produce more than one classes of fullerenol from a single selected synthesis route (where classification of fullerenol is based on level of hydroxylation achieved from the synthesis). The research approached this question by selecting one synthesis route to investigate and develop synthesis protocols that are capable of producing more than one specifiable classes of fullerenol from this single route. This research is the first within the fullerenol research community to investigate the effect of synthetic process parameters on level of hydroxylation (in this case, amount of phase-transfer catalyst, amount of hydroxide ions, and reaction time). Through series of investigations and analyses, synthesis protocols to produce three specifiable classes of fullerenol within practical range of the selected route (TBAH-NaOH) have been developed. The achievement also extends to reporting minimum requirements of process design for fullerenol manufacturing, and recommendations for fullerenol characterisation.

To complete the picture, the research also used the products synthesised from the developed protocols to investigate a practical end-application candidate of currently producible fullerenol mentioned in earlier paragraphs – the application in supercapacitors.

Experiments in this research are thereby divided into two main parts:

- *Part One – Synthesis protocol experiments*
- *Part Two – Supercapacitor experiments*

Part One experiments are for the development of synthesis protocols capable of producing more than one classes of fullerenol with specifiable level of hydroxylation. The experiments consist of selection of fullerenol synthesis route,

evaluation of production consistency in terms of level of hydroxylation, investigation on the effect of selected process parameters on level of hydroxylation, developing the aimed synthesis protocols, and scale-up productions of selected classes of fullerenol.

The products from scale-up syntheses were then used in energy storage application, an area which is still not much studied for fullerenol, in *Part Two* of the research. Equally important as the purpose to investigate the effect of level of hydroxylation on performance of symmetric activated carbon supercapacitor when fullerenol is used as electrode additives, the experiments in *Part Two* also wish to demonstrate the fact that the experimental materials should be produced from the same synthesis route, so that comparison and analysis could be made without concerns regarding variations from different routes.

This thesis consists of 7 chapters in a traditional (monograph) format, which follows the sequence of introduction, literature review, research aims and objectives, methodology, results and discussion, limitations, conclusions, and future work. In the next chapter (Chapter 2) background information for this research is provided, which contains a brief summary of information for C_{60} fullerene (the parent material for this research), fullerenol, and supercapacitor fundamentals. Current trends in fullerenol and supercapacitor researches are also provided in this chapter. Following the information from the literature review, where the gap or weakness in the current fullerenol research was identified, the aims and objectives of this research are stated in Chapter 3. Since all the experiments in *Part One* used the same set of characterisation techniques, Chapter 4 starts from listing and describing each technique, then moves into the methodology of each experiment (from experimental design to experimental and analysis procedures). Results and discussion of all experiments are given and described in Chapter 5. The conclusions are stated in Chapter 6 and suggestions for further work given in Chapter 7. Appendices can be found after the list of references.

2 LITERATURE REVIEW

2.1 The parent material – C_{60} fullerene

Until 1985, the year of the revolution of carbon science, it was known to scientists that carbon naturally existed in two allotropes – graphite and diamond. In 1985, Kroto and colleagues accidentally made a world-changing discovery on the existence of a new structure of carbon cluster which consisted of 60 atoms of carbon in a molecule with the structural arrangement that was completely different from graphite and diamond. The structure consists of 12 pentagons, 20 hexagons, forming the shape of a truncated icosahedron (simply known as a football shape) as shown in Figure 2-1. Aesthetics of its shape, as well as molecular symmetry, has drawn a great deal of attention from many researchers to uncover more of its secrets. The discovered carbon cluster was named 'Buckminsterfullerene' or, in short, 'Fullerene' following the fact that the principle of its structure, consisting of only pentagons and hexagons, is similar to that of the famous geodesic domes designed by the architect Buckminster Fuller. Fullerene was then recognised as the third allotrope of carbon, in addition to the already known graphite and diamond, and the first synthetic allotrope (Kroto et al., 1985; Hirsch, 2010; Max-Planck-Institut für Festkörperforschung, 2017). Later, two more synthetic allotropes of carbon were reported, i.e. carbon nanotubes (Iijima, 1991) and graphene (Novoselov et al., 2004).

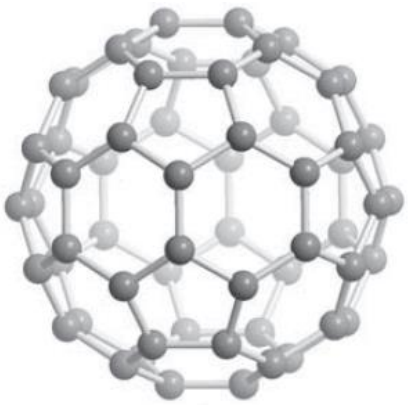

Figure 2-1 Ball-and-stick model for molecular structure of C_{60} fullerene, a truncated icosahedron (Hirsch and Brettreich, 2005)

Following the discovery of C_{60} fullerene, it was found that there were other possible types of fullerene with different number of carbon atoms that forms closed, hollow, three-dimensional, all-carbon molecules. There exist fullerene structures with both higher and smaller number of carbon atoms than C_{60} fullerene. The smallest possible fullerene consists of 20 carbon atoms, while the higher fullerene (i.e. fullerene with more than 60 carbon atoms) could have more than a hundred of carbon atoms in its molecule (Hirsch and Brettreich, 2005). Figure 2-2 shows several molecular structures of fullerene with different number of carbon atoms per molecule.

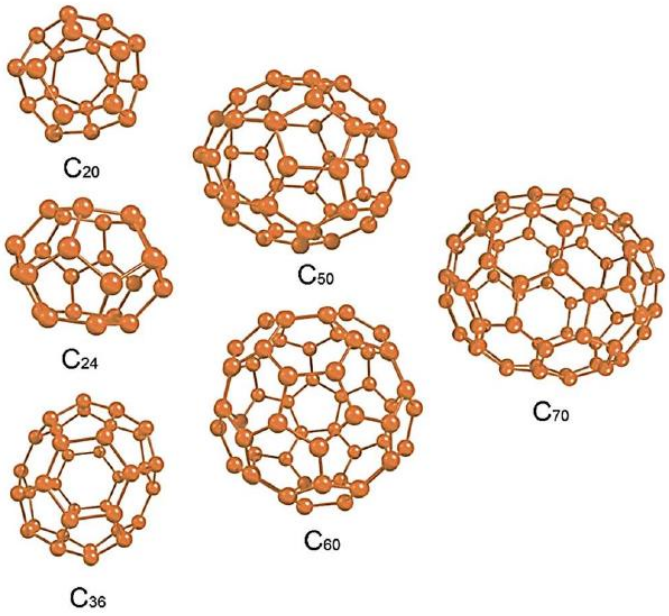

Figure 2-2 Various molecular structures of fullerene with different number of carbon atoms in the molecule (Kausar, 2017)

Fullerene has a good solubility in various organic solvents, especially toluene and carbon disulphide, but it is insoluble in water (Hirsch and Bretteich, 2005; Hirsch, 2010).

In the early days after fullerene discovery, it was possible to produce fullerene in only small quantity until the first macroscopic-scale production was reported by Kratschmer and Huffman in 1990 through evaporating a graphite rod using an arc-discharge technique, and re-condensing the vaporised graphite to yield C_{60} (Withers, Loutfy and Lowe, 1997; Hirsch, 2010). Nowadays, C_{60} can be

produced at an industrial scale and are commercially available to scientists, although each batch contain a certain fraction (by mass) of its relative the C_{70} generated alongside during the production process (Withers, Loutfy and Lowe, 1997).

Due to its unusual and interesting molecular structure and properties, especially electronic configuration, chemistry and reactions of fullerene have been popular with scientists for modification of fullerene in order to extend its application into various fields. There are several ways in which fullerene modification can be achieved as shown in Figure 2-3. The majority of fullerene modifications in fullerene research community are exohedral modifications of fullerene where one or more adducts (or addends) are attached onto the outside of the fullerene cage through addition reactions, making use of the fully conjugated system of π-electrons in the cage. It is reported that exohedral addition onto the fullerene molecule possesses regioselectivity. The adduct is generally attached onto the fullerene cage where two hexagons meet, rather than the edge between a hexagon and a pentagon, possibly because the first scenario possesses more double-bond behaviours compared to the latter (Hirsch and Brettreich, 2005; Hirsch, 2010).

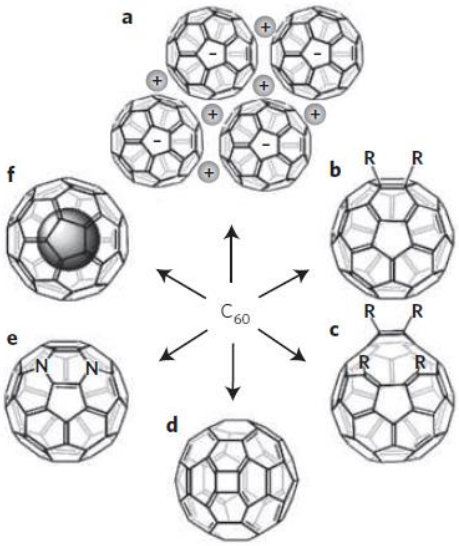

Figure 2-3 Possible fullerene modifications into a) fullerene salt, b) exohedral-modified fullerene, c) open-cage fullerene, d) quasi-fullerene, e) heterofullerene, f) endohedral fullerene (Hirsch, 2010)

Fullerene has been used in various applications, however it is most studied as electron acceptor in photovoltaic systems, especially organic solar cells. Through chemical modification of fullerene, performance improvement of fullerene-containing electron acceptors can be explored (Zhang et al., 2015). It is also reported to enhance catalytic activity and stability of the anode, as well as support oxygen reduction at the cathode when it is used as an electrocatalyst, and increase conductivity of proton conducting membrane in fuel cell applications (Coro et al., 2016). Due to its hydrophobic nature, direct use of fullerene in biological scenarios are limited. However, researchers have been drawn to its radical-scavenging properties and fullerene has been constantly researched on its biomedical merits as potential antioxidants, as well as its protective effects on diseases and disorders related to oxidative damages and reactive oxygen species (ROS). Another popular investigation on fullerene in biomedical area is its use as enhanced medical imaging agents, especially for computerised tomography (CT) and magnetic resonance imaging (MRI) where the presence of fullerene greatly enhances contrasts of the images (Satoh and Takayanagi, 2006; Yang, 2014). The antioxidative capacity of fullerene also leads to the applications in the field of dermatology and cosmetics (Mousavi, Nafisi and Maibach, 2017). Benefits of fullerene in biological applications also extents to agriculture where there were reports of fullerene contributing to an increase of yield, water retention and biomass in plants (Husen and Siddiqi, 2014).

2.2 Fullerenol, a water-soluble fullerene derivative

To tackle the limitation of fullerene application in aqueous situations, several modifications of fullerene molecule have been explored to achieve water-soluble fullerene derivatives, such as hydroxylation and carboxylation. The resulting product after hydroxylation (introduction of hydroxyl groups) of fullerene was found to have a good solubility in water, hence eliminates the limitation. The product has been called by several terms, including ‘fullerol’, ‘fullerenol’, ‘hydroxyfullerene’, and ‘hydroxylated fullerene’. In this work, the term ‘fullerenol’ is used throughout.

Generally, for a fullerenol molecule to be soluble in water, hydroxyl groups are required to be attached onto the fullerene cage, increasing hydrophilic domains of the molecule. As multiple hydroxylation reactions are involved, many articles used another term 'polyhydroxylated fullerene (PHF)' to refer to fullerenol as well. Figure 2-4 illustrates the molecule of fullerenol, which is the product from multiple hydroxylation of fullerene, in comparison to the parent material C_{60} fullerene.

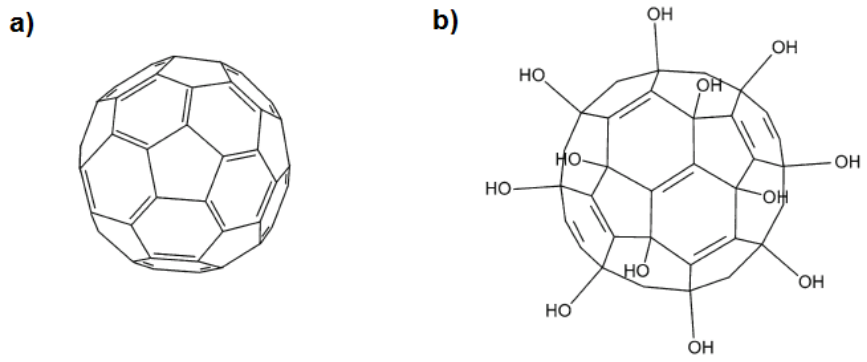

Figure 2-4 Two-dimensional representation of a) C_{60} fullerene, b) fullerenol (Injac, Prijatelj and Strukelj, 2013)

Despite a large number of research on fullerenol applications, the knowledge on properties of the material itself is still very limited. It is suggested that solubility in water of a fullerenol molecule depends on the number of hydroxyl groups it contains – the higher, the more soluble. The size of an individual fullerenol particle was reported to be as small as 1 nm in diameter. Inherited from its parent molecule, fullerenol is also an excellent radical scavenger (Kokubo, 2012).

2.3 Syntheses of fullerenol

To date, there are several routes reported to achieve synthesis of fullerenol. Each route utilises different sets of chemicals, and is reported to give unique results on number of hydroxyl groups per fullerene cage. A summary of fullerenol synthesis routes available is provided in Table 2-1 and Table 2-2.

Table 2-1 Summary of available publications on fullerenol synthesis routes

Route	Year	Research team	Brief description of synthesis route	$n_{(OH)}$	Note
1	1992	Chiang et al.	C_{60} in mixture of H_2SO_4 and HNO_3	14-15	
2	1992	Chiang, Upasani and Swirczewski	Nitronium chemistry with C_{60}, followed by hydrolysis of intermediate	18-20	Long, complex process
3	1993	Li et al.	TBAH-NaOH (C_{60} with NaOH in the presence of TBAH)	26	Simple process
4	1994	Chiang et al.	C_{60} with fuming H_2SO_4, followed by hydrolysis of precursor	10-12	Long, complex process
5	1994	Schneider et al.	Hydroboration of C_{60}	N/A	
6	1996	Chiang et al.	C_{60} with HNO_3 and $NaNO_2$, followed by hydrolysis of intermediate	16	Long, complex process
7	2000	Djordjevic	Formation of $C_{60}Br_{24}$, followed by substitution reaction in alkaline media	24	
8	2001	Chen et al.	C_{60} with lithium camphor in THF, followed by quenching with O_2 and acidified methanol	24	Product form of $C_{60}H_2(OH)_{24}$
9	2003	Arrais and Diana	C_{60} with liquid Na/K alloy	10	Competitive reactions present

Table 2-2 Summary of available publications on fullerenol synthesis routes (continued)

Route	Year	Research team	Brief description of synthesis route	$n_{(OH)}$	Note
10	2003	Zhang et al.	Solid-state reaction of C_{60} with KOH using high-speed vibration milling	27	
11	2005	Ratnikova et al.	C_{60} with tetra-butyl-peroxide, followed by strong acid treatment	2-12	Very limited synthesis information
12	2005	Troshin et al.	Hydrolysis of halogenated fullerene	N/A	Product formula contains K; Very limited synthesis information
13	2005	Wang et al. (2005a)	Solvent-free hydroxylation of C_{60} with NaOH using mechanical grinding	16	Simple process
14	2008	Kokubo et al.	Reaction of product from the route reported by Chiang and colleague (1994) with H_2O_2	36-40	High $n_{(OH)}$
15	2010	Zhang et al.	Thermolysis of a precursor followed by multi-steps	8	Very long, complex process
16	2011	Kokubo et al.	C_{60} with NaOH and H_2O_2 in the presence of TBAH	44	High $n_{(OH)}$

The first fullerenol was synthesised by Chiang and co-workers in 1992, by reacting C_{60} with an aqueous mixture of sulfuric acid (40% V/V) and nitric acid (40% V/V) at an elevated temperature between 85°C to 115°C. Upon the completion of the reaction, the mixture appeared clear, yellowish-brown. After separating out the unreacted C_{60} from the mixture, sodium hydroxide (NaOH) solution was added for neutralisation, followed by precipitation and drying under vacuum at 50°C to obtain the final brown product. The team reported that the number of hydroxyl addends achieved was 14-15 groups.

In the same year, a route utilising nitronium chemistry was reported by Chiang and colleague (Chiang, Upasani and Swirczewski, 1992) for synthesis of fullerenol containing 18-20 hydroxyl groups per molecule. A brown mixture of C_{60}, nitronium tetrafluoroborate, benzoic or p-bromobenzoic acid, and methylene chloride (solvent) was stirred for 48 hours under an inert atmosphere at ambient temperature. Solvent was removed and the remaining mixture was added dropwise into icy water and stirred for 3 hours. Following some workup procedures, the retrieved solid was mixed with tetrahydrofuran (THF) and added dropwise into a 1:1 mixture of diethyl ether and hexane. The resulting mixture was stirred vigorously to produce precipitates. Following some separation steps, the intermediate (polyhydroxyorganocarboxylated fullerene) was formed. The intermediate was then hydrolysed overnight at 60-70°C in the presence of sodium hydroxide. After further separation steps, fullerenol was eventually obtained. This route is an example of a rather long and complex process involving quite a number of chemicals and generation of intermediate along the way, which certainly would not suit this research. Therefore, other long and complex route will not be explained here but the corresponding references are provided in Table 2-1 and Table 2-2.

In 1993, another synthesis route to obtain fullerenol with the help of a phase-transfer catalyst, tetrabutylammonium hydroxide (TBAH), was reported by Li and colleagues. The dark violet solution of benzene-C_{60} (80 mg C_{60} in 60 ml toluene) was added with sodium hydroxide solution (2 g NaOH in 2 ml water) containing 3 drops of TBAH. The resulting mixture changed from dark violet into

colourless with the presence of brown sludge within a few minutes after it was vigorously stirred under ambient condition. Benzene was decanted and evaporated under reduced pressure for a few hours. With additional water added, the mixture was further stirred for 10 hours, giving a brown solution. After removing insoluble particles, the remaining solution was concentrated to approximately 5 ml and methanol was added to give brown precipitate. The precipitation step was repeated 3 times before the precipitate was dried under reduced pressure to give the final product of brown solid (115 mg). Through elemental analysis, the product was determined to contain approximately 26 hydroxyl addends. The presence of oxygen is very crucial for the reaction step as Li and colleagues (1993) had also reported in the same literature that the reaction progressed very slowly in absence of oxygen, and that most of the product collected from the reaction conducted under argon atmosphere was insoluble in water. Nevertheless, this route appears to be the most popular synthesis among fullerenol researchers, probably due to its simplication, ease of operation, and reasonable isolated yield. Some publications made modifications to this route to improve production capacity of the synthesis (Semenov et al., 2010; Semenov et al., 2012).

Fullerenol was also synthesised by reacting C_{60} with oleum (fuming sulfuric acid) at 65°C under nitrogen atmosphere for 5 hours (Chiang et al., 1994). The obtained brown suspension was added dropwise into anhydrous diethyl ether to form orange solid, an intermediate in the production process. Hydrolysis (using water) of this intermediate at 85°C gave a dark brown suspension which, when further separation, washing and drying under reduced pressure at 40°C were completed, resulted in the product of brown solid. Using mass spectrometry, as well as complementary information other analytical techniques, the product was reported to have 10-12 hydroxyl groups per cage.

Another approach to the synthesis of fullerenol reported in 1994 was the work of Schneider and colleagues (1994) where they reacted C_{60} fullerene with excess mixture of borane-tetrahydrofuran (BH_3-THF) for 2-3 hours followed by addition of hydrogen peroxide (H_2O_2) and sodium hydroxide solutions. Completion of the

reaction was determined by the reaction mixture changing its colour from brown to orange with brown solid inside. The mixture was left to settle overnight before toluene was removed and brown solid, the product, was filtered out. However, the mechanism of this route was not fully understood, and no analysis on determining hydroxyl addends was given.

In 2005, Wang and colleagues report the solvent-free, mechanical grinding hydroxylation approach to produce fullerenol. Pristine C_{60} fullerene was mechanically ground together with sodium hydroxide pellets and hydrogen peroxide solution (30%) in a mortar for 15 minutes, giving a yellow-brown mixture. Added with water, the resulting mixture was stirred for 10 minutes before the insoluble solids were filtered out, and the filtrate was concentrated to approximately 5 ml. Methanol was added dropwise into the concentrated filtrate, giving brown precipitate. After washing with methanol was repeated 3 times and drying under reduced pressure, the final brown product was retrieved. The literature provided values of wavenumbers from infrared absorption peaks and reported that the results were similar to those of fullerenol reported in previous other literatures, however the actual spectra was not shown (Wang et al., 2005a).

The first fullerenol with number of hydroxyl groups per molecule towards the high end of the spectrum was achieved and reported by Kokubo and colleagues in 2008. The team successfully synthesised fullerenol with 36 and 40 hydroxyl groups per molecule by first obtaining product from the route reported by Chiang and colleagues (1994) and the product was vigorously stirred with 30% hydrogen peroxide solution at 60°C for 4 days. After cooled down, the resulting mixture was then mixed with a mixture of 2-propanol, diethyl ether and hexane (1:1:1). Milky white precipitate is formed. Following separation steps, fullerenol was obtained as pale yellowish-brownish powder with estimated formula of $C_{60}(OH)_{36}.8H_2O$. Fullerenol with 40 hydroxyl groups per molecule was achieved when the vigorous mixing step lasted for 2 weeks.

The latest discovered fullerenol synthesis route was also reported by Kokubo and colleagues in 2011. Unlike the previous route in 2008, this route now did

not rely on product from other existing routes. The solution of C_{60} in toluene was stirred with a mixture of hydrogen peroxide (30%) solution and TBAH (40% in water) at 60°C for 16 hours. After cooling down and separation of liquid, the aqueous layer was mixed with a mixture of 2-propanol, diethyl ether and hexane (7:5:5) to form milky white precipitates. Following some steps for separation, fullerenol was obtained as pale-yellow powder, and was estimated to contain 44 hydroxyl groups per molecule.

2.4 Fullerenol characterisation techniques

At present, although there is yet an established standard protocol for characterisation of fullerenol, a selection of analytical techniques has been used among fullerenol researchers.

2.4.1 Fullerenol identification

Fourier-Transform infrared (FTIR) and nuclear magnetic resonance (NMR) spectroscopic tecnhiques are the two key techniques for confirming fullerenol identity, with FTIR appears to be more often used probably due to its less complicated operation and analysis compared to NMR. A typical infrared spectum of fullerenol (Figure 2-5) has a broad ν O–H absorption band around 3400 cm^{-1}, and has its characteristic absorptions around wavenumbers 1620, 1370 and 1080 cm^{-1} which correspond to ν C=C, δ C–O–H, and ν C–O absorptions respectively (Li et al., 1993; Kokubo et al., 2011).

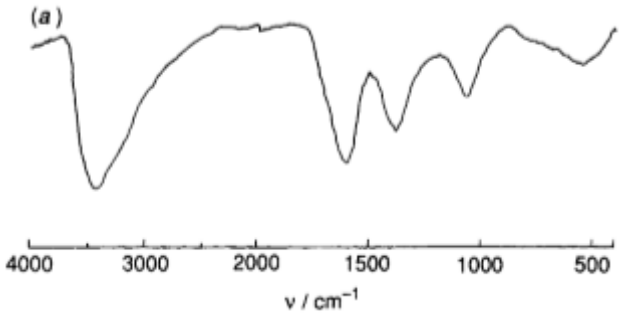

Figure 2-5 Infrared spectrum of fullerenol from Kokubo et al. (2011)

Another important technique to confirm fullerenol identity is X-ray photoelectron spectroscopy (XPS). XPS allows very detailed characterisation to the atomic

level, revealing electronic configurations and bonding within the sample by analysis of its XPS spectra (Chiang et al., 1992). Although XPS seems to be the most accurate technique for identification, not all researches incorporated the use of XPS. This is probably due to the fact that FTIR and NMR are more accessible as they are basic analytical facilities which are available in almost every institution.

Other techniques which have been used in complement to previously mentioned techniques for confirmation of fullerenol identity include mass spectrometry and UV-visible light (UV-Vis) spectroscopy (Chiang et al, 1992; Alves et al, 2006).

2.4.2 Estimating level of hydroxylation

Apart from confirming identity of fullerenol, another important feature of the product to determine is the number of hydroxyl groups attached on the fullerene cage, an important feature of a fullerenol molecule. Up to date, there are 4 methods to which this number is estimated.

- Elemental analysis method

  This is the oldest and most frequently used method for estimating the number of hydroxyl groups in fullerenol. Using flash combustion elemental analyser, percentages of elements present in the sample can be obtained and used to derive empirical formula of the sample in the form of $C_{60}(OH)_n$, hence determining the number of hydroxyl groups in the molecule 'n'. This method was widely used, especially in the early days of fullerenol syntheses.

- Thermogravimetric (TGA) method

  In 2004, Goswami and colleagues reported a new method to estimate the number of hydroxyl groups in fullerenol $n_{(OH)}$ using information obtained from TGA thermogram of the sample.

$$n_{(OH)} = \frac{(720)(x)}{(y)(17)} \qquad \textbf{(2-1)}$$

where x is percentage weight loss of the sample from 150°C to 570°C, and y is the remaining percentage weight after 570°C. The numbers 720 and 17 correspond to molecular masses of C_{60} and hydroxyl group respectively.

- TGA-Elemental analysis method

  In 2008, Kokubo and colleagues introduced the new concept of using both TGA and elemental analysis to obtain a more accurate formula of fullerenol product, accounting for the water molecules attached or trapped in the molecule (Kokubo et al., 2008). Information on moisture content of the sample is obtained from TGA thermogram. Combining this information with percentages of elements present in the sample obtained from elemental analysis, the hydrated formula of the sample can be derived, giving a more accurate estimation of the number of hydroxyl groups in fullerenol molecule. This method was also used in the work of Kokubo and colleagues in 2011.

2.4.3 Particle size measurement

For characterisation of particle size, dynamic light scattering (DLS) and mass spectrometry have been used, with DLS as the more popular technique. Complementing these techniques, scanning or transmission electron microscopy (SEM or TEM) have also been used to obtain microscopic images of fullerenol for particle size characterisation. In 2011, Kokubo and colleagues introduced the used of a new technique based on induced grating (IG) method developed by Shimadzu Corporation (Kyoto, Japan). The technique is specially for the measurement of particles of which diameters are in the range of 1-10 nm.

2.5 Applications of fullerenol

Researchers have been investigating the applications of fullerenol in various fields, with the majority being medical applications. Due to its antioxidative and radical-scavenging properties, as well as ability for further functionalisation,

fullerenol are widely used in medical researches as potential therapeutic agents against oxidative damages in various organs across the body (Chen and Lai, 2002; Cai et al., 2008; Saitoh et al., 2010), and drug delivery system (Knezevic et al., 2015; Jovic et al., 2016). There have been several reports on protective effects of fullerenol against drug-induced toxicity, such as doxorubicin (an anti-cancer drug) (Injac et al., 2009; Srdjenovic et al., 2010; Torres et al., 2010; Jacevic et al., 2017), radiative damages (Vesna et al., 2016), and neurodegenerative damages (Jin et al., 2000; Rade et al., 2008; Silva, 2010; Fluri et al., 2015; Ye et al., 2016; Darabi and Mohammadi, 2017). Its response upon UV radiation to generate ROS is also used in cancer treatment via photodynamic and photothermal therapy (Vileno et al., 2007; Krishna et al., 2010; Chen et al., 2012; Grobmyer and Krishna, 2012; Rokitskaya and Antonenko, 2016). Another popular use of fullerenol in medical applications is in the development of enhanced contrast agents for medical imaging technologies such as magnetic resonance imaging (MRI) and computerised tomographic (CT) scans (Okumura et al., 2002; Anderson, Lee and Frank, 2006; Miyamoto et al., 2006; Heckl, 2007; Chen et al., 2012). The recently emerged field of theranostic in nanomedicine has also sought for the use of fullerenol in the development of theranostic agent, where therapeutic and diagnostic agents could be attached on to the same fullerenol molecule through functionalisation, creating new potentially more effective and faster ways to tackle diseases (Budde and Frank, 2009; Chen et al., 2012; Sriramoju, Kanwar and Kanwar, 2015). The antioxidative and radical-scavenging properties of fullerenol have also led it into the science of anti-aging (Cong et al., 2015).

Fullerenol also finds its many applications outside biological and medical areas, including composite materials, manufacturing, catalyst, and energy. It has been incorporated into several composite materials, such as polyurethane (PU) (Kyokane et al., 2004; Dobashi, Matsunaga and Tajima, 2014), and polyvinyl alcohol (PVA) (Saotome et al., 2011; Penkova et al., 2014; Penkova et al., 2016; Penkova et al., 2017) to improve its property. It is also used to synthesise other materials, such as fullerene-based materials and graphene (Singh and Goswami, 2008; Singh and Goswami, 2011; Kumar et al., 2014; Prekodravac et

al., 2014; Bourlinos et al., 2017). In manufacturing, fullerenol have been explored as abrasive (Tachika et al., 2009; Takaya et al., 2009; Kano et al., 2010; Murai et al., 2014) and water-based lubricants (Liu et al., 2012). There are a few reports on the successful application of fullerenol as catalyst (Niu et al., 2011; Sun et al., 2014; Bai et al., 2017). In the energy sector, fullerenol has been used during fabrication of solar cell materials (Liu et al., 2008; Kumar et al., 2014; Wang et al., 2014), as well as material for lithium-ion battery (Wang et al., 2012).

2.6 Current situation and trends in fullerenol research

To understand the current situation and trends within fullerenol research, information on fullerenol publications were collected, classified and analysed. Excluding review papers, fullerenol research publications can be divided into computational and non-computational (i.e. experiment-based) categories. The non-computational publications consist of three sub-categories: fullerenol synthesis, studies on fullerenol properties, and investigations on applications of fullerenol. Publications on fullerenol applications could be further classified by themes or subject areas. The hierarchy of fullerenol research is thus presented in Figure 2-6.

The collected information was classified according to the hierarchy (Figure 2-6) and analysed, results presented as a pie chart in Figure 2-7. The top five applications of fullerenol are in the themes of medicinal applications, fullerenol-containing composite materials for enhanced properties, uses of fullerenol as intermediate or precursor in synthesis of some materials, fullerenol toxicity, and molecular biology applications.

Alongside its beneficial medical effects and other applications mentioned in Section 2.5, investigations on adverse effects of fullerenol have been conducted for various situations. Several reports suggested its cytotoxicity which caused changes in morphology of the living cells or organelles (Yang et al., 2016; Jin et al., 2016). It could also influence on elasticity of cells (Liu, Wang and Wang, 2015). Genotoxicity of fullerenol has also been reported that it could alter

genetic expression. Preliminary determination of toxic doses of fullerenol administration in vivo was conducted on mice (El-Nagar et al., 2016).

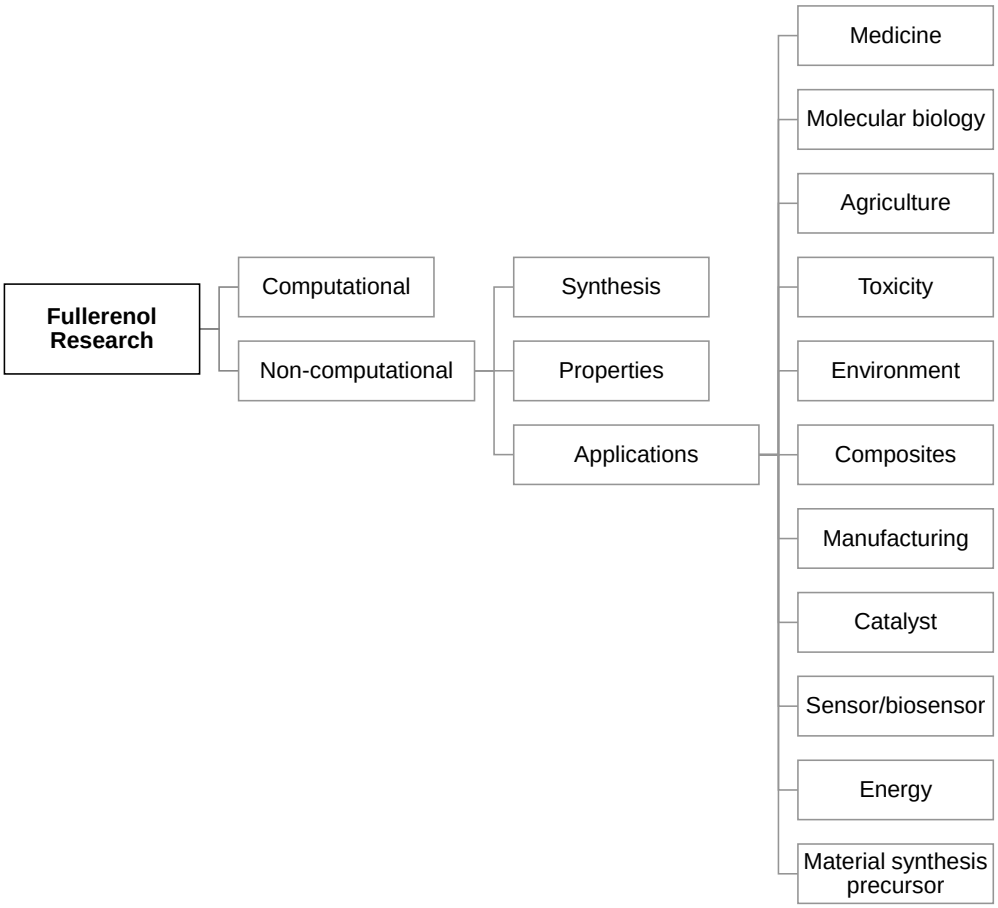

Figure 2-6 Hierarchy of fullerenol research

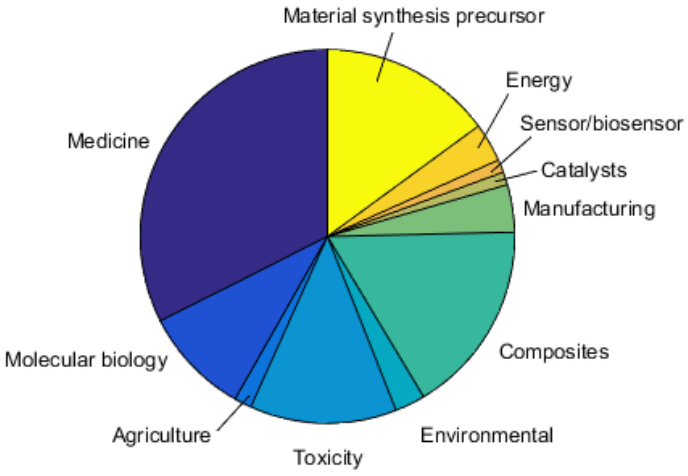

Figure 2-7 Pie chart illustrating proportions of research under the theme of fullerenol applications (data as of July 2017)

Interactions between fullerenol and other molecules, especially biomolecules such as proteins (Yang et al., 2008; Bobylev, Marsagishvili and Podlubnaya, 2010; Grebowski, Krokosz and Puchala, 2013), cell membrane (Rokitskaya and Antonenko, 2016; Liu et al., 2015; Zhu et al., 2016), and genetic material (Pinteala, Dascalu and Ungurenasu, 2009) are also of increasing interests as they form important aspects of biocompatibility, hence safety, of the material.

Although the majority of fullerenol researches are on the applications of the material in various fields, there is a growing number of researches on physicochemical properties of the material in selected environmental conditions or system; the fullerenol used in the studies were also of different, selected number of hydroxy groups (Zhu et al., 1996; Mohan et al., 1998; Mirkov et al., 2004; Kong et al., 2009; Semenov et al., 2011; Penkova et al., 2014; Semenov et al., 2014). In additional to experimental studies, a lot of computational and simulative studies on fullerenol have been conducted using computational methods such as density function theory (DFT) (He et al., 2011; Tachikawa, Iyama and Abe, 2011; Addicoat et al., 2012; Pushkarchuk et al., 2016).

While reviewing published non-computational literatures on fullerenol properties and applications, it was noticed that different research groups used different routes to synthesise fullerenol for use in their experiments. There was also quite a portion using purchased fullerenol available from a few manufacturers. A sample of 45 publications were randomly selected from the available publications on fullerenol properties and applications. The origins of fullerenol for these publications, i.e. either through a synthesis route or purchasing, were identified and analysed as shown in Figure 2-8. Route 3 (TBAH-NaOH route) has the largest proportion (38%), followed by the equal proportions (11% each) of second largest for Route 7 and purchased fullerenol. Other routes identified from this sample were Route 1 (9%), Route 4 (9%), Route 6 (9%), Route 13 (4%), Route 14 (2%) and Route 15 (4%). The list of 45 references used for this analysis is provided in Appendix B.

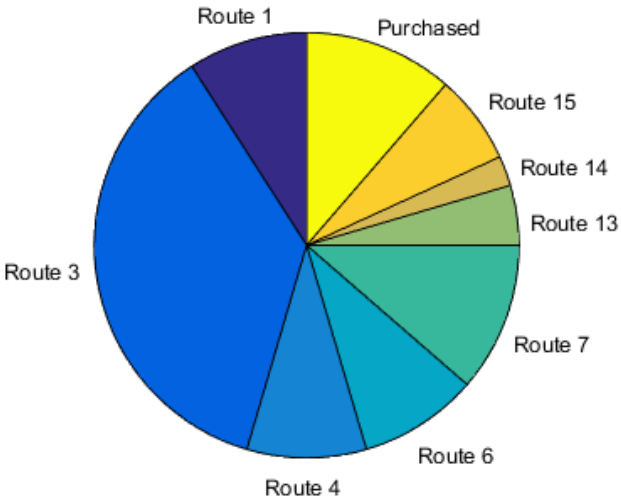

Figure 2-8 Pie chart illustrating proportions of various origins of fullerenol as experimental material used in researches on its applications and material properties. Information was collected from randomly selected 45 publications.

With different research groups using different routes to obtain fullerenol for their studies, further uses of these information poses concerns over their validity for comparison and integration.

2.7 Supercapacitor

With reference to Chapter 1, supercapacitor was selected as the end-application for this research. In this section, background information for supercapacitor application is provided.

2.7.1 Supercapacitor classification

Supercapacitor is one form of energy storage systems. Based on charge-storage mechanism, supercapacitors can be classified into 3 main classes, namely electrochemical double-layer capacitor (EDLC), pseudocapacitor and hybrid supercapacitor (Winter and Brodd, 2004). The type of electrode materials used in the fabrication of the supercapacitor could also be used to determine the class of the supercapacitor, since each class only uses specific type of materials as summarised in Figure 2-9.

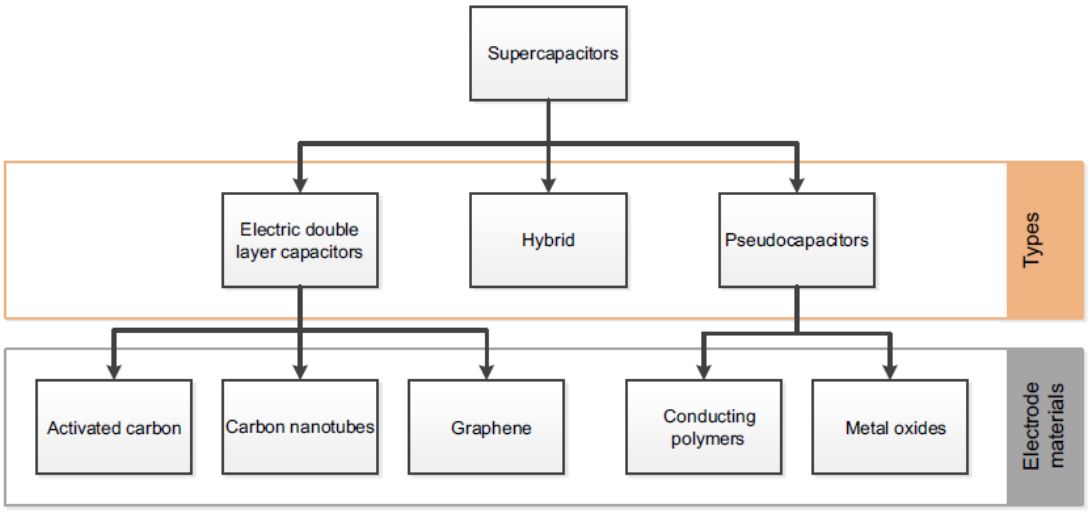

Figure 2-9 Classification of supercapacitor and their associated choices of electrode materials (Winter and Brodd, 2004)

During charging of an EDLC type supercapacitor, separation of charges occurs at the interface between electrode and electrolyte and charge storage is based on direct adsorption of ions from the electrolyte onto the electrode surface. This forms a double layer which acts as a capacitor. Several models have been established for explanation of this double-layer phenomenon, from the simplest Helmholtz model to the more complex model by Stern as seen in Figure 2-10. There is no Faradic process at the surface of the electrode, therefore fast adsorption and desorption of charges can be achieved, and the electrodes do not swell. Generally, EDLCs can achieve a large number of cycles but limited maximum energy density compared to that of a lithium-ion battery. Attempts have been made to increase maximum achievable energy density in EDLC through various factors including electrode materials and electrolytes. Materials used as electrode for EDLCs are high surface area activated carbon or carbon nanomaterials, such as carbon nanotube and graphene (Winter and Brodd, 2004; Zhang and Zhao, 2009; Sharma and Bhatti, 2010; Vangari, Pryor and Jiang, 2013; Gonzalez et al., 2016).

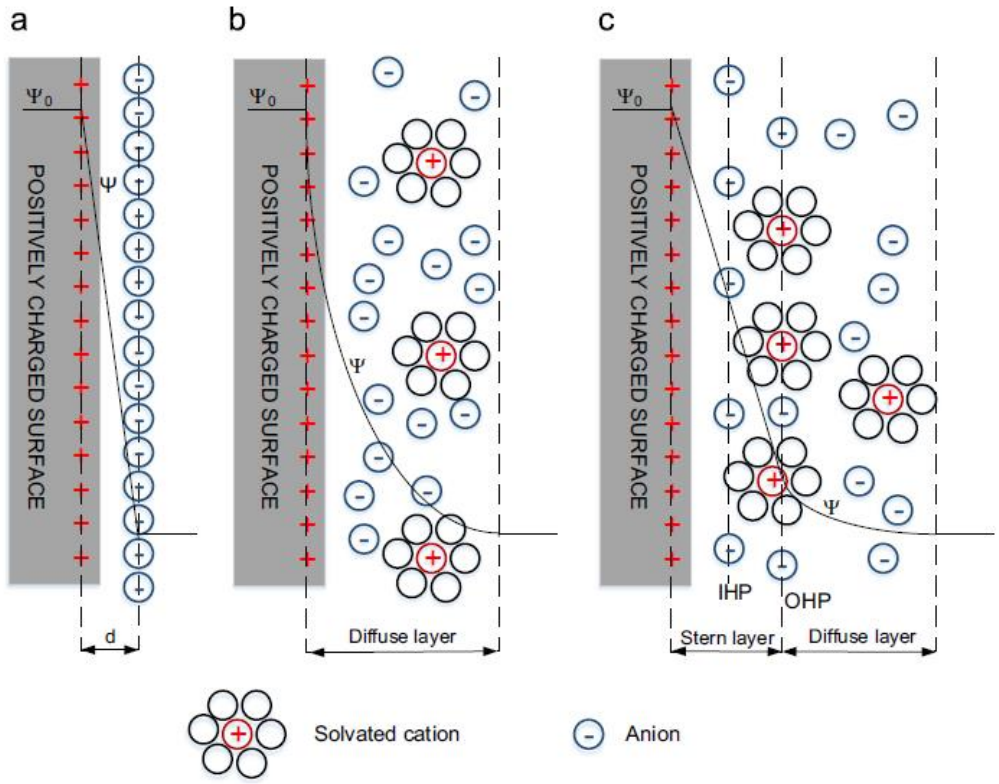

Figure 2-10 Illustration of different models for electrochemical double-layer capacitance. a) Helmholtz, b) Guoy-Chapman, c) Stern (Winter and Brodd, 2004)

On the contrary, pseudocapacitors store charges via redox reactions occurring at the electrode surface or sub-surface. Electrode materials for this type of supercapacitor are metal oxides and conducting polymers. While it is true that pseudocapacitors can achieve higher capacitance compared to EDLCs, the downside is their much lower cycle numbers due to the fact that the charges are stored through redox reactions. Originally, this type of supercapacitor suffered from low electrical conductivity. However, this has been tackled by incorporating carbon nanomaterials to form improved composite materials (Pryor and Jiang, 2013; Choi and Yoon, 2015; Wang et al., 2015).

The final type of supercapacitor combines features from EDLC and pseudocapacitor together into a single cell, having one electrode made of carbonaceous material and another made of pseudocapacitive materials, i.e. hybrid supercapacitor. As a result, charge storage mechanisms at anode and

cathode are different. Electrode materials for hybrid-supercapacitor anode are battery's anode materials, such as TiO_2 and $Li_4Ti_5O_{12}$. The cathode is often made of high surface-area carbon materials (Pryor and Jiang, 2013; Choi and Yoon, 2015).

2.7.2 Components of a supercapacitor

A supercapacitor consists of four key components which are electrodes (anode and cathode), electrolyte, separator and current collectors (Figure 2-11). Each component is described in the following sections.

Figure 2-11 Simplified schematic diagram of supercapacitor components

2.7.2.1 Electrodes

Good electrode materials should exhibit high conductivity, high surface area, high cycle life and good thermal stability. There are several types of materials currently used for supercapacitor electrodes, including carbonaceous materials, conducting polymer, and metal oxides.

Carbonaceous electrodes are the most common for both research and commercial non-Faradaic supercapacitors. General-grade carbon materials were previously used for electrode fabrication. Recent generations of supercapacitors have shifted towards using activated carbon with large surface area and controlled pore size and structures. Current trends in development of carbon-based electrodes for supercapacitor applications involve the use of carbon nanomaterials and carbon aerogels. Carbon nanomaterials, such as carbon nanotubes (CNTs) and graphene have excellent electrical conductivity, surface area, mechanical properties and thermal stability. They can also be further functionalized to achieve the desired modified properties. Carbon aerogels have also received attention alongside other carbon nanomaterials

due to the fact that they have low charging resistance, while showing an increased in capacitance and cycle life as well as flexibility (Davies and Yu, 2011; Gonzalez et al., 2016).

For pseudocapacitors, where redox reactions at the electrodes are essential to the working mechanism, transition-metal oxide nanoparticles and conducting polymers are preferred types of materials for electrode fabrication. RuO_2 and MnO_2 are the most studied metal oxide materials for supercapacitor electrodes, however RuO_2 has concerns over its toxicity. Other metal oxide nanoparticles for electrode materials include TiO_2, NiO_2, CoO_2, SnO_2 and VO_2. Recently, carbon nanomaterials have also been involved to fabricate carbon-metal oxide composite nanomaterial for improved material properties (Davies and Yu, 2011; Chandra, 2012; Jiang et al., 2012; Roldan et al., 2015). Conducting polymers may have an advantage over metal oxides in terms of production cost but they have lower rate of adsorption and desorption of ions due to lower ion mobility in the bulk polymer. Examples of commonly used conducting polymers are polyaniline and polypyrrole (Choi and Yoon, 2015; Wang et al., 2015).

2.7.2.2 Current collectors

This component collects the current and sends it to electrical wire going out from the electrode. The most common current collectors in supercapacitor research are aluminium foil and stainless steel. The quality of surface contact between electrode and current collector contributes to a component of the cell's impedance. Researches have been conducted on developing new materials as current collector with higher degrees of surface contact, such as CNT- and graphene-based sheets (Davies and Yu, 2011).

2.7.2.3 Separator

The separator prevents two electrodes from touching – circuit shorting – while it also serves as ion-permeable membrane, allowing only transportation of ions between anode and cathode. In general, aqueous-electrolyte supercapacitors use separators made from ceramic or glass-fibre materials, while organic-electrolyte supercapacitors use separators made from paper or polymeric

material. A good separator should have high electrical resistance, high ionic conductivity, and very small thickness (Davies and Yu, 2011).

2.7.2.4 Electrolyte

There are several classes of electrolyte used in supercapacitor applications, including aqueous, organic, ionic liquids, and solid electrolytes. Each class features different operating voltage range. Aqueous electrolytes were the first to be used in research but they have lowest operating voltage range. Common aqueous electrolytes are potassium hydroxide and sulfuric acid. Although organic electrolytes can cope with larger voltage windows, their safety concerns (such as flammability) must be carefully considered in designing the construction. Commonly used organic electrolytes include tetraethylammonium tetrafluoroborate ($TEABF_4$) in propylene carbonate or acetonitrile. Solid electrolytes, including polymer gel electrolytes, have been increasingly explored as promising and safer alternatives to liquid electrolytes as the concerns with leakage could be eliminated. Recently, ionic liquid electrolytes have gained an increased attention from researchers as they have a wide operating window, less charge loss in comparison to other liquid electrolytes, and remain stable up to 300°C (Davies and Yu, 2011; Qi et al., 2016).

2.7.3 Evaluating performance of a supercapacitor

Electrochemical techniques can be applied to a supercapacitor to obtain measurement data from which performance metrics could be estimated and used for evaluation. The common techniques include cyclic voltammetry (CV), galvanostatic charge-discharge (GCD), and electrical impedance spectroscopy (EIS).

2.7.3.1 Cyclic voltammetry

Cyclic voltammetry is among one of the most commonly used electrochemical techniques. Its principle involves variation of the voltage applied to the working electrode between the specified initial and final values, and measurement of the resulting current (Stoller and Ruoff, 2010). The current is plotted against voltage, forming a cyclic voltammogram (or CV curve). In the ideal situation, CV

curve of a capacitor appears as a rectangle as shown in Figure 2-12a. However, in real situations, there are several components of resistance within the cell which cause deviation from ideal conditions, such as resistance due to current collector-electrode contact or ion diffusion within the electrolyte (Yang and Mai, 2014). Accordingly, CV curve of a real supercapacitor is generally a distorted rectangle as seen in Figure 2-12b. Cyclic voltammetry can be used to determine the voltage window of an electrolyte (Stoller and Ruoff, 2010).

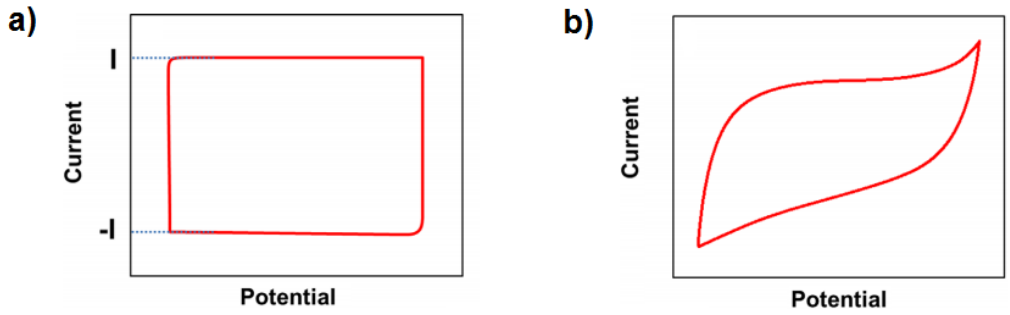

Figure 2-12 Cyclic voltammograms of a) ideal capacitor and b) real supercapacitor (Yang and Mai, 2014)

2.7.3.2 Galvanostatic charge-discharge

In this technique, constant-current charging and discharging are performed on the cell during a specified duration, and voltage is recorded. Voltage is plotted against time, forming a GCD curve. For an ideal capacitor, GCD curve appears as a perfect triangle (Figure 2-13a). However, due to several resistance components in real supercapacitors, GCD curve of a real supercapacitor is generally a slightly distorted triangle (Figure 2-13b) (Yang and Mai, 2014).

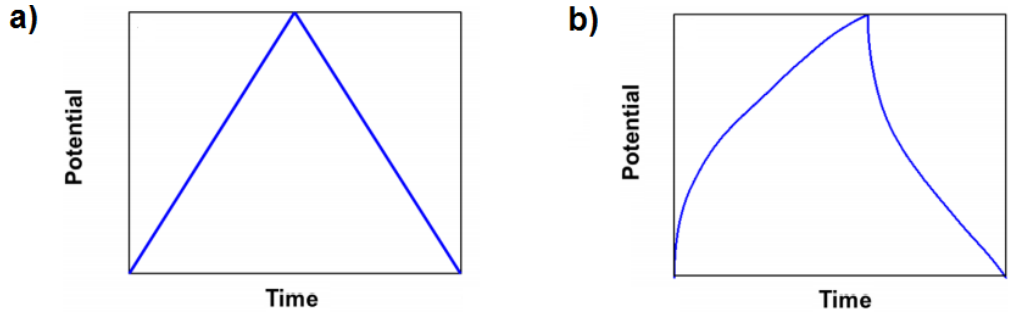

Figure 2-13 GCD curves of a) ideal capacitor and b) real supercapacitor (Yang and Mai, 2014)

Specific capacitance of the supercapacitor cell ($C_{sp,cell}$) can be calculated from a GCD curve using the following equation (Stoller and Ruoff, 2010):

$$C_{sp,cell} = \frac{I}{m \cdot \left(\frac{dV}{dt}\right)} \quad \textbf{(2-2)}$$

where I refers to the applied current (unit, A) during the measurement, m refers to total mass of two electrodes (unit, g), and $\left(\frac{dV}{dt}\right)$ refers to slope of the discharge curve (units, V/s).

Energy density of the cell can be calculated from (Stoller and Ruoff, 2010):

$$E = \frac{1}{2} C_{sp} V^2 \quad \textbf{(2-3)}$$

where E, C_{sp} and V refer to energy density (units, J/g), specific capacitance (units, F/g) and potential difference (unit, V) respectively.

Maximum power achievable of the supercapacitor (P_{max}) is estimated by:

$$P_{max} = \frac{V^2}{4(ESR)} \quad \textbf{(2-4)}$$

where P_{max}, V and ESR are maximum power (unit, Watt), potential difference (unit, V) and equivalent series resistance (unit, Ω) respectively (Yu et al,. 2012). ESR is related to the potential drop at the beginning of a discharge part in each GCD cycle, and can be calculated from (Stoller and Ruoff, 2010):

$$ESR = \frac{V_{drop}}{2I} \quad \textbf{(2-5)}$$

where V_{drop} refers to potential drop at the beginning of the discharge curve of the GCD curve (unit, V) and I refers to the current applied in the measurement (unit, A).

2.7.3.3 Electrochemical impedance spectroscopy

Electrical impedance is another important parameter in evaluating the performance of a supercapacitor cell as it is a measure of the ability to resist the flow of electron within the cell (Bard and Faulkner, 2001). In an EIS measurement, a voltage of specified frequency is applied to the working electrode, and the resulting current is measured. Impedance is defined as the ratio of the amplitude of the oscillating voltage to the amplitude of measured current, hence represented in the form of complex number (Gamry, 2017). Plotting the negative values of imaginary part of the impedance against values of real part forms a Nyquist Plot. The plot can be used to determine solution resistance (R_{Ω}) and charge-transfer resistance (R_{ct}) from the intercepts between the semi-circle part of the plot and the horizontal axis (left and right respectively) (Bard and Faulkner, 2001).

3 AIMS AND OBJECTIVES

From Chapter 1 and 2, it can be seen that fullerenol is a versatile nanoparticle and is continuously being explored on its properties and applications in many areas, especially medical applications. However, it was also found that different research teams utilised different synthesis routes to obtain fullerenol for their studies.

Concerning the fact that each synthesis route results in different forms of fullerenol (i.e. different number of hydroxyl groups per molecule), it may be considered that researchers have actually been studying behaviours of particular forms of fullerenol produced from the particular synthesis routes only, not the other forms and not from any other routes. However, fullerenol with other levels of hydroxylation from the same route might give a better performance for the application. It is necessary to investigate on the influence of level of hydroxylation on performance of fullerenol and determine the optimum conditions in order to harvest the ultimate benefits of fullerenol for each application.

It is also extremely crucial to carefully and critically consider the nature of the product when comparing the products which are synthesised from different routes, including residual components, contaminations, and profiles of properties (such as particle sizes). With variations in these factors, comparing products from different routes may not yield meaningful results.

To facilitate investigation on the influence of level of hydroxylation on fullerenol performance in application, variations on these factors should be eliminated as much as possible. This research sees that it is necessary to develop protocols which are based on a single synthesis route to produce fullerenol with specifiable level of hydroxylation, where the set of process conditions in each protocol is specific to each level of hydroxylation achievable.

The question for this research is established – whether it is possible to produce fullerenol with specifiable level of hydroxylation based on a single synthesis route.

To answer this question, the research therefore aims to develop synthesis protocols capable of producing fullerenol with specified level of hydroxylation. This is the main aim of this research. Nevertheless, as previously mentioned in Chapter 1, the research also wishes to complete the view of this issue by demonstrating comparison of performance of different classes of fullerenols (all produced from the developed protocols based on the same route) in an unexplored application, i.e. supercapacitor. Comparison and analysis can be achieved without concerns on effects from variations associated with different synthesis routes since all materials are produced from the same route. This becomes the complementary aim of this research.

Research aims and objectives are thereby stated as follows:

Aims

1. To develop synthesis protocols, based on a single route, from which fullerenol with specified level of hydroxylation can be produced
2. To demonstrate comparison of the effects of different classes of fullerenol (i.e. different levels of fullerene hydroxylation) in an unexplored area of supercapacitor as electrode additives for energy storage application

Objectives

1. Synthesis of fullerenol from a single route, characterisation and estimation of level of hydroxylation
2. Investigation on relationships between selected process parameters and level of achieved hydroxylation
3. Fabrication of fullerenol-containing electrodes and analysis of results from electrochemical experiment of the assembled symmetric activated carbon supercapacitors

4 METHODOLOGY

In order to achieve the ultimate aims and objectives stated in Chapter 3, a series of experiments on fullerenol synthesis (*Part One*), and a set of supercapacitor experiments (*Part Two*), were conducted. All experiments in *Part One* used the same set of characterisation techniques. To provide a good flow of information in the thesis, the first section in this chapter lists and explains the techniques involved in characterisation of fullerenol, which were consistently used throughout this research. The remaining sections in this chapter then describe methodologies for all experiments conducted to achieve research aims and objectives.

4.1 Fullerenol characterisation

4.1.1 Fourier-Transform infrared spectroscopy (FTIR)

Infrared spectroscopy was used to confirm chemical identity of the product achieved from a synthesis. All measurements were conducted using an ALPHA (Bruker) FTIR spectrometer, transmission mode. The spectra were recorded in the range of wavenumbers from 4000 to 400 cm^{-1}. A measurement disc for transmission-mode measurement was prepared by grinding a small amount of sample with dried potassium bromide (KBr) powder, which was pressed into a disc using high pressure. (KBr powder was stored in a desiccator to avoid contact with moisture.) The obtained infrared spectra were analysed and compared against related literatures (Li et al., 1993; Kokubo et al., 2011).

4.1.2 Thermogravimetric analysis (TGA)

TGA was used as a method for estimating the level of hydroxylation in fullerenol, i.e. number of hydroxyl groups present per fullerenol molecule ($n_{(OH)}$). All TGA measurements were conducted using a TG50 (Mettler Toledo) instrument, in a nitrogen atmosphere, with the heating rate of 10 °C/min, temperature range of 50-1000°C, sample mass of approximately 5 mg and aluminium oxide crucibles with lids (Mettler Toledo). Each TGA thermogram

obtained was analysed to determine parameters (x and y) for calculating $n_{(OH)}$ using Equation (2-1).

4.1.3 Dynamic light scattering (DLS)

DLS was chosen as an approach for particle size characterisation. All measurements were conducted using a ZEN1600 Nano-S Zetasizer (Malvern Instrument). Each DLS measurement consisted of five records, with three replications per record. Sample preparation was done by dissolving fullerenol into de-ionized water and transfer 1.1 ml of the solution into a disposable cuvette. Distribution of particle diameter by number (%) was obtained at the end of each measurement. DLS results were analysed in conjunction with electron micrographs in each experiment.

4.1.4 Scanning/Transmission electron microscopy (SEM/TEM) and energy dispersive X-ray spectroscopy (EDX)

Electron microscopy was used to obtain information on both particle morphology and size distribution of the products in the form of electron micrographs.

Due to the issues of instrument conditions and availability, as well as other constraints (including limited funding and time) during the course of this research, it was not possible to use one electron microscope as the source of microscopic information throughout, and the project had to adapt to using whichever facility accessible at the time the characterisation was required. A CM20 (Philips) TEM was first used and involved with characterisation of products from the experiment for evaluation of production consistency, but was very little involved in later experiments due to associated costs and availability issues. To reduce the analytical cost and minimise the amount of sample required, TEM was replaced with SEM. An XL30 (Philips) SEM was involved but, due to its severe and recurring issues of instrument conditions and availability, the project then had to seek access to a Supra 40 (Zeiss) at the National Physical Laboratory (London) and used it for the rest of the research.

Both SEMs were equipped with INCA X-sight (Oxford Instruments) for EDX elemental analysis function.

TEM sample preparation included dissolving fullerenol into de-ionized water and applying the solution onto a TEM copper grid. The loaded grid was left to dry in ambient atmosphere for a few hours before use. In case of SEM, the sample powder was sprinkled onto an SEM stud which was already applied with a thin layer of Silver Dag.

To obtain EDX results for each sample, information on elemental composition was taken from 3 different areas. The results (after subtracting signals from the Silver Dag) were obtained as percentages of elements present in the sample.

4.2 Selection of fullerenol synthesis route: assessing the solvent-free hydroxylation route as a potential alternative to TBAH-NaOH

Among the discovered routes to the synthesis of fullerenol (Section 2.3) the process of fullerene hydroxylation by sodium hydroxide in the presence of TBAH (Li et al., 1993) is rather simple, and is often used by many researchers as a method to produce fullerenol. However, there was also a route which did not involve any solvent in the reaction step, the solvent-free hydroxylation method proposed by Wang and colleagues in 2005 (Wang et al., 2005a). If valid, it would be a very attractive process with the advantages of having minimal risks and concerns related to solvents. The advantages would be not only in terms of good image as green manufacturing, but also reduced costs associated with waste treatment. This process could be a potential alternative to the TBAH-NaOH route. Although the authors provided numerical data from infrared spectroscopy, the spectrum itself was not present. Therefore, it was decided to assess this route and determine the missing information. The conclusion from this experiment was considered as the selection of fullerenol synthesis route for this research.

This section starts from describing procedures of the solvent-free hydroxylation method, followed by explanation on design of experiment.

4.2.1 The solvent-free hydroxylation route for fullerenol synthesis

With reference to the work published by Wang and colleagues (2005a), pristine C_{60} (72 mg), sodium hydroxide (240 mg), and hydrogen peroxide (180 µl) were thoroughly ground together for 15 minutes in a glass mortar. De-ionized water (50 ml) was added into the mixture, which was then stirred for 10 minutes. The mixture was filtered through a nylon-6,6 membrane (0.45 µm pore size), and the concentrated filtrate was added with 40 ml of methanol to form precipitates. Precipitation was repeated before the precipitate was collected and dried below 80°C for 30 minutes. The final product (brown solid) was stored in a tightly sealed container, in a cool and dry place, away from sunlight.

C_{60} (99.5+%) was purchased from Sigma-Aldrich, UK. Sodium hydroxide pellets (NaOH, 98.50%) was supplied by Acros Organics. Hydrogen peroxide (H_2O_2, general laboratory grade) and methanol (CH_3OH, HPLC grade) were purchased from Fisher Scientific. Nylon-6,6 filter membranes (0.45 µm pore size) were supplied by Fluka Analytical. De-ionised water was purchased from ReAgent.

4.2.2 Design of experiment

The purpose of this experiment was to assess feasibility of the solvent-free hydroxylation method, as well as its practicability to be used in this research for achieving the ultimate aims and objectives.

Following the procedures described in Section 4.2.1, synthesis using solvent-free hydroxylation method was conducted. The product was characterised using infrared spectroscopy. If fullerenol identity was confirmed in the infrared spectra and there were no practical issues with the route, estimation of the product's n_{OH} using TGA would then be performed, as well as particle size characterisation.

Information obtained from product characterisation, as well as other practical aspects during the syntheses, was used for assessing and deciding whether this solvent-free hydroxylation method would be used instead of the TBAH-NaOH route for this research.

4.3 Evaluation of production consistency of the selected route

Following the results and discussion of the first experiment (Section 5.1), it was found that there were significant practical concerns with the solvent-free hydroxylation method, and TBAH-NaOH route was selected as the fullerenol synthesis route to be used throughout this research.

Prior to further experimentation, production consistency of the selected route must be evaluated. The purpose of this experiment was to assess the production consistency of the selected synthesis route in terms of level of fullerene hydroxylation (i.e. number of hydroxyl groups per fullerene cage).

This section starts from describing procedures of fullerenol synthesis which was used as the base throughout the research, and was slightly modified from the original procedures (Li et al., 1993) in response to the need to adapt to accessible and available equipment. Design of experiment and explanation on associated statistical evaluation are also provided.

4.3.1 Fullerenol synthesis procedures (modified TBAH-NaOH route)

A clear, deep violet C_{60}-toluene solution was prepared by dissolving pristine C_{60} (80 mg) into toluene (60 ml). To this solution, 24 drops of tetrabutylammonium hydroxide (TBAH) were added using a narrow-tip disposable Pasteur pipette (one drop equivalent to 0.0223 ± 0.0004 ml TBAH calculated from density 0.995 g/ml and mean mass 0.0222 ± 0.0004 g per drop of TBAH – 95% confidence interval determined from 30 measurements), followed by 2 ml sodium hydroxide solution (100% W/V). The mixture was vigorously stirred for 20 minutes. Within a few seconds after vigorous stirring, the deep violet mixture turned colourless and black semi-solid was formed inside the reaction flask. Toluene was removed using a rotary evaporator. De-ionized water (10 ml) was added before the resulting mixture was moderately stirred for 12 hours at room temperature. When completed, further 20 ml of de-ionized water was added into the mixture, before it was filtered using a nylon-6,6 membrane of 0.45 µm pore size. Adding 40 ml of methanol (CH_3OH) to the concentrated filtrate gave red-brown precipitate. Precipitation was repeated once before the precipitate was retrieved

by filtering through a nylon-6,6 membrane (0.45 µm pore size), and oven-dried below 80°C for 30 minutes. The final product was obtained as brown powder, and stored in a tightly sealed container, in a cool and dry place, away from sunlight.

C_{60} (99.5+%) and toluene (C_7H_8, ACS reagent grade) were purchased from Sigma-Aldrich. TBAH ($C_{16}H_{37}NO$, 40% in water) and nylon-6,6 filter membranes (0.45 µm pore size) were supplied by Fluka Analytical. Sodium hydroxide pellets (NaOH, 98.50%) was supplied by Acros Organics, and methanol (CH_3OH, HPLC grade) was from Fisher Scientific. De-ionized water was purchased from ReAgent. The narrow-tip disposable Pasteur pipettes (1.0-1.5 mm tip, 150 mm length) were supplied by Kimble.

4.3.2 Design of experiment

This experiment involved fullerenol syntheses and product characterisation, with the focus on applying analysis of variance (ANOVA) as a tool for evaluating production consistency of the selected synthesis route.

The experiment was designed to produce four batches of fullerenol following the synthesis procedures described in Section 4.3.1. The products were labelled as Batch 1 to Batch 4 respectively. Each batch was subjected to infrared spectroscopy to confirm fullerenol identity. DLS ad TEM characterisation were also conducted.

To satisfy the requirements of ANOVA, the concept of completely randomised design (CRD) was applied throughout the experiment. From each batch, three samples (each of approximately 5 mg) were randomly taken. This gave a total of twelve samples from the four batches. Each sample was assigned with a unique number from 1 to 12, and lottery tickets for these twelve numbers were prepared. For each TGA measurement, a ticket was randomly drawn without replacing, and the sample that was assigned with the same number was selected as the sample of that measurement. This process was repeated until TGA measurements of all samples were completed. TGA thermograms of all samples were analysed and $n_{(OH)}$ values were calculated using equation (2-1).

ANOVA was then performed on the $n_{(OH)}$ values, and hypothesis testing and inference were performed. For this experiment, the null hypothesis (H_0) was:

$$\mu_1 = \mu_2 = \mu_3 = \mu_4 \quad \textbf{(4-1)}$$

where μ_i refers to the mean of $n_{(OH)}$ values from batch i $(i = 1,2,3,4)$. In other words, the null hypothesis assumes that values of the average $n_{(OH)}$ from each batch are equal. Accordingly, the alternative hypothesis (H_1) assumes that there is at least one μ_i that is different from other values.

4.3.3 Analysis of variance (ANOVA) for evaluation of production consistency

One-way ANOVA using significance level of 0.05 was performed on the calculated $n_{(OH)}$ values. The obtained test statistics, F and critical value of F (F_{crit}) were used for hypothesis testing. Inference of the outcomes was used to statistically evaluate production consistency.

4.4 Effect of TBAH on level of hydroxylation in TBAH-NaOH route for fullerenol synthesis

In the previous experiment (Section 4.3), production consistency of the selected synthesis route was statistically evaluated. To achieve the main research aim, studies on effects of selected key process parameters of the selected route were required. In this experiment, the first process parameter, amount of catalyst (TBAH) was studied for its influence on level of hydroxylation achieved in the production of fullerenol.

4.4.1 Design of experiment

Following the general procedures described in Section 4.3.1, a total of seven fullerenol syntheses were performed using different amount of TBAH for the reaction: 3, 6, 12, 24, 48, 96 and 192 drops. Products were labelled as Product 1 to 7 respectively. All products were characterised following the characterisation procedures described in Section 4.1.

The obtained $n_{(OH)}$ values from all products were plotted against corresponding amount (drops) of TBAH added for the reaction.

4.5 Effect of NaOH on level of hydroxylation in TBAH-NaOH route for fullerenol synthesis

In this experiment, the second process parameter, amount of source of hydroxide ions (sodium hydroxide solution) was studied for its influence on level of hydroxylation achieved.

4.5.1 Design of experiment

Referring to the procedures described in Section 4.3.1, a total of five fullerenol syntheses were performed using different amount of sodium hydroxide solution: 0.5, 1.0, 2.0, 4.0 and 8.0 ml. Products were labelled as Product 8 to 12 respectively. All products were characterised following the procedures explained in Section 4.1.

The obtained $n_{(OH)}$ values from all products were plotted against corresponding volume (ml) of sodium hydroxide solution added for the reaction.

4.6 Effect of reaction time on level of hydroxylation in TBAH-NaOH route for fullerenol synthesis

The purpose of this experiment was to study the effect of the final selected process parameter, reaction time, on level of hydroxylation achieved.

4.6.1 Design of experiment

Following the procedures described in Section, 4.3.1, a total of five fullerenol syntheses were conducted using different reaction time: 10, 15, 20, 25 and 30 minutes. Products were labelled as Product 13 to 17 respectively. All products were characterised following the procedure explained in Section 4.1.

The obtained $n_{(OH)}$ values from all products were plotted against corresponding reaction time.

4.7 Scale-up fullerenol syntheses using the developed synthesis protocols based on TBAH-NaOH route

This experiment served as a bridge between *Part One* and *Part Two* of the research. After the analyses in *Part One* were completed, three synthesis protocols were develped to achieve three classes of fullerenol (different $n_{(OH)}$) at a bigger production capacity (Section 5.7). This experiment is thus both an investigation on scalability of the developed synthesis protocols, as well as the production of experimental materials for *Part-Two* experiments.

4.7.1 Design of experiment

To achieve a sufficient amount of each fullerenol planned for the supercapacitor experiments in *Part Two* of the research, process scale-up, as well as multiple batches, were required for production of the three products. All productions followed the general procedures described in Section 4.3.1 but using different specific process condition summarised in Table 4-1 and Table 4-2.

To produce the experimental material with the lowest $n_{(OH)}$ (Product A), 3 drops of TBAH together with 2.0 ml of sodium hydroxide solution were used as normal-scale process conditions (Protocol 1, later described in 5.7.1). The total of seven productions, each of scaling factor = 3, were required. The seven batches were labelled as Product A, Batch A1-A7 respectively.

For Product B which has a medium $n_{(OH)}$, normal-scale process conditions use 24 drops of TBAH together with 2.0 ml of sodium hydroxide solution (Protocol 2, later described in Section 5.7.2). Two productions using scaling factor = 2, and another production at the normal scale, were required. The three batches were labelled as Product B, Batch B1-B3 respectively.

The normal-scale process conditions for producing Product C, which has the highest $n_{(OH)}$ among the three products, 24 drops of TBAH together with 8.0 ml of sodium hydroxide solution were used as the normal-scale synthesis (Protocol 3, later described in Section 5.7.3). Only one production (scaling factor = 2) was required. The product was labelled as Product C.

Table 4-1 Summary of normal-scale synthesis reagents for the three classes of fullerenol

$n_{(OH)}$	Denotation	Protocol	Normal-scale synthesis reagents			
			C_{60} (mg)	Toluene (ml)	TBAH (drops)	NaOH (ml)
Low	Product A	1	80	60	3	2.0
Medium	Product B	2	80	60	24	2.0
High	Product C	3	80	60	24	8.0

Table 4-2 Summary of synthesis reagents used for each actual batch in Scale-up Experiment

Batch	Synthesis reagents used in Scale-up Experiment			
	C_{60} (mg)	Toluene (ml)	TBAH (drops)	NaOH (ml)
A1-A7	240	180	9	6.0
B1-B2	160	120	48	4.0
B3	80	60	24	2.0
C	160	120	48	16.0

Due to the issues of instrument availability, as well as limited time, funding and amount of fullerenol material available for the supercacitor experiments, it was not possible to perform every characterisation on every single batch. Consequently, the project had to adapt to this problem by limiting characterisation on individual batches to FTIR and TGA only, since the techniques hold critical chemical information of the batch. For each product, if all batches pass FTIR and TGA characterisation (fullerenol identity confirmed), the batches would then be thoroughly mixed together to form a combined stock of corresponding product. Then, samples from each combined product were used for the remaining characterisation (DLS, SEM, and EDX). All characterisation followed the procedures given in Section 4.1. $n_{(OH)}$ of each product was determined.

4.8 Investigation on the effect of fullerenol as additives in activated carbon anode electrode for supercapacitor

This set of experiments belongs to *Part Two* of this research. The experiment was conducted both as a complement to *Part One* and as an investigation on an unexplored fullerenol application.

Experimental material for this experiment were Product A, B and C produced from scale-up syntheses in *Part One*. The products were used as additives of activated carbon electrodes for symmetric supercapacitor, to study the effect of different levels of hydroxylation in the additives on the performance of the supercapacitor.

4.8.1 Design of experiment

Part-Two experiments involved fabrication, assembly and electrochemical characterisation of five different symmetric activated carbon supercapacitors. Activated carbon was chosen as electrode's active material in all supercapacitors. Apart from the control (additive-free), each supercapacitor incorporated a different electrode additive material as shown in Table 4-3. All electrode additives were incorporated at the same proportion of 10% of the mass of total electrode material. All supercapacitor used 5M potassium hydroxide (KOH) as electrolyte.

Table 4-3 Summary of different designs of supercapacitor electrodes for the five symmetric activated carbon supercapacitors for *Part-Two* experiments

Supercapacitor	Electrode materials
S1	Activated carbon (100%)
S2	Activated carbon + 10% (wt) C_{60}
S3	Activated carbon + 10% (wt) Product A
S4	Activated carbon + 10% (wt) Product B
S5	Activated carbon + 10% (wt) Product C

CV, GCD and EIS were performed and analysed for all supercapacitors. Values of C_{sp}, ESR, R_{Ω}, R_{ct}, E and P_{max} of each supercapacitor were determined. The

parameters were plotted against the corresponding $n_{(OH)}$ values of the additive materials incorporated within the supercapacitors.

4.8.2 Electrode fabrication

The procedure for electrode fabrication was adapted from the work of Liu and colleagues (2014). N-methyl-2-pyrrolidine (NMP, 6 ml) was stirred with poly(vinylidene fluoride) (PVDF, 0.36 g) until PVDF was completely dissolved. Conductive carbon (0.01 g) was added and the mixture was stirred for 30 minutes. Electrode active material (1.138 g) was then added and the mixture was stirred for 150 minutes to form electrode slurry. Each supercapacitor had different composition of electrode material as described in Table 4-3. The slurry was casted onto a piece of aluminium foil using a manual casting knife applicator (Figure 4-1). After drying below 60°C on a hotplate, electrode discs were punched out from the foil, and stored in a tightly sealed container, in a cool and dry place, away from sunlight.

N-methyl-2-pyrrolidine (NMP, C_5H_9NO, 99%), activated carbon (DARCO®, 100 mesh powder), and conductive carbon black (Super-P®) were purchased from Fisher Scientific, Sigma-Aldrich, and TIMCAL respectively. Poly(vinylidene fluoride) (PVDF, $–(C_2H_2F_2)_n–$) was supplied by Alfa Aesar.

Figure 4-1 Manual casting knife applicator used in electrode fabrication

4.8.3 Supercapacitor cell assembly

The supercapacitor cell was built on-site using a PTFE union tube fitting as housing (detailed drawing as illustrated in Figure 4-2), and two stainless steel rods (diameter 12 mm, length 4 cm) as current collectors. A small hole was drilled into the middle part of the housing for draining of excess electrolyte. To provide points of contact for crocodile clips from the potentiostat/galvanostat for electrochemical measurements, a small hole was drilled into one end of each stainless-steel rod, and a ring-style blade connector was attached onto this end of the rod using a screw. Figure 4-3 shows supercapacitor housing installed with current connectors.

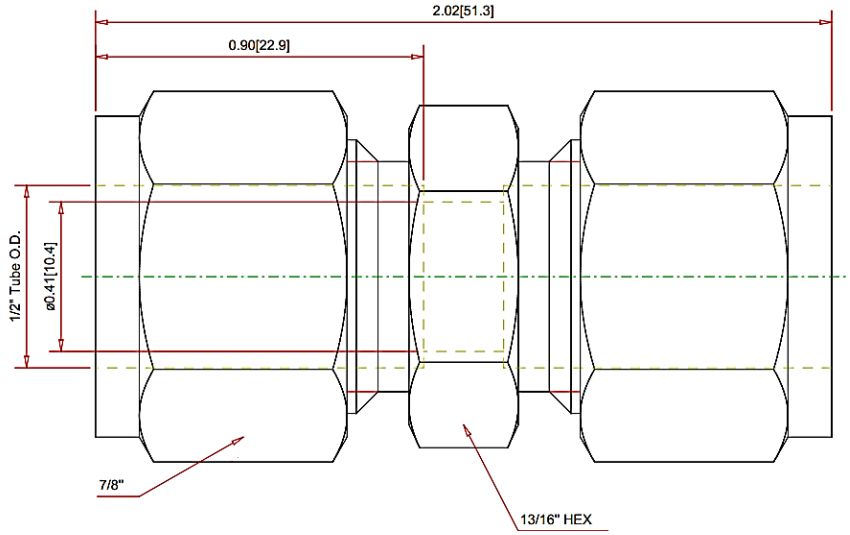

Figure 4-2 Drawing for the PTFE union tube fitting used as supercapacitor housing

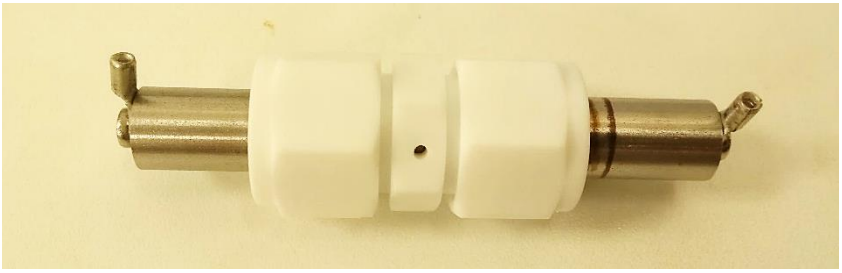

Figure 4-3 Supercapacitor housing with both current collectors installed

Separator discs were punched out from the separator film. Potassium hydroxide aqueous solution (KOH, 5M) was prepared to be used as electrolyte. KOH

(85%, pellets) was supplied by Acros Organics, and de-ionised water was purchased from ReAgent.

To assemble the cell, an electrode was placed on a current connector which was installed to one end of the housing. Electrolyte was added and the separator was placed. Another electrode was then placed on top of the separator, followed by the second current collector which was tightly screwed to the housing. Crocodile clips from the potentiostat/galvanostat were attached at each end of the cell, ready for measurements (Figure 4-4).

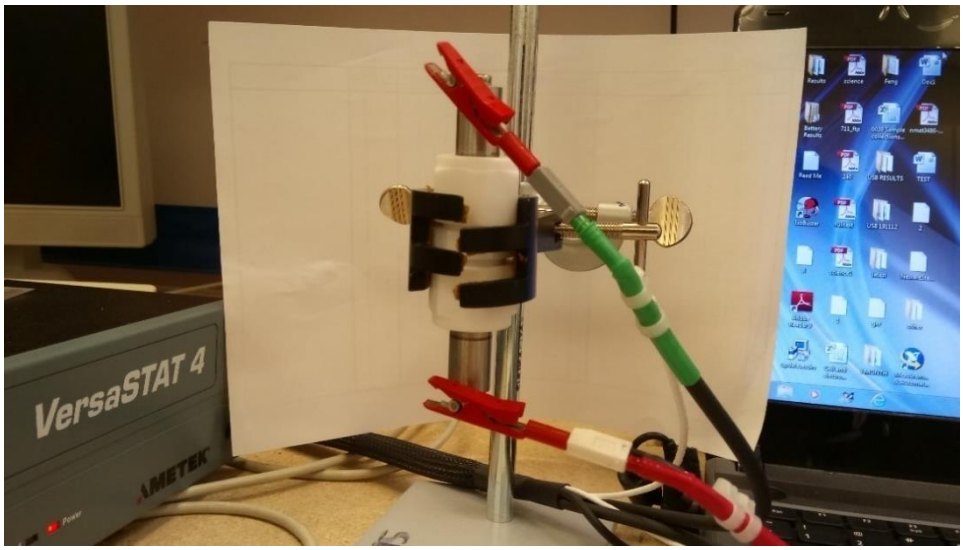

Figure 4-4 Assembled supercapacitor connected to VersaSTAT 4 potentiostat/galvanostat ready for measurements

4.8.4 Electrochemical measurements

All electrochemical measurements of the assembled supercapacitors were conducted using a VersaSTAT 4 (Princeton Applied Research) potentiostat/galvanostat and its software package VersaStudio. The software was also used for data analysis. For each supercapacitor, CV was conducted between 0.00 – 0.85 V at the scan rate of 0.05 V/s. GCD was performed using a current of 0.0005 A, and a cycle time of 1 minute. Frequency range for EIS was set for 10,000 to 1 Hz. Values of C_{sp}, ESR, R_{Ω}, R_{ct}, E and P_{max} using equations described in Section 2.7.3. Results were analysed and compared among the five supercapacitors.

5 RESULTS AND DISCUSSION

5.1 Selection of fullerenol synthesis route

Having identified the desired product (fullerenol), the next critical task towards the development of synthesis protocols is the selection of synthesis route. Usually, the selection is influenced by several constraints, for example, resources, physical laws, economic constraints, safety regulations, standards, and time (Sinnott, 2005).

For this research, the following factors were used in consideration of the likely candidates among the discovered synthesis routes to produce fullerenol:

- Process feasibility
- Possible product impurity, such as residual components, by-products, and other contaminations
- Health and safety concerns
- Process simplicity
- Overall process time
- Practicability based on the actual working environment during the course of this research
- Characterisation data
- Isolated yield

Several synthesis routes to produce fullerenol have been published. From literature review (Section 2.3), it could be seen that most of the routes have lengthy processes and involve several hazardous substances, such as strong acids, strong oxidising agents, and highly flammable substances. However, the route reported by Li and colleagues in 1993 (TBAH-NaOH route) appears different from others in the following aspects:

- The process is considerably simple (one-step reaction, followed by basic product separation processes).
- The process involves a small number of chemicals (only C_{60}, toluene, NaOH, TBAH and methanol).

- Overall process time is considerably shorter than most routes.

Apart from C_{60}, other chemicals in this route are general chemicals which could be conveniently sourced at commercial scale. These aspects support the suggestion that this route is highly favourable for the development of large-scale production of fullerenol. This route also has been widely accepted and frequently used by many researchers for fullerenol synthesis. Considering all aspects, the TBAH-NaOH route was therefore listed as the first candidate of routes for this research. A smaller number of substances in the process also implies the smaller probability of product impurity from residual components.

From the aspect of process simplicity, there is another route which might offer an even simpler process than TBAH-NaOH route. It is the solvent-free hydroxylation method reported by Wang and colleague in 2005 (Wang et al., 2005a). While TBAH-NaOH route requires toluene to dissolve C_{60} before hydroxylation takes place, reaction in the solvent-free hydroxylation method occurs during manual grinding of pristine C_{60} with sodium hydroxide pellets and a small volume of hydrogen peroxide solution. Table 5-1 summarises and compares the lists of chemicals involved in TBAH-NaOH and solvent-free hydroxylation routes for fullerenol synthesis.

Table 5-1 Involved chemicals in TBAH-NaOH and solvent-free hydroxylation routes for fullerenol synthesis

Process step	Process chemicals	
	TBAH-NaOH	**Solvent-free hydroxylation**
Reaction	C_{60} Toluene NaOH TBAH	C_{60} H_2O_2 NaOH
Product separation	Methanol	Methanol

The absence of solvent is beneficial in many ways. Not only the process is safer, but associated costs are also reduced (including solvent removal process and waste treatment).

Despite its advantages and attractiveness, this route unexpectedly has not been much used in fullerenol research. In addition, although the authors gave numeric spectroscopic data in their publication (Wang et al., 2005a), no graphical spectrum was provided. As a result, it could not be certain if fullerenol identity was actually confirmed in the spectra. However, the process seemed very attractive and it was decided that assessment on this process would be beneficial. If proven feasible, this route could offer the greenest and most attractive process for fullerenol manufacturing.

Apart from TBAH-NaOH, the route reported by Kokubo and his colleagues in 2011 was also attractive. In this route, hydroxylation of fullerene occurs when hydrogen peroxide solution and TBAH are added into C_{60}-toluene solution. However, the reaction required working at an elevated temperature in an open system with toluene in presence for a prolonged period of time. Also, in addition to toluene in the reaction step, the route requires two more hazardous solvents during product separation (diethyl ether and hexane). As a result, this route was removed from consideration of likely candidates because there were significant health and safety concerns regarding using this route in the working environment where this experiment was conducted.

5.1.1 Synthesis and characterisation of product from solvent-free hydroxylation route

After grinding all starting materials continuously for 15 minutes using glass mortar and pestle, a slightly moist, brown paste was obtained (Figure 5-1a). The paste was dissolved into 50 ml of de-ionised water, giving a brown liquid, which was stirred for 10 minutes to dissolve soluble product. Filtering the liquid resulted in a layer of black filter cake on the filter membrane, and a clear, brown filtrate. Adding methanol into the concentrated filtrate yielded brown precipitate Figure 5-1b).

The precipitate was retrieved as a layer of brown filter cake on the filter membrane. Precipitation with methanol was repeated once before the obtained filter cake was oven-dried to give the final product in the form of brown powder (Figure 5-1c).

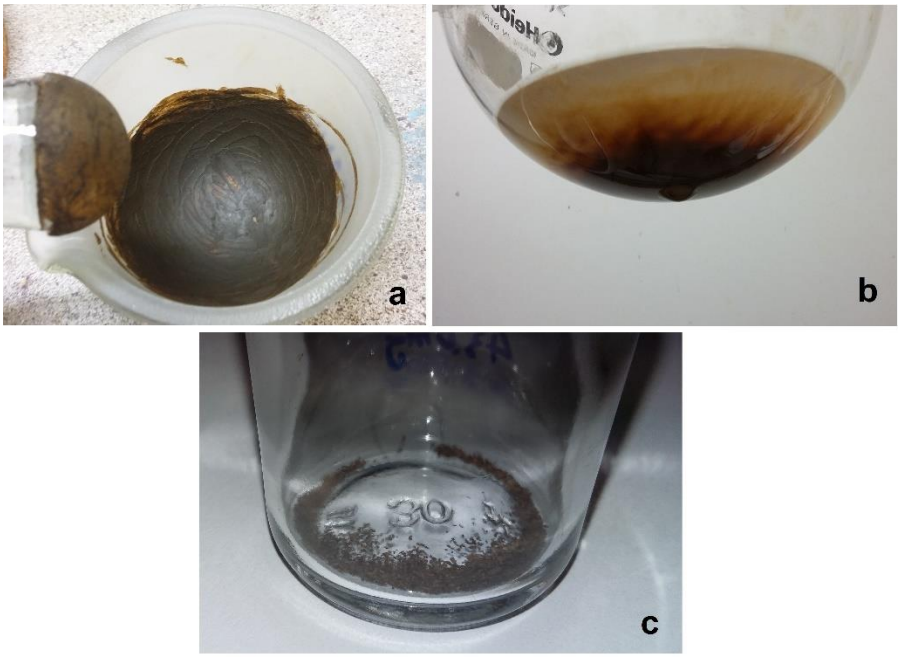

Figure 5-1 Major observations from solvent-free hydroxylation route. a) reaction mixture after 15 minutes of grinding, b) brown precipitate formed in a reservoir of methanol, and c) the final product

In the original literature of this route, the authors proposed a possible mechanism of their reaction as shown in Figure 5-2. The $–OOH^-$ moiety, produced from the reaction between hydrogen peroxide and sodium hydroxide, attacks the fullerene cage to produce $C_{60}(O)_m$ (Intermediate A). Next, nucleophilic attack by $–OH^-$ on Intermediate A takes place to produce either Intermediate B1 or Intermediate B2, depending on which carbon of the 6-membered ring of fullerene cage was attacked. Hydrolysis of Intermediate B resulted in $C_{60}(OH)_n$ (Wang et al., 2005a).

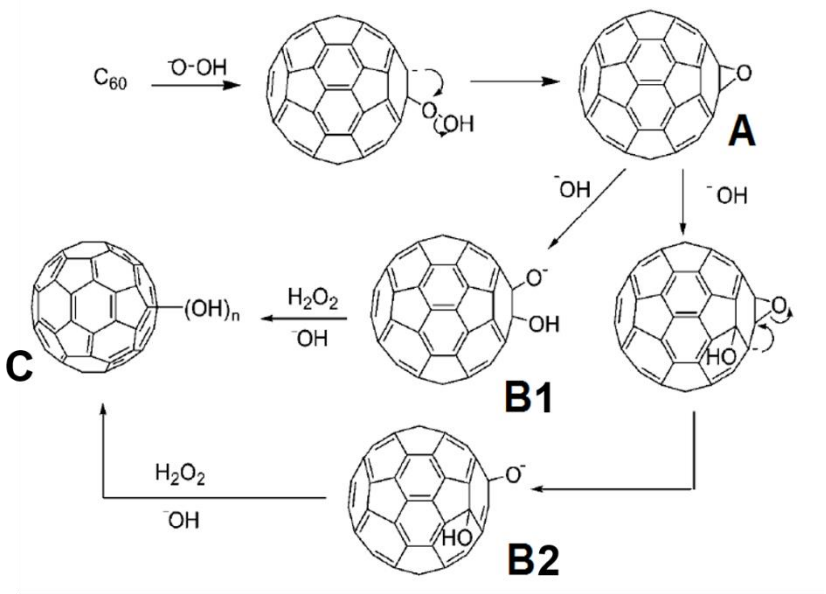

Figure 5-2 Possible reaction mechanism of solvent-free synthesis of fullerenol (Wang et al., 2005a)

Infrared spectroscopy was used to characterise the product, and the resulting spectrum (baseline corrected) is given in Figure 5-3. Confirmation of fullerenol identification was done by comparing the obtained spectrum with the spectrum of fullernol from other published literature. In this case, infrared spectrum of fullerenol from the work of Kokubo and colleagues (Figure 5-4) was chosen due to the fact that their process also used hydrogen peroxide and sodium hydroxide solutions as the source of hydroxylation, hence most similar to the route in question.

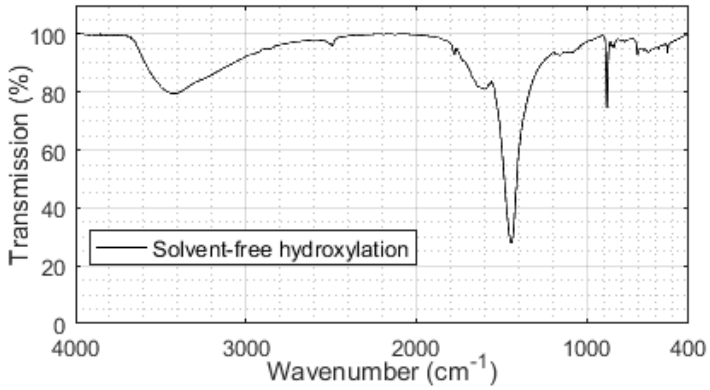

Figure 5-3 Infrared spectrum of product from solvent-free hydroxylation route

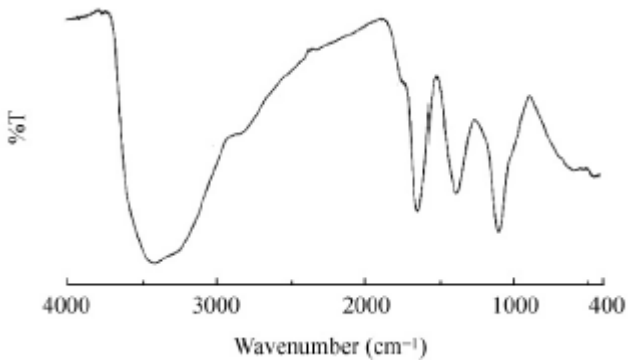

Figure 5-4 Infrared spectrum of fullerenol from Kokubo et al. (2011)

From Figure 5-4, fullerenol characteristic absorptions are clearly shown. There is a broad ν O–H absorption band around 3400 cm^{-1}, and other 3 absorptions at approximately 1620, 1370 and 1080 cm^{-1} which correspond to ν C=C, δ C–O–H, and ν C–O absorptions respectively (Kokubo et al., 2011). Figure 5-3, clearly different from the spectrum of C_{60} shown in Figure 5-5, shows a broad ν O–H absorption band around 3400 cm^{-1}. However, absorptions below 2000 cm^{-1} appears different from fullerenol spectrum in Figure 5-4, apart from the absorption centred around 1600 cm^{-1} which corresponds to ν C=C.

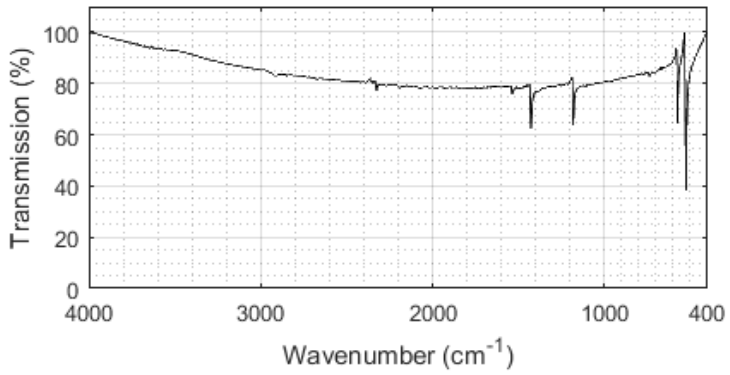

Figure 5-5 Infrared spectrum of pristine C_{60}

Absorption associated with epoxides was also detected in the spectrum – the unexpected sharp peak at 880 cm^{-1}. Referring to the possible reaction mechanism in Figure 5-2, this might suggest the existence of Intermediate A (fullerene epoxide) within the retrieved product, meaning that there were parts of the reaction mixture which could not achieve complete reactions. Although it might be temped to assign the combination of a spike around 2500 cm^{-1} and a

shoulder around 1700 cm^{-1} to the presence of carboxylic groups, the fact that absorption around 1450 cm^{-1} was strongest in the entire spectrum might suggest for some other substances. The possibilities of other substances should not be excluded based on only information from this spectrum as well. Ideally, the research also would like to conduct other characterisation using other techniques on the product to identity what else was present. However, since it was found that there were some practical concerns regarding the solvent-free hydroxylation route (which is discussed in more detail in the next section), and due to limitations on available research resources (especially time and budget), other characterisation was not conducted on the product.

5.1.2 Overall assessment and final decision on the selection of fullerenol synthesis route

While it is true that the overall process time for the entire synthesis using solvent-free hydroxylation route is very short (only approximately 3 hours), and that the route involves the smallest number of chemicals among all the reported routes, the downside of this route was also realised from this experiment.

Considering the nature of this route, the reaction step relies on solid processing – mechanical grinding and mixing – and generally there are concerns regarding mixing efficiency and product uniformity when solid processing is involved. In case of the solvent-free hydroxylation route, the evidence supporting this argument is the presence of epoxide absorption in the infrared spectrum of the product (Figure 5-3), which might suggest for incomplete reaction. Incomplete reaction leads to poor yield and product quality.

Closely related to the concerns for the reaction which relies on solid processing, the problem with practicability of using this route to achieve the ultimate aims of this research was realised through a few additional tests – modification of the amount of hydroxylating agent (hydrogen peroxide and/or sodium hydroxide). When the mass of sodium hydroxide pellets used was doubled, grinding became ineffective within 5 minutes after started. The reaction mixture quickly hardened and became solid, tightly adhered onto the grinding surfaces of both

mortar and pestle as shown in Figure 5-6). It was not possible to achieve any proper mixing further and the production could not proceed.

Figure 5-6 Reaction mixture after 5 minutes of grinding from the solvent-free hydroxylation route when using excess amount of solid sodium hydroxide (doubled), showing solidified reaction mixture and lumps of materials

A more extreme condition was also tested by using only a quarter of an original amount of hydrogen peroxide in another production (without changing the mass of solid sodium hydroxide from the original description). Here, the liquid portion of reaction mixture was not sufficient to provide a good mixing, and the material started forming lumps. The surface of the reaction mixture quickly solidified, covering several lumps of untouched starting materials buried deepy at the bottom of the mortar as shown in Figure 5-7.

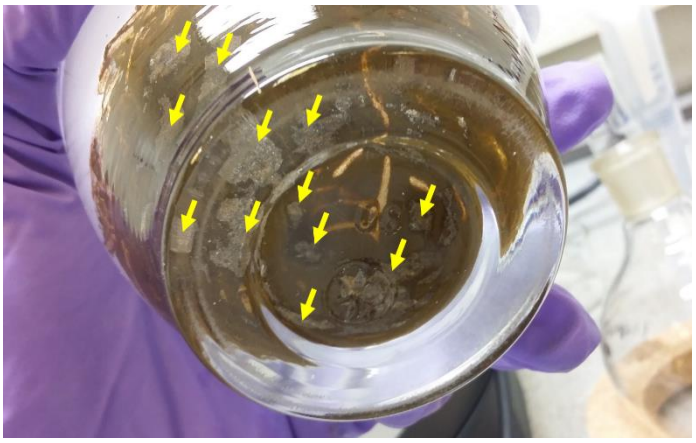

Figure 5-7 Untouchable lumps of materials (marked by yellow arrows) buried under solidified reaction mixture in solvent-free hydroxylation route using a reduced amount of hydrogen peroxide solution

Underlying significant health and safety concerns were also noticed while performing the synthesis in the laboratory. Waste water from quick washing of the mortar and pestle used for grinding of reaction mixture was stored in a new and empty waste container with its cap on. The container swelled after 5-6 hours, and the cap had to be loosen to release gas built up inside.

The amount of water used for washing was considerably large in relation to the small amount of both chemicals remained on surface of the mortar and pestle. Therefore, waste water from washing should already be a rather dilute mixture of hydrogen peroxide and sodium hydroxide aqueous solutions. Through an investigation to explain this phenomenon, it was suggested that the gas which built up inside resulted from decomposition of hydrogen peroxide catalysed by sodium hydroxide, expressed by the following chemical equations:

$$OH^- + H_2O_2 \rightleftharpoons HOO^- + H_2O \quad \textbf{(5-1)}$$

$$H_2O_2 + HOO^- \longrightarrow H_2O + O_2 + OH^- \quad \textbf{(5-2)}$$

The presence of hydroxide ion (OH^-) induces the reaction in Equation (5-1) when it comes into contact with hydrogen peroxide, forming hydroperoxide ion (HOO^-) and water. However, the reaction tends to go forward of the equilibrium due to the fact that pK_a of water is slightly larger than that of hydrogen peroxide (Kokubo et al., 2011). Hydroperoxide ion then reacts with hydrogen peroxide as shown in Equation (5-2), generating oxygen gas. The net expression for sodium hydroxide-catalysed decomposition of hydrogen peroxide is thus (Hart, Houtman and Hirth, 2013):

$$2H_2O_2 \longrightarrow 2H_2O + O_2 \quad \textbf{(5-3)}$$

From Equation (5-3), it can be suggested that the gas build-up inside the waste water container was oxygen gas (generated through decomposition of hydrogen peroxide catalysed by the presence of sodium hydroxide). Hart, Houtman and Hirth (2013) conducted an experiment to study the kinetics of this reaction and found that this exothermic reaction was capable of self-acceleration resulting in rapid generation of a large amount of oxygen gas, as well as massive energy

release which was observed as a lot of steam plume. There were also cases in chemical plants where pumps exploded due to the two incompatible chemicals coming in contact inside the pump, causing serious injuries and damages (Hart, Houtman and Hirth, 2013).

In an open working space, the release of oxygen poses risk of ignition which leads to fire. In the closed container, if the container is not strong enough and there is a build-up of pressure cause by oxygen generated from this reaction, this poses the risk of explosion (Hart, Houtman and Hirth, 2013).

The actual working environment during the course of this research was a fume cupboard in a small chemistry laboratory which was shared with many other students and staffs. With limited space, it was sometimes difficult to gain control over the arrangement of the shared working space. However, appropriate and safe experiment setup and arrangement should not be compromised when health and safety are concerned. Therefore, for health and safety, it was concluded that the solvent-free hydroxylation route was not suitable for this environment due to its associated chemical and thermal hazards, and risks of fire and explosion.

Beside this phenomenon, there is also another rapid exothermic reaction between hydrogen peroxide and sodium hydroxide leading to formation of sodium peroxide (Na_2O_2) which is a strong oxidiser and poses chemical hazards. This reaction is shown in Equation (5-4) (California FACE Program, 2010).

$$2NaOH + H_2O_2 \longrightarrow Na_2O_2 + 2H_2O \quad \textbf{(5-4)}$$

Considering the fact that there were significant health and safety concerns, this route was thus eliminated.

Based on results from this experiment and discussion in this section, fullerene hydroxylation by sodium hydroxide in presence of TBAH (TBAH-NaOH route) was thereby selected as the fullerenol synthesis route for this research.

5.2 Evaluation of production consistency of the selected route

Before proceeding to further stages in developing the aimed synthesis protocols, it is important to evaluate production consistency of the selected route. Appropriate statistical analysis was used to support and provide information on confidence of the evaluation.

Several parameters can be used to evaluate consistency of a chemical process, for example, yield, particle size distribution, colour, or physical form. Other characters of the product such as moisture content, contaminants and impurity could also be considered. Based on research aims and objectives (Chapter 3), production consistency of the selected fullerenol synthesis route (TBAH-NaOH) was evaluated in terms of level of hydroxylation ($n_{(OH)}$) achieved, i.e. number of hydroxyl groups introduced per fullerene cage.

In this section, synthesis and product characterisation are discussed, followed by estimation of level of hydroxylation and statistical analysis for the evaluation of production consistency. For ease of clarification, this experiment is hereby referred as ‘Consistency Evaluation Experiment’.

5.2.1 Synthesis and characterisation of fullerenol

Prior to the actual experiment, a trial synthesis using the original TBAH-NaOH route as described in the work of Li and colleagues (1993) (using 3 drops of TBAH for the reaction) was conducted to assess its performance based on accessible equipment and available time.

During product separation, it would have been ideal to separate the final precipitate from methanol reservoir using centrifugation followed by decantation and finally drying under vacuum. However, drying under vacuum takes a rather long time based on the accessible vacuum source. This choice of process was not suitable to this research, which had quite a number of syntheses to conduct under limited time frame. Consequently, collection of precipitate for this research used filtration followed by oven-drying instead. Although the modified steps greatly reduced the process time for each synthesis, this came with the price of a decrease in mass of isolated product due to dead space from filtration

(i.e. a certain amount of product retained in the filter membrane). This point should be taken into account when considering the yield of each synthesis.

From the trial synthesis and the accessible equipment, it was found that the amount of isolated final product (approximately 15 mg) was far from being sufficient to cover all the required characterisations of each batch.

For this experiment which aimed to statistically evaluate production consistency, each characterisation was design to have a number of replications. It was extremely essential that each single batch was produced at a capacity from which sufficient amount of material for all the required characterisation of the batch could be supplied. Consequently, modification to the original TBAH-NaOH route was necessary to ensure a sufficient amount of isolated product for a single batch, and the amount of TBAH added into the reaction mixture was changed from 3 drops to 24 drops instead. The combined modification to synthesis steps resulted in the synthesis procedures described in Section 4.3.1 which was used as a basis throughout this research. This modified version of TBAH-NaOH is hereby referred as ‘the selected route’ throughout this research.

All products in this experiment were synthesised following the procedures described in Section 4.3.1. Four batches of fullerenol (Batch 1 to Batch 4) were synthesised.

Observations during the production of each batch were similar. Black pristine C_{60} was dissolved into toluene to give a clear, deep violet solution (Figure 5-8a). The solution was added with TBAH and sodium hydroxide solution, and was vigorously stirred in air at room temperature for 20 minutes using a magnetic stirrer. The deep violet colour faded within 3 seconds, with black semi-solid started forming simultaneously and increasingly as vigorous stirring progressed. Upon completion, the resulting reaction mixture turned into a colourless liquid with black semi-solid formed (Figure 5-8b). This marked the end of the reaction step of the synthesis.

Product separation started from removing toluene (colourless liquid) from the black semi-solid using an evaporator. De-ionised water was added into the

reaction flask to dissolve soluble parts (the desired product) from the bulk of black semi-solid, resulting in a black suspension. The suspension was moderately stirred for 12 hours to dissolve soluble product as much as possible into the aqueous liquid phase. When completed, the suspension was filtered. Insoluble solids were retained on a filter membrane and a clear, brown filtrate (Figure 5-8c) was obtained in the filtering flask. Water was evaporated from the filtrate to obtain concentrated filtrate, which was added with methanol to yield brown precipitate (Figure 5-8d). Precipitation occurred immediately when methanol was poured into the concentrated filtrate, however the mixture was left to sit for 5 minutes to allow time for precipitation. Filtering the mixture resulted in a layer of brown filter cake on membrane (Figure 5-8e) and a clear colourless filtrate. To further remove traces of sodium hydroxide, the filter cake was re-dissolved into de-ionised water, and concentration and precipitation were repeated. The final filter cake of brown precipitate was oven-dried to give the final product as brown powder (Figure 5-8f).

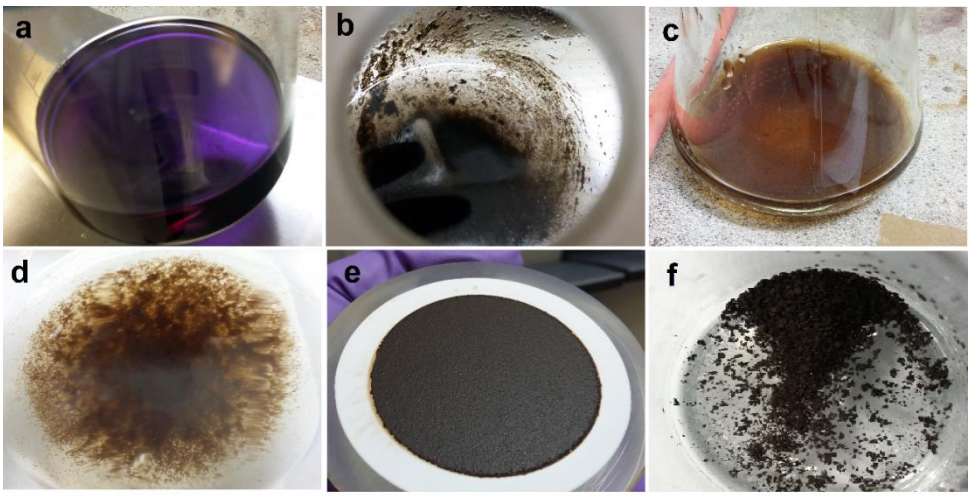

Figure 5-8 Major observations from fullerenol synthesis using the selected route (TBAH-NaOH). a) Deep violet solution of C_{60}-toluene, b) Reaction mixture upon completion of vigorous stirring, c) Brown filtrate containing water-soluble product, d) Brown precipitate immediately formed when methanol was added into concentrated filtrate, e) Precipitate obtained as brown filter cake on a membrane, f) Final product in the form of brown powder

All batches were produced at an original scale (production basis of 80 mg C_{60}). Table 5-2 shows the amount of C_{60} used and isolated product from each batch. It should be noted that the isolated product in Batch 4 was lower than other batches due to accidental loss of some product while transferring into a container before weighing (it was roughly estimated that the lost portion was 30-40 mg). The products from all batches were characterised by infrared spectroscopy, DLS and TEM to confirm chemical identity as well as particle morphology and size distribution.

Table 5-2 Record of the amount of starting material C_{60} and isolated products from Batch 1 to Batch 4

	Amount of C_{60} used (mg)	**Isolated product (mg)**
Batch 1	82.4	105.4
Batch 2	81.5	96.1
Batch 3	80.4	110.9
Batch 4	80.4	68.1

Infrared spectra of Batch 1-4 and pristine C_{60}, are shown in Figure 5-9. The spectra of all batches, clearly different from the spectrum of pristine C_{60}, resembled each other and fullerenol spectra in published literatures (Li et al., 1993; Kokubo et al., 2011). All spectra show fullerenol characteristic absorptions: a broad band centred around 3430 cm^{-1} corresponding to ν O–H, and three more peaks centred around 1600 cm^{-1}, 1370 cm^{-1}, and 1080 cm^{-1} corresponding to ν C=C, δ C–O–H, and ν C–O respectively. In addition to these characteristic absorptions, the spectrum of sample from Batch 2 (Figure 5-9b) contained a small peak around 1200 cm^{-1} which was suggested to come from the fullerene cage (also seen in Figure 5-9e). In summary, infrared spectra suggested that fullerenol identity, hence successful hydroxylation of fullerene, was confirmed in all four batches.

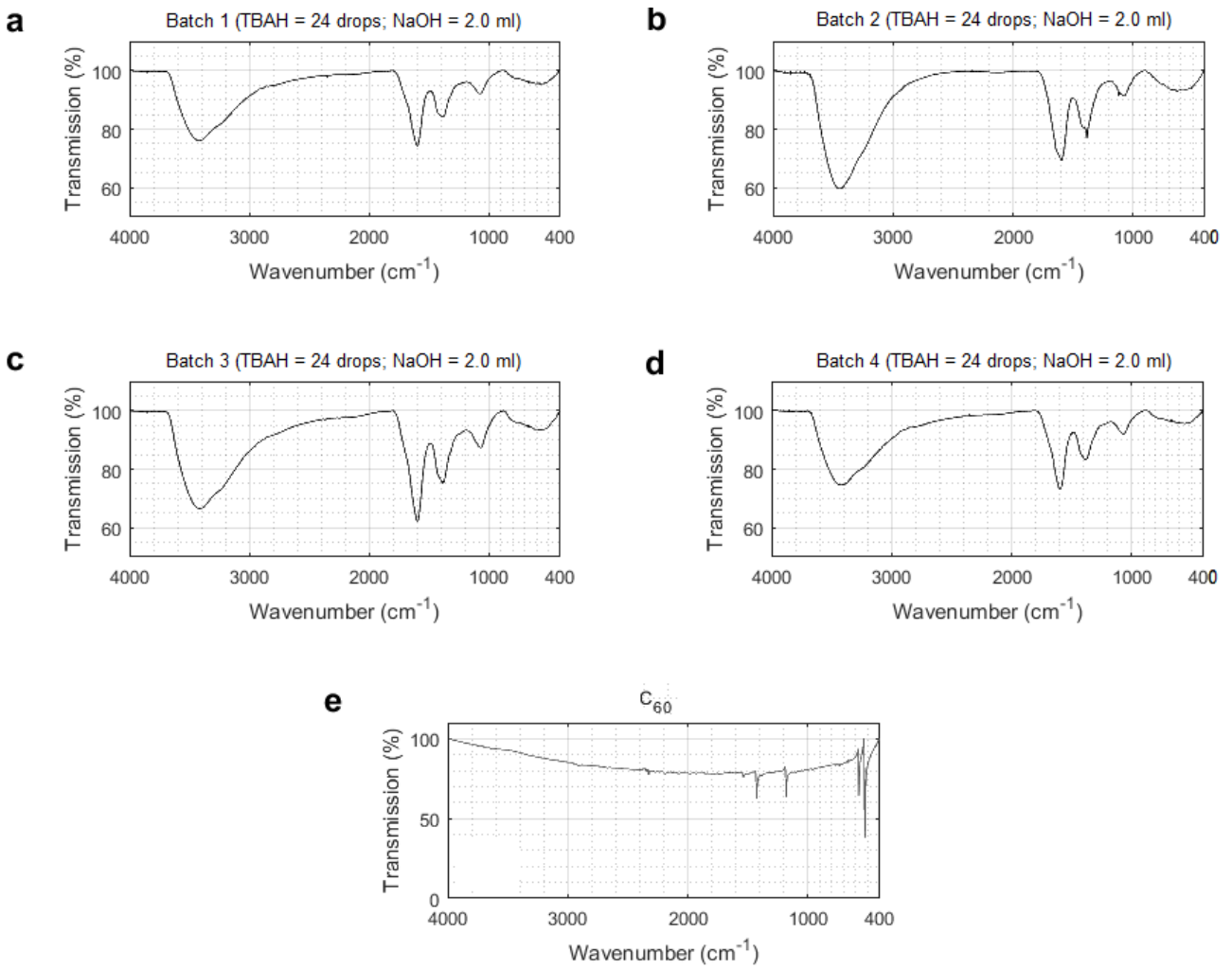

Figure 5-9 Infrared spectra of products from Consistency Evaluation Experiment (Batch 1-4; a-d respectively) and C_{60} (e)

Results from DLS were used in conjunction with TEM micrograph for particle size characterisation. Figure 5-10 shows DLS results of the produced fullerenol as distribution of particle diameter by number (%). The measurement was set to consist of five records (with three replications per record).

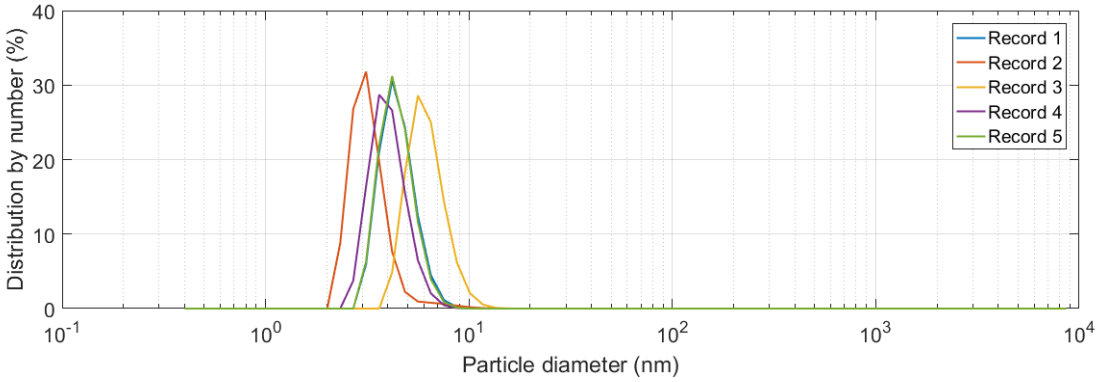

Figure 5-10 DLS results of the produced fullerenol (Record 1 and Record 5 perfectly coincided)

It might be difficult to differentiate but Record 1 and Record 5 coincided perfectly in Figure 5-10. From the figure, most particles in the sample from the produced fullerenol were approximately 3-7 nm in diameter, with the smallest detected diameter approximately 1.5 nm, and the biggest diameter just above 10 nm. These findings were supported by the TEM micrograph of the sample in Figure 5-11, revealing the existence of very small spherical particles of different sizes. Most particles in the image are smaller than 5 nm. However, slightly bigger particles (diameter less than 15 nm) are also observed in the micrograph.

Results from particle size characterisation were in agreement with published literature where Kokubo and colleagues (2011) reported the size of individual fullerenol particles to be approximately 1 nm. It was suggested that existence of larger diameters detected in both DLS results and TEM micrograph were created through aggregation of smaller fullerenol particles due to the fact that fullerenol tends to easily aggregate and form clusters of particles (Kokubo, 2012).

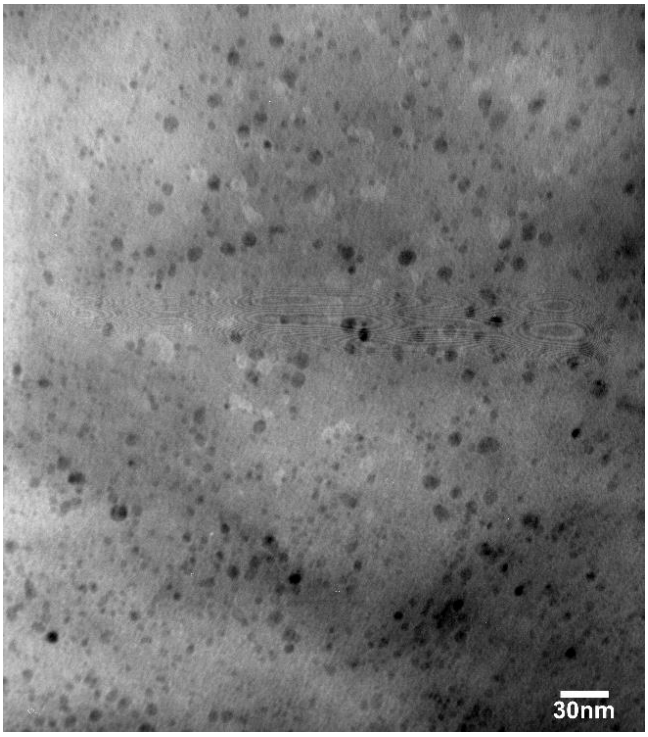

Figure 5-11 TEM micrograph (200kx) of the produced fullerenol

Based on chemical and particle characterisation, it can be concluded that the synthesised products were fullerenol.

In the selected route, the reaction mixture consisted of two immiscible phases: organic (toluene) and aqueous (sodium hydroxide solution) phases. C_{60} molecules existed in the organic phase, while hydroxide ions (OH^-) were in the aqueous phase. The role of sodium hydroxide solution was the source of hydroxide ions for polyhydroxylation of C_{60}. Naturally, the reaction between C_{60} and hydroxide ions could not occur as they existed in different, immiscible phases and could not come together. TBAH, a phase-transfer catalyst, is the key which makes this reaction possible by bringing hydroxide ions from the aqueous phase to meet C_{60} molecules in the organic phase where the desired reaction takes place (Li et al., 1993; Kokubo, 2012).

In addition to TBAH, it is known that fullerenol synthesis via TBAH-NaOH route also requires the presence of oxygen in order to achieve the desired products (Li et al., 1993; Alves et al., 2006; Kokubo, et al., 2011; Kokubo, 2012). Based on the fact that C_{60} is well-known as an excellent photosensitizer, this research

proposed that the role of oxygen gas is the source of ground state oxygen for generation of singlet oxygen (by C_{60}) which are essential for the mechanism of reaction between hydroxide ions and C_{60} molecules to form fullerenol, illustrated in Figure 5-12.

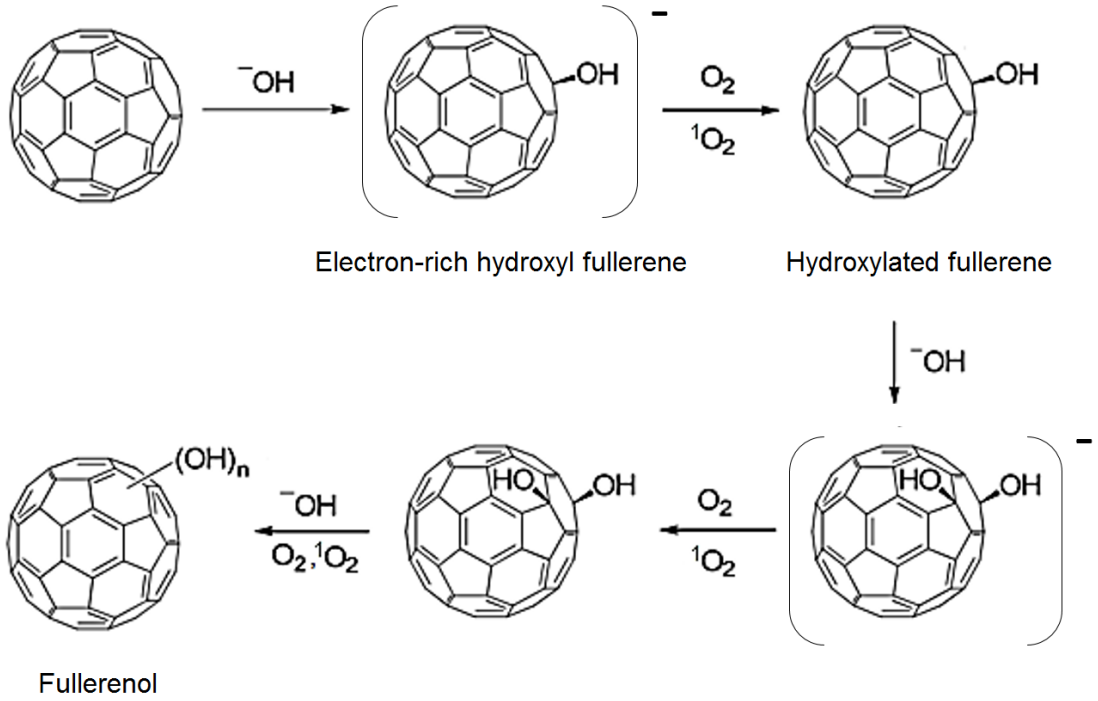

Figure 5-12 Proposed reaction mechanism for C_{60} hydroxylation in TBAH-NaOH route to produce fullerenol. Single oxygen ($^1O_2$) is proposed to play an important part in the reaction pathway (figure modified from Kokubo (2012))

C_{60} molecule can be transformed into an excited triplet state when stimulated by light, and energy of the excited C_{60} can be transferred to nearby ground-state oxygen molecule to form singlet oxygen ($^1O_2$) in the system (Stasheuski et al., 2014). Once the hydroxide ion has been transferred from the aqueous phase to meet with C_{60} in the organic phase by TBAH, the nucleophilic hydroxide ion attacks the C_{60} molecule (nucleophilic addition) and forms an electron-rich hydroxyl-fullerene. The singlet oxygen receives the excess electron and forms charge-transfer complex with hydroxyl-fullerene, which consequently dissociates into hydroxylated fullerene and ground state oxygen (Hulliwell and Gutteridge, 2015). Several repetitions of nucleophilic attacks by hydroxide ions

and transferring excess electrons to singlet oxygen finally result in the formation of fullerenol.

5.2.2 Thermogravimetric analysis (TGA) and estimation of level of hydroxylation by 'TGA method'

As the method for estimation of level of hydroxylation relies on TGA information, it was important to explore the thermograms of the products.

For each TGA measurement, a constant flow of nitrogen gas was supplied into furnace of the TGA instrument before and throughout the measurement to eliminate unwanted reactions between the sample and atmospheric components. Each sample was subjected to a linear heating (10°C/min). Sample weight was recorded against furnace temperature throughout the measurement, presented as a TGA thermogram. Figure 5-13 to Figure 5-16 show TGA thermograms from all replications of the four batches. Key analyses included the first derivative of thermogravimetric curve (DTG), and identification of important weight losses. DTG curve is plotted on the same horizontal axis as the TGA curve, with its vertical axis is on the right side (shown in pink).

Under normal situation, i.e. contamination-free, TGA curve of fullerenol can be divided into three parts associated with decomposition of different chemical species. The first part is the loss of physically bound water molecules which occurs from room temperature up to 150-180°C. The second part extends from 150°C or 180°C to around 570°C, and is associated with degradation of the introduced hydroxyl groups. The final part covers weight loss above 570°C which is related to degradation of fullerene structure (Chiang et al., 1993; Goswami et al., 2004; Kokubo et al., 2011; Kokubo, 2012). In general, thermograms from Figure 5-13 to Figure 5-16 follow this normal pattern in their first two parts. However, unexpected decomposition behaviour deviated from the normal pattern is observed in the final part. To approach this problem, it is a good idea to start from observing how pristine C_{60} decomposes under the same conditions.

Thermal decomposition of pristine C_{60} (Figure 5-17) starts with very small and gradual decrease in sample mass from 670°C to 800°C. Then, a major weight loss (almost 70% of sample mass) occurs within the range of 800-950°C, due to sublimation of C_{60} (degradation of fullerene structure). This is in agreement with report on thermal stability of C_{60} from other literature (Cataldo, 2002). A small weight loss from 950-1000°C could come from degradation of C_{70} molecules (Weber, 2009). It is possible that C_{70} could be present as contamination in a small proportion from C_{60} manufacturing, according to purity information (99.5+%) provided by the manufacturer (Sigma-Aldrich). For a fullerenol sample, a step weight loss around 700-900°C is thus expected in the final part of the TGA curve.

An observation was recalled upon realisation of unexpected decomposition behaviour above 570°C of the samples. When the brown filtrate (which contained the product) was collected in the flask after filtering out the insoluble solids, a layer of opaque substance was observed (from the side of the flask) on as a top layer bove the filtrate as shown in Figure 5-18. This layer was not obvious in a bird's eye view. In an attempt to find the possible source this layer, all chemicals involved in the synthesis were investigated and the entire synthesis procedures were scrutinised, including all apparatus. It was realised that silicone grease, the lubricant applied at the glass joint for vent of the the glass condenser for rotary evaporator, could be the source of the opaque layer.

An SEM micrograph of the product, shown in Figure 5-19, provided another evidence supporting the argument that silicone contamination was present in the product. Several sheets of solid were observed existing together with the spherical product particles. It was thought that some parts of these sheets were broken possibly during the sample preparation stage (where the sample powder was thoroughly ground before sprinkled onto the sample mount) and shown here as long fragments. With reference to the observation of an opaque layer during the syntheses, it was suggested that these sheets could be dried silicone grease.

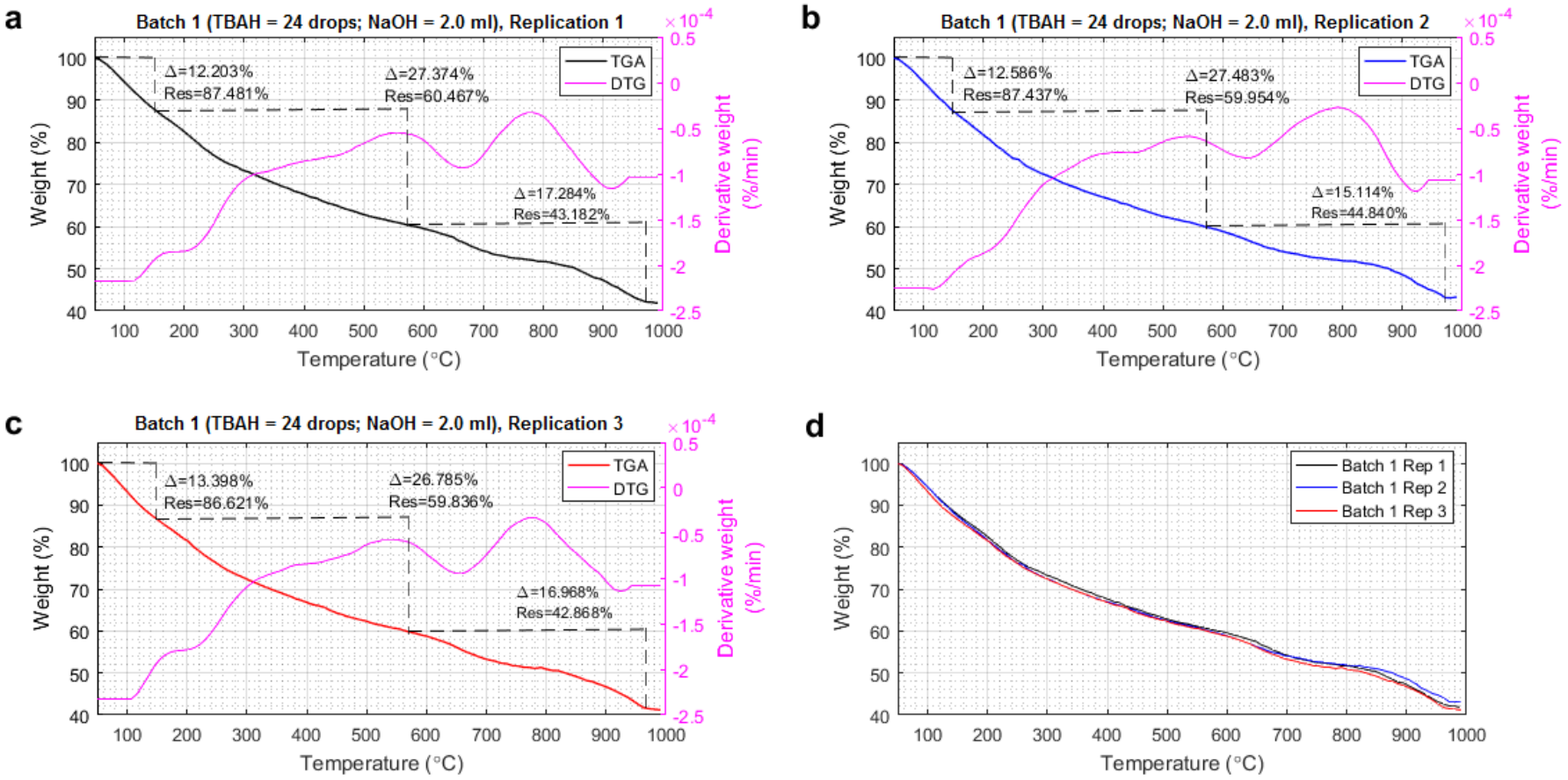

Figure 5-13 Individual (a-c) and superimposed (d) TGA thermograms from Batch 1, Consistency Evaluation Experiment

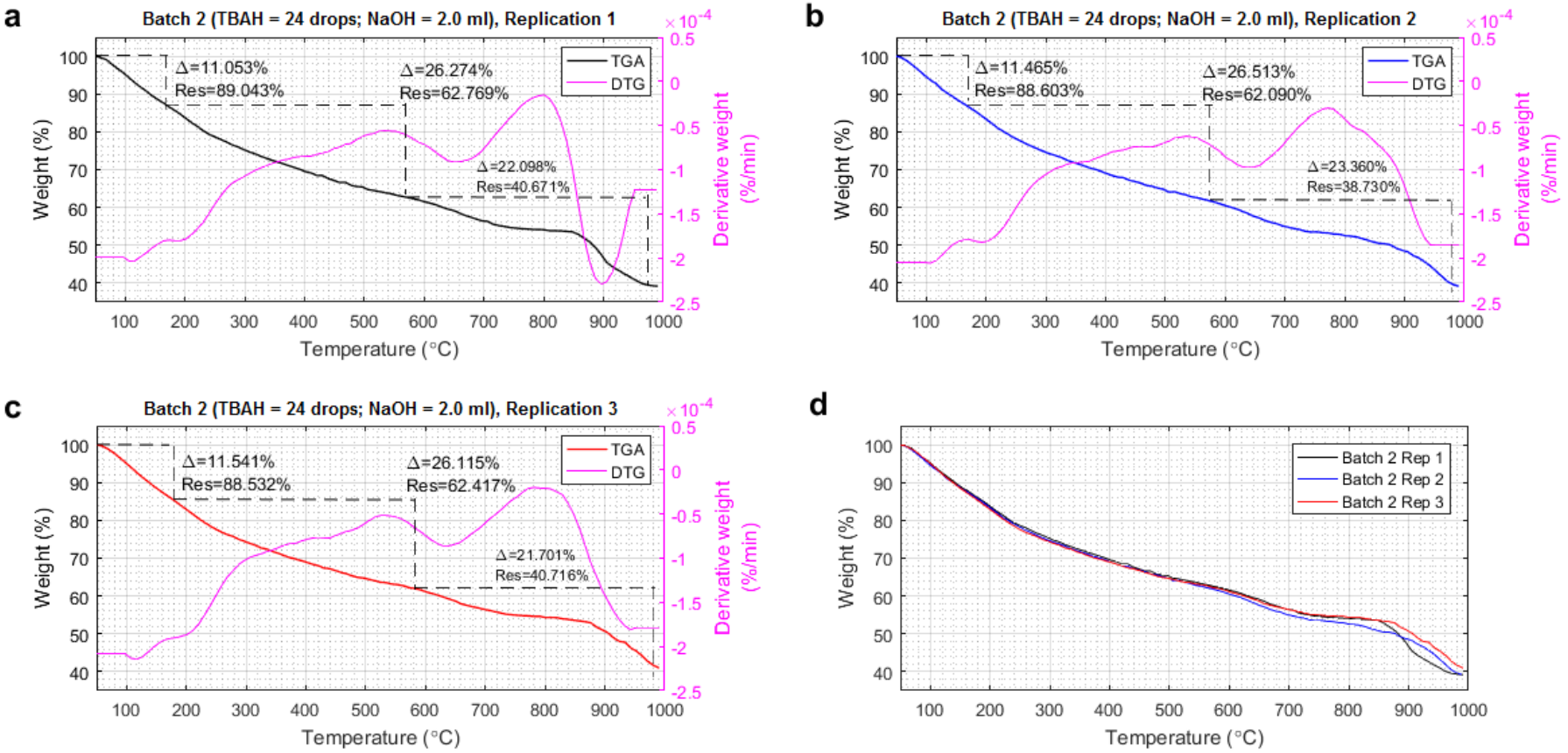

Figure 5-14 Individual (a-c) and superimposed (d) TGA thermograms from Batch 2, Consistency Evaluation Experiment

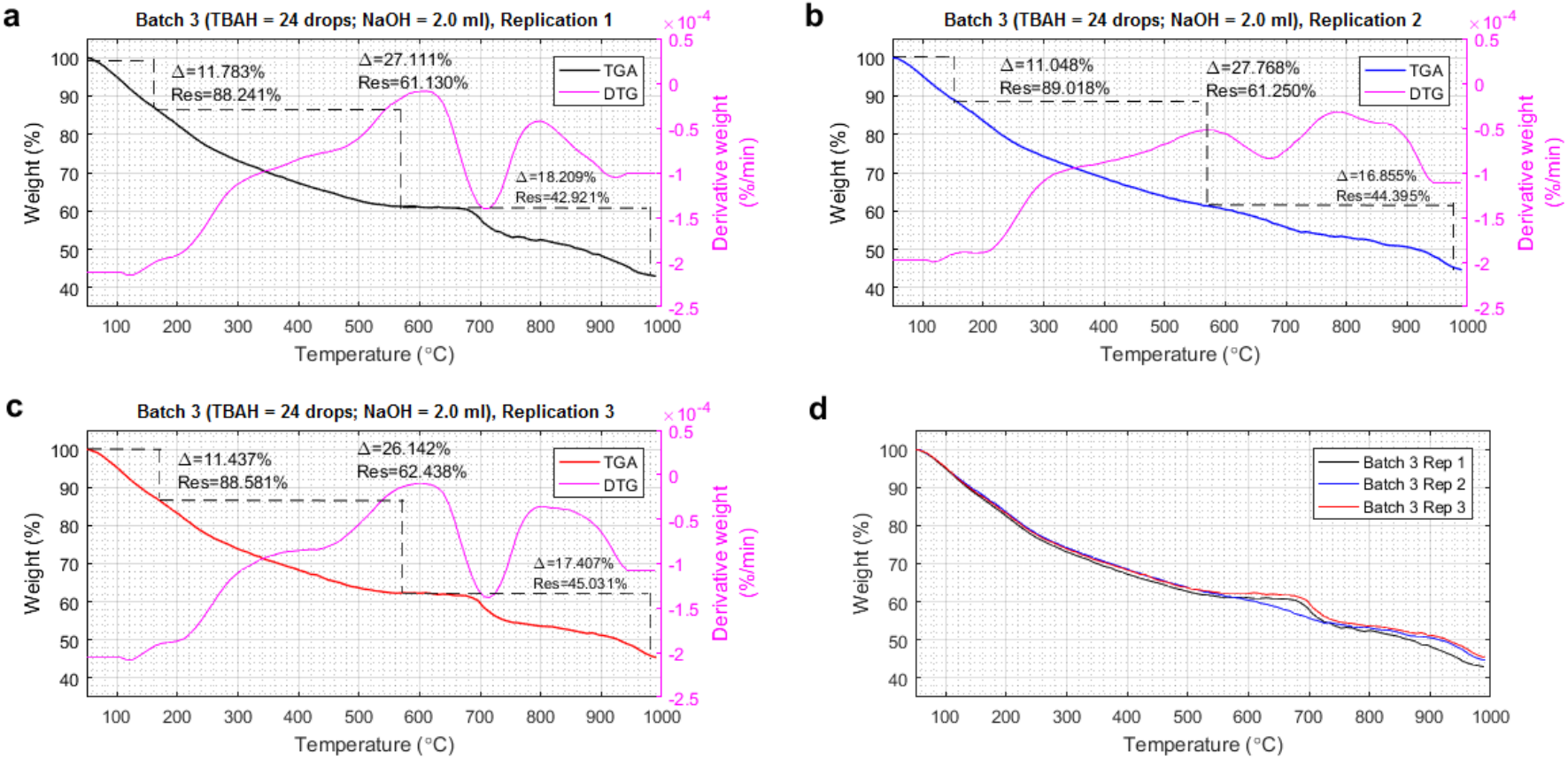

Figure 5-15 Individual (a-c) and superimposed (d) TGA thermograms from Batch 3, Consistency Evaluation Experiment

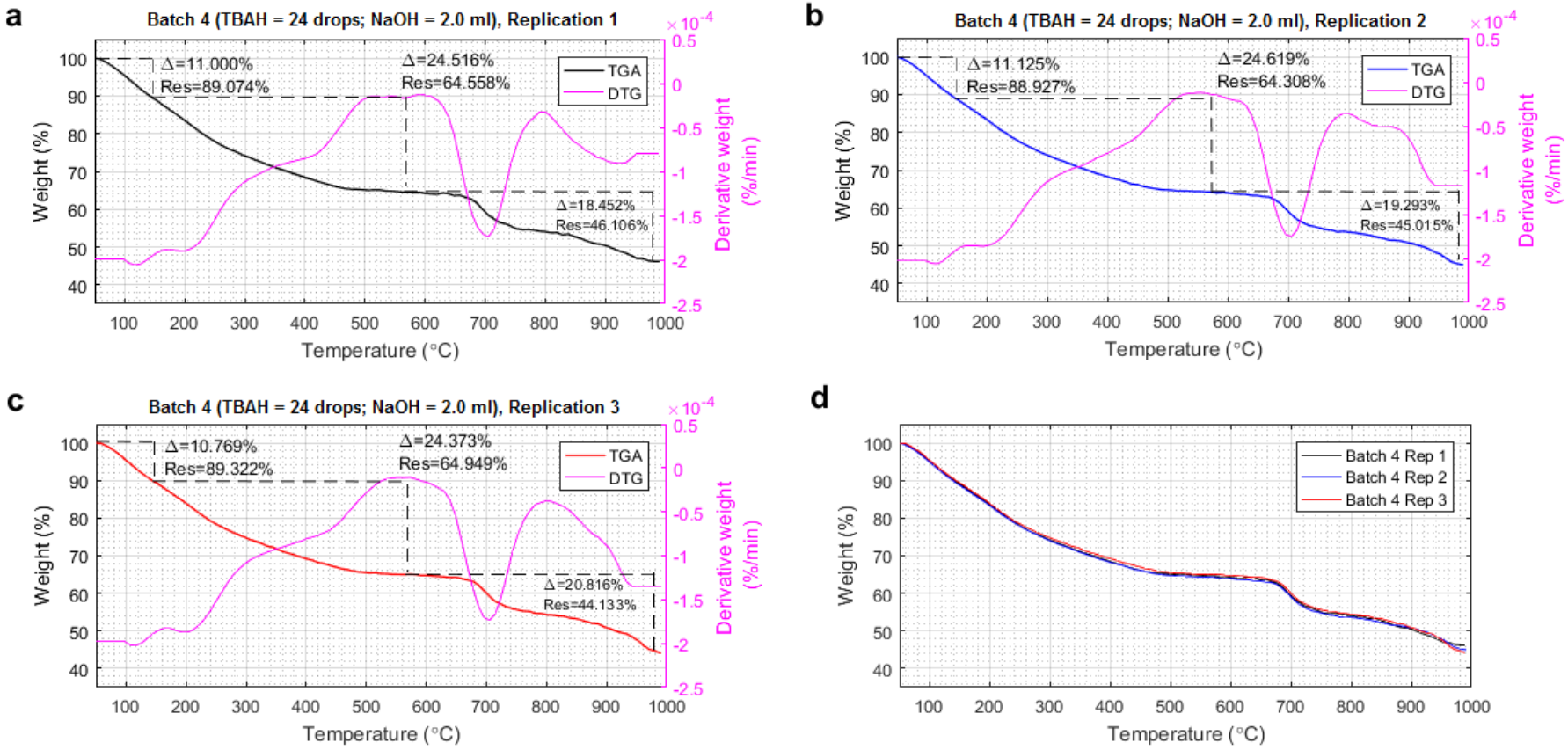

Figure 5-16 Individual (a-c) and superimposed (d) TGA thermograms from Batch 4, Consistency Evaluation Experiment

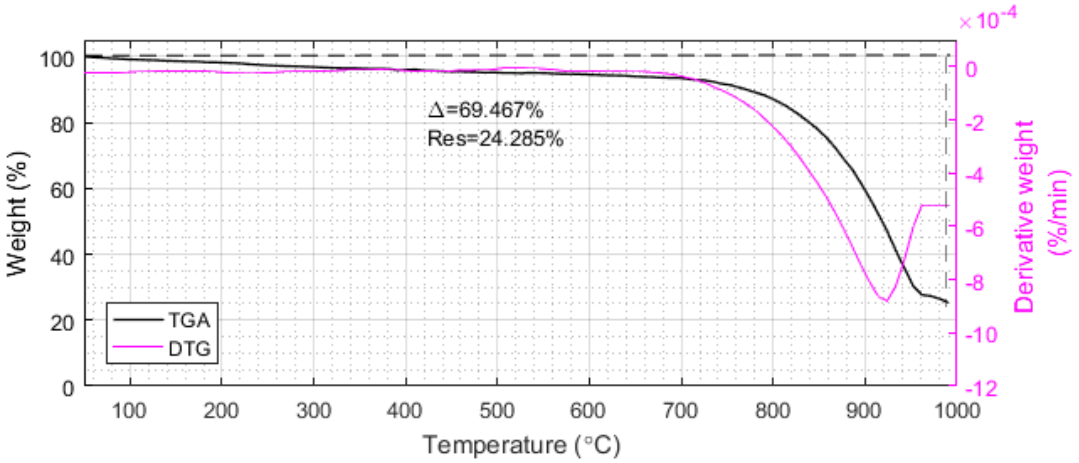

Figure 5-17 TGA thermogram of pristine C_{60}

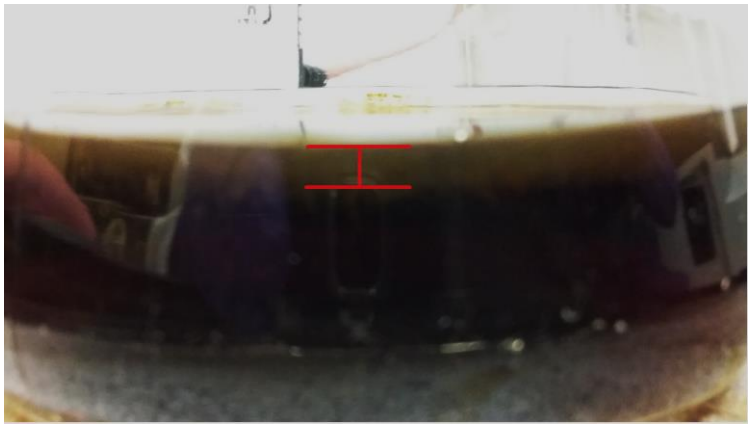

Figure 5-18 A layer of opaque substance observed (indicated in red) on top of product-containing filtrate during product separation steps of the synthesis

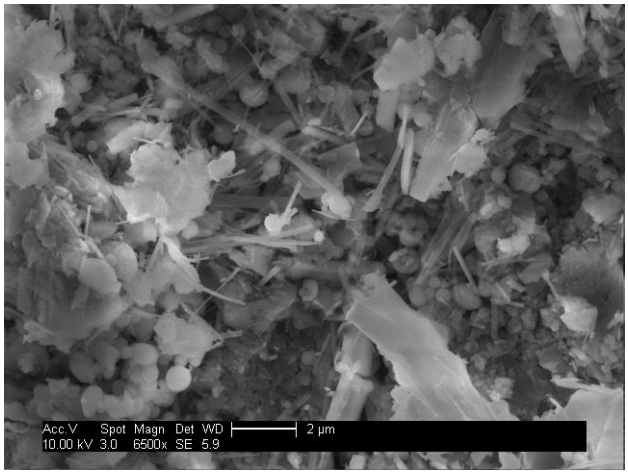

Figure 5-19 SEM micrograph (100kx) of the product revealing sheets of solid existing together with the product (spherical particles). (Image produced by SEM facilities at Cranfield University.)

A sample of silicone grease (5 mg) was subjected to a TGA measurement under the same condition as the products and pristine C_{60}. The obtained TGA thermogram (Figure 5-20) shows a two-step decomposition covering the range of 300-550°C.

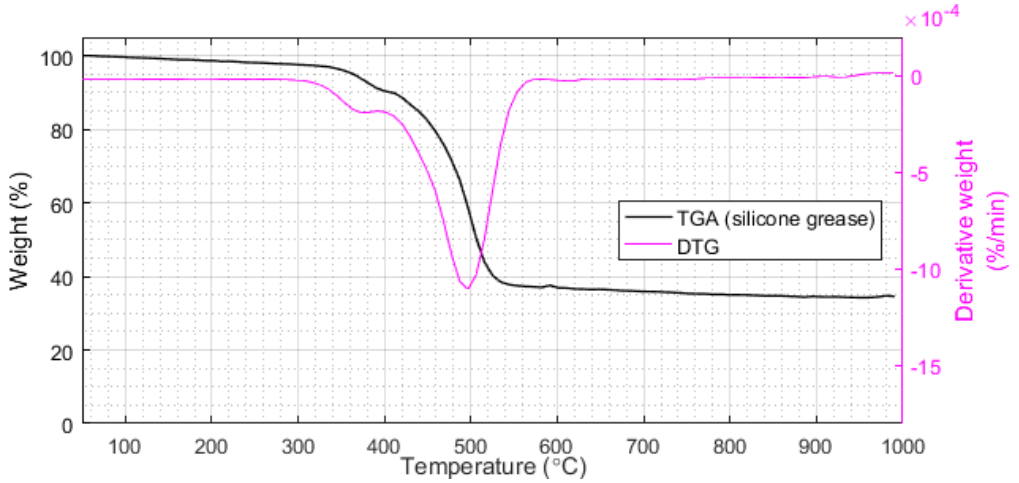

Figure 5-20 TGA thermogram of silicone grease

Plotting the temperature ranges for weight loss above 570°C of sample from the products, and thermal decomposition of pristine C_{60} and silicone grease on the same temperature scale (Figure 5-21) reveals that, although the beginning of

weight loss above 570°C of sample from the products lies between the range for decomposition of silicone grease and C_{60}, almost half of the sample weight loss above 570°C still fall into the temperature range of C_{60} decomposition. Although still not clearly understood, it was proposed that existence of silicone contamination within the products caused this unexpected deviation of decomposition behaviour of the products above 570°C. It could be that silicone grease attached onto the fullerene cage of fullerenol and became more thermally stable, hence decomposing at a higher temperature than usual silicone grease, i.e. above 570°C. As the attached silicone grease decomposed, the contaminated fullerene cages might have also been simultaneously destroyed. Consequently, the detected weight loss of the samples around 570-670°C might be attributed to decomposition of silicone contamination as well as the contaminated fullerene cages. The rest of the cages which were not contaminated could decompose from 670 to 800°C. In some products, such as Product 2, weight loss around 800-950°C was also detected (shown as dotted blue line). This might indicate the existence of survived molecules, i.e. not all fullerenol molecules were contaminated with silicone grease.

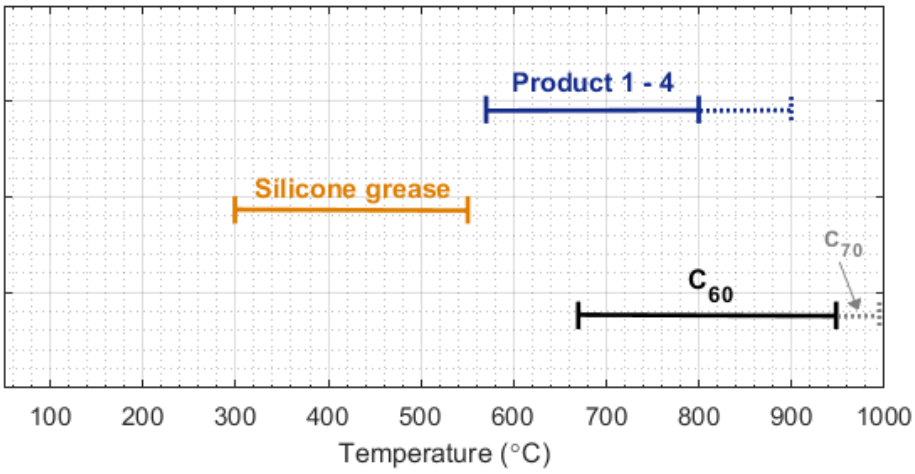

Figure 5-21 Different temperature ranges for weight loss above 570°C of samples from Product 1-4 (blue), thermal decomposition of silicone grease (orange), and thermal decomposition of pristine C_{60} (black)

It is believed that silicone contamination affected thermal decomposition of the products at high temperatures by causing deviation from the normal pattern. Therefore, it is recommended that the use of silicone-based lubricants should be avoided in fullerenol manufacturing of all scales. It would have been ideal to synthesise all products again from the start using a new condenser on the evaporator (without applying silicone grease anywhere). This was not possible due to limited time and budget. Nevertheless, a new condenser set, as well as the complete set of new glassware and other equipment (such as spatulas, storage boxes, and cleaning equipment), were purchased and would be used in the other experiments (i.e. studies on the effects of TBAH, NaOH and reaction time on $n_{(OH)}$, scale-up productions, and investigation on the effect of fullerenol as additives in activated carbon electrodes for supercapacitor).

Despite the discovery of silicone contamination within the products, it was decided to proceed with evaluation of production consistency using these products in order to evaluate consistency under the discovered circumstance (presence of contamination), which could serve as an example of worst-case scenario.

Estimation of level of hydroxylation $n_{(OH)}$ achieved in each synthesis was performed following the procedures described in Section 4.3.2, which relies on the principles for thermogravimetric (TGA) method described in Section 2.4.2 (hereby referred as 'TGA method'). Calculation requires the values of percentage weight loss from 150-570°C (x, corresponding to decomposition of hydroxyl groups), and sample weight remained after 570°C (y, corresponding to degradation of fullerene cage structure). These values were directly determined from each thermogram. Table 5-3 summarises the extracted values of x and y, and calculated $n_{(OH)}$ from each thermogram. Graphical representation of calculated results is presented in Figure 5-22.

It could be seen that values of $n_{(OH)}$ were reasonably close to each other among the three replications within the same batch, but slight variations were observed when the four different batches were compared. The results were further

analysed with the support from statistical analysis using Analysis of Variance (ANOVA) of which results are discussed in the next section.

Table 5-3 Extracted information and analysis of TGA thermograms of all replications

Batch	Replication No.	x	y	$n_{(OH)}$
1	1	27.374	60.467	19.174
1	2	27.483	59.954	19.415
1	3	26.785	59.836	18.959
2	1	26.274	62.769	17.728
2	2	26.513	62.090	18.085
2	3	26.115	62.417	17.720
3	1	27.111	61.130	18.783
3	2	27.768	61.250	19.201
3	3	26.142	62.438	17.733
4	1	24.516	64.558	16.084
4	2	24.619	64.308	16.214
4	3	24.373	64.949	15.894

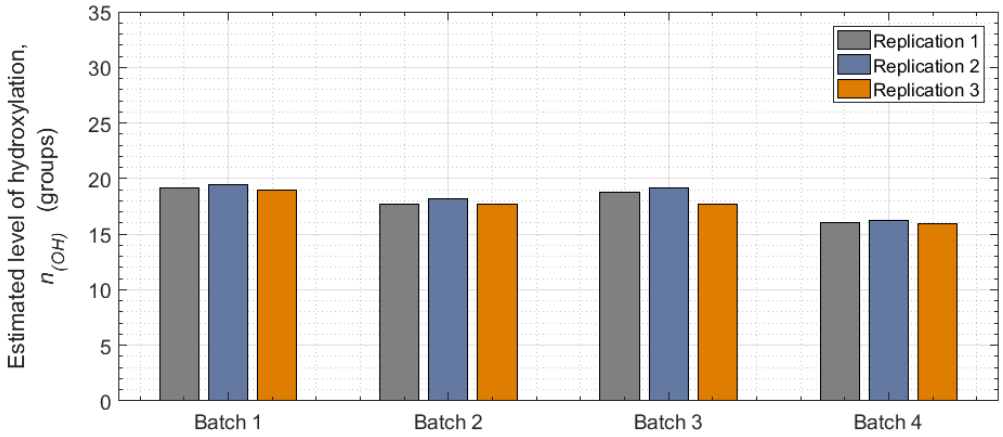

Figure 5-22 Graphical representation of estimated $n_{(OH)}$ values from all individual TGA measurements

5.2.3 Statistical analysis for evaluation of production consistency using One-way ANOVA

Results from the previous section (Figure 5-22) showed that, although calculated values of $n_{(OH)}$ within the same batch might be reasonably close to each other, slight variations were observed when different batches were compared. In practice, it is impossible to always obtain exactly the same results as real-life situations involve numerous factors which naturally can cause error in a system of interest. As a result, the point to consider is whether or not the observed variations are significant; this can be done by statistical analysis using an appropriate statistical test. If the result of the test indicates that there is no significant difference among the information, a value which represents the population can be determined. For this experiment, this would imply that it would be acceptable to treat the average of the involved $n_{(OH)}$ values as the representative of the number of hydroxyl groups per fullerenol molecule for the synthesis route. The synthesis route could then be considered to have an acceptable production consistency at the significance level (α) used in the analysis. On the other hand, if the result indicates that the observed variations are significant, it is inappropriate to conclude such property to a single number, and the route does not offer an acceptable consistency at the significance level being considered.

The goal of this experiment was to evaluate production consistency of the synthesis route in terms of level of hydroxylation achieved ($n_{(OH)}$). The evaluation could be conducted by comparing $n_{(OH)}$ values from samples within the same batch and between batches. Statistical analysis which suits the nature of this evaluation is thus one-way analysis of variance (ANOVA), which is used to verify whether data from different groups of a factor of interest have a common mean (Montgomery, 2009; MathWorks, 2016).

The principle of ANOVA is based on assumptions that sample populations follow a normal distribution and qualify for a completely randomised design (CRD) (Montgomery, 2009). In this regard, collection of data in this experiment was specially designed and strictly followed to ensure that the collected

information was certified for a CRD, extending even to sample preparation for TGA measurements (which was the source of data to be analysed). From each batch, three samples of equal mass (approximately 5 mg) were randomly taken out to be used as TGA samples for the batch, stored in three separate but identical containers. Each of the total of twelve TGA samples (three samples per batch) was assigned with a unique number from 1 to 12. Prior to each TGA measurement, lotto was used as a method to randomly select a sample to run. A number was drawn out without replacing and the sample assigned with that particular number was put into the TGA furnace for a measurement. As a preliminary testing before the actual ANOVA, means and variances of $n_{(OH)}$ for each batch were calculated and shown in Table 5-4.

Table 5-4 Means and variances of estimated $n_{(OH)}$ values from Batch 1-4

Groups	Mean, $\bar{x}$	Variance, S^2
Batch 1	19.182	0.052
Batch 2	17.845	0.043
Batch 3	18.572	0.572
Batch 4	16.064	0.026

Box-and-whisker plots (Figure 5-23) were made to visually present the differences within and between batches. In a box-and-whisker plot, the top of the box represents the 25th percentiles of the sample, and the bottom represents the 75th percentiles. The red horizontal line within the box represents median of the batch. The whiskers are lines extending from the top and bottom of each box to the furthest data on each side within the whisker length (MathWorks, 2016). From Figure 5-23, it can be seen that Batch 1-3 are roughly close to each other. Although Batch 4 appears to be different from the other 3 batches, it does have a smaller variance and skewness of data (judging from locations of medians) compared to Batch 2 and Batch 3.

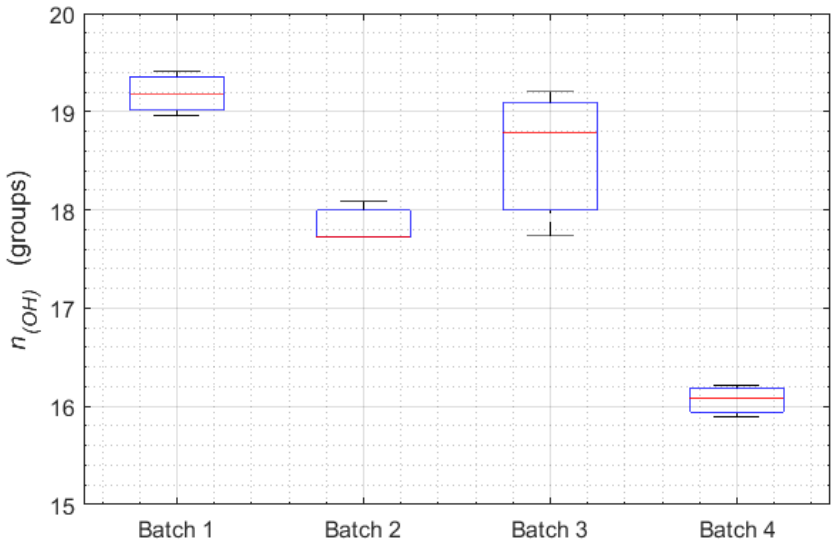

Figure 5-23 Box-and-whisker plots of estimated $n_{(OH)}$ values from Batch 1-4

Upon seeing the results in Table 5-4 and Figure 5-23, laboratory records were consulted to check for any abnormal incidence. It was recorded that, during the synthesis of Batch 4, readings of the precision balance accessible at that time fluctuated rather significantly and it took much longer than usual until the reading was settled for each weighing. This made the condition and origin of Batch 4 different from the others.

From this note, it was proposed that these variations within and between batches might have resulted from silicone contamination and other factors which might affect accuracy of the production, especially reliability and accuracy of measuring instruments. More discussion on this topic is provided in Section 5.6.3. Nevertheless, it should be taken into consideration that the results in Figure 5-23 were not absolute and the plots might have shown less difference and skewness of data had a larger number of data been available (i.e. more batches produced and more replications of TGA measurement conducted per batch). This was not possible due to limited amount of product, available time and budget. This research thus decided to proceed forward with one-way ANOVA based on these collected and available data.

Significance level (α) is an important parameter for statistical analysis as it affects the size of critical region of the collected data, hence criteria for rejecting the null hypothesis. Conventionally, α = 0.05 is specified (Montgomery, 2009). One-way ANOVA was performed on $n_{(OH)}$ values from Table 5-3 to determine test statistics F and the critical value of F (F_{crit}), which were then used for hypothesis testing. The outcome of hypothesis testing determines whether or not the values of $n_{(OH)}$ involved in the analysis are significantly different, thus implies whether an acceptable production consistency in terms of $n_{(OH)}$ is achieved at the specified α.

It had been made aware of the fact from the preliminary testing that inclusion of data from Batch 4 in the analysis might lead to rejection of the null hypothesis. However, variance within Batch 4 itself is rather small and this might be a hint towards variations as a result of external factors. Consequently, the first analysis (referred as 'Analysis 1') was performed on all 12 values of $n_{(OH)}$, including values from Batch 4, to assess the worst situation. Results of the analysis was presented as an ANOVA table, shown in Table 5-5. It is found that the value of F-statistic is much larger than its corresponding F_{crit} (31.542 >> 4.066) and the null hypothesis was therefore rejected, i.e. the sample means were significantly different from each other. Inference could be made that the synthesis route could not achieve an acceptable production consistency in terms of $n_{(OH)}$ at α = 0.05. It was believed that the cause behind this was the issue with reliability of the precision balance during the synthesis of Batch 4 as previously mentioned.

Table 5-5 ANOVA table for Analysis 1 (α = 0.05; data from Batch 1-4)

Source of Variation	SS	df	MS	F	p-value	F_{crit}
Between Groups	16.412	3	5.471	31.542	8.799E-05	4.066
Within Groups	1.388	8	0.173			
Total	17.799	11				

Considering the issue with precision balance during the synthesis of Batch 4, along with Figure 5-23 and the results from Analysis 1, it was decided that information from Batch 4 should not be included in statistical analysis as it was significantly different from others. Consequently, Analysis 2 was performed using one-way ANOVA with α = 0.05 on $n_{(OH)}$ values from only Batch 1-3, results shown in Table 5-6. Here, the value of F was greatly reduced to 6.046 but still slightly larger than F_{crit} (5.143). Although the null hypothesis was rejected again, it was not to the same extent as in Analysis 1. Statistical interpretation of this result was that the sample means were still significantly different from each other. Inference could be made that, although production consistency of the synthesis route in terms of $n_{(OH)}$ improved when only Batch 1-3 are considered, the route still could not achieve an acceptable consistency at α = 0.05.

Table 5-6 ANOVA table for Analysis 2 (α = 0.05; data from Batch 1-3)

Source of Variation	SS	df	MS	F	p-value	F_{crit}
Between Groups	2.692	2	1.346	6.046	0.036	5.143
Within Groups	1.336	6	0.223			
Total	4.027	8				

Without prior knowledge of behaviour or performance of the synthesis route, the original plan was to only use the convention α = 0.05 for statistical analysis of the collected data. Although the null hypothesis was rejected in Analysis 2, the estimated $n_{(OH)}$ values from Batch 1-3 in Table 1 did show a scattering over a narrow range of numbers. It was possible that working condition, equipment condition, and quality of chemicals at the time of conducting this experiment might not be good enough for the selected synthesis route to not reject the null hypothesis at α = 0.05. However, it might be possible that the null hypothesis would not be rejected at a lower α. By doing so, the analysis would be performed at the criteria which was less possible to reject H_0. Analysis 3 was thus performed at a slightly lower α of 0.025 on data from Batch 1-3, results

shown in Table 5-7. This time, F-statistics was still 6.046 but now smaller than F_{crit} (7.260). The test failed to reject the null hypothesis. Statistical interpretation of this result was that there was no significant difference among the sample means. It also meant that it was acceptable to treat the average of the collected values as a representative of the samples. The average value (to the nearest whole number) was determined to be 19. From statistical analyses, it could be inferred that, based on available equipment and working conditions, the selected synthesis route achieved a consistent production (in terms of level of hydroxylation) at significance level of 0.025, producing fullerenol with 19 hydroxyl groups per molecule.

Table 5-7 ANOVA table for Analysis 3 (α = 0.025; data from Batch 1-3)

Source of Variation	SS	df	MS	F	p-value	F_{crit}
Between Groups	2.692	2	1.346	6.046	0.036	7.260
Within Groups	1.336	6	0.223			
Total	4.027	8				

Table 5-8 shows a summary of results from all analyses and hypothesis testing in this experiment. In Analysis 1, when Batch.4 which contained some error was still included, rejection of null hypothesis flagged the fact that there was something wrong during the process. By consulting the laboratory records, the possible source of error was found. After eliminating the error-containing information, Analysis 2 was performed and, although still rejecting H_0, a less extreme result was obtained. Analyses 1 and 2 exhibited the potential power of statistical analysis as a tool to detect error in a process, providing that systematic and well-designed laboratory record was available.

Table 5-8 Summary of Analysis 1-3 including key results from ANOVA tables and testing outcomes

	Source of data	α	p-value	F	F_{crit}	Outcomes
Analysis 1	Batch 1-4	0.05	8.799E-05	31.542	4.066	Reject H_0
Analysis 2	Batch 1-3	0.05	0.036	6.046	5.143	Reject H_0
Analysis 3	Batch 1-3	0.025	0.036	6.046	7.260	Fails to reject H_0

Another potential power of statistical analysis can be realised by considering Analysis 2 and 3. The significance level at which the test fails to reject the null hypothesis can be used to imply reliability of the synthesis route. A synthesis route which fails to reject the null hypothesis at a level of significance lower than 0.05 is less reliable than a route which fails to reject the null hypothesis at a significance level greater than or equal to 0.05. It was suggested that further improvement to the route which fails to reject the null hypothesis at a significance level lower than 0.05 (such as using synthesis equipment which offer higher precision, and minimising cross-contamination from the working environment) could raise consistency of production.

5.3 Effect of TBAH on level of hydroxylation in TBAH-NaOH route for fullerenol synthesis

With production consistency of the route evaluated, the research now entered the main parts of developing the aimed synthesis protocols – studies of the effects of three selected process parameters on level of hydroxylation ($n_{(OH)}$). This experiment focused on the response of achieved $n_{(OH)}$ on different amount of phase-transfer catalyst (TBAH) added into the reaction. For convenience, this experiment is hereby referred as 'TBAH Experiment'.

It should be noted that, as a result of major organisation-level restructuring within the university, all syntheses from this point onwards were conducted in another laboratory which was different to the one where the syntheses for Consistency Evaluation Experiment were conducted.

In response to silicone contamination identified in the products from the Consistency Evaluation Experiment (Section 5.2.2), all apparatuses that had possibilities of being contaminated with silicone grease were permanently removed from this research, and replaced with clean and new items. This included the entire condenser set of the rotary evaporator, all glassware (e.g. beakers, flasks, funnels, measuring cylinders), cleaning brushes, tubing, spatulas, and storage containers of these apparatuses. No silicone grease or any other lubricant was applied to the joint at vent point of the condenser set at all. This was to prevent complications from any possible product contamination from lubricants.

Following the design of experiment in Section 4.4.1, syntheses using different amount of TBAH in the reaction (3, 6, 12, 24, 48, 96 and 192 drops) were conducted. The products, labelled as Product 1 to Product 7 respectively, were obtained as dark brown powder or flake (Figure 5-24). The flake form was suggested to result from pressurised packing of filter cake (fine precipitates) during the final vacuum precipitation during the synthesis.

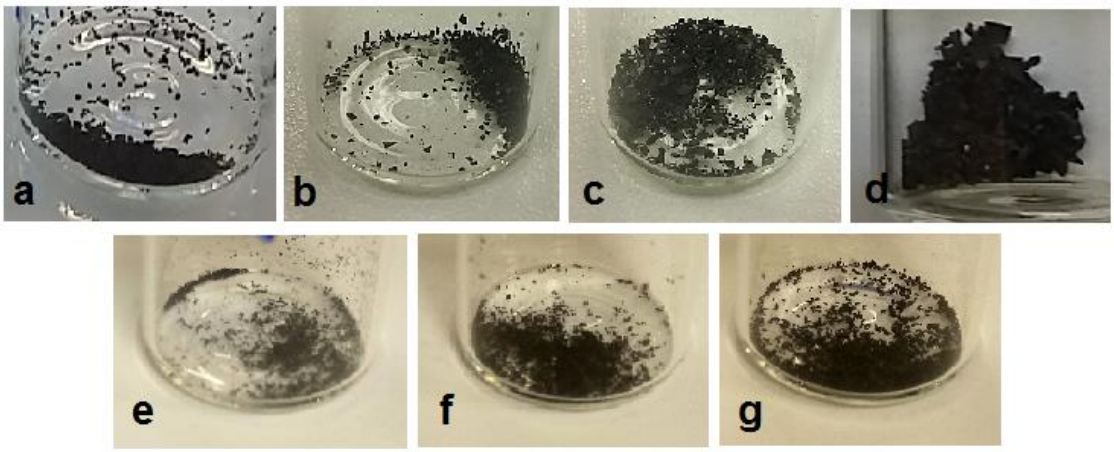

Figure 5-24 Product 1-7 (a-g respectively) obtained as dark brown powder/flakek brown powder/flake

Since silicone grease had been removed from the system, the opaque layer did not appear anymore, and observations from all syntheses were generally in agreement with description in Consistency Evaluation Experiment (Section 5.2.1). Nevertheless, all syntheses commonly had an observation that was never seen before. During product separation steps, a trace of white solid was observed on the glassware's wall where the product-containing liquid flowed (Figure 5-25). The trace could be washed by water. This observation would be very critical to the analysis of characterisation results.

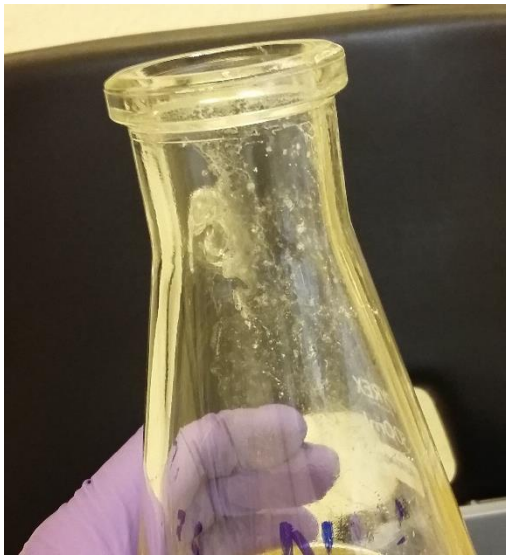

Figure 5-25 A trace of white solid on the flask wall left behind by the product-containing liquid during product separation steps

5.3.1 Analysis of characterisation results

Infrared spectra of Product 1-7 are shown in Figure 5-26 and Figure 5-27. The four characteristic absorptions of fullerenol were observed in all products (absorptions centred around 3430, 1600, 1370 and 1080 cm^{-1} corresponding to ν O–H, ν C=C, δ C–O–H, and ν C–O respectively). Additional absorptions were also observed, i.e. broad shoulder covering 3000-2000 cm^{-1} and a small peak around 1770 cm^{-1}. An exception is in Figure 5-26d where the absorption around 1440 cm^{-1} is even stronger than the absorption of ν O–H and a weak peak around 880 cm^{-1} is present. Analysing and assigning these additional absorptions required supporting information from SEM, EDX, as well as observations during the synthesis.

Figure 5-28 shows SEM micrographs of samples from each product taken at low magnifications. Figure 5-28a and Figure 5-28d reveal clear existence of needle-like objects on the product surface, while other micrographs show some pattern of solids formed on the surface. EDX was also performed on the samples (results shown in Table 5-9). It was found that, in addition to the expected detection of carbon (C) and oxygen (O), each product also contained a significant percentage of sodium (Na).

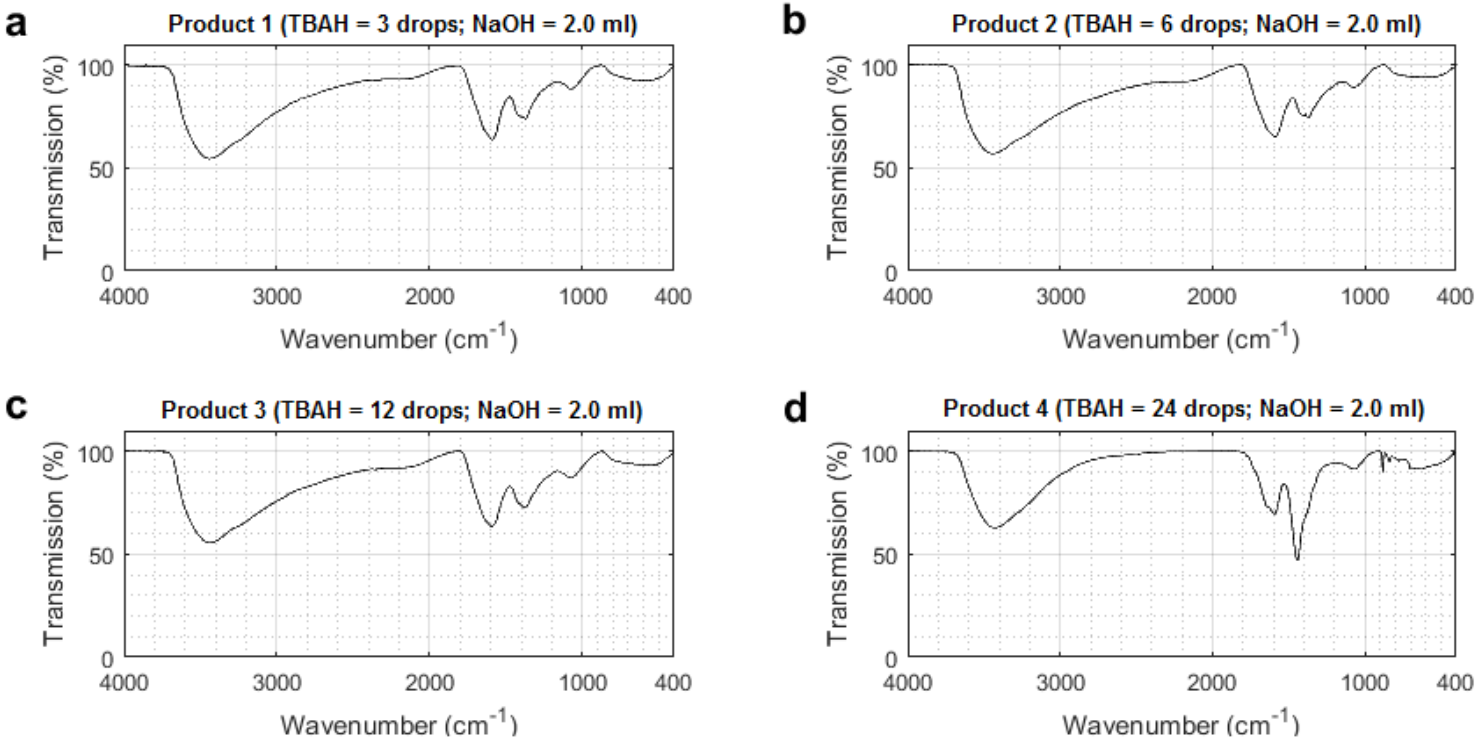

Figure 5-26 Infrared spectra of Product 1-4 (using different amounts of TBAH during syntheses) from TBAH Experiment

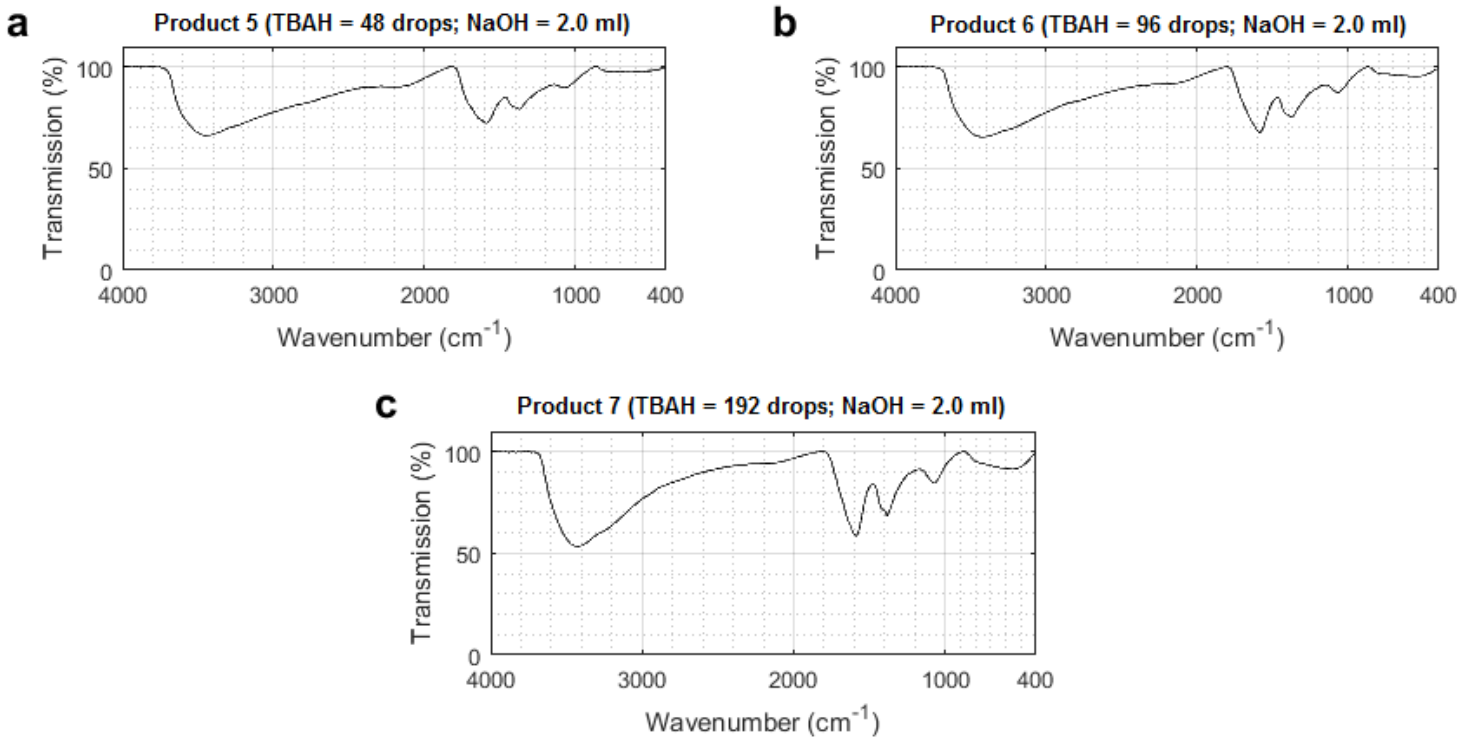

Figure 5-27 Infrared spectra of Product 5-7 (using different amounts of TBAH during syntheses) from TBAH Experiment

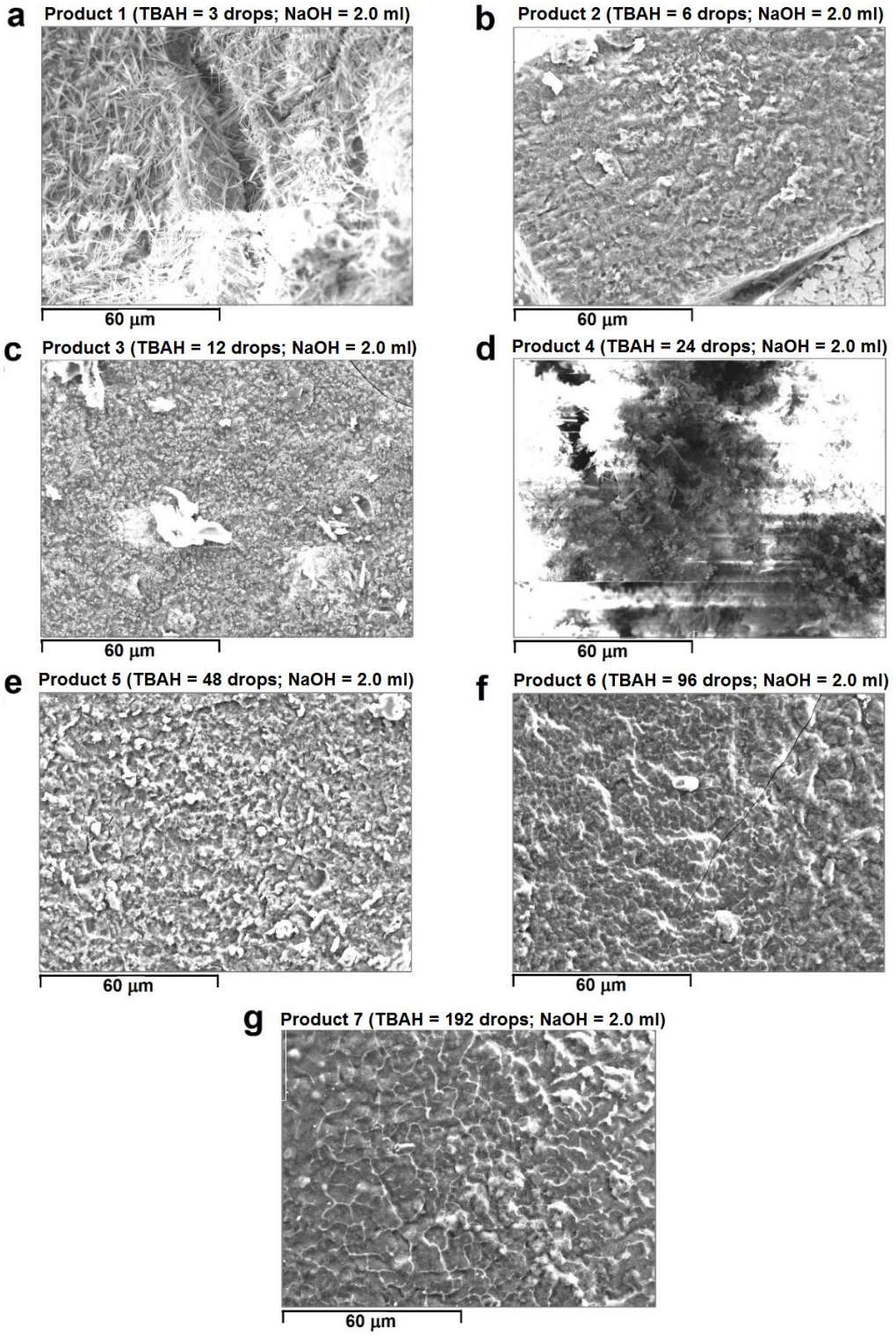

Figure 5-28 SEM micrographs of products from TBAH Experiment showing existence of needle-like objects (a and d), and patterns formed on the surface of product powder (b, c, e, f, and g). (Images produced by SEM/EDX facilities at National Physical Laboratory, London)

Table 5-9 EDX results of Product 1-7 showing major elements (%wt)

Product	TBAH added (drops)	% C	% O	% Na
1	3	44.47	38.62	15.34
2	6	43.61	40.25	14.70
3	12	43.68	40.33	15.29
4	24	37.49	42.64	19.15
5	48	44.82	38.53	15.33
6	96	49.48	36.78	13.02
7	192	50.94	35.55	12.88

The following points could be drawn from a combination of synthesis observation, SEM micrographs and EDX results:

- A certain water-soluble substance was present in the product-containing liquid.
- The substance in dry form was a white solid.
- Needle-like crystals (or pattern of possibly white substance) were formed on the product surface.
- Na was detected in each product, in addition to C and O.

Altogether, these points suggested for the existence of sodium carbonate (Na_2CO_3) in the product. Nevertheless, sodium carbonate was not incorporated as parts of fullerenol structure but only co-existing within the same space, as revealed in SEM micrographs. Formation of sodium carbonate was thought to occur as a result of a chemical reaction between carbon dioxide (which could come from the atmosphere or other possible sources, such as experiments of other projects sharing the same fume cupboard) and sodium hydroxide:

$$CO_2 + 2NaOH \longrightarrow Na_2CO_3 + H_2O \qquad \textbf{(5-5)}$$

When all the required reagents were added, the majority of liquid in the reaction mixture was toluene. There was only a small volume of concentrated sodium hydroxide solution in the mixture. Based on different densities, sodium

hydroxide solution sank to the bottom of the reaction flask. At this stage, it was suggested that toluene had protected sodium hydroxide solution from being exposed to ambient carbon dioxide, hence no formation of sodium carbonate yet. It was suggested that the majority of sodium carbonate present in each product was formed during product separation steps from the moment toluene was removed from the product-containing mixture until the dried product powder was collected at the end of the process. Infrared spectrum of sodium carbonate is provided in Figure 5-29, showing a strong absorption around 1450 cm^{-1}, a medium absorption around 880 cm^{-1}, and other weak absorptions around 3000, 2500, 2400, 1780, 1000 and 700 cm^{-1}.

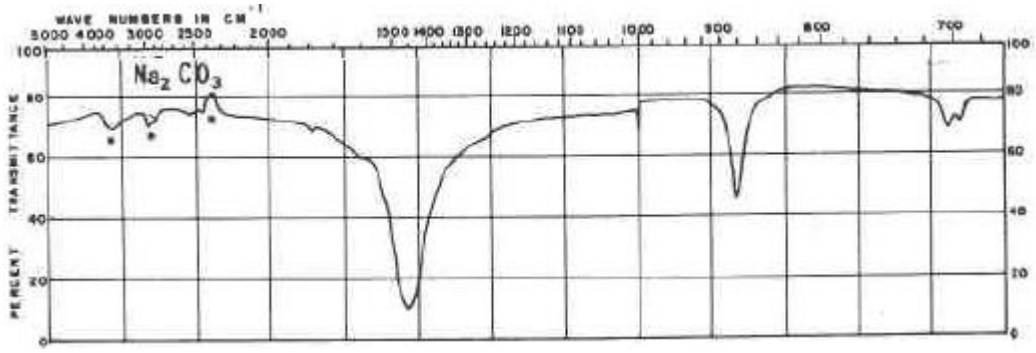

Figure 5-29 Infrared spectrum of sodium carbonate (Huang and Kerr, 1960)

It was now possible to assign absorptions additional to fullerenol characteristics in the infrared spectra of the products (Figure 5-26 and Figure 5-27). The broad shoulder extending from around 3000 to 2000 cm^{-1}, as well as the small peak around 1770 cm^{-1}, were due to the presence of sodium carbonate in the product.

Product 4 was synthesised using 24 drops of TBAH for the reaction, which was the same amount used in all syntheses in Consistency Evaluation Experiment. Although fullerenol characteristic absorptions were observed, the spectrum of this product (Figure 5-26d) showed some variations from those in Figure 5-9. Usually, the absorption around 1370 cm^{-1} of fullerenol characteristics was of medium strength. However, the spectrum in Figure 5-26d shows a strong absorption around 1440 cm^{-1} with a shoulder around 1380 cm^{-1}. This strong absorption, almost covering up δC–O–H peak, also arose from the existence of

sodium carbonate, possibly existing at a higher amount compared to other products. In addition to this, a weak but sharp absorption around 880 cm^{-1} was observed in Figure 5-26d. Two possibilities were related to this absorption: a contribution from sodium carbonate, or an existence of epoxide functional groups. Both chemical species give a weak but sharp absorption around 880 cm^{-1} (Huang and Kerr, 1960; Creegan et al., 1992; Wohlers et al., 1996; Pavia et al., 2001; Evtushenko et al., 2003; Gonzalez et al., 2012; Wade, 2014). To identify whether this was one of the two, or both, TGA thermograms (Figure 5-30 and Figure 5-31) needed to be consulted.

Under normal conditions (no contamination), fullerenol shows 3 main steps (weight losses) in the thermogram: loss of physically bound water molecules (up to 200°C), loss of hydroxyl groups (150-570°C), and degradation of fullerene structure (above 570°C). Most of the thermograms in Figure 5-30 and Figure 5-31 resemble the normal thermogram of fullerenol. However, Figure 5-30d shows a different behaviour. After the usual loss of physically bound water molecule, there is a large weight loss with an onset temperature around 380°C (inflection point around 400°C). Weight loss above 570°C did not give a clear step. The onset temperature of 380°C matches with thermal degradation of fullerene epoxide (Chibante and Heymann, 1993). Combining these facts with the absorption around 880 cm^{-1} from the infrared spectra of Product 4, it was suggested that epoxide groups were also present in the product, possibly in the form of fullerene epoxide (the C_{60} cage only contains epoxide groups) or as fullerenol with epoxide groups on the C_{60} cage in addition to the desired hydroxyl groups. The existence of epoxide groups within the product might resulted from a chemical reaction between C_{60} and ozone present in the atmosphere in the working environment. The resulting fullerene epoxide could have a formula of $C_{60}O$, $C_{60}O_2$, or $C_{60}O_3$, although the latter two would be in a relatively small proportion hence omitted from analysis (Heymann and Chibante, 1993a). To solve the problem regarding which of these possibilities were present in the product structure, more characterisation data, such as XPS, was required.

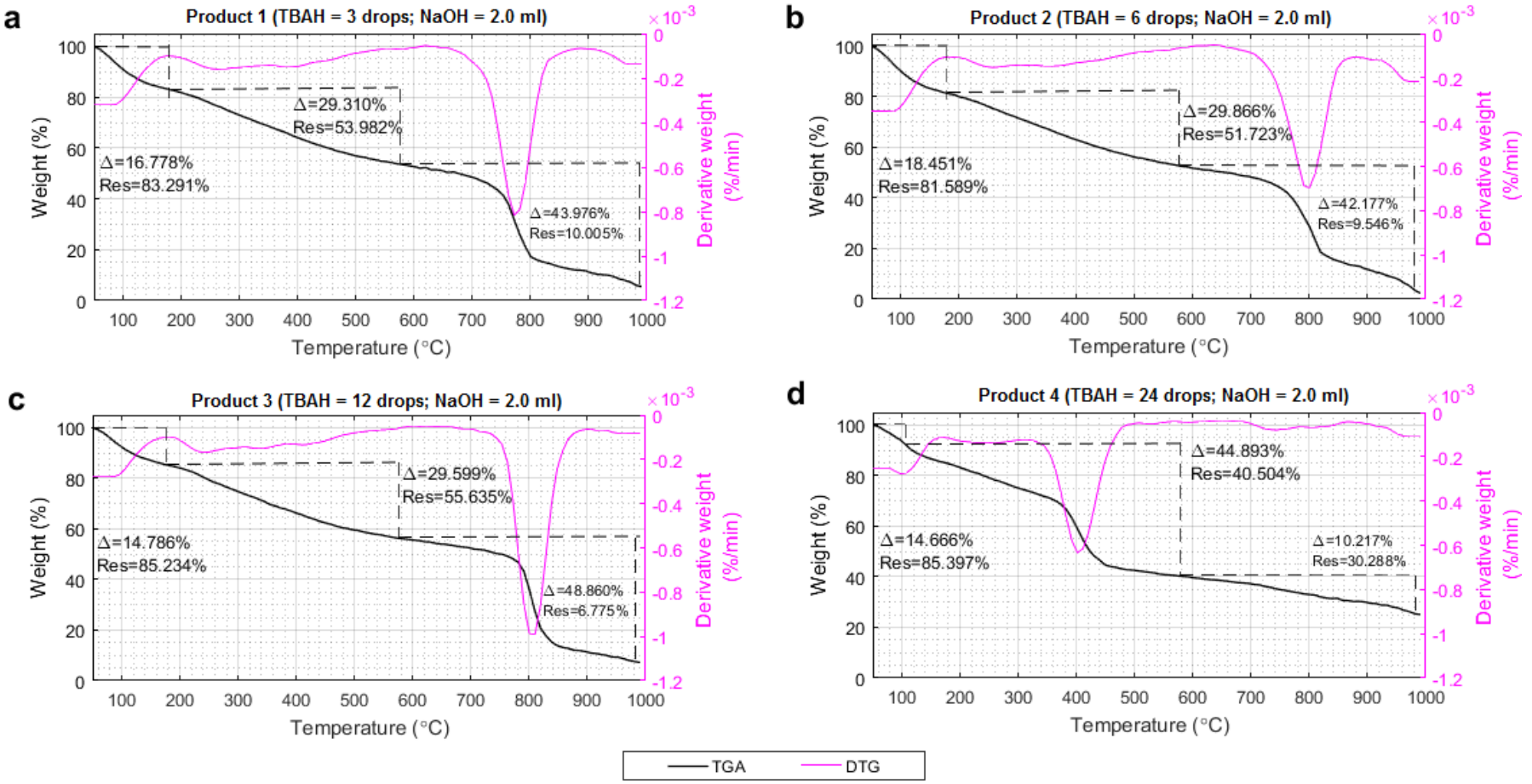

Figure 5-30 TGA thermograms of Product 1-4 (using different amounts of TBAH during syntheses) from TBAH Experiment

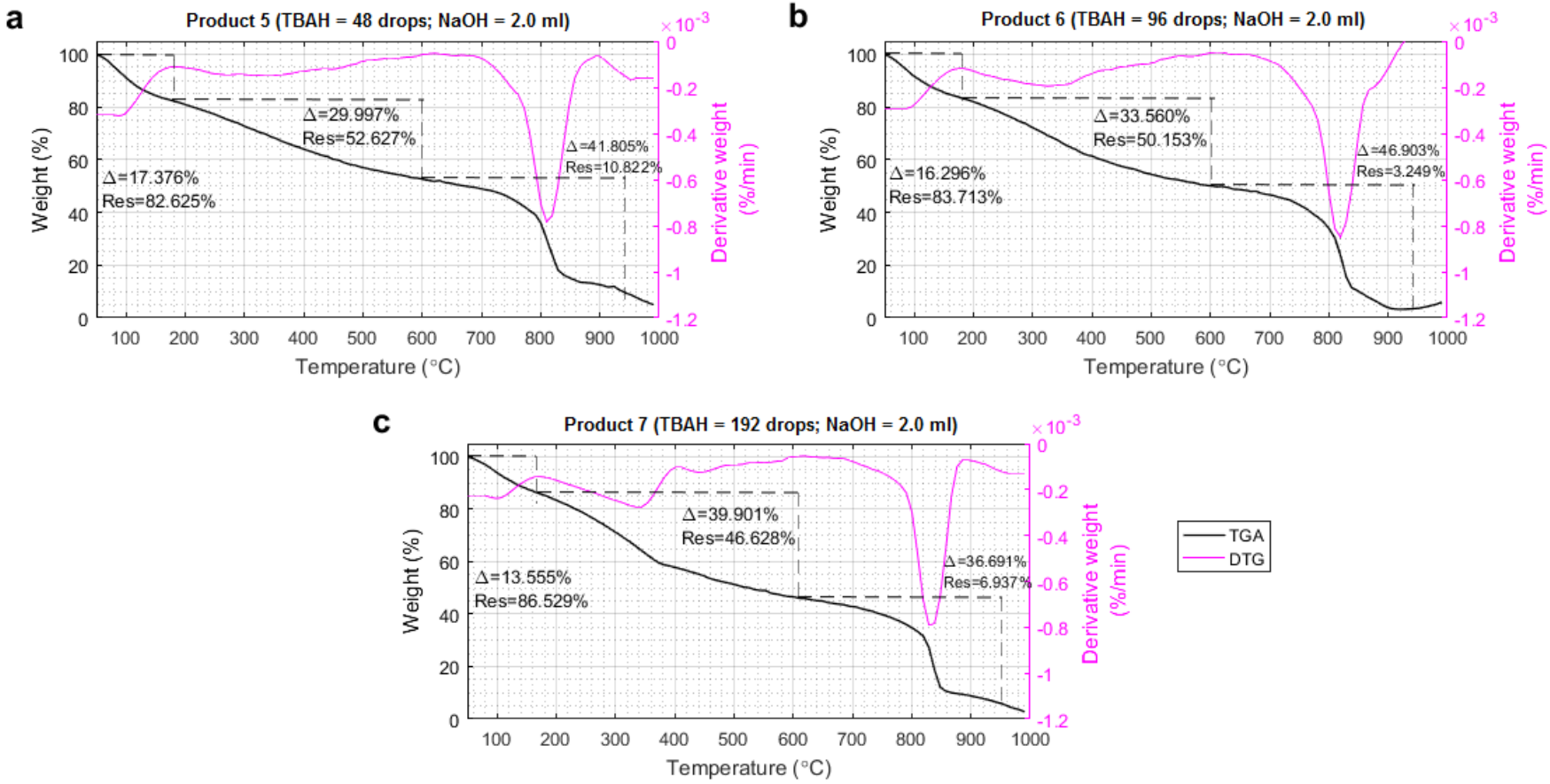

Figure 5-31 TGA thermograms of Product 5-7 (using different amounts of TBAH during syntheses) from TBAH Experiment

Unfortunately, the research could not access XPS due to limited budget. More discussion on the presence of epoxide groups is given in Section 5.6.6.

For particle size characterisation, DLS results of Product 1-7 are shown in Figure 5-32 and Figure 5-33. The majority of detected particles in Product 1, 2, 3, 6 and 7 were in the range of 30-200 nm in diameter. However, the majority of detected particle diameters in Product 4 and 5 were generally between 2-20 nm.

It would have been ideal if SEM micrographs at high magnification could be obtained for each product to be used in conjunction with DLS results for particle size characterisation. However, it was not possible due to several circumstances and limitations on available time and budget, leading to very limited SEM/EDX services affordable. Only one high-magnification SEM micrograph could be obtained for this experiment (Figure 5-34) and was taken from Product 7. Figure 5-34 shows a large number of small spherical particles with the majority having diameters around 45 and 70 nm. Particles with diameter around 90-100 nm were also observed. This is in agreement with DLS results of Product 7 in Figure 5-33c. It was assumed that, had SEM micrographs of other products been obtained, the sizes shown would have been in agreement with their associated DLS results as well.

From the analysis of characterisation results, it can be concluded that fullerenol were successfully synthesised from each synthesis. However, the isolated product also contained sodium carbonate together with fullerenol particles. There was also evidence of epoxide groups present in one product (Product 4) and it was assumed that the form of fullerene epoxides present was all $C_{60}O$.

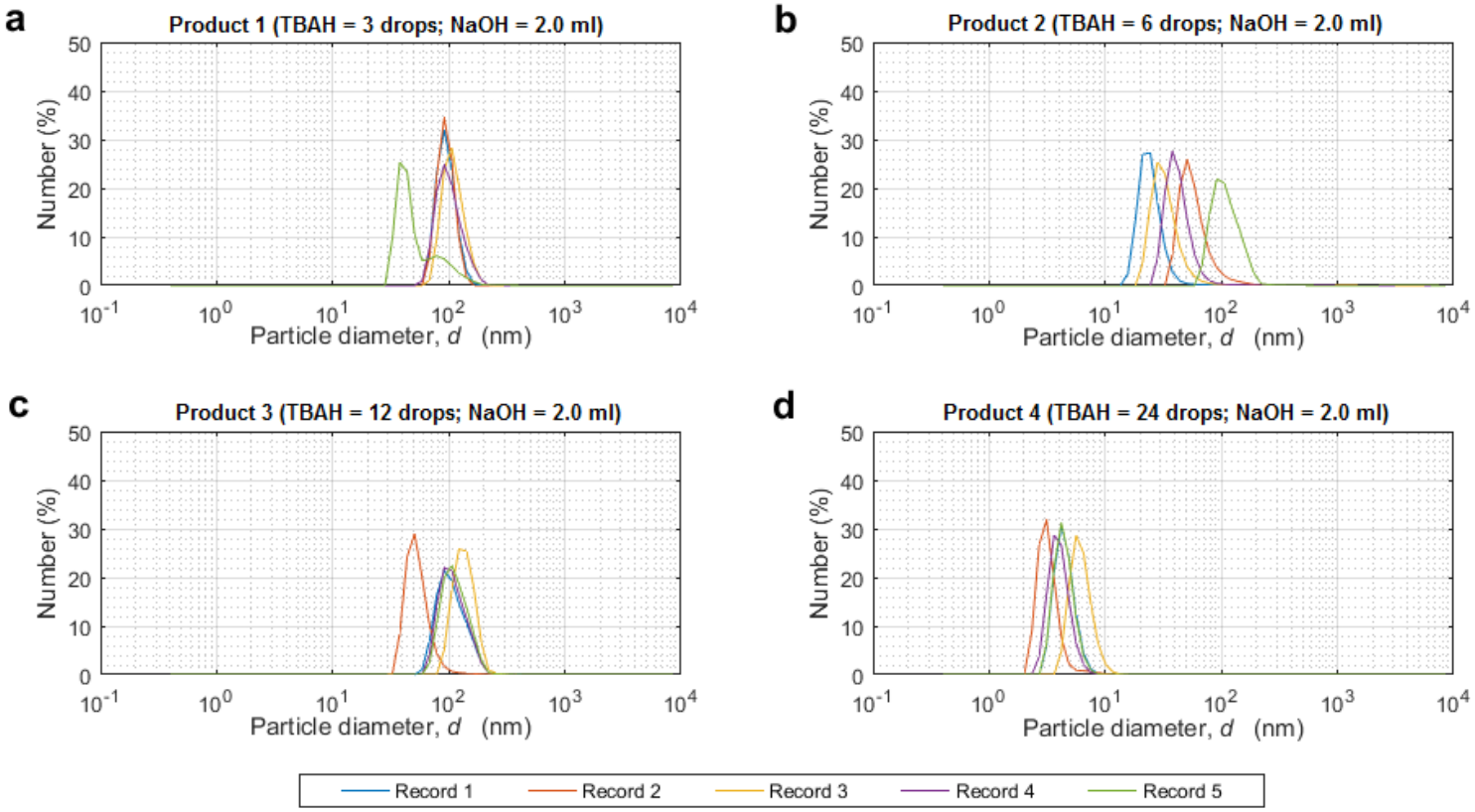

Figure 5-32 DLS results of Product 1-4 (using different amounts of TBAH during syntheses) from TBAH Experiment

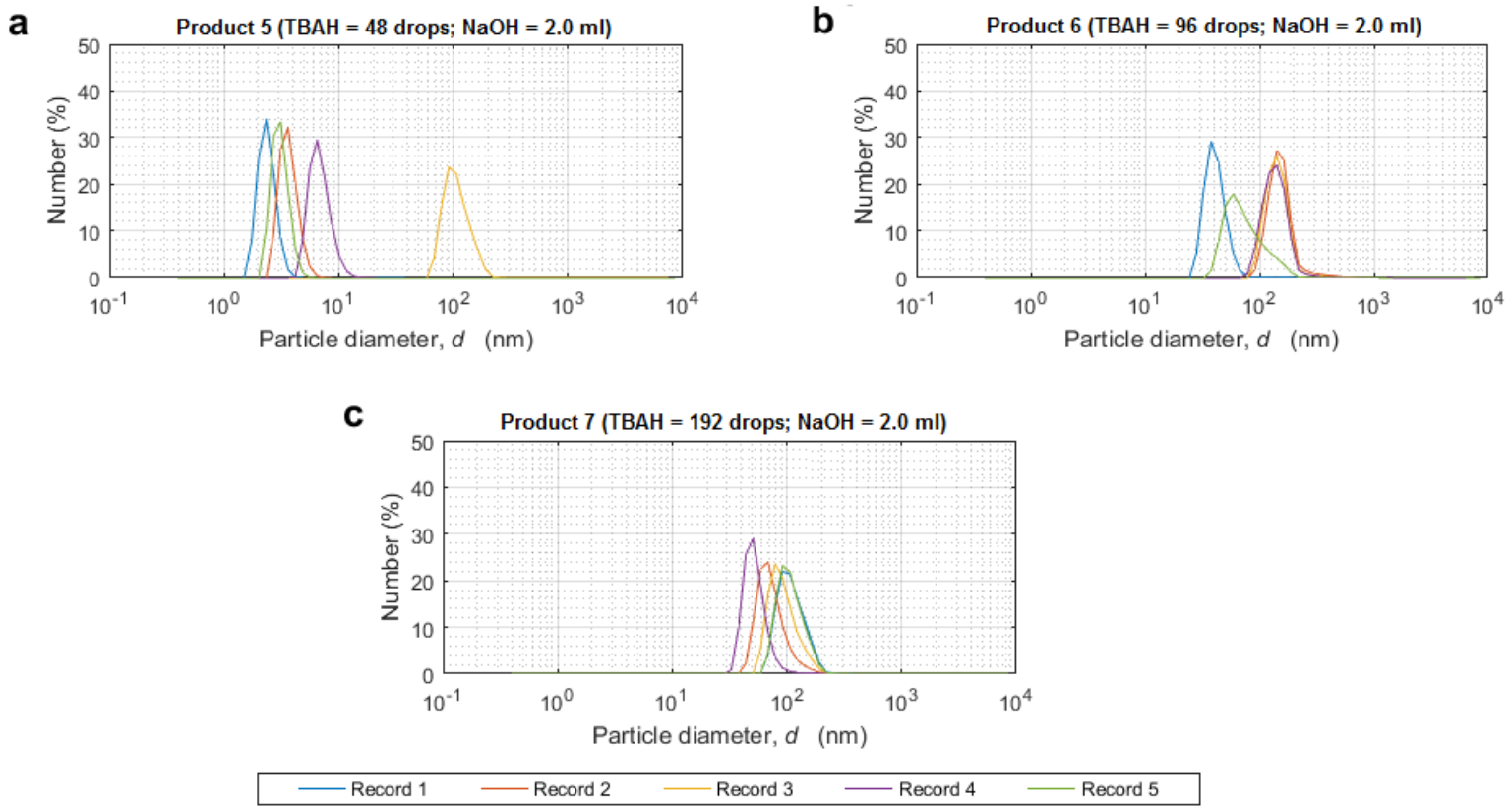

Figure 5-33 DLS results of Product 5-7 (using different amounts of TBAH during syntheses) from TBAH Experiment

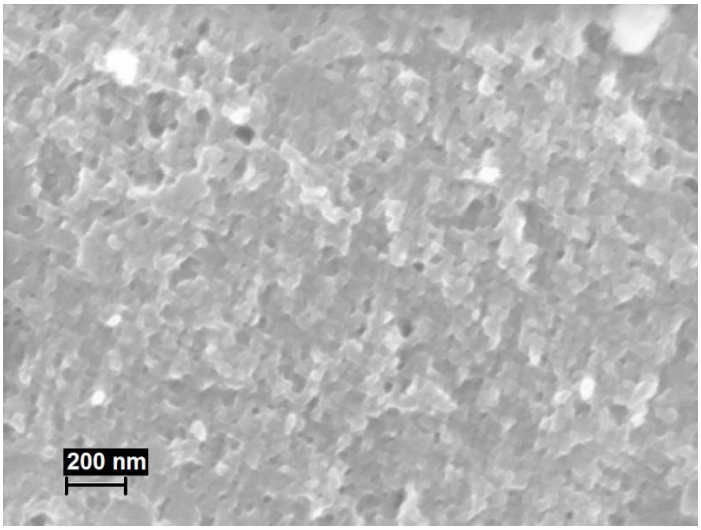

Figure 5-34 SEM micrograph of Product 7 (TBAH = 192 drops; NaOH = 2.0 ml) at 160kx (Image produced by SEM/EDX facilities at National Physical Laboratory, London)

5.3.2 Estimation of level of hydroxylation and development of systematic calculations for the estimation using TGA and EDX (TGA-EDX method)

Using 'TGA method' (principles and procedures described in Section 2.4.2 and 4.1.2) $n_{(OH)}$ of each product was estimated. TGA thermograms in Figure 5-30 and Figure 5-31 were used to extract values of weight loss associated with hydroxyl groups (x) and the remaining sample weight above 570°C (y), which are required to calculate $n_{(OH)}$ for each product. Extracted TGA information and $n_{(OH)}$ of each product are summarised in Table 5-10. Values of $n_{(OH)}$ were plotted against their corresponding amount of TBAH added for the reaction during synthesis, referred as '$n_{(OH)}$-TBAH plot', and shown in Figure 5-35.

Table 5-10 Estimation of $n_{(OH)}$ for Product 1-7 using 'TGA method'

Product	TBAH added for reaction (drops)	x	y	$n_{(OH)}$
1	3	29.310	53.982	23
2	6	29.866	51.723	25
3	12	29.599	55.635	23
4	24	44.893	40.504	47
5	48	29.997	52.627	25
6	96	33.560	50.153	29
7	192	39.901	46.628	37

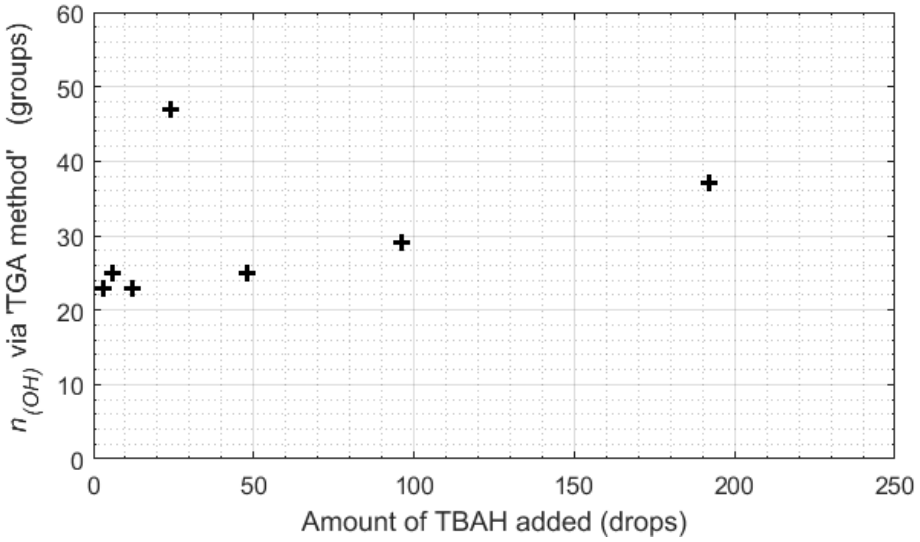

Figure 5-35 $n_{(OH)}$-TBAH plot of $n_{(OH)}$ (determined by 'TGA method') against the amount of TBAH added for the reaction, showing a non-linear relationship

From Table 5-10, $n_{(OH)}$ of Product 4 (TBAH = 24 drops) were unusually higher than those of the products in Consistency Evaluation Experiment. This was because, according to 'TGA method', x was always extracted from the thermogram as weight loss which occurred approximately between 150°C and 570°C (Goswami et al., 2004). This method is suitable for fullerenol without contaminants that could interfere with weight loss in this temperature range. However, Product 4 did not belong to this category since its thermogram shows

an unusually big step in this temperature range. This implied that, in addition to hydroxyl groups, there was some other unexpected substance that contributed to the recorded weight loss in this temperature range. It was suggested that this extra weight loss was associated with fullerene epoxide as the onset temperature for this weight loss in Figure 5-30d coincided with thermal decomposition behaviour of the substance (Heymann and Chibante, 1993a; Heymann and Chibante, 1993b). Using 'TGA method' with Product 4 thus yielded an unusually large value of $n_{(OH)}$, which did not truly reflect the actual property of the product. Therefore, TGA method was no longer suitable for estimation of $n_{(OH)}$ for these products.

Literature review (Section 2.4.2) was consulted in search of a method which could cope with this problem, and the TGA-Elemental analysis method reported by Kokubo and colleagues (2008; 2011) was seen as the most promising. This problem was different to the problem from silicone contamination in Consistency Evaluation Experiment. Sodium carbonate has a definite formula, i.e. Na_2CO_3, and the principles and calculations of elemental analysis can be applied to determine how much of the substance is present per molecule of the desired product. On the contrary, silicone grease is a polymer and it is therefore difficult to specify information regarding its molecular structure or formula for such calculations.

To gain a clear understanding of the TGA-Elemental analysis method, contacts had been made directly to Professor Ken Kokubo (Graduate School of Engineering, Osaka University, Osaka, Japan) who has kindly provided generous support on explanation and advice on the method that he and his team had published.

It is true that the TGA-Elemental analysis method could be directly used for estimating $n_{(OH)}$ while taking into account the physically bound water molecules, giving a more accurate estimation than the 'TGA method'. However, Product 1-7 also contained another substance which must be included in elemental analysis – sodium carbonate. This raised quite a complication when the TGA-Elemental analysis method was used, due to an increase in number of variables

involved, and the nature of this method which involve iterative loop calculations. For this kind of calculation, the first guessing is rather important. The closer it is compared to the correct value, a fewer number of iterations is required to obtain the solution. A certain amount of time was required to arrive at the solution for one product. Therefore, considering the fact that there were 7 products to analyse and that Product 1-7 had more complicated compositions to the products in the work of Prof Kokubo and his team (Kokubo et al., 2008; Kokubo et al., 2011), modifications to this method was necessary.

This had led to the development of the systematic and quick calculations for estimating level of hydroxylation in fullerenol using information from TGA and EDX elemental analysis, hereby named as 'TGA-EDX method'. The development combines the concept of TGA-Elemental analysis method (established by Prof Kokubo and his team) and the fundamental of empirical formula and elemental analysis calculations, together with application of solving a finite system of simultaneous algebraic equations. No guessing or iterative calculation is required for a product. The 'TGA-EDX method' successfully developed in this research consists of 3 steps, shown in Figure 5-36.

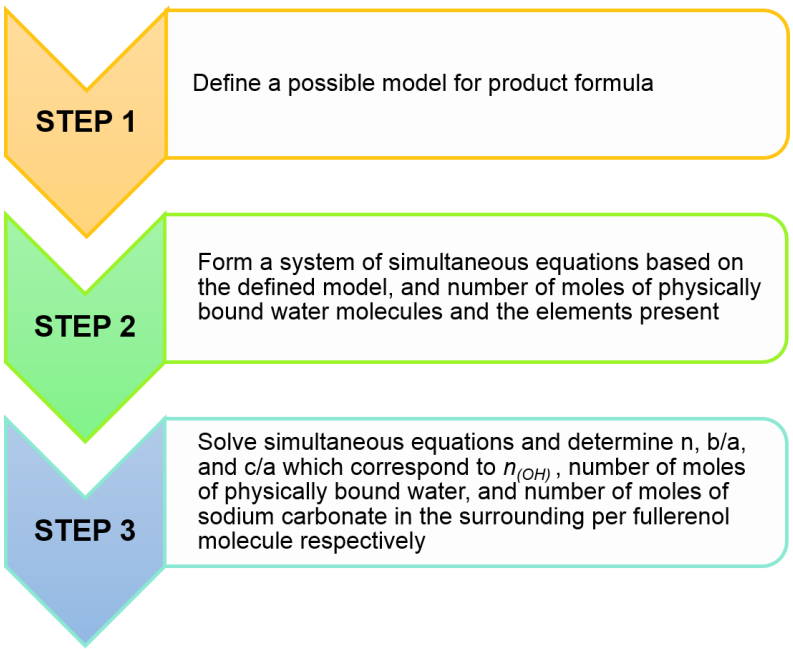

Figure 5-36 Flow chart of steps in 'TGA-EDX method' for estimation of $n_{(OH)}$ developed in this research

The following demonstration of using 'TGA-EDX method' for estimating $n_{(OH)}$ and product formula is based on information from Product 4.

It was assumed that the produced fullerenol was in the form of $\mathbf{a C_{60}(OH)_n \cdot b H_2O}$ **with** $\mathbf{c Na_2CO_3}$ **as its surrounding**, where a, b, and c are number of moles of the chemical substance they preceed, and n is number of hydroxyl groups per fullerenol molecule. Based on EDX results of Product 4 in Table 5-9 and the TGA thermogram in Figure 5-30d, number of moles of physically bound water and elemental C, O and Na present in the product were calculated (shown in Table 5-11).

Table 5-11 Number of moles of physically bound water molecules, and elemental C, O and Na present in Product 4

	%wt	Number of moles
H_2O	14.666	4.07389×10^{-5}
C	37.49	1.56208×10^{-4}
O	42.64	1.33250×10^{-4}
Na	19.15	4.16304×10^{-5}

A system of simultaneous equations can be formed accordingly:

$$b = 4.07389 \times 10^{-5} \quad \textbf{(5-6)}$$

$$60a + c = 1.56208 \times 10^{-4} \quad \textbf{(5-7)}$$

$$an + b + 3c = 1.33250 \times 10^{-4} \quad \textbf{(5-8)}$$

$$2c = 4.16304 \times 10^{-5} \quad \textbf{(5-9)}$$

Solving the above equations thus gives:

$$c = 2.08152 \times 10^{-5} \quad \textbf{(5-10)}$$

$$a = 2.25655 \times 10^{-6} \quad \textbf{(5-11)}$$

$$n = 13.32363 \quad \textbf{(5-12)}$$

The variable n represents the number of hydroxyl groups per fullerenol molecule. It should be noted that n should be rounded up to 14 to better represent the situation (as rounding the number down to 13 would ignore a fraction which actually existed). Therefore, for Product 4, $n_{(OH)}$ = 14.

Number of moles of the physically bound water and the surrounding sodium carbonate per molecule of fullerenol could be determined from b/a and c/a respectively. Rounding these numbers should also follow the same principle as described above for n. Therefore, number of moles of water and sodium carbonate per fullerenol molecule are 19 and 10 respectively.

Through TGA-EDX method, empirical formula of Product 4 was determined to be **$C_{60}(OH)_{14}\cdot 19H_2O$ with 10 moles of Na_2CO_3 as its surrounding**.

To verify validity of the developed 'TGA-EDX method', percentage weight of C, O, and Na based on the derived formula were calculated and compared to the original values from EDX results. Table 5-12 shows that the calculated percentages were very close to the original values from EDX, assuring validity of the developed method.

Table 5-12 Comparison between percentage weight of elements calculated from the estimated formula (by 'TGA-EDX method') and original values from EDX

	%wt calculated	%wt from EDX
C	35.59	37.49
O	42.71	42.64
Na	19.49	19.15
H	2.20	N/A

.

Table 5-13 Calculation results using 'TGA-EDX method' for Product 1-7 showing determined product empirical formula and analysis on molecular and elemental compositions

Product	TBAH added (drops)	Calculation results using 'TGA-EDX method' and composition analysis							
		Product empirical formula	%wt $C_{60}(OH)_n$	%wt H_2O	%wt Na_2CO_3	%C	%O	%Na	%H
1	3	$C_{60}(OH)_9 \cdot 17H_2O$ with $6Na_2CO_3$	48.10	16.86	35.04	43.64	38.79	15.21	2.37
2	6	$C_{60}(OH)_{10} \cdot 19H_2O$ with $6Na_2CO_3$	47.64	18.31	34.05	42.40	40.26	14.78	2.57
3	12	$C_{60}(OH)_{13} \cdot 15H_2O$ with $7Na_2CO_3$	48.18	13.82	37.99	41.17	40.14	16.49	2.20
4	24	$C_{60}(OH)_{14} \cdot 19H_2O$ with $10Na_2CO_3$	40.59	14.49	44.92	35.59	42.71	19.49	2.20
5	48	$C_{60}(OH)_8 \cdot 18H_2O$ with $6Na_2CO_3$	47.14	17.84	35.02	43.61	38.77	15.20	2.42
6	96	$C_{60}(OH)_9 \cdot 15H_2O$ with $5Na_2CO_3$	52.18	16.14	31.68	46.62	37.30	13.75	2.33
7	192	$C_{60}(OH)_{10} \cdot 12H_2O$ with $5Na_2CO_3$	54.40	13.20	32.40	47.68	36.19	14.06	2.08

Based on this model ($aC_{60}(OH)_n \cdot bH_2O$ with cNa_2CO_3), 'TGA-EDX method' was used to estimate values of $n_{(OH)}$ through determination of empirical formulae of Product 1-7. Calculation results and analysis of molecular and elemental composition of the products are presented in Table 5-13. However, it was recalled from characterisation of Product 4 that epoxide functional groups were also present in the product. Therefore, a new model was specially created for Product 4. It was assumed that, in Product 4, each C_{60} cage contained several hydroxyl groups along with one epoxide group (epoxide-contaminated fullerenol). This special model, hereby named 'epoxide model', was thus in the form of **$aC_{60}O(OH)_n \cdot bH_2O$ with cNa_2CO_3 as surroundings**. A new estimation using 'TGA-EDX method' with information from Product 4 based on the epoxide model was conducted. The new empirical formula of Product 4, which considered the existence of epoxide groups within the product, was determine to be $C_{60}O(OH)_{13} \cdot 19H_2O$ with $10Na_2CO_3$. Compared to the formula determined by the first model, number of moles of physically bound water and the surrounding sodium carbonate remained constant, while number of hydroxyl groups per fullerenol molecule had decreased by only one group.

Taking characterisation results into account, it was decided that estimation of $n_{(OH)}$ for Product 1-3 and Product 5-7 could be achieved using 'TGA-EDX method' with the normal model for possible product formula, i.e. no epoxide. However, the estimation of $n_{(OH)}$ for Product 4 should use the epoxide model. Analysis and interpretation of these results are provided in the next section

5.3.3 Effect of TBAH on level of hydroxylation

Differences and similarities of the three series of estimation can be visually observed in Figure 5-37 where values of $n_{(OH)}$ were plotted against the amount of TBAH added for the reaction. It could be seen that, although both methods for estimation of $n_{(OH)}$ gave results in a similar non-linear trend, 'TGA method' was noticeably different from 'TGA-EDX method' as it gave higher values of $n_{(OH)}$ for every product. Nevertheless, as previously discussed towards the

beginning of Section 5.3.2, ‘TGA method’ was deemed to be unsuitable especially for Product 4 due to complications from the presence of epoxide groups in the product hindering calculation based on TGA thermogram. Further analyses thus utilised $n_{(OH)}$ values estimated by the developed ‘TGA-EDX method’.

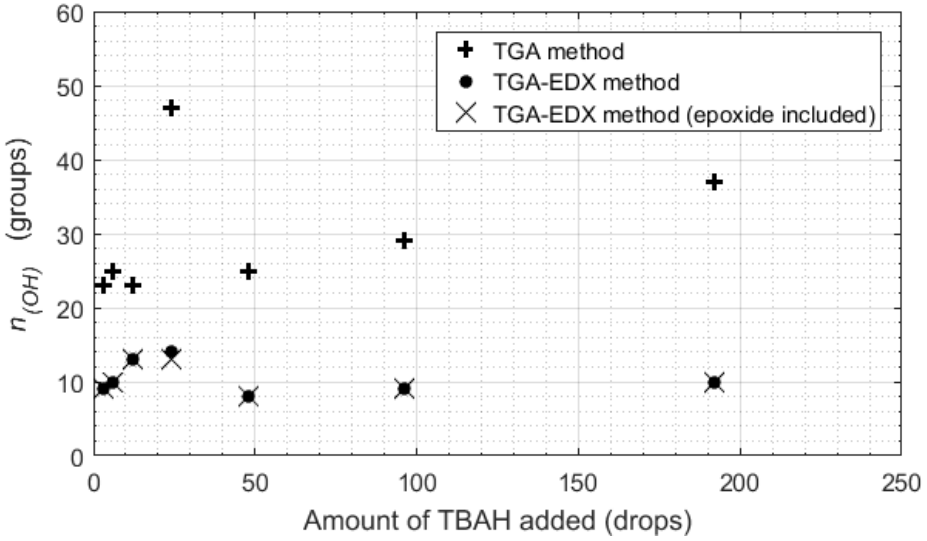

Figure 5-37 $n_{(OH)}$-TBAH plots comparing results from ‘TGA method’, ‘TGA-EDX method’, and ‘TGA-EDX method’ (epoxide included, accounting for presence of epoxide groups in Product 4)

Results from estimation of $n_{(OH)}$ using ‘TGA-EDX method’ were plotted as two series. The first series (black dots) are estimations using the normal model for all products including Product 4. The second series (marked with ×) accounts for the presence of epoxide groups in Product 4, therefore uses epoxide model only for Product 4 and normal model for all other products (referred as ‘TGA-EDX method (epoxide included)’ in the figure). From Figure 5-37, it can be seen that both series of estimation were generally indifferent in terms of $n_{(OH)}$, except for Product 4 where the value with epoxide model was lower by one group. To arrive as close as possible to the true natures of the products, the second series was chosen to represent the relationship between the amount of TBAH added for the reaction and the resulting $n_{(OH)}$.

It would have been ideal if the research could conduct more syntheses in this region to determine which of the two situations actually represented the

behaviour of the influence the amount of TBAH involved had on $n_{(OH)}$ in the product. However, this was not possible due to several limitations including available time, working space and budget.

From this experiment which was conducted under certain limitations, this parameter (amount of TBAH added for the reaction) was capable of controlling $n_{(OH)}$ in a non-linear manner with a local maximum of 14 hydroxyl groups per fullerenol molecule at TBAH = 24 drops, and a local minimum of 8 groups for TBAH = 48 drops.

Production capacity should also be taken into account during development of synthesis protocols. As an elementary measure based on isolated yield, a ratio of mass of isolated product to mass of C_{60} fullerene starting material was calculated, and hereby termed 'PPF mass ratio'. Values of $n_{(OH)}$ and PPF ratios of all products were plotted against the corresponding amount of TBAH added for the reaction, shown in Figure 5-38. It can be seen that PPF mass ratio also generally follows the same trend as $n_{(OH)}$, although with different amplitudes and now the smallest PPF mass ratio comes from when 3 drops were used.

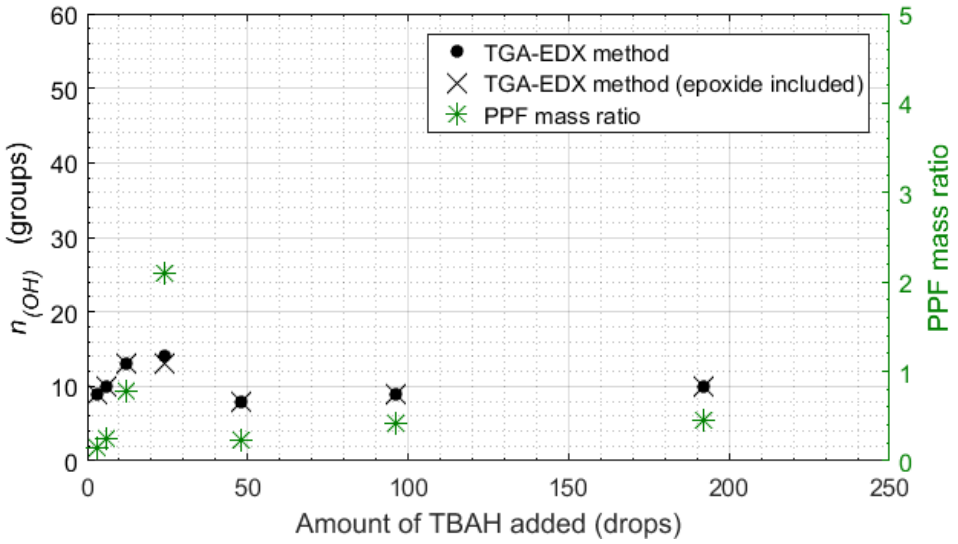

Figure 5-38 $n_{(OH)}$-PPF-TBAH plot comparing $n_{(OH)}$ and PPF mass ratio

Nevertheless, PPF mass ratios are not suitable for comparing between two or more products as the values are on different bases. A conventional measure of reaction performance which can be used for comparing different products is percent yield of a chemical reaction, and is defined as:

$$\text{Percent yield} = \frac{\text{Actual yield}}{\text{Theoretical yield}} \times 100 \quad \textbf{(5-13)}$$

where 'actual yield' refers to the actual amount of product collected from the reaction, and 'theoretical yield' refers to the maximum achievable yield according to the balanced chemical equation of the reaction (Chang and Goldsby, 2016).

As the reaction of fullerene hydroxylation in the TBAH-NaOH route for the synthesis of fullerenol is not yet fully understood and stoichiometry of the reaction is not established, the accurate theoretical yield, hence percent yield, of the reaction could not be obtained. However, it is useful to obtain some approximation of the measure of reaction performance. Although it was not possible to properly determine the conventional percent yield from stoichiometric information of the reaction, it was still possible to calculate an approximation of theoretical yield, hence percent yield, of the reaction using the values of mass and molar mass of the starting material (C_{60} fullerene) and the product (fullerenol). To preserve the flow of content in this thesis, detailed explanation and demonstration of calculations for approximation of theoretical yield and percent yield of the products are given in Appendix C. Calculation results regarding percent yield of the syntheses in TBAH Experiment is summarised in Table 5-14. The values were also plotted against their corresponding $n_{(OH)}$ and amount of added TBAH, shown in Figure 5-39. The observed percent yield pattern was similar to that of PPF mass ratio. Further discussion associated with percent yield is provided in Section 5.6.3.

Results and discussion in this experiment would be used in conjunction with those from the studies of other 2 selected parameters to develop the aimed synthesis protocols, which is provided in Section 5.7.

Table 5-14 Approximation of theoretical yield, actual yield and percent yield of products from TBAH Experiment

Product	TBAH (drops)	Estimated empirical formula	Theoretical yield (mg)	Actual yield (mg)	% yield
1	3	$C_{60}(OH)_9 17H_2O$ with $6Na_2CO_3$	97.0	7.7	8.0
2	6	$C_{60}(OH)_{10} 19H_2O$ with $6Na_2CO_3$	99.4	9.6	9.7
3	12	$C_{60}(OH)_{13} 15H_2O$ with $7Na_2CO_3$	106.1	30.7	29.0
4	24	$C_{60}O(OH)_{13} 19H_2O$ with $10Na_2CO_3$	111.0	71.0	63.9
5	48	$C_{60}(OH)_8 18H_2O$ with $6Na_2CO_3$	95.9	8.8	9.2
6	96	$C_{60}(OH)_9 15H_2O$ with $5Na_2CO_3$	98.0	17.7	18.1
7	192	$C_{60}(OH)_{10} 12H_2O$ with $5Na_2CO_3$	99.1	19.9	20.1

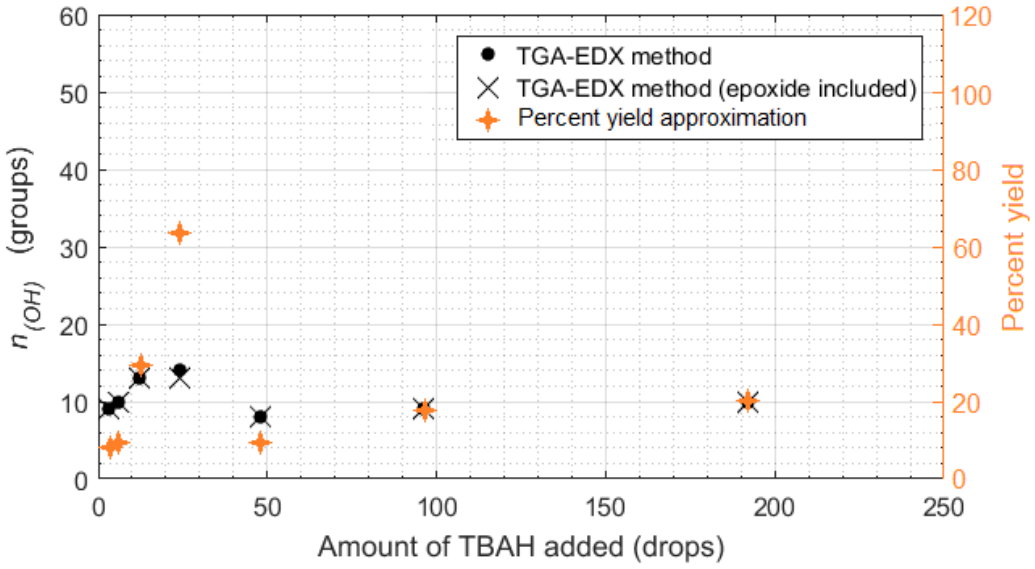

Figure 5-39 $n_{(OH)}$-Percent yield-TBAH plot comparing $n_{(OH)}$ and percent yield

5.4 Effect of NaOH on level of hydroxylation in TBAH-NaOH route for fullerenol synthesis

This experiment focused on the second selected process parameter, source of hydroxide ions (i.e. sodium hydroxide solution), and its influence on $n_{(OH)}$ achieved. For ease of clarification, this experiment is referred as 'NaOH Experiment'. Following the design of experiment and procedures in Section 4.5, five fullerenol syntheses were conducted using different volumes of sodium hydroxide solution (0.5, 1.0, 2.0, 4.0 and 8.0 ml). The products were labelled as Product 8 to Product 12 respectively.

The heart of this experiment was the varying amount of source of hydroxide ions for the reaction. From a scientific point of view, it would have been ideal to change the amount by changing concentration, so that the total volume of the reaction mixture remains constant. However, this approach encountered some impactful practical constraints.

If this approach were to be pursued, the design of experiment would have consisted of a series of fullerenol syntheses using different concentrations of sodium hydroxide solution (but equal ivolume): the original concentration, two

higher concentrations, and two lower concentrations. With solubility of sodium hydroxide (20°C) being 109 g/100 ml (Centers for Disease Control and Prevention, 2015), the original concentration 100% W/V (Li et al., 1993) is already very close to solubility limit and is already rather viscous. While lower concentrations would not be much of a problem, it would be more difficult to force the solution of higher concentrations down the liquid transfer equipment into the reaction mixture. Difficulty of the liquid to flow leads to some material remained inside the transfer equipment. The actual amount transferred into the reaction mixture would then be less than the intended amount, hence insufficient for the designed process condition and causing considerable errors to the experiment.

Alternatively, the amount of hydroxide ions present in the reaction mixture could be varied by changing volume of sodium hydroxide solution of a fixed concentration, e.g. the original concentration. Although the total volume of the reaction mixture may vary slightly between different syntheses, the issue may be more tolerable since the amount of solution transferred into the reaction mixture should be closer to the intended amount when compared to the situation when different concentrations are used.

Based on available equipment and scale of production at the time of conducting this experiment, it was suggested that the errors from insufficient amount of source of hydroxide ions (associated with using different concentrations but same volume) would be more severe when compared to the errors from slightly unequal total volume of the reaction mixture (associated with using different volumes of same concentration). Furthermore, from health and safety point of view, working with a more concentrated sodium hydroxide solution is less favourable as it poses a higher risk of chemical and thermal hazards (dissolution of solid sodium hydroxide into water is an exothermic reaction releasing a certain amount of heat). Therefore, this research decided to keep the concentration of sodium hydroxide constant while changing the volume it was added for the reaction mixture instead.

Apart from the varying volume of sodium hydroxide solution, all other process parameters must be kept constant in all syntheses. Throughout this experiment, 24 drops of TBAH were used due to the facts obtained from the TBAH Experiment that maximum $n_{(OH)}$ as well as maximum isolated yield could be achieved at this condition. Also, the condition already had been evaluated for production consistency.

Figure 5-40 shows physical appearances of Product 8-12. Product 8-10 were obtained as dark brown powder or flake. Product 11 and 12, however, had considerably lighter shades of brown when compared to Product 8-10, and appeared as 'fluffy' powder. The colour of Product 12 also appeared to be slightly lighter than that of Product 11.

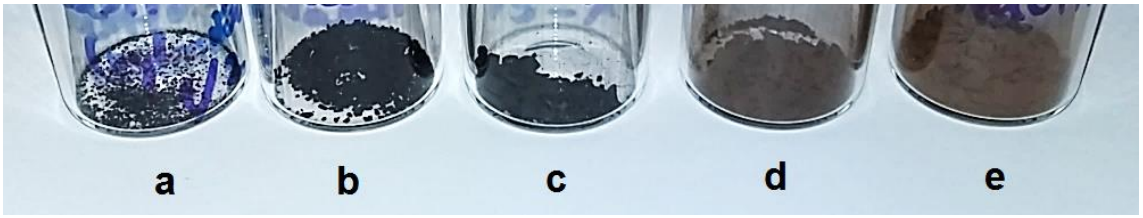

Figure 5-40 Product 8-12 (a-e respectively). Product 11 and 12 show noticeably lighter shades of brown, compared to Product 8-10.

Observations during syntheses of all products were as same as in TBAH Experiment, including the trace of water-soluble white solid on the flask wall where the product-containing liquid flowed (as seen in Figure 5-25). Analysis of characterisation results thus followed the same path as performed in TBAH Experiment.

5.4.1 Analysis of characterisation results

Having observed the trace of water-soluble white solid during product separation steps, it was presumed that sodium carbonate were also present in these products, similar to TBAH Experiment. Characterisation requires an integration of results from IR spectroscopy, SEM, EDX and TGA.

Infrared spectra of Product 8-12 are shown in Figure 5-41. The four characteristic absorptions of fullerenol were observed in all products

(absorptions centred around 3430, 1600, 1370 and 1080 cm^{-1} corresponding to ν O–H, ν C=C, δ C–O–H, and ν C–O respectively).

For Product 8-9, broad shoulder extending from around 3000 to 2000 cm^{-1} present in Figure 5-41a and Figure 5-41b was due to the presence of sodium carbonate in the product. This argument was supported by observation of the pattern of solids (formed on the surface of product powder) in SEM micrographs of the two products (Figure 5-42a and Figure 5-42b), and detection of sodium element in Table 5-15. It was suggested that these products did not contain epoxide groups since their thermograms (Figure 5-43a and Figure 5-43b) did not show a distinct step weight loss around 380°C.

On the other hand, Figure 5-41c to Figure 5-41e show deviations from normal fullerenol similar to the one observed in the spectrum of Product 4 (Figure 5-26d) in Section 5.3.1. The δ C–O–H absorption in the spectra of the three products appears as a shoulder around 1380 cm^{-1}, almost covered by a strong absorption around 1440 cm^{-1}. This strong absorption was suggested to arise from the presence of sodium carbonate at a higher proportion in these products compared to Product 8-9. Observation of needle-like crystals in SEM micrographs in Figure 5-42, as well as EDX results in Table 5-15 supported this suggestion. Infrared spectra of these products also show weak but sharp absorption around 880 cm^{-1}. These evidences pointed towards the presence of sodium carbonate and epoxide functional groups in Product 10-12. TGA thermograms were thus used to confirm whether epoxide groups were actually present in these products. Figure 5-43c to Figure 5-43e reveal the presence of epoxide groups in Product 10-12 from the distinct step weight loss around 380°C.

Therefore, it can be concluded that fullerenol were successfully synthesised from all conditions, although sodium carbonate was also present in all products as surroundings and Product 10-12 contained epoxide groups in addition to the desired hydroxyl groups.

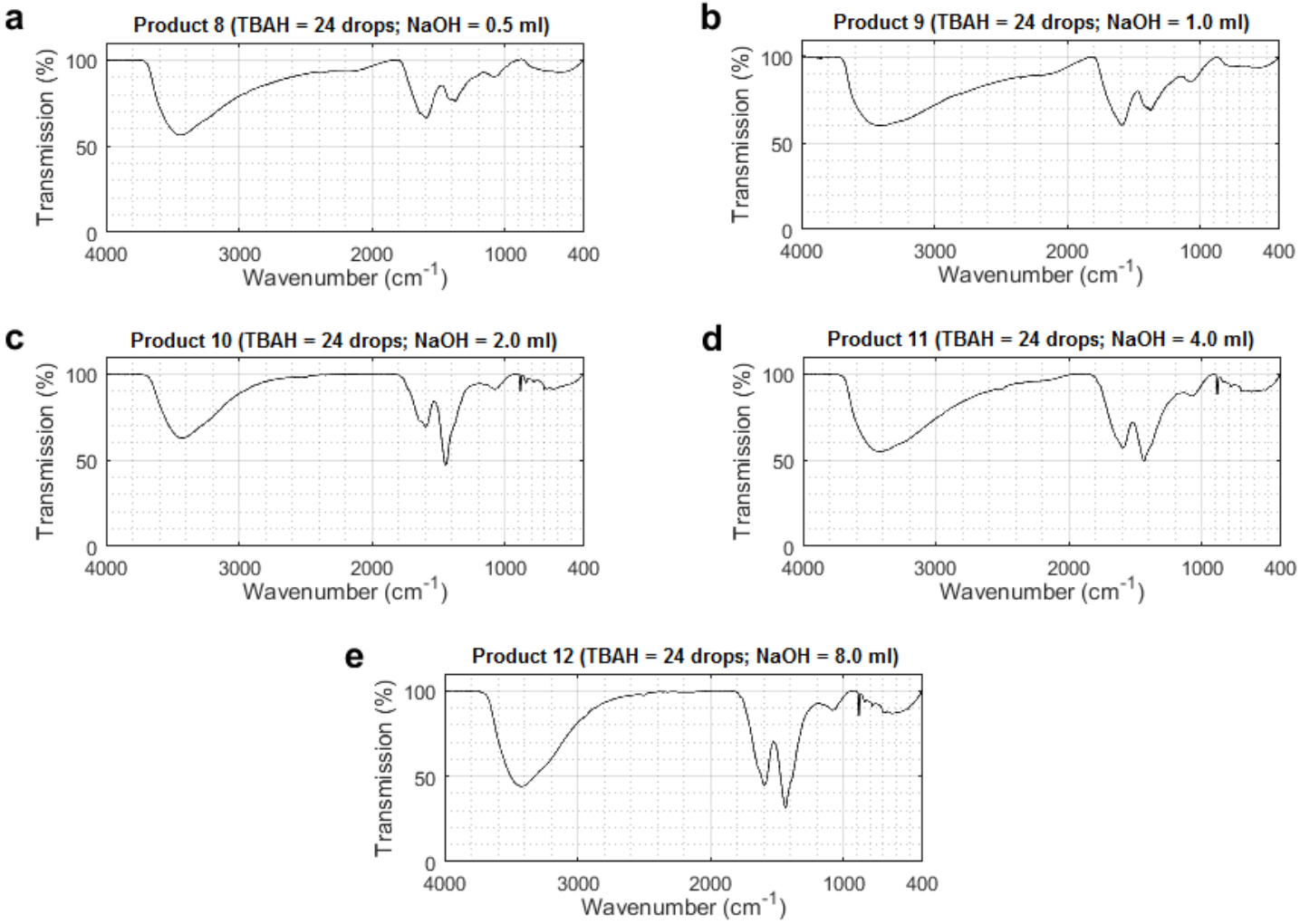

Figure 5-41 Infrared spectra of Product 8-12 (using different volumes of NaOH during syntheses) from NaOH Experiment

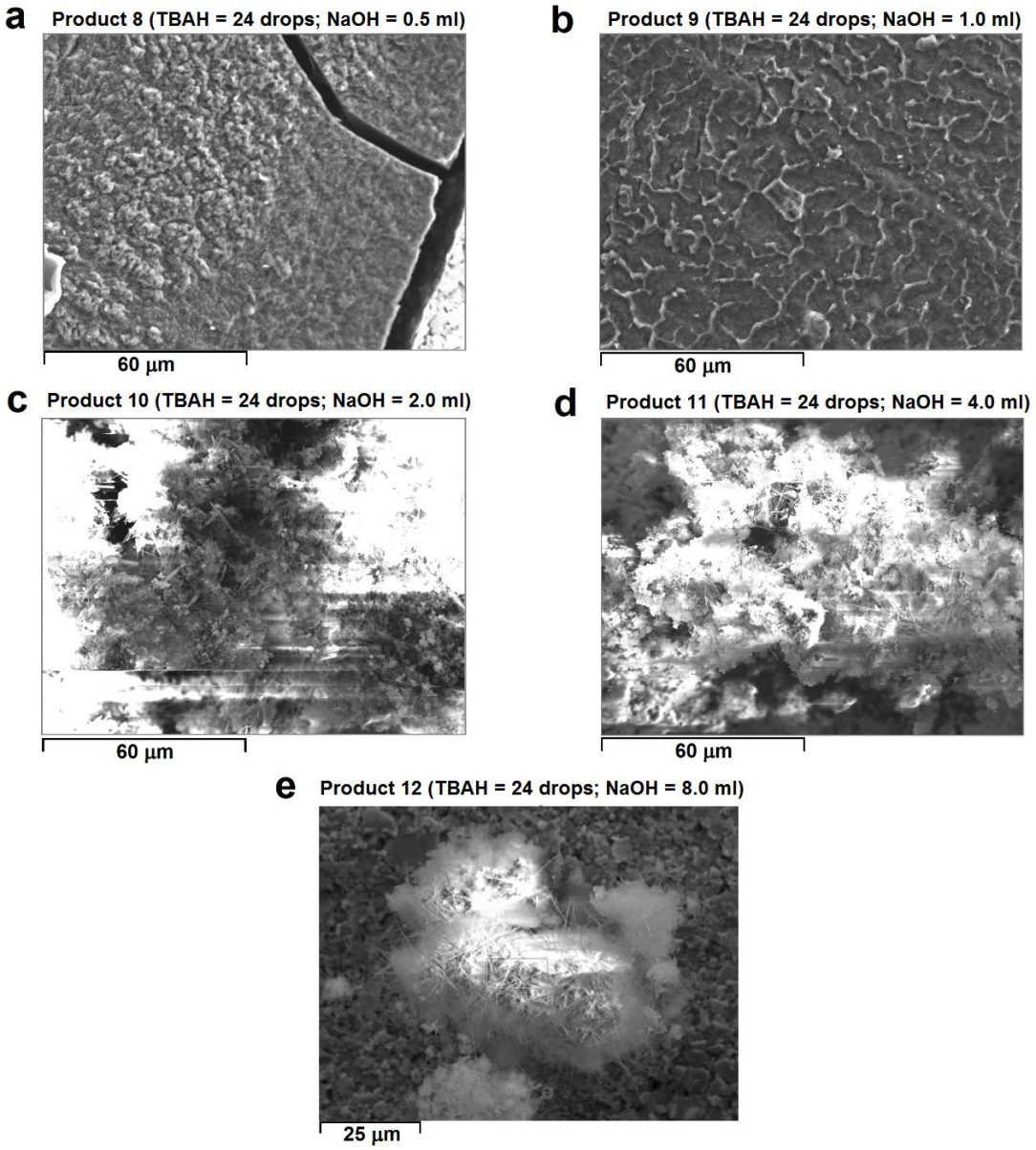

Figure 5-42 SEM micrographs of products from NaOH Experiment showing patterns formed on the surface of product powder (a and b) and existence of needle-like objects (c, d and e) (Images produced by SEM/EDX facilities at National Physical Laboratory, London)

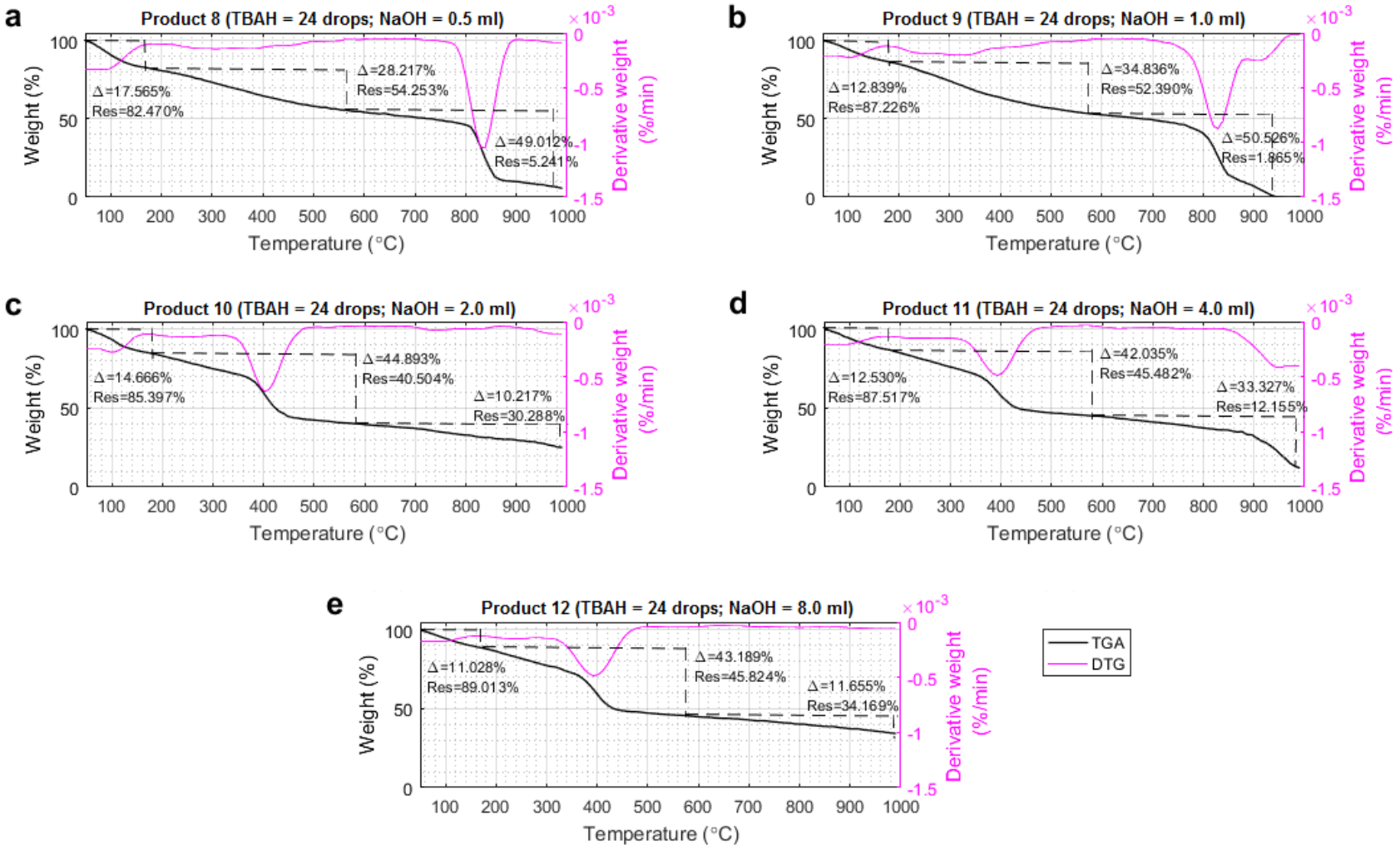

Figure 5-43 TGA thermograms of Product 8-12 (using different volumes of NaOH during syntheses) from NaOH Experiment

Table 5-15 EDX results of Product 8-12 (%wt)

Product	NaOH added (ml)	% C	% O	% Na
8	0.5	46.77	37.75	14.15
9	1.0	46.76	37.57	14.97
10	2.0	37.49	42.64	19.15
11	4.0	36.37	42.31	19.29
12	8.0	41.29	40.71	17.73

For particle size characterisation, it can be seen from Figure 5-44 that DLS results can be divided into two groups: Product 8-9, and Product 10-12. Product 8 and 9 showed distributions of particle diameters at a higher range when compared to those of Product 10-12. For Product 8-9, the smallest detectable particle was about 25 nm in diameter, and the largest of around 200 nm. The majority of particles were of 40-80 nm in diameter. On the other hand, distributions of particle diameter in Product 10-12 covered the range of only 1.5-10 nm, with the majority of diameters between 3-6 nm.

Similar to the TBAH Experiment, only one high-magnification SEM micrograph could be obtained for one product from this experiment, due to very limited SEM/EDX services affordable under limited budget. The obtained micrograph was from a sample of Product 8, taken at 160kx (Figure 5-45). The micrograph reveals the sizes of the majority of particles in the frame to be in agreement with the DLS results, i.e. around 80 nm in diameter. Again, it was presumed that, had the high-magnification SEM micrographs of other products been obtained, they should show particle distributions in agreement with the corresponding DLS results.

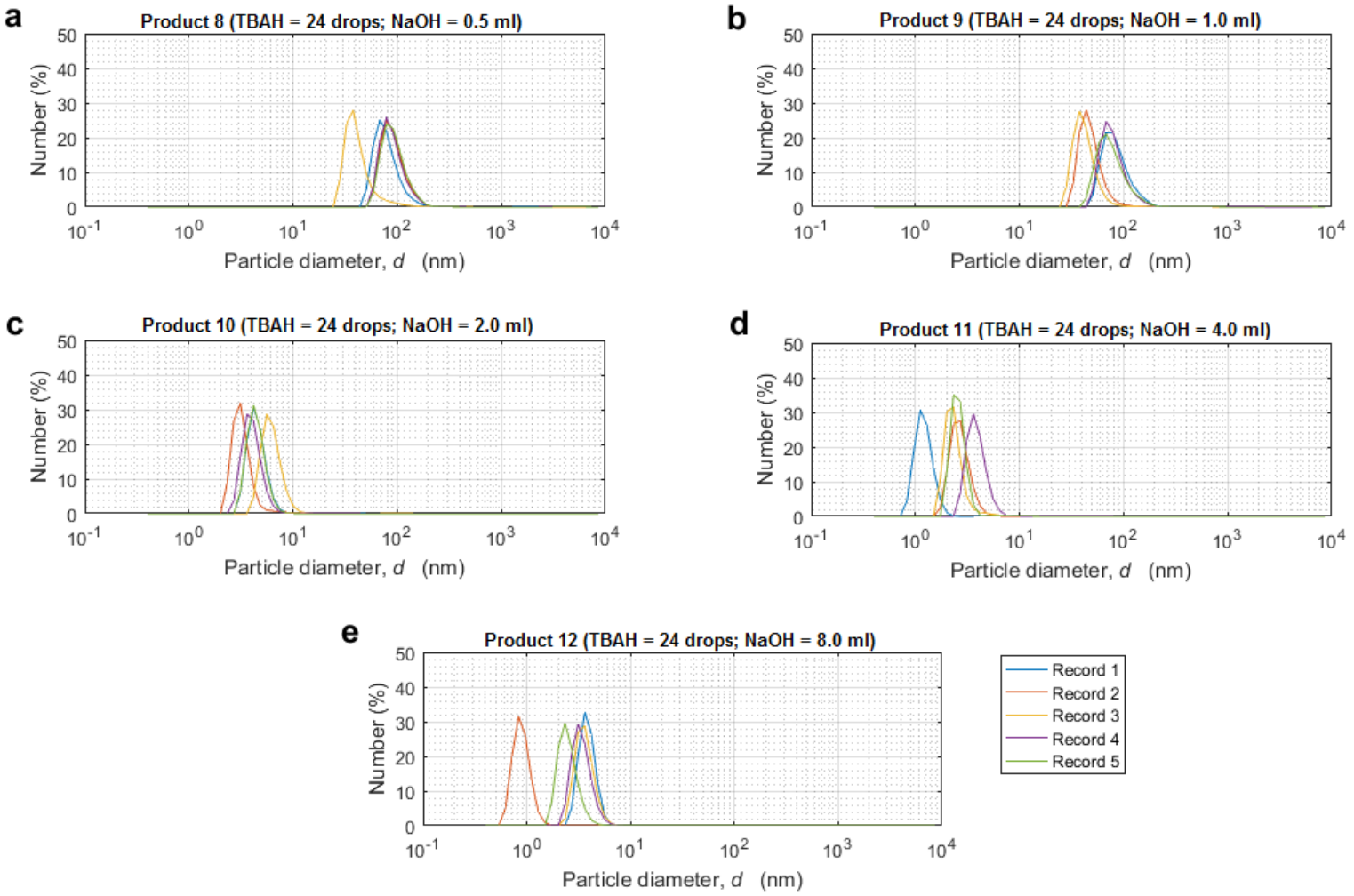

Figure 5-44 DLS results of Product 8-12 (using different volumes of NaOH during syntheses) from NaOH Experiment

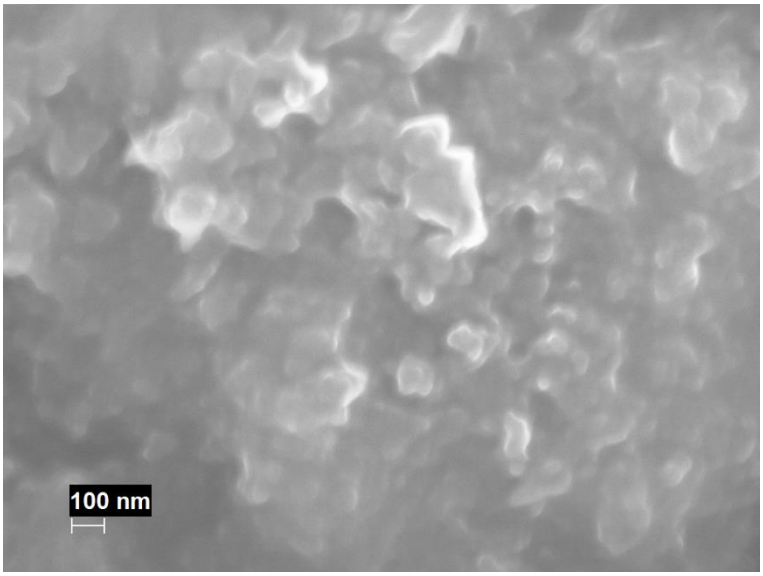

Figure 5-45 SEM micrograph of Product 8 (TBAH = 24 drops; NaOH = 0.5 ml) from NaOH Experiment at 160kx (Image produced by SEM/EDX facilities at National Physical Laboratory, London)

5.4.2 Estimation of level of hydroxylation

Based on the analysis of characterisation results which suggested for the presence of sodium carbonate and epoxide groups in the fullerenol obtained in this experiment (Product 8-12), 'TGA method' was deemed unsuitable for estimation of $n_{(OH)}$ of the products. Table 5-16 shows results from estimation using 'TGA method', which confirmed the argument as $n_{(OH)}$ values seem unusually high, especially the reference condition (NaOH = 2.0 ml) and lower (NaOH of 0.5 and 1.0 ml). The plot of results ($n_{(OH)}$-NaOH plot) is shown in Figure 5-46.

Table 5-16 Estimation of $n_{(OH)}$ for Product 8-12 using 'TGA method'

Product	NaOH added (ml)	x	y	$n_{(OH)}$
8	0.5	28.217	54.253	23
9	1.0	34.836	52.390	29
10	2.0	44.893	40.504	50
11	4.0	42.035	45.482	40
12	8.0	43.189	45.824	40

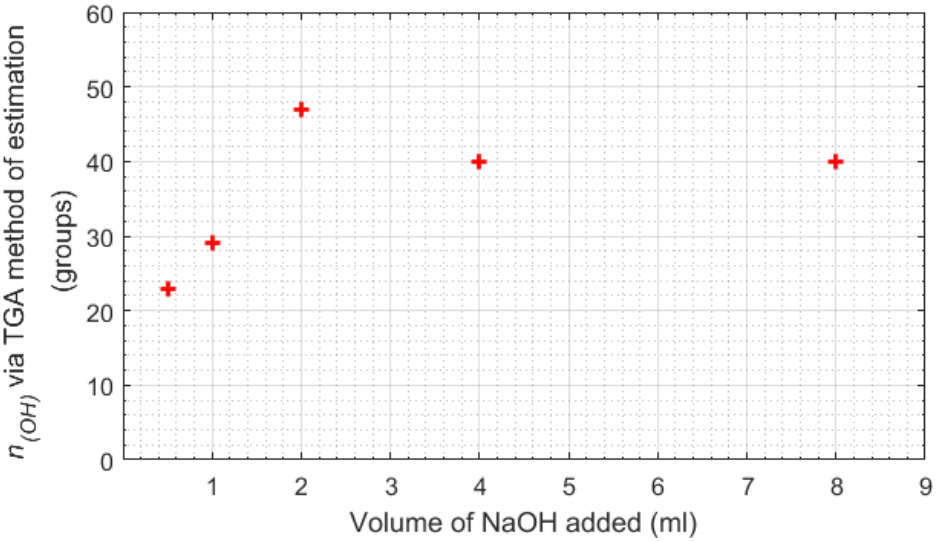

Figure 5-46 $n_{(OH)}$-NaOH plot using $n_{(OH)}$ determined by 'TGA method'

The 'TGA-EDX method' developed in this research was therefore used for estimation of $n_{(OH)}$ of the products. Again, two series of estimations were conducted for comparison. The first series used the normal model **$aC_{60}(OH)_n{\cdot}bH_2O$ with cNa_2CO_3 as surroundings** for calculations of all products. The obtained results and analysis of compositions are shown in Table 5-17.

However, as determined from product characterisation, Product 10-12 contained epoxide groups in addition to the desired hydroxyl groups. Estimation of $n_{(OH)}$ of these products should be conducted based on the epoxide model, i.e. **$aC_{60}O(OH)_n{\cdot}bH_2O$ with cNa_2CO_3 as surroundings**. The second series of estimations was therefore conduced using the epoxide model for Product 10-12, and normal model for Product 8-9. Results obtained from epoxide model including composition analyses for Product 10-12 are present in Table 5-18. Similar to TBAH Experiment, values of $n_{(OH)}$ estimated using the epoxide model were lower from that of the normal model by only 1 group, while the number of moles of physically bound water and the surrounding sodium carbonate did not change (for each Product).

Table 5-17 Calculation results using 'TGA-EDX method' for Product 8-12 showing determined product empirical formula and analysis on molecular and elemental compositions

Product	NaOH added (ml)	Calculation results							
		Product empirical formula	%wt $C_{60}(OH)_n$	%wt H_2O	%wt Na_2CO_3	%C	%O	%Na	%H
8	0.5	$C_{60}(OH)_8.17H_2O$ with $6Na_2CO_3$	47.61	17.02	35.37	44.05	38.26	15.35	2.34
9	1	$C_{60}(OH)_{12}.12H_2O$ with $6Na_2CO_3$	52.03	12.16	35.81	44.59	37.84	15.54	2.03
10	2	$C_{60}(OH)_{14}.19H_2O$ with $10Na_2CO_3$	40.59	14.49	44.92	35.59	42.71	19.49	2.20
11	4	$C_{60}(OH)_{16}.16H_2O$ with $10Na_2CO_3$	42.39	12.31	45.30	35.90	42.39	19.66	2.05
12	8	$C_{60}(OH)_{16}.13H_2O$ with $8Na_2CO_3$	47.83	11.28	40.89	39.34	40.89	17.74	2.03

Table 5-18 Calculation results using 'TGA-EDX method' with epoxide model for Product 10-12 showing determined product empirical formula and analysis on molecular and elemental compositions

Product	NaOH added (ml)	Calculation results ('TGA-EDX method' with epoxide model)							
		Product empirical formula	%wt $C_{60}O(OH)_n$	%wt H_2O	%wt Na_2CO_3	%C	%O	%Na	%H
10	2	$C_{60}O(OH)_{13}.19H_2O$ with $10Na_2CO_3$	40.57	14.50	44.93	35.61	42.73	19.50	2.16
11	4	$C_{60}O(OH)_{15}.16H_2O$ with $10Na_2CO_3$	42.37	12.31	45.32	35.91	42.41	19.67	2.01
12	8	$C_{60}O(OH)_{15}.13H_2O$ with $8Na_2CO_3$	47.80	11.29	40.91	39.36	40.91	17.75	1.98

5.4.3 Effect of NaOH on level of hydroxylation

Values of $n_{(OH)}$ estimated via 'TGA method', 'TGA-EDX method' using the normal model for all products, and 'TGA-EDX method' using epoxide model for Product 10-12 were plotted against volume of sodium hydroxide solution added for the reaction, shown in Figure 5-47. Again, although both methods for estimation of $n_{(OH)}$ give results in a non-linear manner, 'TGA-EDX method' gave lower values of $n_{(OH)}$, but presumably closer to the reality, for every product.

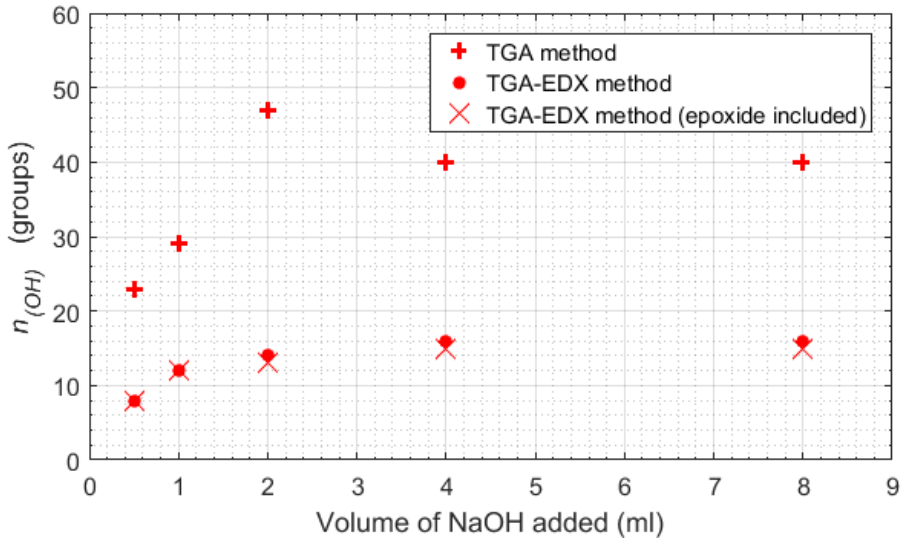

Figure 5-47 $n_{(OH)}$-NaOH plots comparing results from 'TGA method', 'TGA-EDX method', and 'TGA-EDX method' (epoxide included, accounting for presence of epoxide groups in Product 10-12)

Within the two series of estimations using 'TGA-EDX method', the second series, which accounted for the presence of epoxide groups in Product 10-12, was believed to provide more accurate estimations. Further analyses were therefore based on $n_{(OH)}$ values from the second series of estimations.

The smallest volume of sodium hydroxide solution of 0.5 ml added for the reaction gave the smallest value of achieved $n_{(OH)}$ (8 groups). From Figure 5-47, as added volume increases, the resulting $n_{(OH)}$ also increases in a non-linear manner until it levels off after added volume equals to 4.0 ml. Both 4.0 and 8.0 ml of sodium hydroxide solution added gave the same $n_{(OH)}$ which is a maximum value of this experiment (15 groups).

Basic curve fitting on the $n_{(OH)}$-NaOH from the 'TGA-EDX method' (with consideration towards the presence of epoxide groups in Product 10-12). It was found that the mathematical function which offerred the biggest value of R^2 (a parameter for assessing Goodness of Fit) was a 2-term power function with an expression described in Equation (5-14). R^2 was determined to be 0.9810. Plotting Equation (5-14) together with the corresponding $n_{(OH)}$-NaOH gives Figure 5-48.

$$f(x) = -3.993x^{-0.9313} + 15.68 \quad \textbf{(5-14)}$$

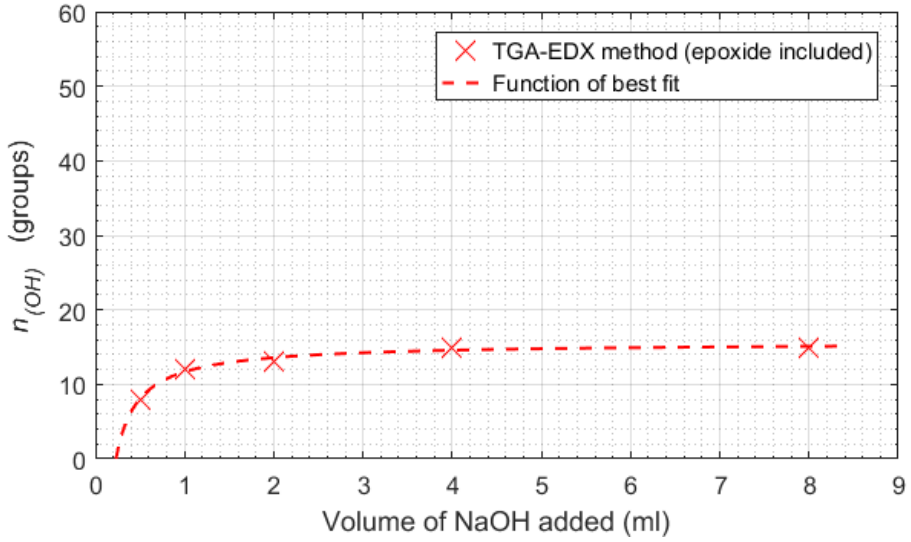

Figure 5-48 Function of best fit (2-term power function) for $n_{(OH)}$-NaOH plot of results from 'TGA-EDX method' (epoxide included, accounting for presence of epoxide groups in Product 10-12)

The phenomenon of introducing hydroxyl groups onto fullerene cages in a reservoir of toluene liquid might be considered as liquid-solid adsorption. One of the most popular equations used to describe adsorption isotherm of liquid-solid systems is known as Freundlich Adsorption Isotherm, shown in Equation (5-15):

$$C'_s = \alpha_2 (C^*)^{1/k} \quad \textbf{(5-15)}$$

where C'_s refers to mass of adsorbate per unit mass adsorbent, C^* refers to concentration of adsorbate in the solution (in equilibrium with concentration of the adsorbate on the solid), and α_2 and k are constants (Richardson et al.,

2002). Equation (5-14), hence the $n_{(OH)}$-NaOH plot, resembled the original form of Freundlich Adsorption Isotherm equation in such a way that it could be considered as Equation (5-15) with an extra term (although it could not be certain at this point whether this extra term was another constant or a parameter). Taking natural log of Equation (5-15) gives:

$$\ln(C'_s) = \ln(\alpha_2) + \left(\frac{1}{k}\right)\ln(C^*) \quad \textbf{(5-16)}$$

which is generally used in analysis of experimental data from the study of liquid-solid adsorption processes.

Natural log of $n_{(OH)}$ values were plotted against natural log of the added sodium hydroxide solution, shown in Figure 5-49. Basic curve fitting using a linear model shows that the following linear function could be fitted to the plot with R^2 = 0.8423:

$$f(x) = 0.2415x + 2.382 \quad \textbf{(5-17)}$$

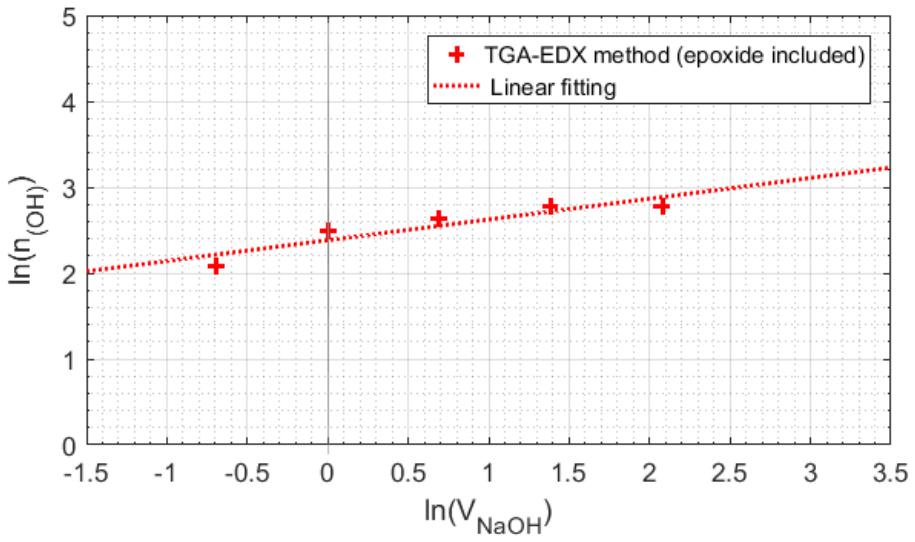

Figure 5-49 Plot of natural log of $n_{(OH)}$ values against natural log of volume of sodium hydroxide solution added for the reaction, fitted with a linear function Equation (5-17)

It can be argued that the $\ln(n_{(OH)})$-$\ln(V_{NaOH})$ plot follows Freundlich Adsorption Isotherm. By comparing Equation (5-16) with Equation (5-17), the slope of the plot gives an indication to the constant k from Freundlich Adsorption Isotherm

for this process of hydroxylation of C_{60}, and the intercept with the vertical axis gives an indication to another constant α_2.

From this discovery, it was suggested that hydroxylation of C_{60} by sodium hydroxide solution in the TBAH-NaOH route to produce fullerenol could be considered as a liquid-solid adsorption process (also suggested to be a chemisorption type as the introduced hydroxyl groups form chemical bonds with the fullerene cage).

$n_{(OH)}$ and PPF ratios of Product 8-12 were plotted against the corresponding volume of sodium hydroxide solution added for the reaction, shown in Figure 5-50. From the figure, it can be seen that PPF mass ratio increases as the volume of sodium hydroxide solution added into the reaction increases. Based on available information, it could not be certain whether a volume of sodium hydroxide solution larger than 8.0 ml would actually result in an even bigger PPF mass ratio. Nevertheless, it might be argued that PPF mass ratio seemed to be more affected by the amount of hydroxide ions than the amount of phase-transfer catalyst present in the reaction mixture.

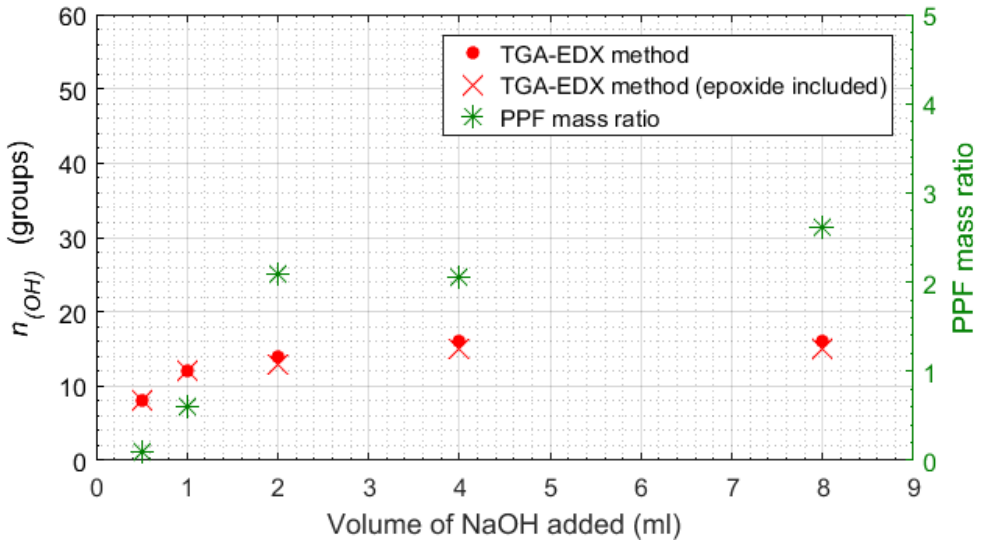

Figure 5-50 $n_{(OH)}$-PPF-NaOH plot comparing $n_{(OH)}$ and PPF mass ratio

Similar to TBAH Experiment, calculation results for approximation of theoretical yield and percent yield of products from NaOH Experiment followed the approach explained in Appendix C. The results are given in Table 5-19 and Figure 5-51. Further discussion associated with percent yield is provided in Section 5.6.3.

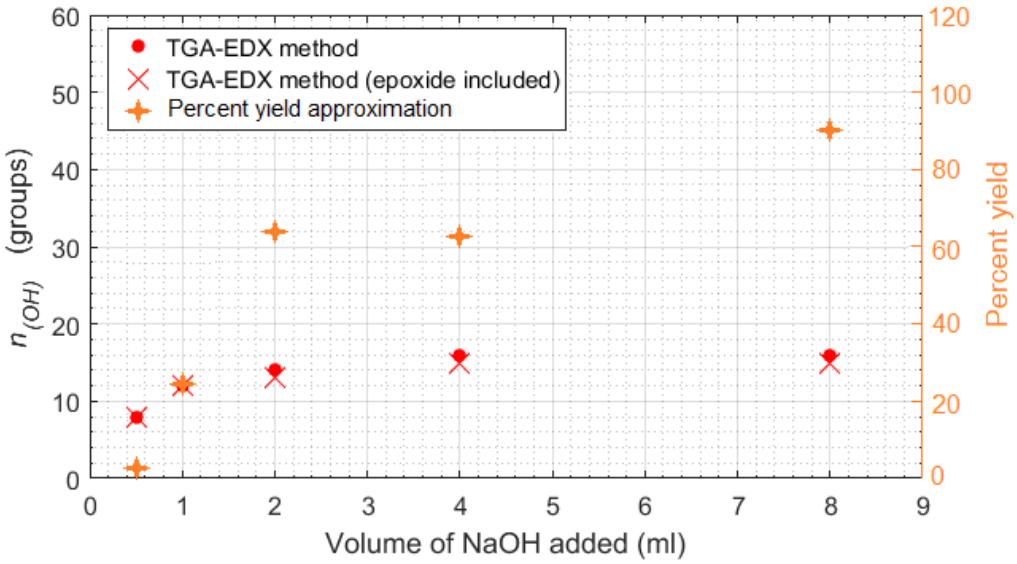

Figure 5-51 $n_{(OH)}$-Percent yield-NaOH plot comparing $n_{(OH)}$ and percent yield

From this experiment which was conducted under certain limitations, this parameter (volume of sodium hydroxide solution added for the reaction) was capable of controlling $n_{(OH)}$ in a non-linear manner, with a local maximum of 16 hydroxyl groups per fullerenol molecule after 4.0 ml and a local minimum of 8 groups per fullerenol molecule at 0.5 ml of sodium hydroxide solution.

Results and discussion in this experiment would be used in conjunction with those from the studies of other 2 selected parameters to develop the aimed synthesis protocols, which is provided in Section 5.7.

Table 5-19 Approximation of theoretical yield, actual yield and percent yield of products from NaOH Experiment

Product	NaOH (ml)	Estimated empirical formula	Theoretical yield (mg)	Actual yield (mg)	% yield
8	0.5	$C_{60}(OH)_8.17H_2O$ with $6Na_2CO_3$	193.0	7.0	3.6
9	1.0	$C_{60}(OH)_{12}.12H_2O$ with $6Na_2CO_3$	103.1	25.2	24.4
10	2.0	$C_{60}O(OH)_{13}.19H_2O$ with $10Na_2CO_3$	111.0	71.0	63.9
11	4.0	$C_{60}O(OH)_{15}.16H_2O$ with $10Na_2CO_3$	110.5	69.7	63.1
12	8.0	$C_{60}O(OH)_{15}.13H_2O$ with $8Na_2CO_3$	113.0	102.7	90.9

5.5 Effect of reaction time on level of hydroxylation in TBAH-NaOH route for fullerenol synthesis

This experiment studied the response of $n_{(OH)}$ on the final selected process parameter, reaction time (i.e. the duration of vigorous stirring step). For ease of clarification, this experiment is hereby referred as 'Reaction Time Experiment'.

Based on the same rationale as described towards the beginning of Section 5.4 for specification of the other process parameters which must be kept constant, 24 drops of TBAH together with 2.0 ml of 100% W/V sodium hydroxide solution were used for all syntheses in this experiment.

Following the design of experiment and procedures given in Section 4.6, five fullerenol syntheses were conducted with different duration of the vigorous stirring step (i.e. reaction time): 10, 15, 20, 25 and 30 minutes. It would have been ideal if the research was able to include a wider range of reaction time in the design of experiment, for example, 60 minutes and longer. However, this was not practicable due to certain limitations especially those related to availability of working space and the available time. The products were labelled as Product 13-17 respectively. All five products were obtained as dark brown powder (Figure 5-52), the shade similar to Batch 1-4 from Consistency Evaluation Experiment.

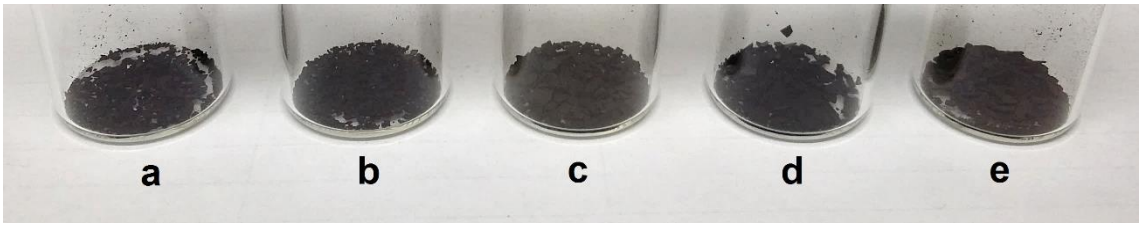

Figure 5-52 Product 13-17 (a-e respectively) obtained as dark brown powder/flake

Synthesis observations were similar among the five syntheses, and were similar to the observations from TBAH and NaOH Experiments. In addition to the major and characteristic observations for fullerenol synthesis (as described in Section 5.2.1), the trace of water-soluble white solid on the flask wall where the product-containing liquid flowed (as seen in Figure 5-25) was observed in all syntheses.

Again, analysis of characterisation results thus followed the same path performed in TBAH and NaOH Experiments.

5.5.1 Analysis of characterisation results

The trace of water-soluble white solid during product separation steps suggested that sodium carbonate was also present in these products, similar to TBAH and NaOH Experiments. Again, product characterisation required an integration of results from IR spectroscopy, SEM, EDX and TGA.

The four characteristic absorptions of fullerenol were observed in the infrared spectra of all products (absorptions centred around 3430, 1600, 1370 and 1080 cm^{-1} corresponding to ν O–H, ν C=C, δ C–O–H, and ν C–O respectively) which are shown in Figure 5-53. Unlike Product 4 and Product 10, infrared spectra of the five products from this experiment did not show a weak, sharp absorption at 880 cm^{-1}. The absence of this absorption suggests that none of these products contain epoxide groups.

From Figure 5-53, the δ C–O–H absorption in each spectrum does not appear as a shoulder, but as the main absorption itself. The signal around 1440 cm^{-1} appears as a shoulder of δ C–O–H absorption instead. Together with the mild broad shoulder extending from around 3000 to 2000 cm^{-1} observed in the spectra, presence of sodium carbonate in the products was suggested (probably in a lower proportion when compared to Product 4 and Product 10). SEM micrographs of the products (Figure 5-54) showing pattern of solids formed on the flake surface, as well as detection of sodium element in samples from Product 13-17 (Table 5-20), supported the suggestion.

Table 5-20 EDX results of Product 13-17 (presented as %wt)

Product	Reaction time (min)	% C	% O	% Na
13	10	51.18	35.11	13.06
14	15	52.32	33.07	14.61
15	20	50.48	34.22	14.58
16	25	51.93	33.65	14.22
17	30	51.24	34.35	13.54

Based on analysis of infrared spectra, it was expected that TGA thermograms of Product 13-17 should exhibit the characteristic weight loss pattern of fullerenol, i.e. weight loss related to physically bound water molecules (up to 180°C), weight loss associated with hydroxyl groups (from 150°C or 180°C to 570°C), and weight loss from degradation of fullerene cage structure (around 700-900°C). However, the thermograms obtained in Figure 5-55 show a completely different picture. An extra step weight loss from around 200°C to up to 450°C was observed in almost all thermograms. These unusual results were not believed to be associated with the presence of epoxide groups within the product due to the fact that epoxide absorption was not present in the infrared spectrum of any product.

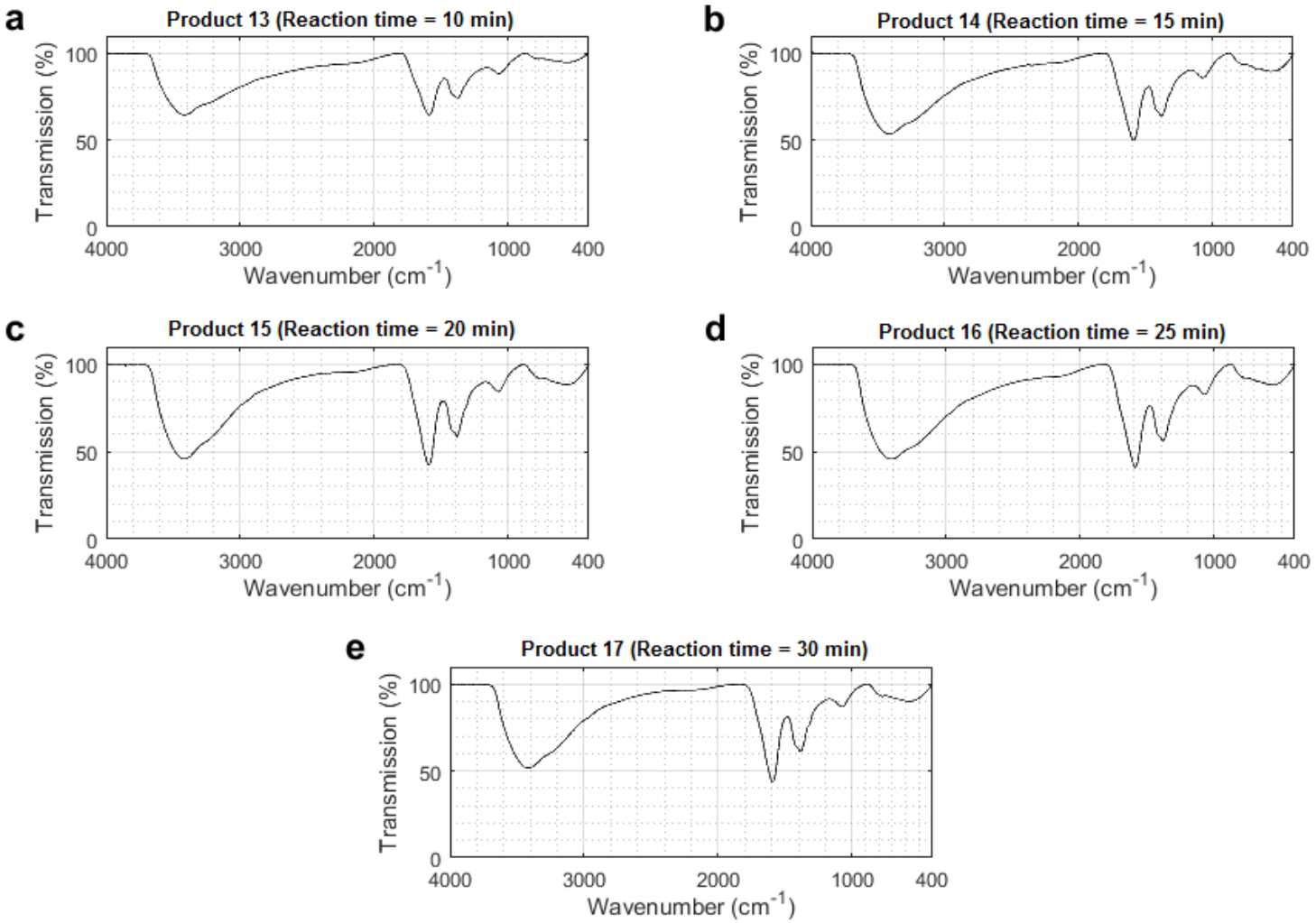

Figure 5-53 Infrared spectra of Product 13-17 (using different lengths of reaction step during syntheses) from Time Experiment

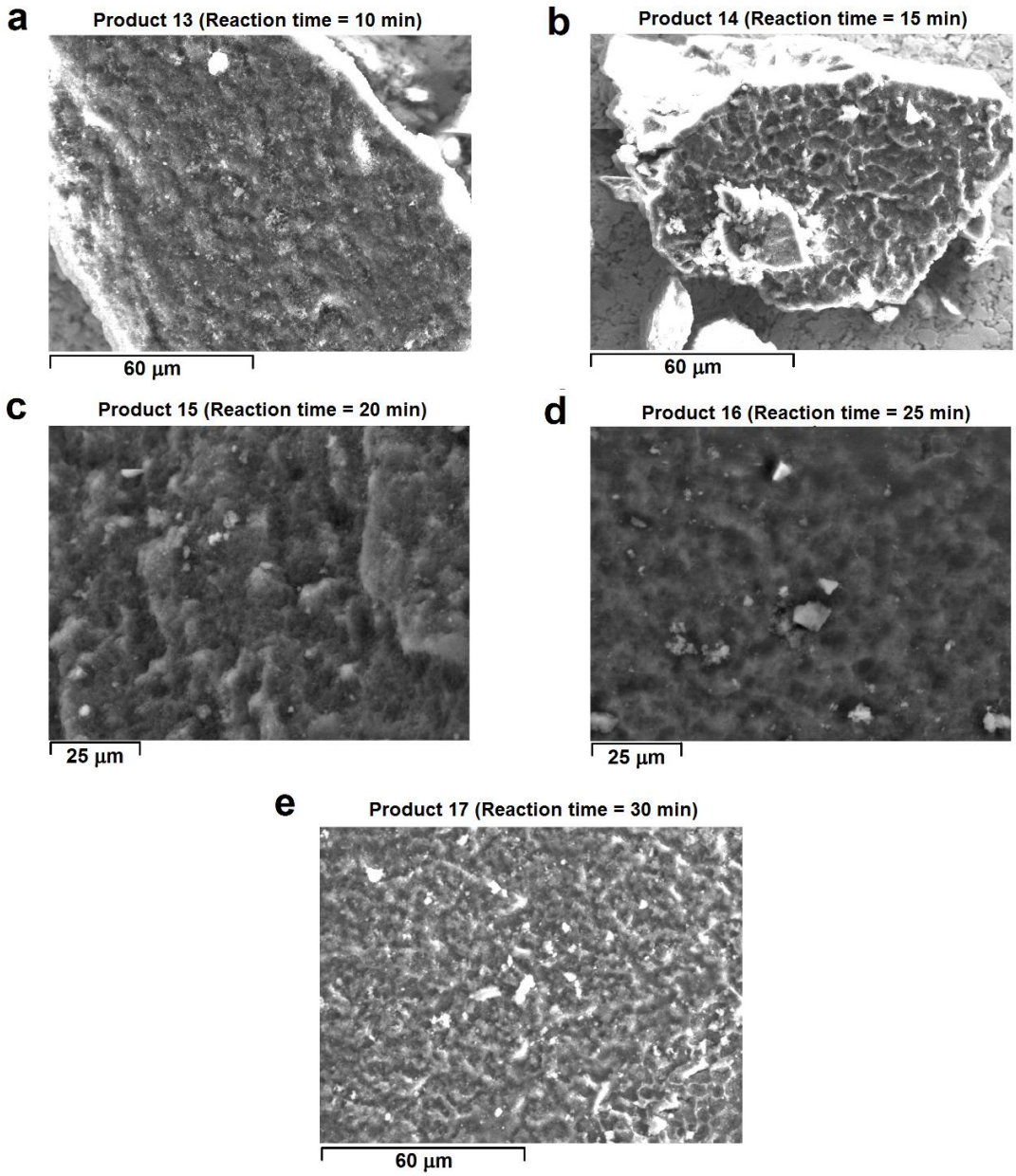

Figure 5-54 SEM micrographs of products from Time Experiment showing patterns formed on the surface of product powder (Images produced by SEM/EDX facilities at National Physical Laboratory, London)

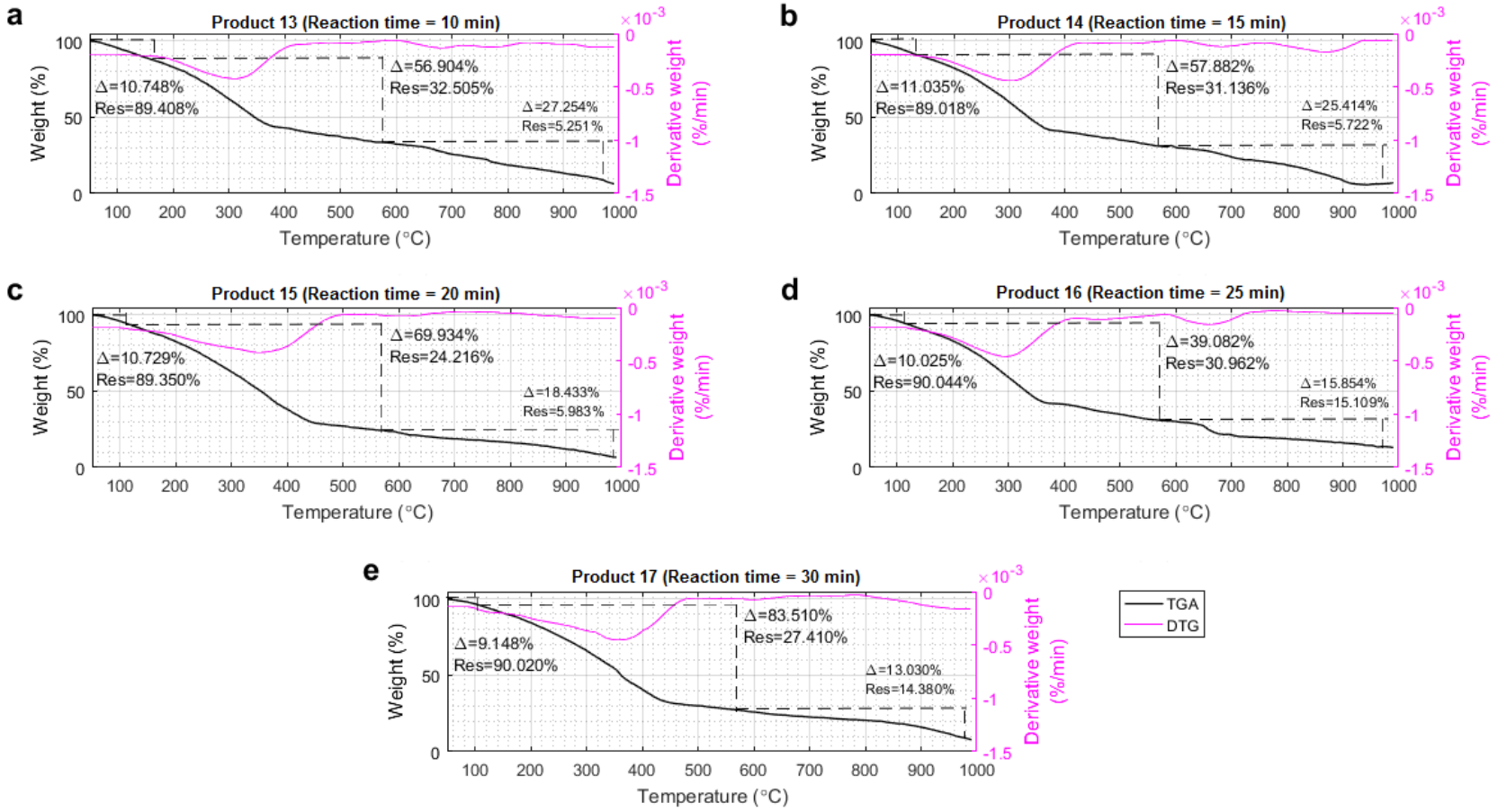

Figure 5-55 TGA thermograms of Product 13-17 (using different lengths of reaction step during syntheses) from Time Experiment

It was recalled that, when TGA measurements for this experiment were required, the team at Shrivenham informed in advance that the TGA instrument was in an extremely busy period (fully booked every day) which would continue for a while. It was such an immense and generous support the research received from the team that, despite the extremely busy schedule, some slots were kindly arranged for this research to access the instrument. Unlike other measurements in this research, as the available measurement schedule became rather tight, it was not possible to include 'furnace cleaning' (a blank run from room temperature to the maximum temperature for burning off any condensates or residues from other substances remaining inside the furnace) prior to the beginning of the measurement schedule for this experiment.

Based on this fact, it was believed that abnormalities of TGA thermograms of Product 13-17 could come from decomposition of condensates or residues from other substances remaining inside the furnace. It was also believed that these condensates and residues accumulated on the parts which could directly affect weight detection, i.e. the hang-down metal sample pan and the small metal chain connecting the sample pan in the furnace to the balance in the top compartment, shown in Figure 5-56. As measurement progressed, these substances came off, resulting in extra loss of weight detected which did not come from the product in the crucible.

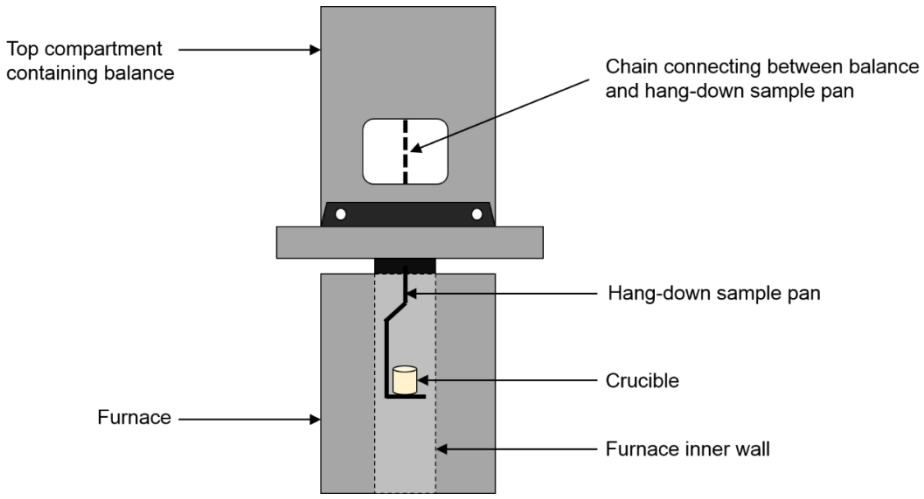

Figure 5-56 Simplified diagram of main components connecting the crucible inside furnace to the balance of the TGA instrument used in this research

Interference from extra weight loss of unidentified residues in the furnace appeared in the TGA thermograms, and affected the calculation of $n_{(OH)}$ according to 'TGA method' as demonstrated in Table 5-21. Again, the method is unsuitable for analysis of these affected data.

Table 5-21 Demonstration of the impact of interference on calculations via 'TGA method' resulting in abnormally high values

Product	Reaction time (min)	x	y	$n_{(OH)}$
13	10	56.904	32.505	75
14	15	57.882	31.136	79
15	20	69.934	24.416	122
16	25	59.082	30.962	81
17	30	63.510	27.410	99

Nevertheless, the interference fortunately did not extend to the first part of TGA curves in most of the products, and information of weight loss before the affected temperatures could still be extracted and used. Although the first part of TGA curve of Product 17 was slightly affected, with careful inspection of DTG curve and selection of appropriate range, some information on the first weight loss could still be extracted and used in 'TGA-EDX method' together with EDX results for estimation of $n_{(OH)}$ of the products.

To avoid errors from including unrelated weight loss, special care was put into inspecting the DTG curves of all thermograms to identify the range of temperature before 200°C that was interference-free in each thermogram, i.e. the range which could be confidently considered to have arisen from the loss of physically bound water molecules.

Although a portion of these molecules might be unavoidably ignored despite their existence, it was suggested that the errors from including false weight loss (i.e. interference) was more severe than the errors from excluding a small percent of physically bound water molecules which could desorb at the problematic temperatures.

For particle size characterisation of the Product 13-17, DLS results in Figure 5-57 reveal that all products generally show similar size distributions, with the biggest portion of the detected particles around 100 nm in diameter and the second biggest portion of particles around 30-40 nm.

Similar to TBAH and NaOH Experiment, only one high-magnification SEM micrograph could be obtained for one product from this experiment, due to very limited SEM/EDX services affordable under limited budget. SEM micrograph of Product 17 at 160kx in Figure 5-58 shows a lot of spherical particles, diameter of approximately 100 nm for almost all observable particles. This is in agreement with its DLS results (Figure 5-57c). Again, it was presumed that, had the high-magnification SEM micrographs of other products been obtained, they should show particle distributions in agreement with the corresponding DLS results.

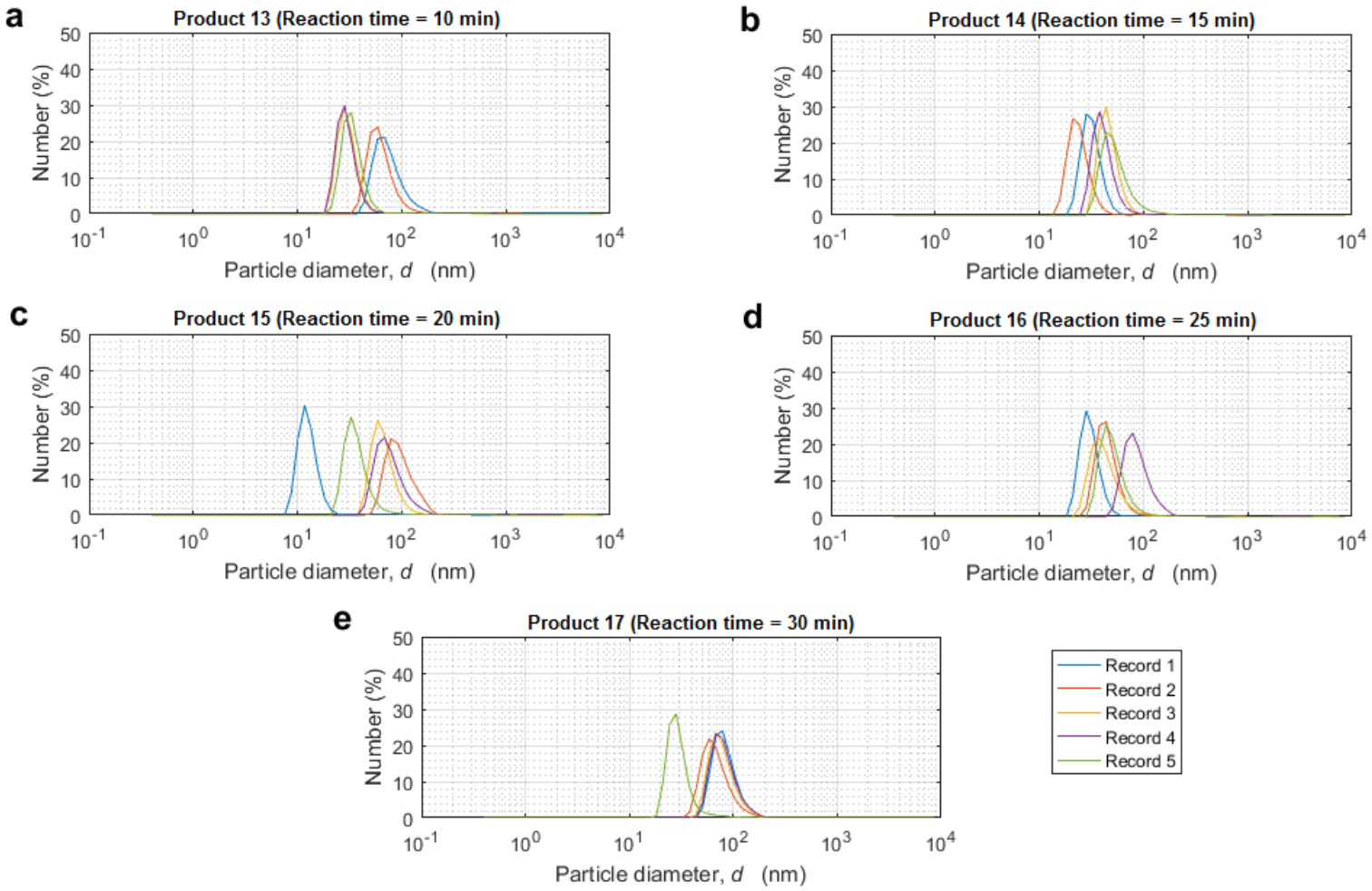

Figure 5-57 DLS results of Product 13-17 (using different lengths of reaction step during syntheses) from Time Experiment

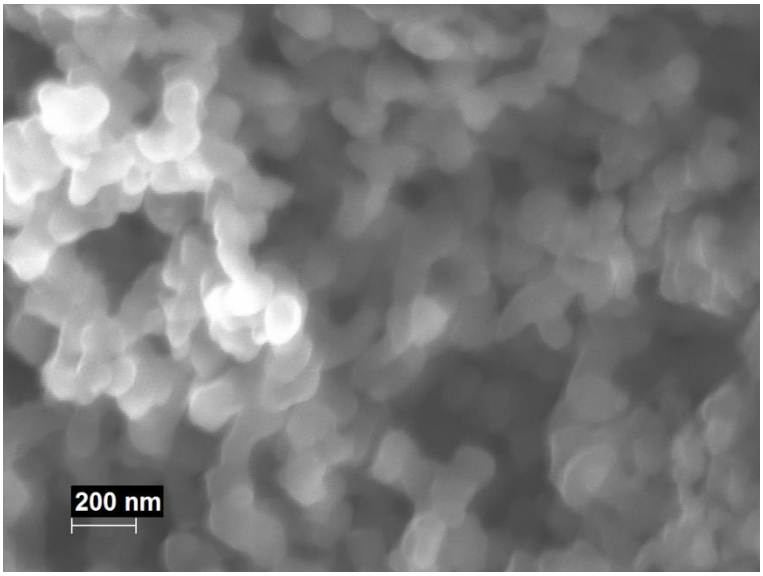

Figure 5-58 SEM micrograph of Product 17 (Reaction time = 30 min) from Time Experiment at 160kx (Image produced by SEM/EDX facilities at National Physical Laboratory, London)

5.5.2 Estimation of level of hydroxylation

Based on the fact that epoxide absorption was not shown in any of the infrared spectra of the products, epoxide group was not included in the model of product formula for the estimation of $n_{(OH)}$.

Accordingly, 'TGA-EDX method' developed in this research was used for estimation of $n_{(OH)}$ of Product 13-17 based on the normal fullerenol model, i.e. **$aC_{60}(OH)_n \cdot bH_2O$ with cNa_2CO_3 as surroundings**. The obtained calculation results and analysis of molecular and elemental compositions of the products are shown in Table 5-22.

Table 5-22 Calculation results using 'TGA-EDX method' for Product 13-17 showing determined product empirical formula and analysis on molecular and elemental compositions

Product	Reaction time (min)	Calculation results							
		Product empirical formula	%wt $C_{60}(OH)_n$	%wt H_2O	%wt Na_2CO_3	%C	%O	%Na	%H
13	10	$C_{60}(OH)_{12}.9H_2O$ with $5Na_2CO_3$	57.18	10.02	32.80	48.27	35.64	14.23	1.86
14	15	$C_{60}(OH)_8.10H_2O$ with $5Na_2CO_3$	54.66	11.49	33.84	49.81	33.72	14.69	1.79
15	20	$C_{60}(OH)_{10}.10H_2O$ with $5Na_2CO_3$	55.63	11.25	33.13	48.75	35.00	14.38	1.88
16	25	$C_{60}(OH)_{10}.9H_2O$ with $5Na_2CO_3$	56.26	10.24	33.50	49.30	34.39	14.54	1.77
17	30	$C_{60}(OH)_{12}.8H_2O$ with $5Na_2CO_3$	57.82	9.01	33.17	48.81	35.04	14.39	1.75

5.5.3 Effect of reaction time on level of hydroxylation

Calculation results from 'TGA method' (Table 5-21), though would not be involved in any further analysis, were plotted together with the results from 'TGA-EDX method' (Table 5-22) against reaction time to visualise the differences between the two methods, shown in Figure 5-59. The figure also served as a final confirmation to exclude the results from 'TGA method' from further analysis.

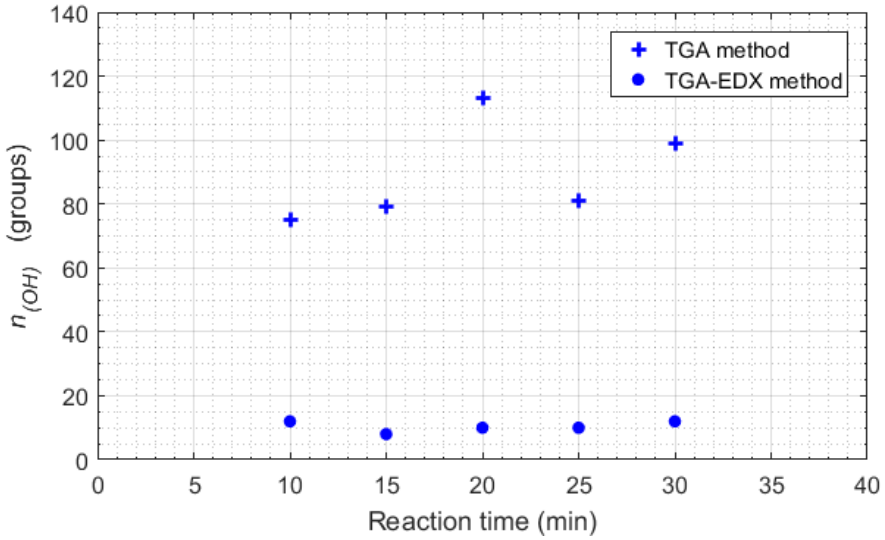

Figure 5-59 $n_{(OH)}$-time plots comparing results from 'TGA method' with 'TGA-EDX method' for Product 13-17

It can be seen from Figure 5-59 that the $n_{(OH)}$-time plot of Product 13-17 ($n_{(OH)}$ values estimated via 'TGA-EDX method') appears horizontally linear. Now excluding unrelated information, a closer inspection was conducted. It was found that the $n_{(OH)}$-time plot of Product 13-17 seems to be a small fluctuation around $n_{(OH)}$ = 10 groups, as can be seen in Figure 5-60. This could mean that the reaction might have already reached saturation even with the reaction time as short as 10 minutes, which is half of the required reaction time in the original procedure (Li et al., 1993). However, these results could not be used to claim that the saturation point of this reaction starts at 10 minutes after the start of the reaction yet since there was no information for reaction time less than 10 minutes available from this experiment.

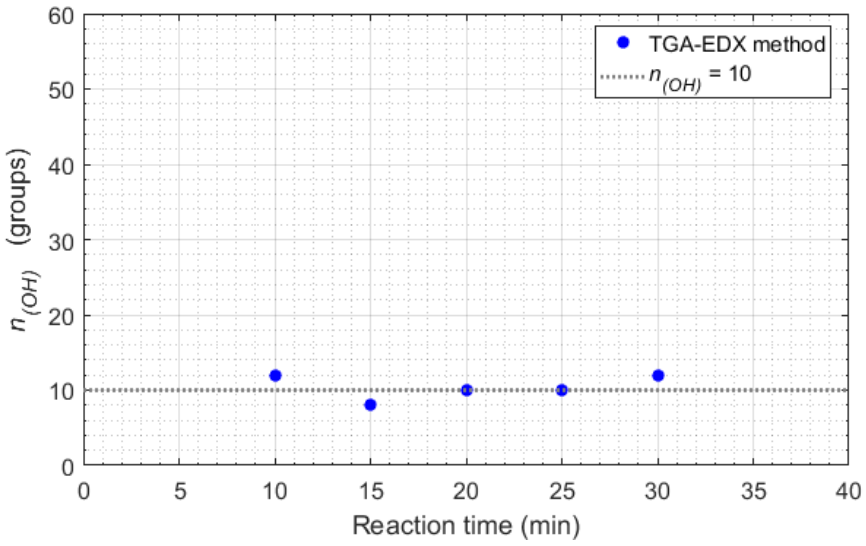

Figure 5-60 Plots of $n_{(OH)}$-time and $n_{(OH)}$=10

With reference to the suggestion from NaOH Experiment that the hydroxylation of C_{60} (in a toluene reservoir) could be considered as a liquid-solid adsorption process, it was further suggested here that the relationship between reaction time and $n_{(OH)}$ might also resemble an adsorption isotherm, i.e. the behaviour of the plot before reaction time equals to 10 minutes could be a convex. From this further suggestion, it seems that the critical region of the relationship lies between reaction time between 0 and 10 minutes. Also, to confirm if the reaction had actually reached a complete saturation, information from reaction time much greater than 30 minutes, for example, 1 hours, several hours, or even days or weeks, is essential.

It might have been possible to discover even more interesting and useful behaviour of the relationship between reaction time (vigorous mixing step) and the resulting level of hydroxylation had this research been able to conduct more syntheses in accordance with the direction guided by analysis of results from Product 13-17. Unfortunately, this was not possible due to several limitations the research had suffered from, especially those related to working space, availability and accessibility of analytical facilities, and time and budget remained.

Although the achieved results and analysis in this experiment came from a narrow range of the parameter of interest, at least it was now known that, within the range of reaction time from 10 to 30 minutes, increasing the time did not cause a significant change in the resulting level of hydroxylation.

Increasing the reaction time (i.e. duration of vigorous mixing step) might not affect much on the level of hydroxylation, however it did increase the amount of isolated yield. By increasing reaction time from 10 to 30 minutes, the resulting PPF mass ratio increases by approximately 60%, as shown in Figure 5-61.

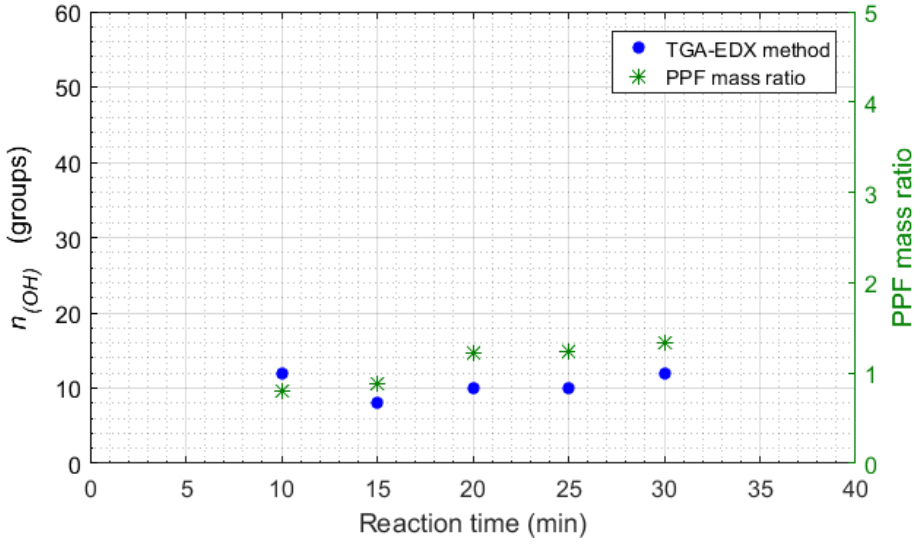

Figure 5-61 $n_{(OH)}$-PPF-Time plot comparing $n_{(OH)}$ and PPF mass ratio

Similar to TBAH and NaOH Experiments, calculation results for approximation of theoretical yield and percent yield of products from Time Experiment followed the approach explained in Appendix C. The results are given in Table 5-23 and Figure 5-62. Further discussion associated with percent yield is provided in Section 5.6.3.

Results and discussion in this experiment would be used in conjunction with those from the studies of other 2 selected parameters to develop the aimed synthesis protocols, which is provided in Section 5.7.

Table 5-23 Approximation of theoretical yield, actual yield and percent yield of products from Time Experiment

Product	Reaction time (min)	Estimated empirical formula	Theoretical yield (mg)	Actual yield (mg)	% yield
13	10	$C_{60}(OH)_{12}.9H_2O$ with $5Na_2CO_3$	103.8	56.4	54.4
14	15	$C_{60}(OH)_8.10H_2O$ with $5Na_2CO_3$	95.8	35.1	36.8
15	20	$C_{60}(OH)_{10}.10H_2O$ with $5Na_2CO_3$	100.1	60.2	60.1
16	25	$C_{60}(OH)_{10}.9H_2O$ with $5Na_2CO_3$	99.5	56.0	56.3
17	30	$C_{60}(OH)_{12}.8H_2O$ with $5Na_2CO_3$	103.6	41.2	39.8

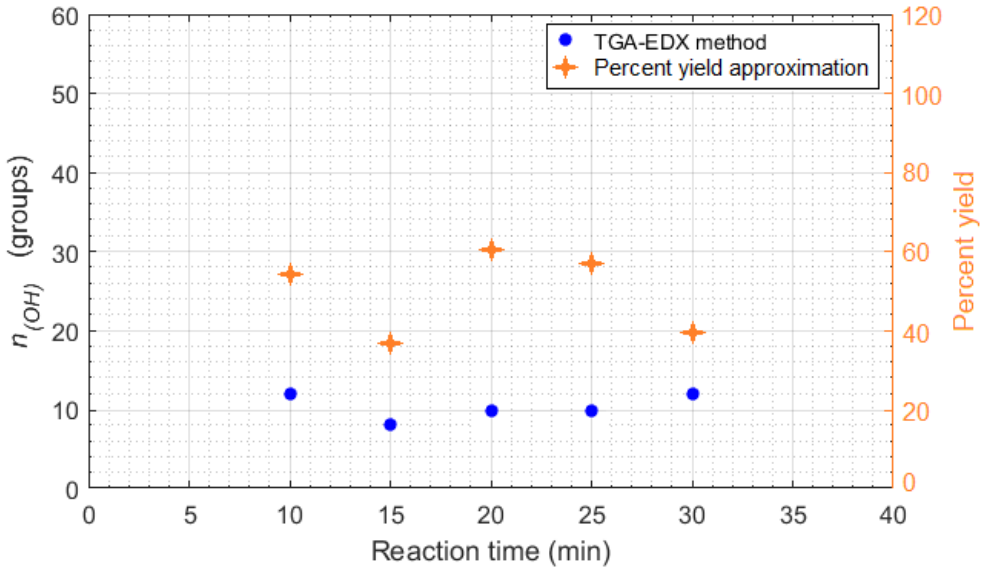

Figure 5-62 $n_{(OH)}$-Percent yield-Time plot comparing $n_{(OH)}$ and percent yield

5.6 Additional discussion on fullerenol synthesis using the selected route, and minimum requirements of process design for fullerenol manufacturing

To avoid distraction and provide a good flow of discussion of results within each experiment, additional aspects of fullerenol synthesis using the selected route is discussed in detail in this section. These include discussion on fullerenol aggregation, consideration on possible sources of variations within the process, precautions towards the use of silicone grease in the production line, and the presence of sodium carbonate and epoxide groups in the product. Combining analysis and discussion throughout *Part One* experiments, suggestions for minimum requirements of process design to achieve effective and efficient fullerenol manufacturing are provided at the end of this section.

5.6.1 Aggregation of fullerenol particles

According to the literatures (Kokubo et al., 2008; Kokubo et al., 2011; Kokubo, 2012), the size of an individual fullerenol particle was reported to be as small as 1 nm based on DLS measurements. However, the majority of particle sizes detected in this research were greater than 1 nm. Among all the fullerenol

synthesised, the largest detected particle diameter was as large as approximately 250 nm. TEM and SEM micrographs clearly revealed the secret that large particles detected were actually a cluster of smaller particles, as can be seen in Figure 5-63 and Figure 5-64. In addition, particle size profiles obtained from electron micrographs were in agreement with the corresponsing DLS results for all products. Therefore, based on the fact that fullerenol identity was confirmed in all products from analysis of characterisation results, DLS results, as well as TEM and SEM micrographs, suggested that the large particles detected resulted of fullerenol aggregation. This argument is supported by the fact that individual fullerenol aggregates very easily and quickly to form larger clusters (Kokubo, 2012).

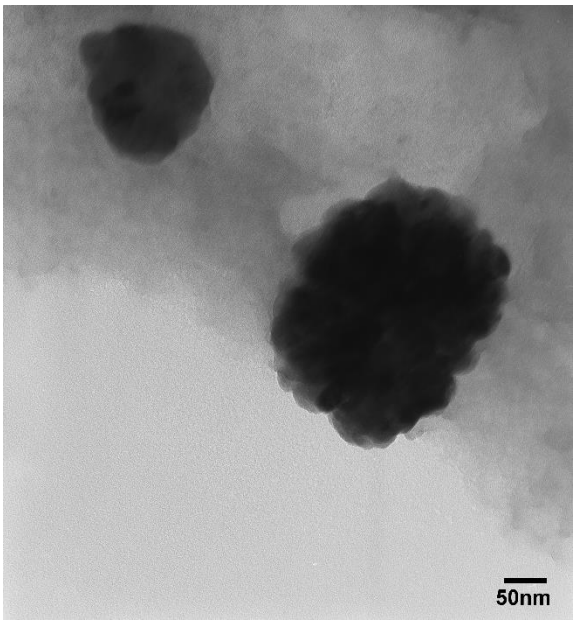

Figure 5-63 TEM micrograph (115kx) of synthesised fullerenol revealing the existence of smaller spherical particles within large detected particles. (Image produced by TEM facilities at Cranfield University.)

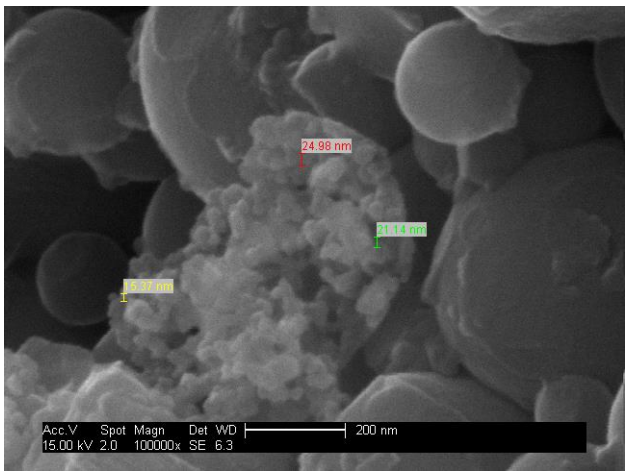

Figure 5-64 SEM micrograph (100kx) of synthesised fullerenol showing a large ruptured particle (approximately 500 nm) which contains a lot of smaller spherical particles inside. The yellow, red and green tags in the micrograph indicate sizes of smallest diameters detectable (reading 15.37, 24.98 and 21.14 nm respectively). (Image produced by SEM facilities at Cranfield University.)

5.6.2 The water-insoluble solids removed during synthesis of fullerenol

During a synthesis of fullerenol using the selected route, water-insoluble black solids were filtered out to obtain product-containing aqueous layer which was further processed to finally yield fullerenol. It was expected that the solids were unreacted fullerene. Samples of these solids were subjected to FTIR and SEM characterisation. Infrared spectrum (Figure 5-65) reveals that the solids comprised of C_{60}, residual toluene, moisture and possibly a certain amount of fullerenol still trapped inside the bulk of insoluble solids. SEM micrograph of the solid (Figure 5-66a) shows a morphology similar to that of pristine C_{60} (Figure 5-66b), but different to the micrographs of the synthesised fullerenol.

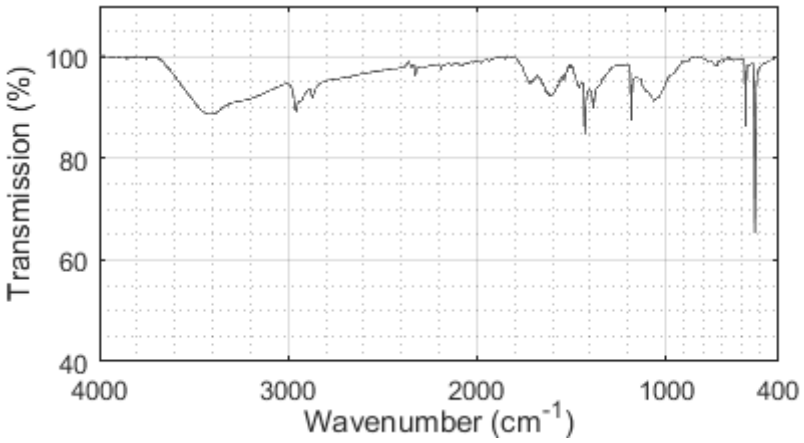

Figure 5-65 Infrared spectrum of the water-insoluble black solids filtered out during product separation process

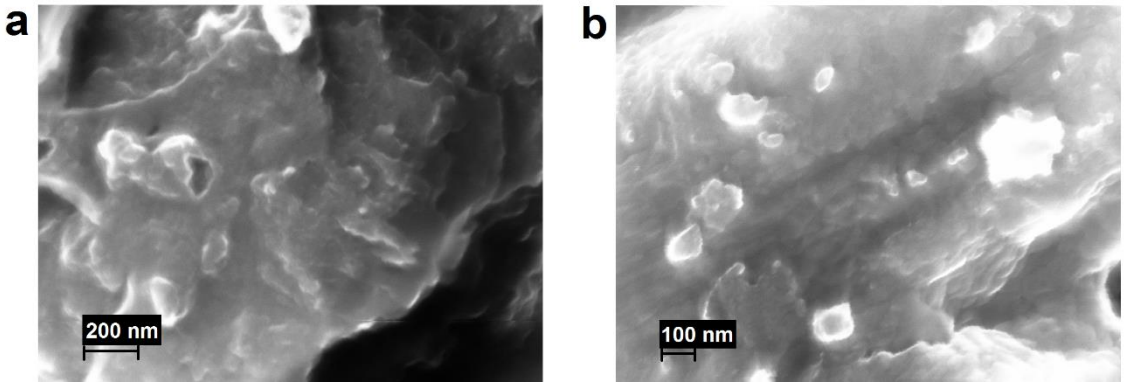

Figure 5-66 SEM micrographs (160kx) of a) water-insoluble solids filtered out during product separation process, and b) pristine C_{60} (Images produced by SEM/EDX facilities at National Physical Laboratory, London)

5.6.3 Comments on yield and production consistency of the selected route and consideration for possible sources of variations

Following the approach to approximate theoretical yield and percent yield of fullerenol synthesis based on the values of mass and molar mass of product and starting material described in Appendix C, percent yield of the original TBAH-NaOH route by Li and colleagues (1993) was 88.5 (see Appendix C.1). However, the TBAH-NaOH route used as a basis throughout this research was a slightly modified version, and was first used in the Consistency Evaluation Experiment from which percent yield was approximated to be 89.7 (see

Appendix C.2.1). This could be used to suggest that, in terms of yield, performance of the modified process was similar to the original version. From TBAH and NaOH Experiments (Figure 5-39 and Figure 5-51), it could be seen that percent yield responded to the amount of phase-transfer catalyst (the key to make the desired reaction feasible) and the amount of source of hydroxyl ions. Within the test range, the highest approximated percent yield was obtained when 24 drops TBAH were used in the TBAH Experiment (63.9%). For NaOH Experiment, using 8.0 ml NaOH solution gave the highest percent yield (90.9). The range of 10-30 minutes reaction time (Figure 5-62) did not seem to cause noticeable changes to percent yield (it should be noted that some of Product 14 and Product 17 were lost during collection step, and total mass was assumed to be similar to other batches from Time Experiment). The lowest percent yield from the three experiments on process parameters was from the synthesis using 0.5 ml NaOH solution (24 drops TBAH).

It was realised that the approximated percent yield of Product 4 (TBAH Experiment), Product 10 (NaOH Experiment) and Product 15 (Time Experiment) were similar among themselves (approximately 60%), but were smaller than that of Consistency Evaluation Experiment (89.7%) despite being produced from the same process conditions (i.e. TBAH = 24 drops, NaOH = 2.0 ml, and reaction time = 20 min). It was suggested that the cause of this difference could come from the filtration step for removing unreacted fullerene from the process.

As a general filtration practice, the filter cake was washed after filtration finished. Each round of filter cake washing used an additional 30-50 ml de-ionised water to extract fullerenol from the water-insoluble filter cake into the brown filtrate, and took approximately 45-60 minutes to complete (based on power of the vacuum pump used as vacuum source for the filtration). For the Consistency Evaluation Experiment, filter cake washing could be done thrice per batch. However, there were limitations on availability of working space during TBAH, NaOH and Time (as well as Scale-up) Experiments, which caused further limitation on available time. To accommodate all the required and planned experiments in this research, filter cake washing had to be reduced

to only once for each batch of these experiments, hence the reduced amount of fullerenol extracted and a smaller percent yield compared to that of the Consisteny Evaluation Experiment.

According to the analysis of results from Consistency Evaluation Experiment, it was determined that the route could offer a consistent production in terms of level of hydroxylation in the product at significance level of 0.025 based on the accessible working environment and equipment. This means that improvement on the process could raise the significance level to 0.05 or even higher, for example, using equipment with greater precision, using chemicals with better grades, and adjusting the working environment to suit the nature of the process.

Excluding external sources of process variations (which were beyond control), other possible sources of variations within the process (internal sources) were considered and discussed here regarding both $n_{(OH)}$ and yield.

The reaction of interest requires a homogeneous solution of C_{60}-containing toluene. According to the original procedures (Li et al., 1993) 80 mg of pristine C_{60} was weighed, added into 60 ml of toluene, and – to achieve a good dissolution – ultrasonication was applied until complete disappearance of the black power of pristine C_{60} was visually confirmed and the colourless liquid of toluene changed into dark violet. Considering this fact, it is suggested relying only on the measured mass of pristine powder added into toluene might not be efficient enough to achieve a high production consistency. The commercially available C_{60} still contains a fraction of other substances such as C_{70} and other possible forms of carbonaceous soot as by-products from C_{60} manufacturing. Each sample of 80 mg pristine powder taken out from the bottle might actually contain less than 80 mg of C_{60}, hence variation to the process. Therefore, to achieve a better production consistency, it is suggested that the synthesis should rely on the actual concentration of C_{60} molecules present in obtained dark violet solution instead. Quick and convenient quantitative analytical technique such as UV-Vis spectroscopy could be applied for this purpose, both in laboratory and industrial scales.

Liquid transfer equipment for transferring TBAH into the reaction mixture was also considered as another possible source of variation. Standard Pasteur pipettes were used for dropping TBAH solution into the reaction mixture. One Pasteur pipette of the same type and same manufacturer was tested for errors by measuring mass of an individual drop of TBAH produced by this pipette for a total of 30 drops. It was determined that a drop of TBAH from this type of pipettes from this supplier equals to 0.0222 ± 0.0004 g (95% confidence interval).

Dissolving solid sodium hydroxide into water (to produce sodium hydroxide solution) is an exothermic process, raising the solution temperature. Solubility of sodium hydroxide at 20°C is 109 g/ 100 ml (Centers for Disease Control and Prevention, 2015). In case of the specified concentration 100% w/v (Li et al, 1993) used for all fullerenol syntheses in this research, the increased solution temperature (due to exothermic dissolution process) might temporarily raise solubility limit, and there could be some recrystallisation of the surplus portion of dissolved sodium hydroxide when the solution has cooled down (forming white solids). Although not visually observed in any of the sodium hydroxide solutions freshly prepared for each synthesis, it might be possible that some recrystallisation was happening at such a very small scale that the recrystallised portion was insufficient to form visible solids. This phenomenon might cause slight variations in actual concentrations of sodium hydroxide solutions between batches, hence another possible factor affecting production consistency.

5.6.4 Precautions towards using silicone-based material as lubricants in the production line

During the syntheses for Consistency Evaluation Experiment, silicone grease was applied to the joint connecting a glass valve (vent) to the condenser of the rotary evaporator. As previously discussed in Section 5.2.2, it was permanently removed from the research (and was strictly prohibited to the rest of the experiments) due to the fact that silicone contamination affected analysis of TGA thermograms, not to mention that the contamination raised an issue with purity and quality of the products.

Silicone grease is a common lubricant used for several applications in both laboratory and industrial scales. Silicone contamination is also among the most common and insidious contaminations within manufacturing plants. Although silicone contamination occurs through a direct physical contact between the silicone material and the surface most of the time, there have been a number of cases reporting a less obvious contamination route, i.e. indirect contact through highly volatile silicone-based molecules travelling in air streams. This is due to the fact that silicone-based material with low molecular weight has high volatility. Not only it is very demanding to identify contamination from silicone, removing is also very difficult and it is not guaranteed if the initial properties of the contaminated material or surface could be brought back (Petrie, 2013).

5.6.5 The presence of sodium carbonate

With reference to the analyses of characterisation results in each experiment, it was found that sodium carbonate was present in almost all products except the four batches in Consistency Evaluation Experiment (which was the only experiment conducted in a laboratory different to the rest of the experiments in this research). Based on graphical evidences from SEM micrographs of each affected product, it could be suggested that sodium carbonate was formed separately, i.e. not incorporated as part of the fullerenol molecule but existed alongside fullerenol particles. As previously discussed in Section 5.3.1, it was suggested that sodium carbonate was formed by the reaction between sodium hydroxide solution and ambient carbon dioxide.

Through SEM micrographs, in conjunction with EDX results, the presence of sodium carbonate was suggested from observation of needle-like crystals or, if present in less amount, pattern of solids covering the surface of the product powder/flake. A sample of water-insoluble solids removed before precipitation step during the synthesis was subjected to SEM characterisation and its micrograph (Figure 5-67) reveals that sodium carbonate was present in these solids as well (possible at a larger proportion when compared to the product, considering the amount of needle-like crystals seen).

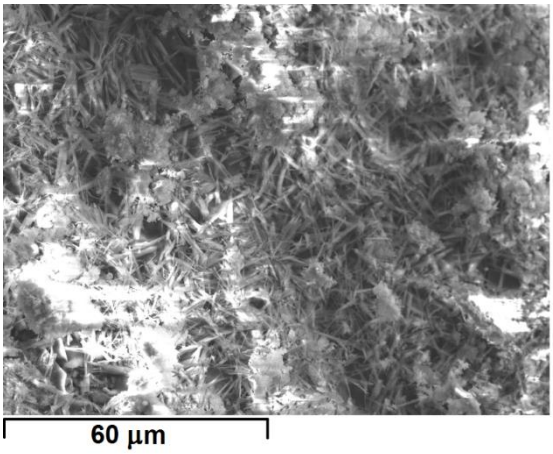

Figure 5-67 SEM micrograph of a sample from water-insoluble solid removed before precipitation step during the synthesis. A numerous amount of needle-like crystals, suggested to be sodium carbonate, is present. (Image produced by SEM/EDX facilities at National Physical Laboratory, London.)

It was possible to analyse infrared absorptions attributed to sodium carbonate from the infrared spectra, however, it might be difficult for TGA thermograms. Noticeable mass loss due to thermal decomposition of pure sodium carbonate begins above 1000°C. However, it could also be observed at lower temperatures such as 900°C if sodium carbonate is mixed with some carbon black (Kim and Lee, 2001) – see Appendix D. Based on this information, it was suggested that weight loss associated with sodium carbonate might be partially present in some TGA thermograms. However, this portion was mostly not seen due to the fact that the maximum operating temperature of the TGA instrument used in this research was only 1000°C. As a result, TGA was not generally involved in suggestion for existence of sodium carbonate in the product.

Referring to the special note that the four batches from the Consistency Evaluation Experiment were the only products which were produced in a different laboratory and their syntheses were the only ones which did not show the trace of white solid, it might be suggested that the ambient levels of carbon dioxide were different between the laboratory used to produce the four batches for consistency evaluation and another laboratory used for the rest of the experiments, with the latter location possibly having a higher level of ambient carbon dioxide.

Although sodium carbonate is generally not highly toxic or harmful to health, its presence is undesirable from the aspects of product purity, characterisation (especially EDX and FTIR), and production quality control. Therefore, carbon dioxide should not be allowed in any synthesis of fullerenol using the selected route. Nevertheless, it should be noted that conducting the synthesis under an inert atmosphere without any supply of oxygen gas would result in a worse situation due to the fact that the reaction between C_{60} and hydroxide ions to form fullerenol required the presence of oxygen (Li et al., 1993; Alves et al., 2006). Therefore, it is suggested that fullerenol synthesis via TBAH-NaOH route should be conducted in a CO_2-free atmosphere and directly supplied with oxygen stream to avoid complications due to formation of sodium carbonate.

5.6.6 The presence of epoxide groups in addition to the desired hydroxyl groups

From analyses of characterisation results in Section 5.3.1 and 5.4.1, the results suggested that some products from TBAH and NaOH and Experiments contained epoxide groups in addition to the desired hydroxyl groups (and the unwanted sodium carbonate). The suggestion was based on the presence of infrared absorption around 880 cm^{-1} in the infrared spectra, and detection of weight loss with general onset temperature around 380°C in TGA thermograms, both of which are characteristics to epoxide functional group as well as fullerene epoxide (Wohlers et al., 1986; Chibante and Heymann, 1993; Evtushenko et al., 2003; Gonzalez et al., 2012). It was therefore suggested that the presence of epoxide groups within the product might be in the form of fullerene epoxide.

Formation of fullerene epoxide in this research was not believed to be part of the reaction pathway (hydroxylation of fullerene to form fullerenol) due to the fact that not every product synthesised from this route showed epoxide signals in characterisation. None of the products from Consistency Evaluation Experiment (and even all products from Reaction Time Experiment which were synthesised in the same laboratory as the affected products) did not show the presence of epoxide groups. Therefore, it was suspected that the origin of

fullerene epoxide in the affected products might come from the working environment.

Product 4 (TBAH Experiment), Product 10 (NaOH Experiment) and Product 15 (Reaction Time Experiment) were synthesised from exactly the same design for process conditions, i.e. TBAH = 24 drops, NaOH = 2.0 ml and reaction time = 20 minutes. Despite this fact, Product 4 and Product 10 showed presence of epoxide groups in both infrared spectra, while none of this was present in the case of Product 15. This fact may be used to suggest that the origin of formation of fullerene epoxide, which was suspected to be in the working environment, was not always or permanently present as well. Therefore, it was suspected that the origin of fullerene epoxide origin coincidently existed in the laboratory when the schedules for the syntheses of the affected products.

It was not appropriate to compare TGA thermograms of the three products as the thermogram of Product 15 were interfered in the range of interest with other unknown condensates and residues inside TGA furnace.

Literature on fullerene epoxide was consulted. Syntheses of fullerene epoxide were found and the reactions generally require special conditions and chemicals, for example, reaction which needs to be directly and continuously irradiated or reaction occurring at -78°C (Creegan et al., 1992, Heymann and Weisman, 2006). These conditions are certainly not applicable to this research and therefore these reactions were not considered as possible paths to explain the phenomenon. Nevertheless, some literature reported that fullerene epoxide can be formed at ambient temperature and pressure via reaction between C_{60} (in toluene) and ozone-containing oxygen streams (Heymann and Chibante, 1993a; Heymann and Chibante, 1993b; Heymann and Cataldo, 2001). Recently, Murdianti and colleagues (2012) also reported that even the ambient-level of ozone could transform C_{60} into fullerene epoxide ($C_{60}O$) and facilitated formation of colloidal fullerene-water system.

Figure 5-68 illustrates the structure of fullerene epoxide $C_{60}O$, which is a C_{60} fullerene cage with one oxygen atom bonded between two carbon atoms of the

cage structure. Although fullerene dissolves in toluene, fullerene epoxide does not (Heymann and Weisman, 2006; Dattani et al., 2015).

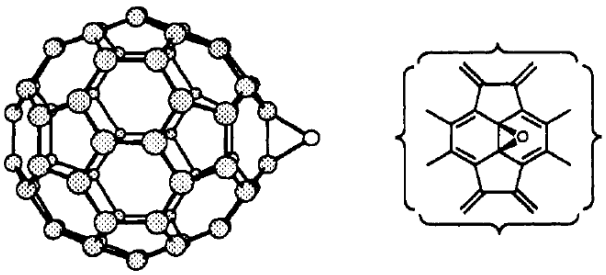

Figure 5-68 Schematic representation of $C_{60}O$ as ball-and-stick model (left) and abbreviated Schlegel diagram (right) (Creegan et al., 1992)

With reference to the point that these experiments were conducted in a laboratory which was different to the one used in Consistency Evaluation Experiment, and another fact that none of the batches from Consistency Evaluation Experiment contained epoxide signals, it was suspected that the two locations had different levels of ambient ozone (with the latter location having a higher level). Therefore, it was suggested that the origin of $C_{60}O$ formation in this research was the ambient ozone level in the laboratory where TBAH, NaOH and Reaction Time Experiment were conducted.

Towards the beginning of each fullerenol synthesis, toluene (colourless) was added into a beaker containing black powder of pristine C_{60}. The mixture was subjected to ultrasonication to facilitate dissolution of C_{60}. The colourless liquid changed into dark violet, and almost all black powder that was initially present in the liquid disappeared. Recalling laboratory records, it was found that a slightly more than usual amount of fine black solids was observed at the bottom of the beaker in some syntheses. The solids did not dissolve in toluene even when subjected to prolonged ultrasonication. It was suggested that the solids were $C_{60}O$ as a result of the reaction between C_{60} (in toluene) and ambient ozone level in the laboratory. This means that a fraction of C_{60} was transformed into $C_{60}O$. Heymann and Weismann (2006) described that the reaction first results in an intermediate 'ozonide' ($C_{60}O_3$) which is unstable and further dissociates into $C_{60}O$ and molecular oxygen (Figure 5-69).

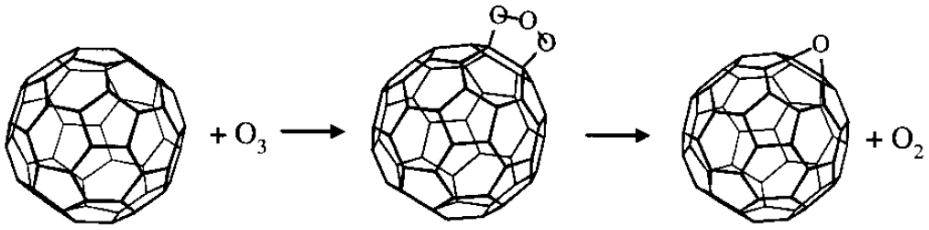

Figure 5-69 Schematic diagram illustrating chemical reaction between C_{60} fullerene and ozone, forming an unstable intermediate (ozonide) which dissociates into fullerene epoxide and molecular oxygen (Heymann et al., 2000)

Although some C_{60} cages were transformed into $C_{60}O$, it is believed that this should not obstruct the synthesis of fullerenol in theory due to the electrophilic nature of epoxide ring which should be reactive towards the nucleophilic hydroxyl ions. Reaction mechanism of this scenario was proposed based on nucleophilic attack on an epoxide ring (Figure 5-70). The reaction occurs in two steps – nucleophilic attack opening the ring, followed by protonation to give a diol structure (Wade, 2014).

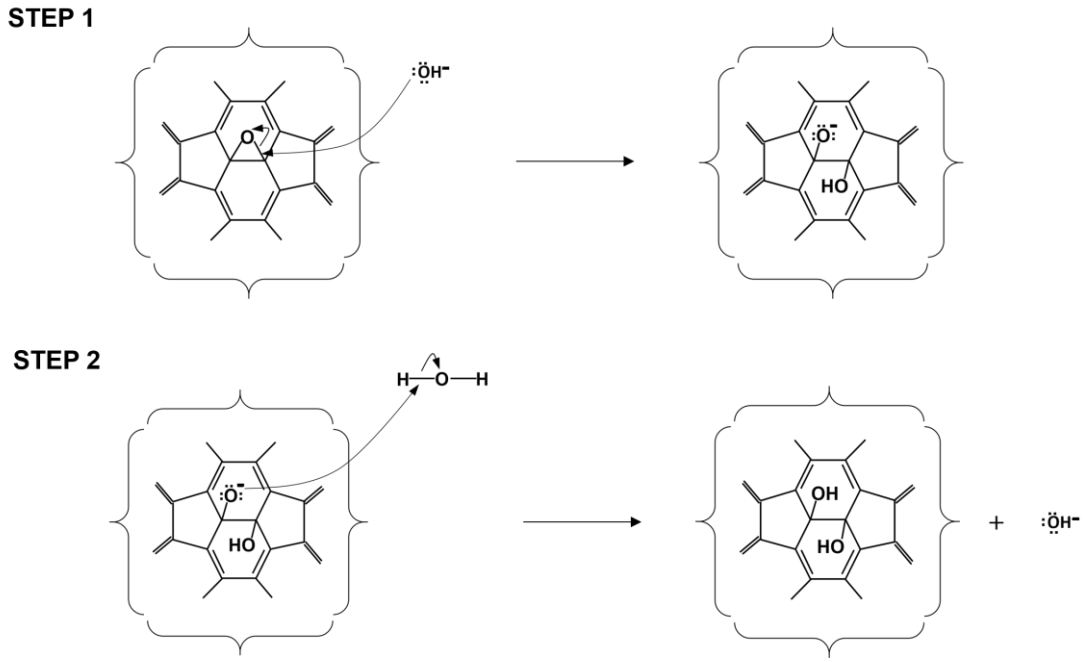

Figure 5-70 Proposed possible reaction mechanism between $C_{60}O$ (represented by simplified Schlegel diagram) and sodium hydroxide solution, resulting in a diol

If this was the case to all $C_{60}O$ molecules present in the system, there should not have been evidence of epoxide groups from product characterisation. However, the real situation was the opposite and indicated that something might have prevented some epoxide rings form being in contact with chemical species from aqueous phase. Here, an explanation was proposed that, once $C_{60}O$ molecules were formed inside toluene reservoir, individual $C_{60}O$ molecules aggregated with the epoxide ring pointing inside the cluster and resulted in a quasi-polar area (Figure 5-71). It was thought that difference in polarity between around the epoxide rings (more polarity) and the rest of the system (non-polar) was an important driving force for the aggregation in this manner (although there might be other factors as well which were still not fully understood).

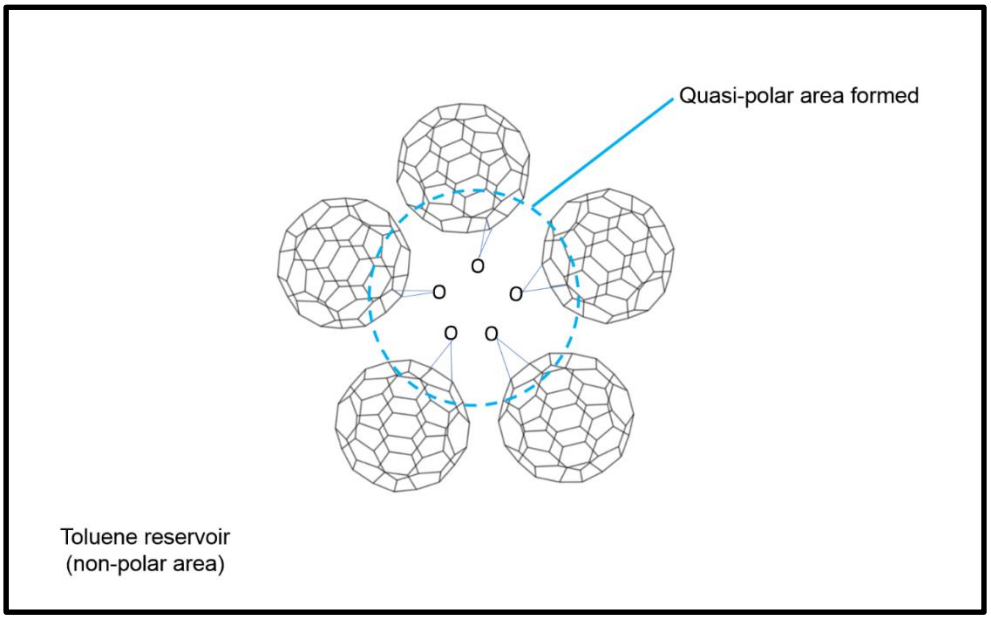

Figure 5-71 Illustration of the proposed formation of quasi-polar area by a first-generation cluster of $C_{60}O$ within the non-polar reservoir of toluene

This explanation is also generally in agreement with mechanism of fullerene epoxide cluster formation reported by Dattani and colleagues (2015). Although their proposed mechanism might be based on a different origin of fullerene epoxide generation (i.e. irradiation-initiated), the steps for cluster formation might apply to the phenomenon in this research from the step $C_{60}O$ is formed. Figure 5-72 illustrates the four steps in formation of $C_{60}O$ clusters. Starting from the initial stage where C_{60} is still well-dissolved in toluene, Stage 1 is reached

when $C_{60}O$ starts to form and starts to aggregate (first-generation of aggregates). Due to the fact that fullerene could also easily aggregate, first-generation aggregates could also come together and form clusters. As aggregation continues, Stage 2 is reached where clusters of a few hundreds nm in size are formed. If aggregation still continues, larger clusters in micron range are formed (Stage 3) and further aggregation leads to densification of the aggregates in the final stage (Stage 4).

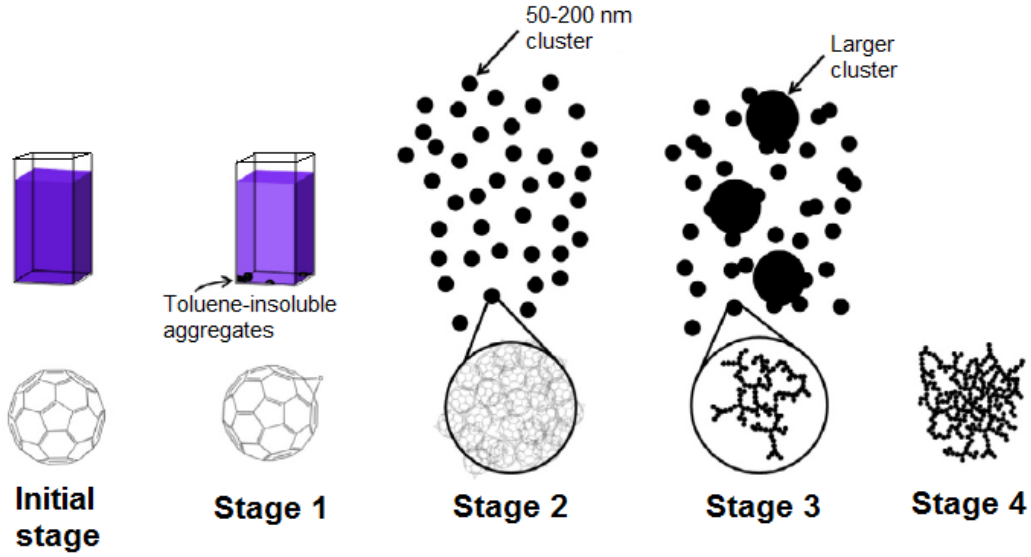

Figure 5-72 Formation of fullerene epoxide clusters within a C_{60}-toluene solution induced by ambient visible-light (figure modified from Dattani et al. (2015))

In a fullerenol synthesis using the selected route, the C_{60}-toluene solution was added with sodium hydroxide solution and TBAH and was vigorously stirred. However, some $C_{60}O$ clusters which were very dense and compact might have survived the vigorous mixing and had not been broken apart, resulting in some epoxide rings being unexposed to hydroxide ions and water molecules. Although the hydroxide ions and water molecule could not access inside these densely aggregated clusters, they could still attack the surfaces which are the C_{60} cages and introduced hydroxyl groups onto the accessible surfaces. Consequently, these hydroxylated $C_{60}O$ clusters could be extracted into water together with the desired fullerenol during product separation, coexisted in the

product and gave rise to epoxide absorptions in the infrared spectra and weight loss of fullerene epoxide in TGA thermograms.

From the aspect of product purity and quality control, it is thus recommended to prevent possible formation of $C_{60}O$ within the product by conducting the synthesis in an ozone-free environment.

5.6.7 Minimum requirements of process design for fullerenol production

It can be concluded from the discussion on presence of sodium carbonate and fullerene epoxide that, to prevent these contaminations and achieve a good result in fullerenol synthesis using the selected route (which is based on TBAH-NaOH route), the working environment should be free from both carbon dioxide and ozone. Guided by these points, the use of glove boxes supplied with nitrogen gas is recommended. To achieve maximum potential of the synthesis route, recommendation for a specially designed working environment is described below.

As protection from exposure to carbon dioxide and ozone are required as early as dissolution of C_{60} in toluene and are extended as far as until the dried product power is collected, it is highly recommended that the entire synthesis, including drying, is conducted inside the controlled atmosphere of a large and specially designed glove box. However, it is also recommended to locate the drying unit in a separate glove box to prevent interference to the synthesis chamber from heat flow. The two boxes could be connected through tightly-sealed lockable doors for transferring the final filter cake of brown precipitate to the drying unit. The main glove box where most of the synthesis work is conducted should have built-in supplies for oxygen gas (required for bubbling into the reaction mixture), de-ionised water, and cooling water (for evaporator's condenser), as well as outlets of gaseous streams from evaporator and vacuum filtration. Ultrasonication equipment should also be located inside the main glove box. Simplified illustration of the recommended design for working environment of laboratory-based fullerenol synthesis is provided in Figure 5-73.

Furthermore, it is highly recommended to avoid using silicone grease as lubricants in any part of the system for any scale of fullerenol synthesis.

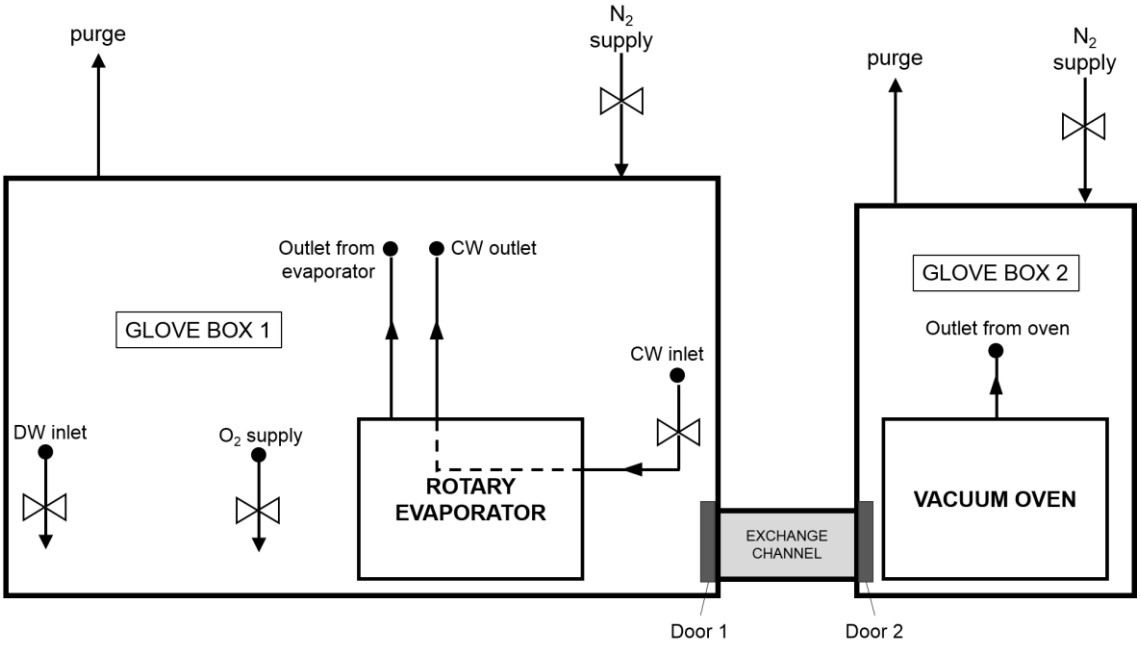

Figure 5-73 Schematic diagram of suggested working environment for laboratory-based fullerenol synthesis using the selected route. For simplication, ultrasonication equipment, glove slots and main doors connecting each glove box to the external environment are not shown in this diagram.

5.7 Synthesis protocols for producing fullerenol with specified level of hydroxylation within practical range based on TBAH-NaOH route

The following points could be made from analyses and interpretation of results from TBAH, NaOH and Reaction Time Experiments (Section 5.3 - 5.5):

- Achievable level of hydroxylation ($n_{(OH)}$) of the selected synthesis route was 8-16 groups (per fullerenol molecule), based on the working environment and equipment used in this research.
- The research has found the way to produce three different classes of fullerenol (i.e. low-, medium-, and high-$n_{(OH)}$) by specifically controlling amount of phase-transfer catalyst (TBAH), and amount of source of hydroxide ions (sodium hydroxide solution).

- Fullerenol with a low level of hydroxylation could be achieved by using either a low amount of TBAH or a low amount of sodium hydroxide solution. However, controlling low values of $n_{(OH)}$ via volume of sodium hydroxide is not favourable due to risk of a rather unappreciable amount of isolated product.
- For fullerenol with medium- and high-$n_{(OH)}$, with a chosen amount of TBAH, level of hydroxylation could be controlled by amount of sodium hydroxide added for the reaction.
- Reaction time might not have much influence on $n_{(OH)}$. However, within the experimented range (10-30 minutes), longer reaction time gave a bigger amount of isolated yield.

Based on the obtained results up to this point, it was realised that the condition of 'NaOH = 2.0 ml' could serve as a basis of developing synthesis protocols for the three different classes of fullerenol as it produced reasonable yield and could be considered as a link between process conditions to produce the low-, medium- and high-$n_{(OH)}$ products. When used together with 24 drops of TBAH for the reaction, medium-$n_{(OH)}$ fullerenol can be produced. When paired with 3 drops of TBAH, low-$n_{(OH)}$ fullerenol could be obtained. On the other hand, changing to NaOH = 8.0 ml and pairing with 24 drops of TBAH resulted in high-$n_{(OH)}$ fullerenol. It should be noted that the terms 'low', 'medium' and 'high' used here were in relation to the route's practical range.

Three synthesis protocols based on the selected route (TBAH-NaOH) for producing three different classes of fullerenol with specified level of hydroxylation within the route's practical range were then developed as described in the following sections.

5.7.1 Protocol 1 – Synthesis of fullerenol with $n_{(OH)} < 10$ groups

1. *Working environment*

   It is highly recommended that the working environment for the entire synthesis is free from ozone and carbon dioxide to avoid undesirable formation of fullerene epoxide and sodium carbonate contaminating the product.

2. *Preparation of homogeneous C_{60}-toluene solution*

   80 mg of pristine C_{60} fullerene is weighed and carefully transferred into a heavy-duty beaker, followed by addition of 60 ml of toluene. The beaker is subjected to ultrasonication for 15 minutes in an ultrasonic bath. Upon completion, a clear, dark violet solution is obtained.

3. *Preparation of sodium hydroxide solution*

   Solid sodium hydroxide is dissolved into de-ionised water at a ratio of 1 g/1 ml (100%w/v).

4. *Preparation of TBAH solution*

   Prior to each use, it is recommended to warm TBAH solution in a water bath at a temperature up to 38°C for a few minutes to re-dissolve any crystallised portion as a result of low temperatures. The stock should be allowed to cool down and thoroughly mixed before use.

5. *Reaction between C_{60} and sodium hydroxide solution in presence of oxygen and TBAH phase-transfer catalyst*

   The prepared homogenous C_{60}-toluene solution is transferred into the reaction flask. Using a standard Pasteur pipette, 3 drops of TBAH solution is added into the C_{60}-toluene solution. 2.0 ml of 100%w/v sodium hydroxide solution is then added into the solution. This forms the reaction mixture. The mixture is vigorously stirred for 20 minutes in presence of oxygen. The dark violet liquid turns colourless within a few seconds after the reaction starts, and black semi-solid substance is formed inside the reaction mixture. Upon completion, the mixture in the reaction flask consists of black semi-solid in a reservoir of clear colourless liquid (toluene).

6. *Separation*

6.1 Toluene removal

Using a rotary evaporator with water in the heating bath preheated up to 90°C (depending on degree of vacuum achievable by the pump of evaporator), toluene is distilled off the mixture from Step 5, leaving black semi-solid inside the evaporating flask. Toluene vapour is condensed and collected as distillate in the collecting flask. The distillate is removed, transferred into toluene waste container and stored in an appropriate waste storage area of the laboratory for flammable liquid.

6.2 Separation of water-insoluble solids

6.2.1 10 ml of de-ionised water is added into the flask containing the black semi-solid, forming a black suspension. The suspension is moderately stirred for 12 hours at room temperature and pressure.

6.2.2 Upon completion, the suspension is transferred to a glass vacuum filtration assembly which consists of borosilicate bottle-top receiver, a nylon-6,6 membrane (0.45 µm pore size), borosilicate fritted funnel fitted with vacuum seal, and a filter flask. A cake of black water-insoluble solids is retained on the nylon membrane, and a clear brown filtrate is collected in the filter flask. The filtrate is transferred into a new evaporating flask.

6.2.3 Water is evaporated off the filtrate at a temperature up to 75°C using the rotary evaporator until the remaining liquid volume is approximately 2 ml.

7. *Product precipitation*

Immediately after water evaporation, 40 ml of methanol is added into the flask. Brown precipitate form immediately. The mixture is allowed to sit for 5 minutes.

8. *Purification*

8.1 The mixture is filtered through a 0.45 µm nylon-6,6 membrane using vacuum filtration. Precipitate is obtained as brown filter cake on the nylon membrane. A clear, colourless filtrate (methanol) obtained in a filter flask is discarded.

8.2 The filter cake is re-dissolved into de-ionised water, forming a clear, brown solution. The solution is concentrated using the same procedure as described in Step 6.2.3.

8.3 A fresh 40 ml of methanol is added into the flask immediately after water evaporation to form brown precipitate. After allowing to stand for 5 minutes, the mixture is filtered through a 0.45 µm nylon-6,6 membrane. Brown filter cake is obtained on the nylon membrane which is transferred into a borosilicate dish. The filtrate (methanol) is discarded.

9. *Drying*

The brown filter cake is dried for 30 minutes in an oven preheated up to 70°C. A vacuum oven is recommended.

10. *Product collection and storage*

The dried product, obtained as brown powder, is stored in a glass bottle, cap tightly screwed, and sealed with parafilm. The product should be stored in a cool and dry place, away from light sources. It is recommended to store the product in a desiccator to avoid contact with moisture.

11. *Precautions and tips*

11.1 Preparation of C_{60}-toluene solution

- If black solids still remain at the bottom of the beaker when ultrasonication completes, it is possible that fullerene epoxide has already been formed and the obtained solution is no longer recommended for production of fullerenol.
- Care should be taken to not overheat water in the ultrasonic bath while in operation. This is to avoid causing process variations associated with solution temperature.

11.2 Preparation of sodium hydroxide solution

If white solids appear on the liquid surface or at the bottom of the container, it is possible that sodium carbonate has already been formed and the solution is no longer suitable for production of fullerenol.

Caution: Dissolution of sodium hydroxide in water is an exothermic reaction. Care and consideration for possible thermal hazards, as well as chemical hazards (severe chemical burns) should be taken when preparing the solution in large quantity.

11.3 Preparation of TBAH solution

- If clear crystals are formed inside, the TBAH stock must be warmed in a water bath at 38°C until the crystals disappears and the stock returns to a complete liquid state. The stock should also be allowed to cool down and thoroughly mixed before use.
- If white solids are observed on the liquid surfaces or at the bottom of the container, it is possible that carbonate compounds have been formed and the stock is no longer suitable for production of fullerenol.

11.4 Storage of nanomaterial waste and nanomaterial contaminated waste

- The black insoluble solid retained on nylon membrane should be double-bagged using air-tight sealable bags and stored in an appropriate area for storage of nanomaterial waste.
- Used nylon membranes should be double-bagged using air-tight sealable bags (separated from nanomaterial waste) and stored in an appropriate area for storage of nanomaterial contaminated waste.
- Used methanol should be transferred into a waste container and stored in an appropriate area for nanomaterial contaminated chemical waste.

5.7.2 Protocol 2 – Synthesis of fullerenol with $10 \leq n_{(OH)} < 15$

1. *Working environment*

   Refer to Protocol 1.

2. *Preparation of homogeneous C_{60}-toluene solution*

   Refer to Protocol 1.

3. *Preparation of sodium hydroxide solution*

   Refer to Protocol 1.

4. *Preparation of TBAH solution*

   Refer to Protocol 1

5. *Reaction between C_{60} and sodium hydroxide solution in presence of oxygen and TBAH as a phase-transfer catalyst*

   The prepared homogenous C_{60}-toluene solution is transferred into the reaction flask. Using a standard Pasteur pipette, 24 drops of TBAH solution is added into the C_{60}-toluene solution, followed by addition of 2.0 ml of 100%w/v sodium hydroxide solution. This forms the reaction mixture. The mixture is vigorously stirred for 20 minutes in presence of oxygen. The dark violet liquid turns colourless within a few seconds after the reaction starts, and black semi-solid substance is formed inside the reaction mixture. Upon completion, the mixture in the reaction flask consists of black semi-solid in a reservoir of clear colourless liquid (toluene).

6. *Separation*

   Refer to Protocol 1 for procedures to remove toluene and water-insoluble solids.

7. *Product precipitation*

   Refer to Protocol 1.

8. *Purification*

   Refer to Protocol 1.

9. *Drying*

   Refer to Protocol 1.

10. *Product collection and storage*

    Refer to Protocol 1.

11. *Precautions and tips*

    Dropping 24 drops of TBAH solution into C_{60}-toluene solution should be completed within a finite amount of time, as quick as possible. If difficulty in dropping starts, or the TBAH solution turns slightly unclear, this portion of liquid is no longer suitable for production of fullerenol and the Pasteur pipette should be replaced. In addition to this, precautions and tips in Protocol 1 are also applicable.

5.7.3 Protocol 3 – Synthesis of fullerenol with $15 \leq n_{(OH)} \leq 20$

1. *Working environment*

   Refer to Protocol 1.
2. *Preparation of homogeneous C_{60}-toluene solution*

   Refer to Protocol 1.
3. *Preparation of sodium hydroxide solution*

   Refer to Protocol 1.
4. *Preparation of TBAH solution*

   Refer to Protocol 1
5. *Reaction between C_{60} and sodium hydroxide solution in presence of oxygen and TBAH as a phase-transfer catalyst*

   The prepared homogenous C_{60}-toluene solution is transferred into the reaction flask. Using a standard Pasteur pipette, 24 drops of TBAH solution is added into the C_{60}-toluene solution, followed by addition of 8.0 ml of 100%w/v sodium hydroxide solution. This forms the reaction mixture. The mixture is vigorously stirred for 20 minutes in presence of oxygen. The dark violet liquid turns colourless within a few seconds after the reaction starts, and black semi-solid substance is formed inside the reaction mixture. Upon completion, the mixture in the reaction flask consists of black semi-solid in a reservoir of clear colourless liquid.
6. *Separation*

   Refer to Protocol 1 for procedures to remove toluene and water-insoluble solids.
7. *Product precipitation*

   Refer to Protocol 1

8. *Purification*

   Refer to Protocol 1.

9. *Drying*

   Refer to Protocol 1.

10. *Product collection and storage*

    Refer to Protocol 1.

11. *Precautions and tips*

    Refer to Protocol 2.

5.7.4 General block flow diagram for the developed synthesis protocols for synthesis of fullerenol based on the selected route

Complement to the developed synthesis protocols (Protocol 1, 2 and 3), a simplified block flow diagram summarising general processes is provided in Figure 5-74. Since the diagram is based on laboratory synthesis, no recycling streams were incorporated into the diagram.

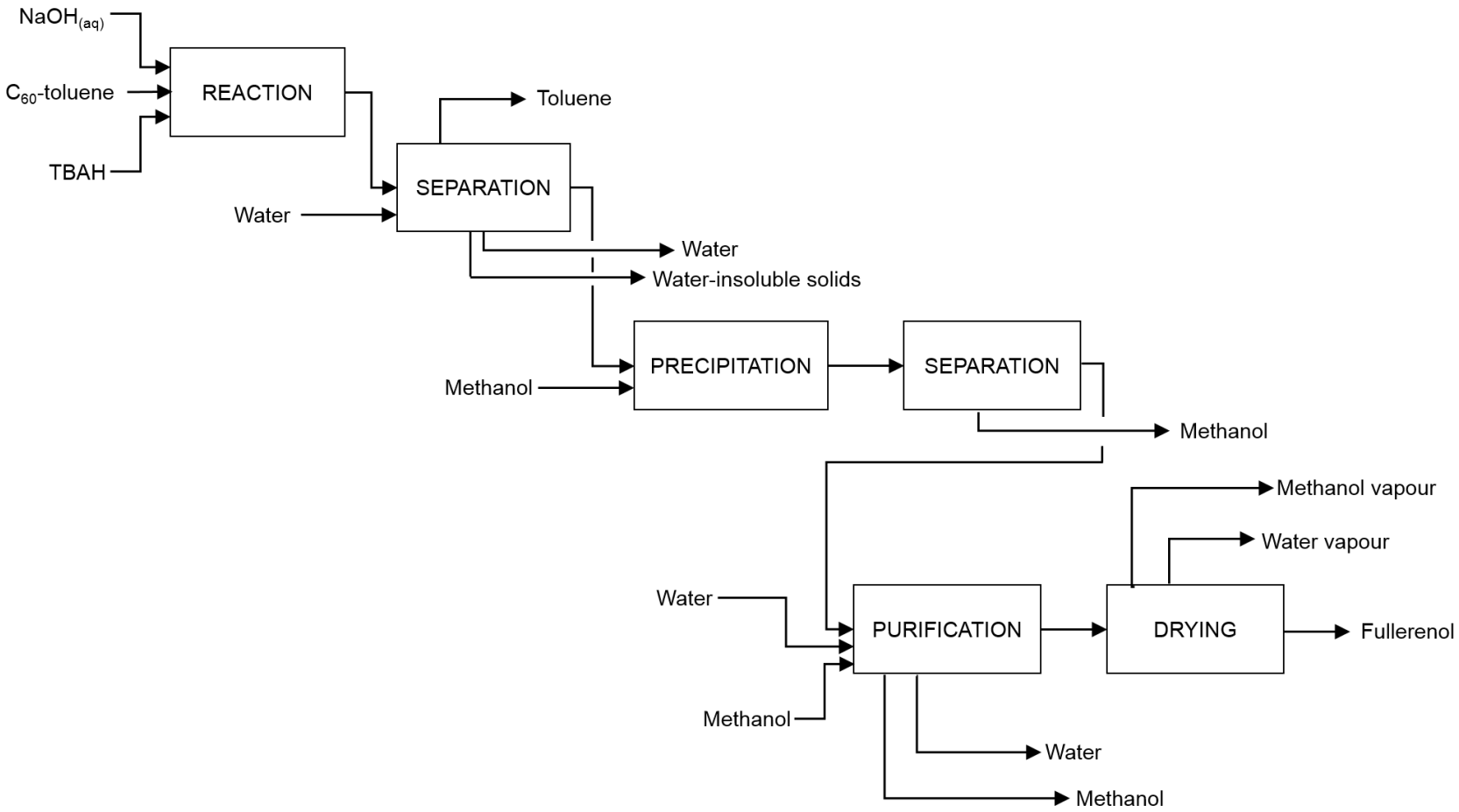

Figure 5-74 Simplified block flow diagram for fullerenol production based on the developed synthesis protocols

5.8 Scale-up syntheses of fullerenol with specified level of hydroxylation using the developed protocols

With the purposes of both confirming scalability of the developed protocols and producing sufficient amount of fullerenol to be used as experimental material in the supercapacitor experiments, the scale-up syntheses served as a bridge between Part One and Part Two of this research. For ease of clarification, this section is hereby called ‘Scale-up Experiment’.

Three different classes of fullerenol (each class with a unique level of hydroxylation) were required as experimental materials for the end-application investigation, and were produced using the developed Protocol 1-3 (Section 5.7):

- Low $n_{(OH)}$: Protocol 1(TBAH = 3 drops, NaOH = 2.0 ml)
- Medium $n_{(OH)}$: Protocol 2 (TBAH = 24 drops, NaOH = 2.0 ml)
- High $n_{(OH)}$: Protocol 3 (TBAH = 24 drops, NaOH = 8.0 ml)

Reaction time for each synthesis was kept constant at 20 minutes.

By using the protocols, the rationale behind development of synthesis protocols also applied to specifying process conditions for material synthesis in this experiment. The condition ‘2.0 ml NaOH’ was selected as the basis for developing the protocols (hence the basis for Scale-up Experiment as well) due to the fact that it produced reasonable yield and could be used to link between process conditions for producing low-, medium- and high-$n_{(OH)}$ fullerenol as previously explained in Section 5.7.

To obtain sufficient amount of each class of fullerenol for the Part Two experiments, scaling up and multiple batches were required. For low-$n_{(OH)}$ fullerenol, the total of seven batches, each with scaling factor = 3, were conducted and the products obtained were labelled as Product A (Batch A1-A7 respectively). For medium-$n_{(OH)}$ fullerenol, the total of 3 batches comprised with two batches of scaling factor = 2 and one normal-scale batch were conducted. The products obtained were labelled as Product B (Batch B1-B3 respectively).

For the high-$n_{(OH)}$ fullerenol, only one batch of scaling factor = 2 was required, and the collected product was labelled as Product C.

Apart from the above-mentioned process conditions specifically selected for each synthesis, scaling factor and plan for multiple-batch syntheses, other procedures were as described in Section 4.3.1. Within the same class of product, the batches showed similar physical appearances. Product A was obtained as powder of the darkest shade of brown. Product B was a powder of a slightly lighter shade but still dark brown. Product C had the lightest shade of brown and the powder seemed 'fluffier' than other two products. Appearances of Product A, B and C (Figure 5-75) were in agreement with their corresponding normal-scale appearances in earlier section.

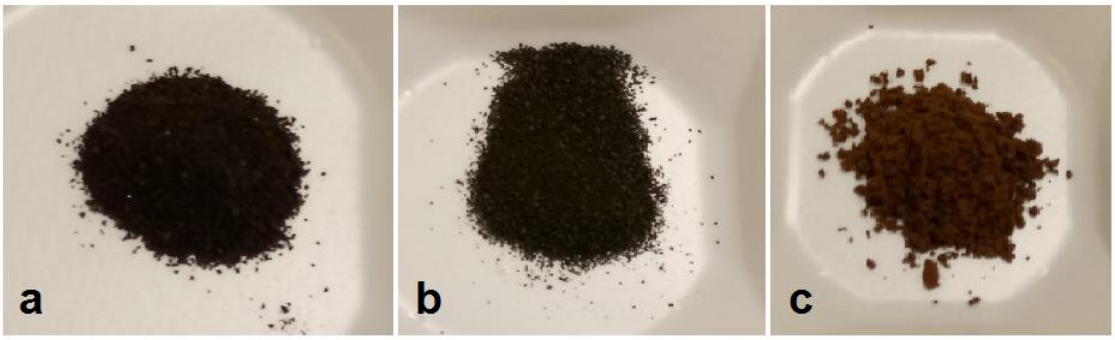

Figure 5-75 Physical appearances of Product A, Product B and Product C (a-c respectively) in agreement with their corresponding normal-scale appearances

Synthesis observations from each synthesis were similar to those from their corresponding normal-scale synthesis in previous experiments. This also included observing the trace of water-soluble white solid on the flask wall where the product-containing liquid flowed (as seen in Figure 5-25) in all syntheses. Again, analysis of characterisation results thus followed the same path performed in TBAH, NaOH and Reaction Time Experiments.

5.8.1 Analysis of characterisation results

Infrared spectra and TGA thermograms of each individual batch of each product were obtained. However, to ensure a sufficient amount of each product remained available *Part Two* experiment, individual batches of the same product after FTIR and TGA measurements were thoroughly mixed together and formed a combined product. Samples for the rest of characterisation were taken from the combined version of each product. All characterisation followed the procedures described in Section 4.1.

The presence of sodium carbonate was expected in all batches based on the trace of white water-soluble solids observed in all syntheses. Supporting evidences were found in infrared spectra, SEM micrographs and EDX results of the products. Characterisation of the products therefore required integration of results from all techniques (i.e. FTIR, TGA, EDX and SEM).

Infrared spectra of the products are shown from Figure 5-76 to Figure 5-78. Fullerenol characteristic absorptions were confirmed in all spectra (absorptions centred around 3430, 1600, 1370 and 1080 cm^{-1} corresponding to ν O–H, ν C=C, δ C–O–H, and ν C–O respectively).

Almost all batches of Product A show normal pattern of relative strength of each absorption (i.e. absorption strength from the strongest to the weakest in an order of ν O–H $>$ ν C=C $>$ δ C–O–H $>$ ν C–O). An exception was from the spectra of Batch A1 (Figure 5-76a) where the overall order of absorption strength changed due to the strong absorption around 1440 cm^{-1} which was related to the presence of sodium carbonate, possibly slightly higher than other batches). Existence of sodium carbonate within Product A was further confirmed by a micrograph showing needle-like crystals covering the surface of product powder (Figure 5-79a), and detection of sodium element in the sample (Table 5-24). Weight losses related to decomposition of fullerene epoxide were observed in TGA thermograms of Batch A1, A3, A4 and A7 (Figure 5-80 and Figure 5-81).

For Product B, infrared spectra of the three batches (Figure 5-78) also follow the normal pattern for absorption strength. There was no strong absorption around 1440 cm^{-1}, however broad shoulder extending from 3000 cm^{-1} to 2000 cm^{-1} was related to the presence of sodium carbonate (supported by observation of needle-like crystals in Figure 5-79b, and detection of sodium element in Table 5-24). Obvious weight loss related to fullerene epoxide was observed only in TGA thermogram of Batch B1 (Figure 5-82a).

Strong absorption around 1440 cm^{-1} in Figure 5-78d together with the evidence of needle-like crystals mixed with small clusters of fluffy solids (Figure 5-79c) and detected sodium element (Table 5-24) suggested for the presence of sodium carbonate in Product C. TGA thermogram (Figure 5-82d) indicated that the product also contained epoxide groups.

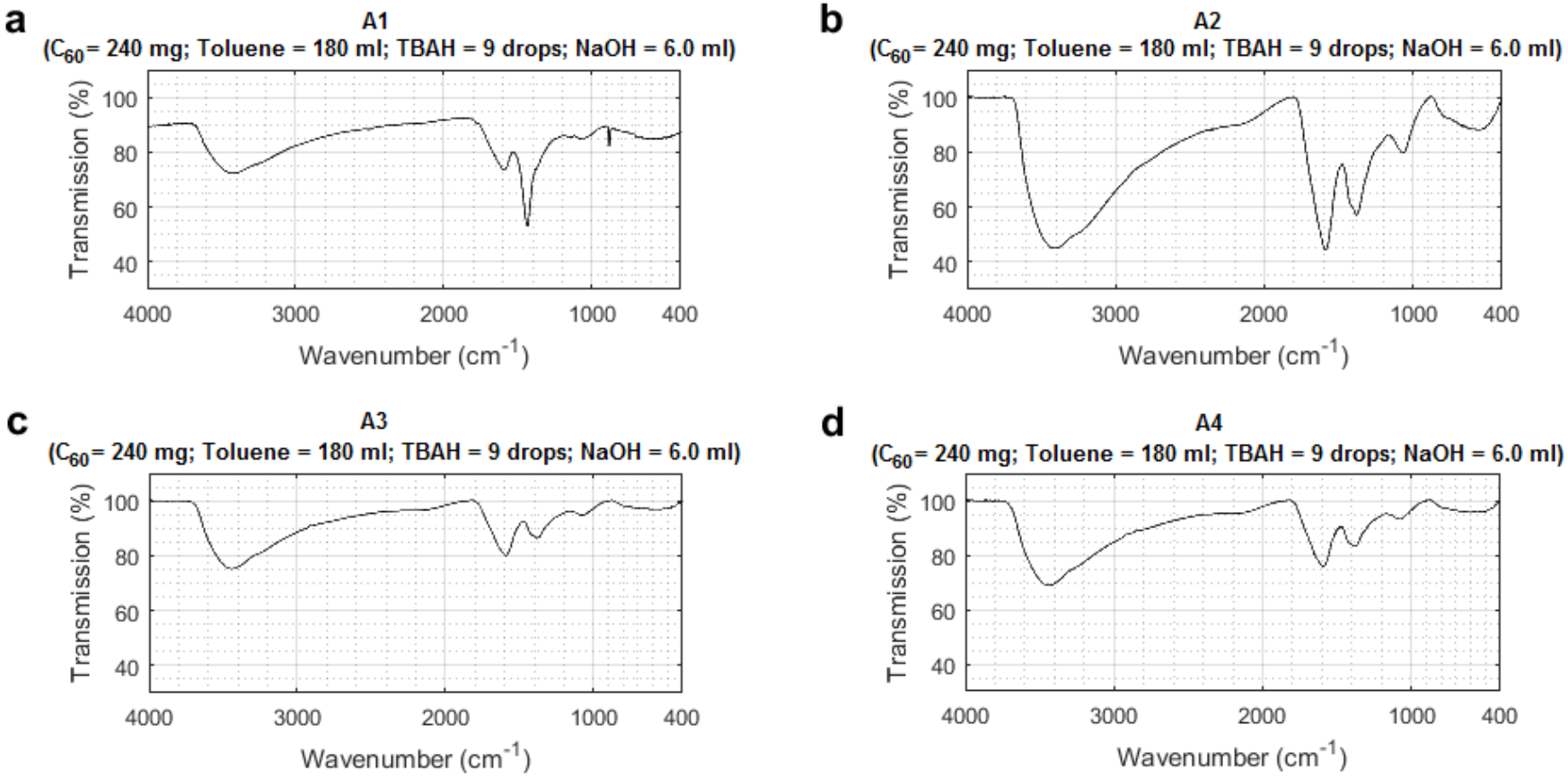

Figure 5-76 Infrared spectra of Product A1-A4 (Protocol 1 with scaling factor = 3) from Scale-up Experiment. Amounts of reagents used for synthesis of corresponding product are shown in brackets above the plots.

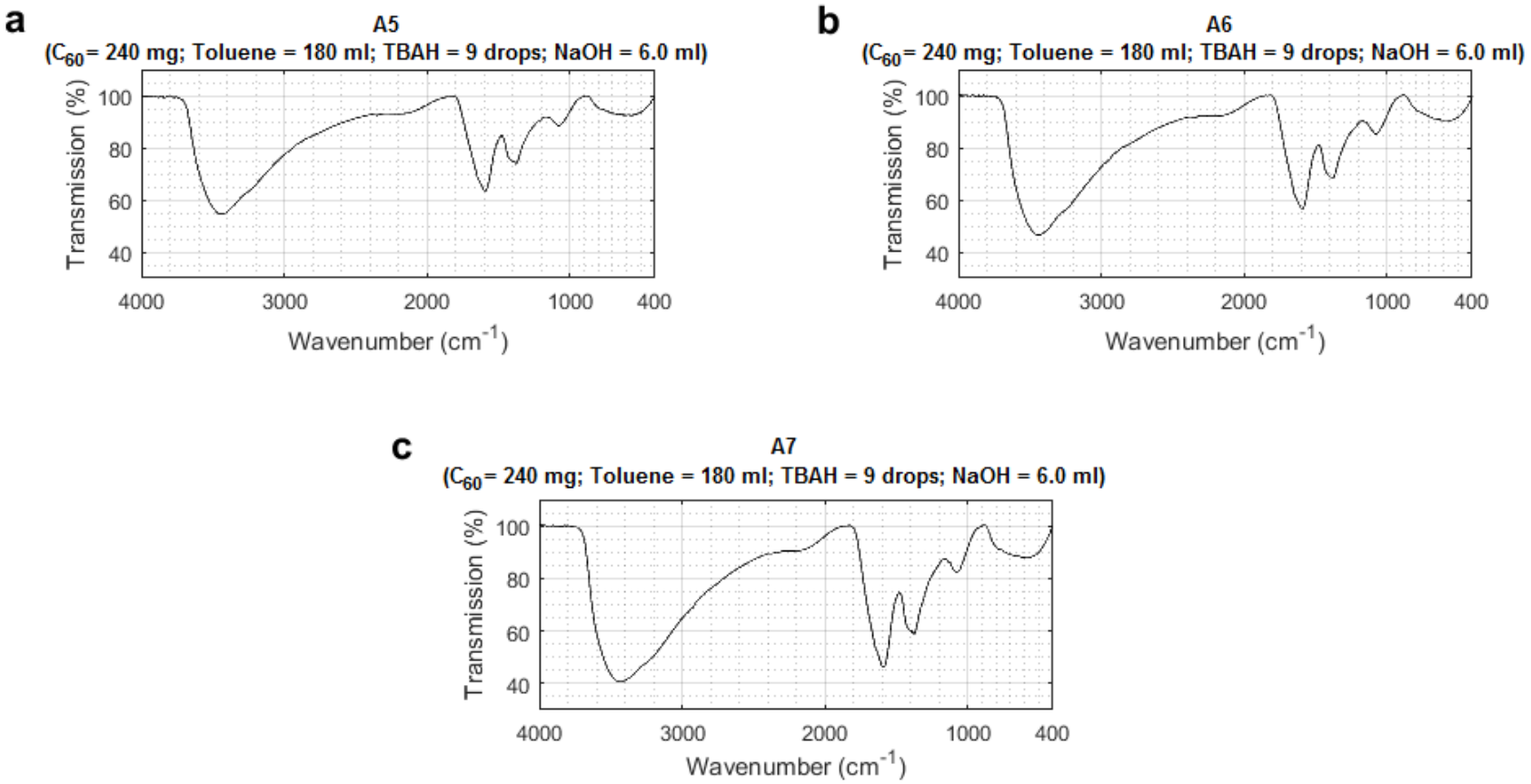

Figure 5-77 Infrared spectra of Product A5-A7 (Protocol 1 with scaling factor = 3) from Scale-up Experiment. Amounts of reagents used for synthesis of corresponding product are shown in brackets above the plots.

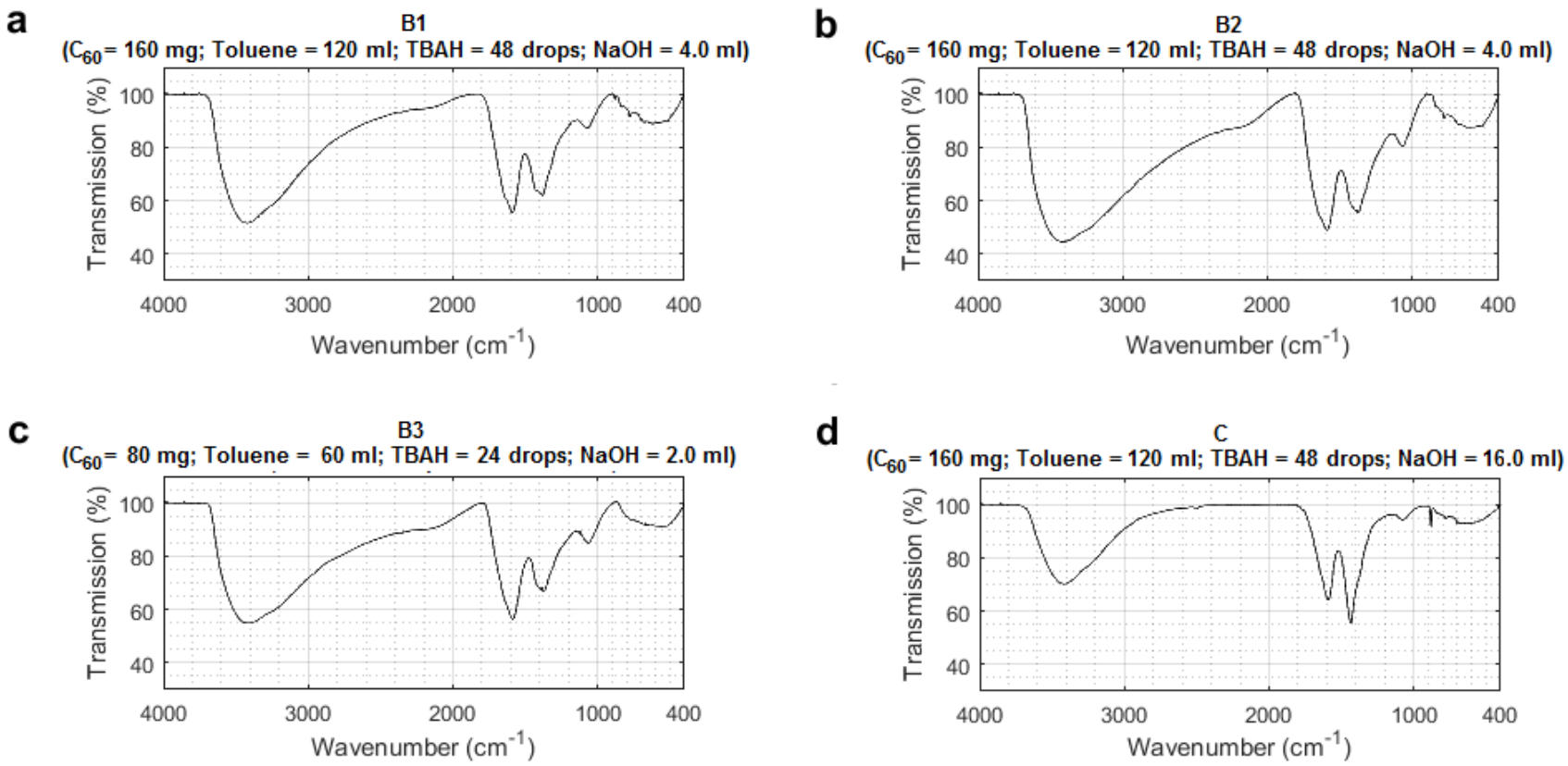

Figure 5-78 Infrared spectra of Product B1-B3 (Protocol 2 with scaling factor = 2 for B1-B2, and normal-scale for B3) and Product C (Protocol 3 with scaling factor = 2) from Scale-up Experiment. Amounts of reagents used for synthesis of corresponding product are shown in brackets above the plots.

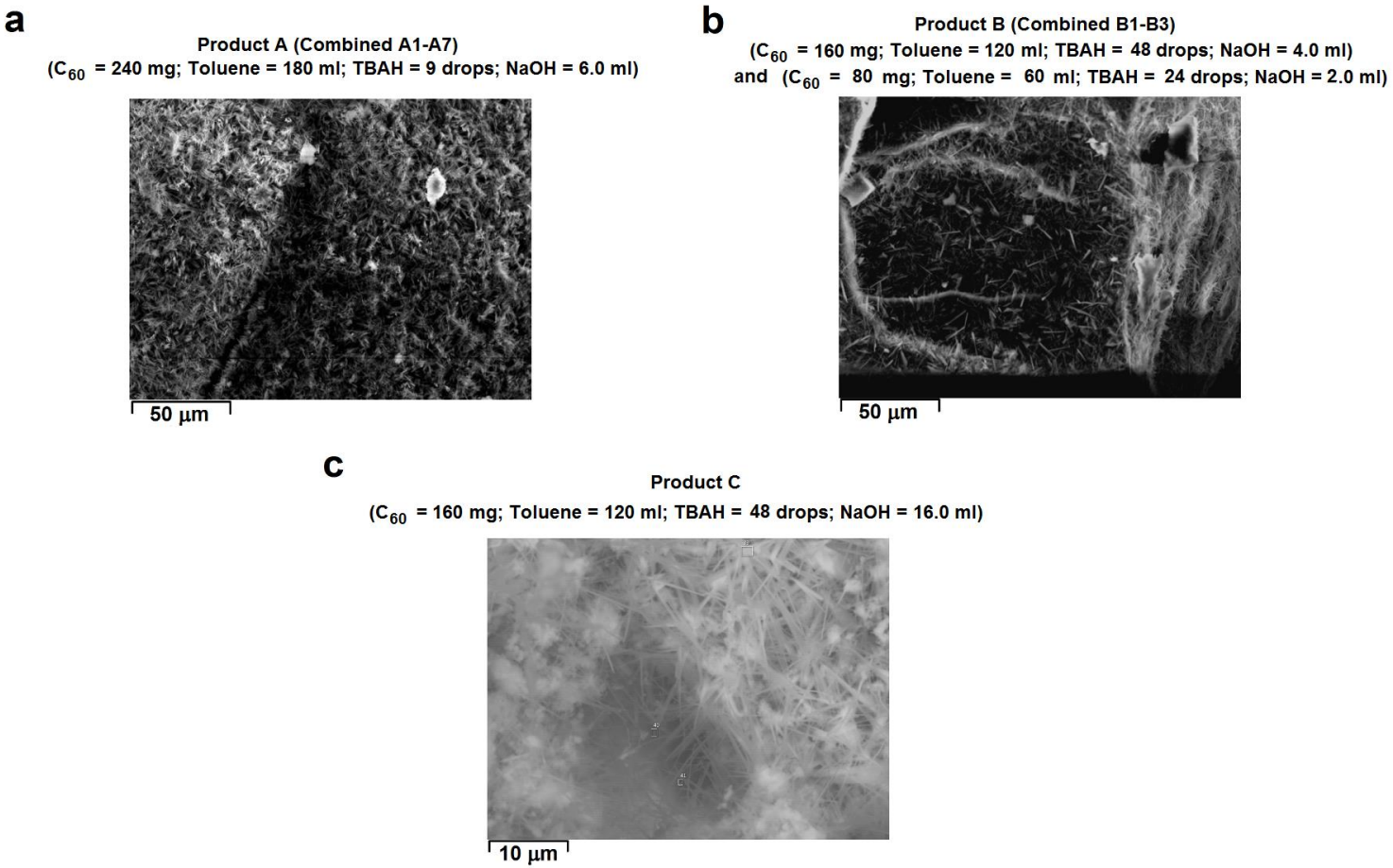

Figure 5-79 SEM micrographs of Product A (combined A1-A7), Product B (combined B1-B3) and Product C from Scale-up Experiment showing needle-like crystals covering product powder. Amounts of reagents used for synthesis of corresponding product are shown in brackets above the images. (Self-operated images obtained from SEM facilities at Cranfield University)

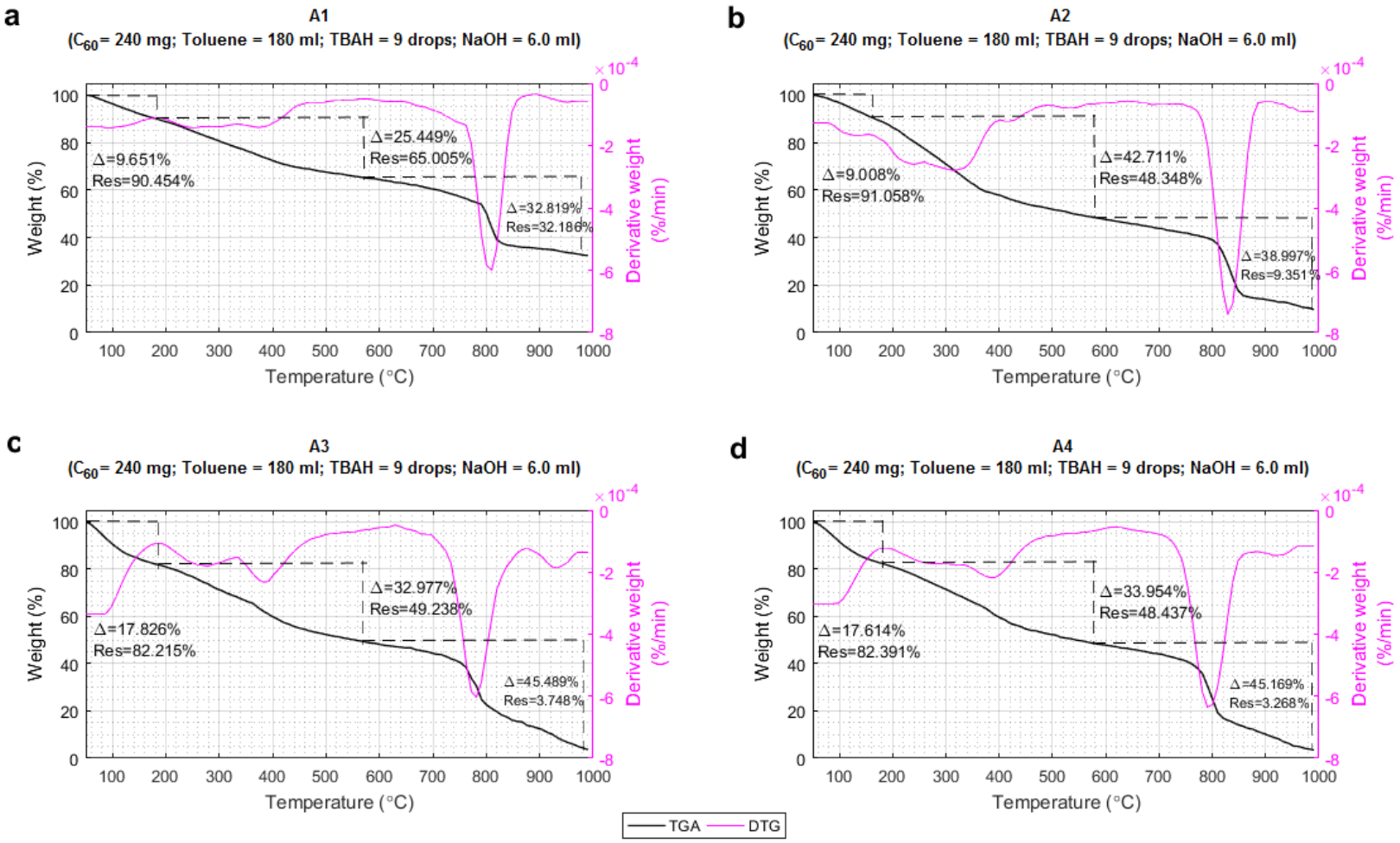

Figure 5-80 TGA thermograms of Product A1-A4 (Protocol 1 with scaling factor = 3) from Scale-up Experiment. Amounts of reactants used for synthesis of corresponding product are shown in brackets above the plots.

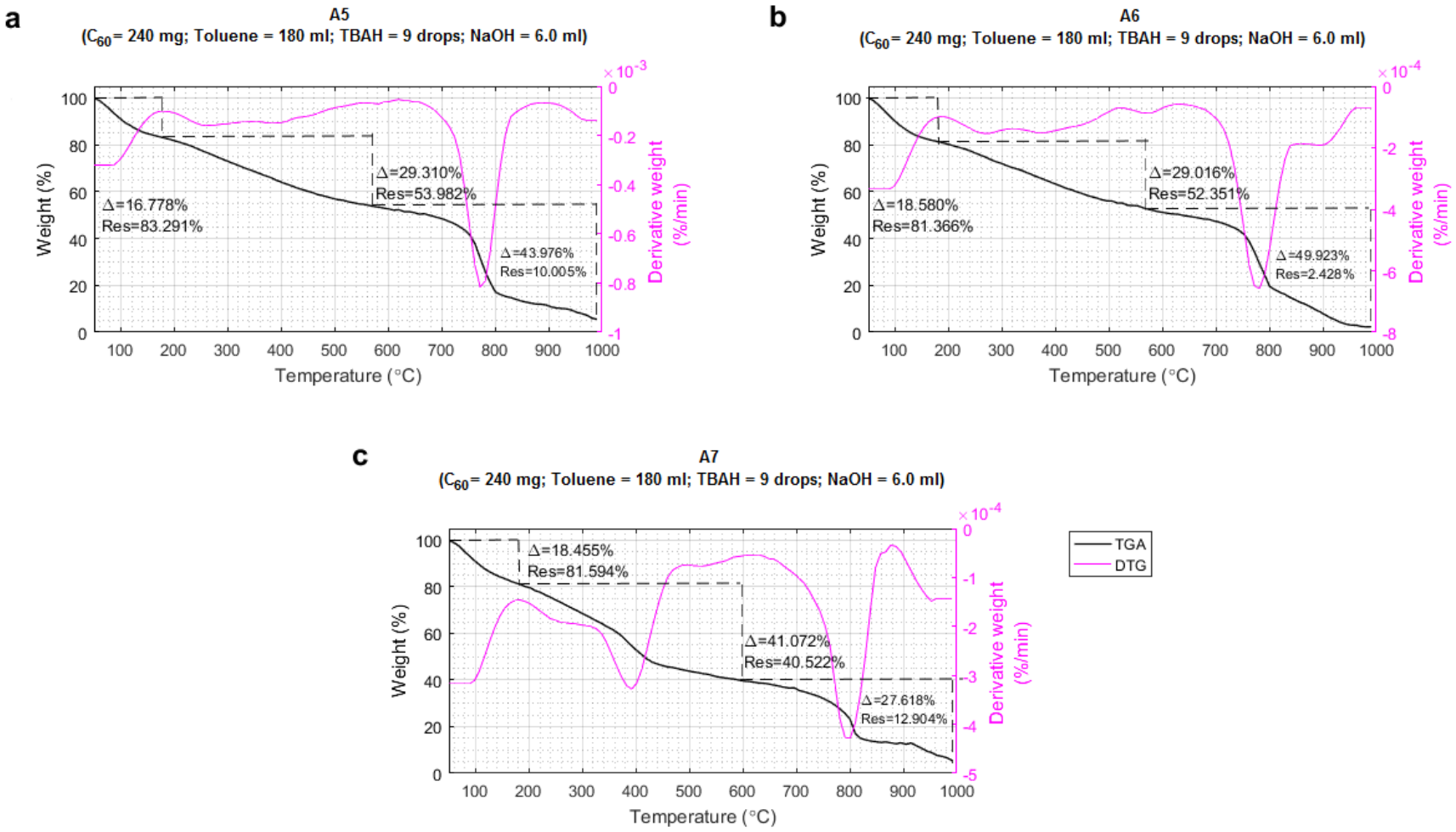

Figure 5-81 TGA thermograms of Product A5-A7 (Protocol 1 with scaling factor = 3) from Scale-up Experiment. Amounts of reagents used for synthesis of corresponding product are shown in brackets above the plots.

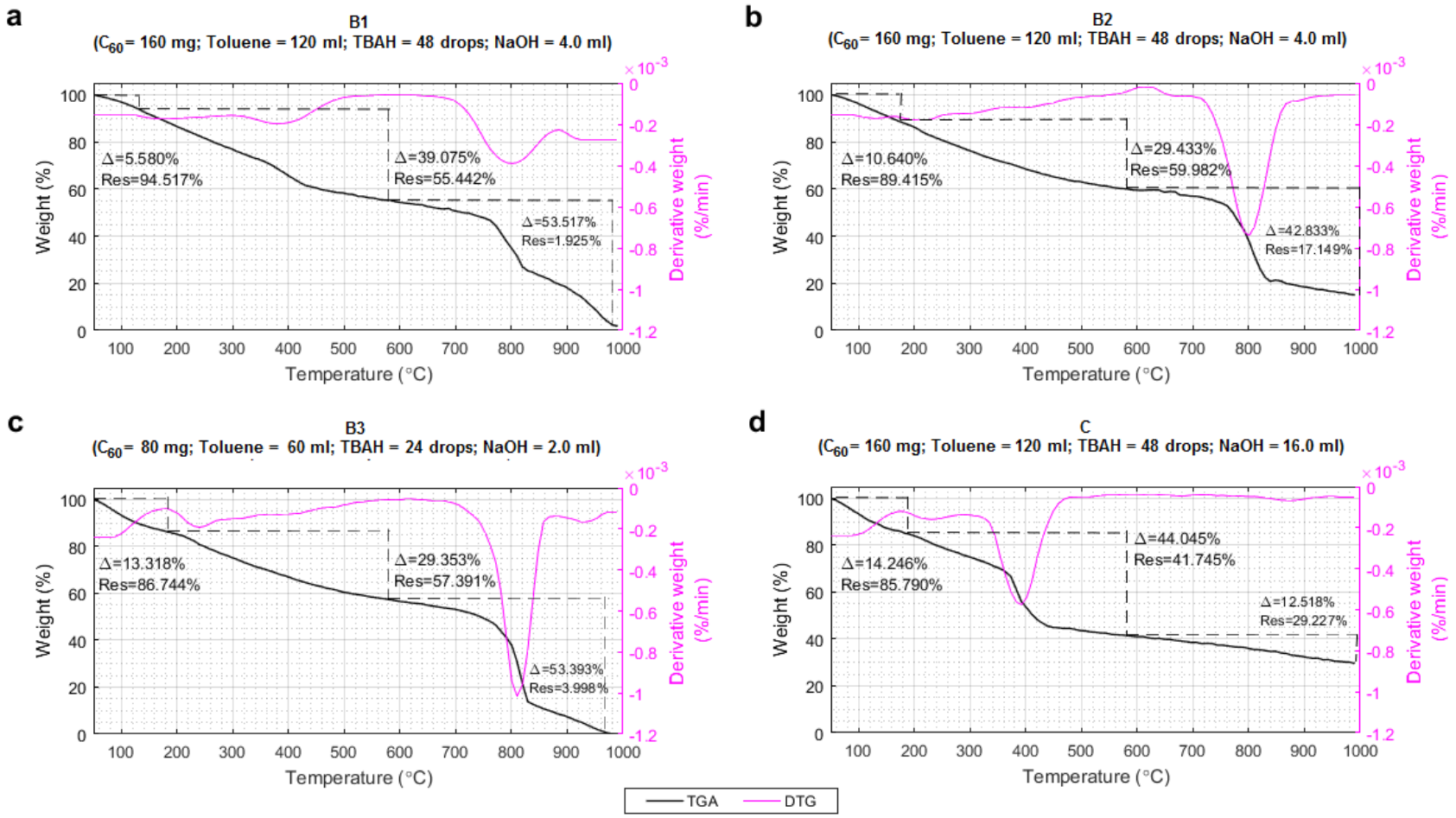

Figure 5-82 TGA thermograms of Product B1-B3 (Protocol 2 using scaling factor = 2 for B1-B2, and normal-scale for B3) and Product C (Protocol 3 with scaling factor = 2) from Scale-up Experiment. Amounts of reagents used for synthesis of corresponding product are shown in brackets above the plots.

Table 5-24 EDX results of Product A, B and C (presented as %wt)

Product	% C	% O	% Na
A (combined A1-A7)	44.47	38.62	15.34
B (combined B1-B3)	47.26	37.66	15.08
C	34.61	44.75	18.59

DLS results of Product A, B and C are shown in Figure 5-83. For Product A, the detected particle diameters range between 25 and 200 nm, with the majority of particles around 40-80 nm. This is in agreement with the high-magnification SEM micrograph of Product A in Figure 5-84. For Product B, the detected particles also have sizes ranging from 25 to 200 nm and the similar range for the majority of particles (40-80 nm), in agreement with SEM micrograph in Figure 5-85. However, Figure 5-83b shows that Product B may have a narrower distribution compared to Product A. The range of detected particle sizes in Product C was lowest among the three products – range of 1 to 50 nm, with most of the particles in the range of 1-10 nm in diameter (Figure 5-83c). However, the dry-form size distribution observed in the SEM micrograph (Figure 5-86) showed the majority of particles, which are also roughly the smallest observable, having diameters of approximately 200 nm. Larger particles of approximately 500 nm are also seen in the frame. It is suggested that these large particles are large clusters resulting from aggregating of a numerous number of individual fullerenol particles.

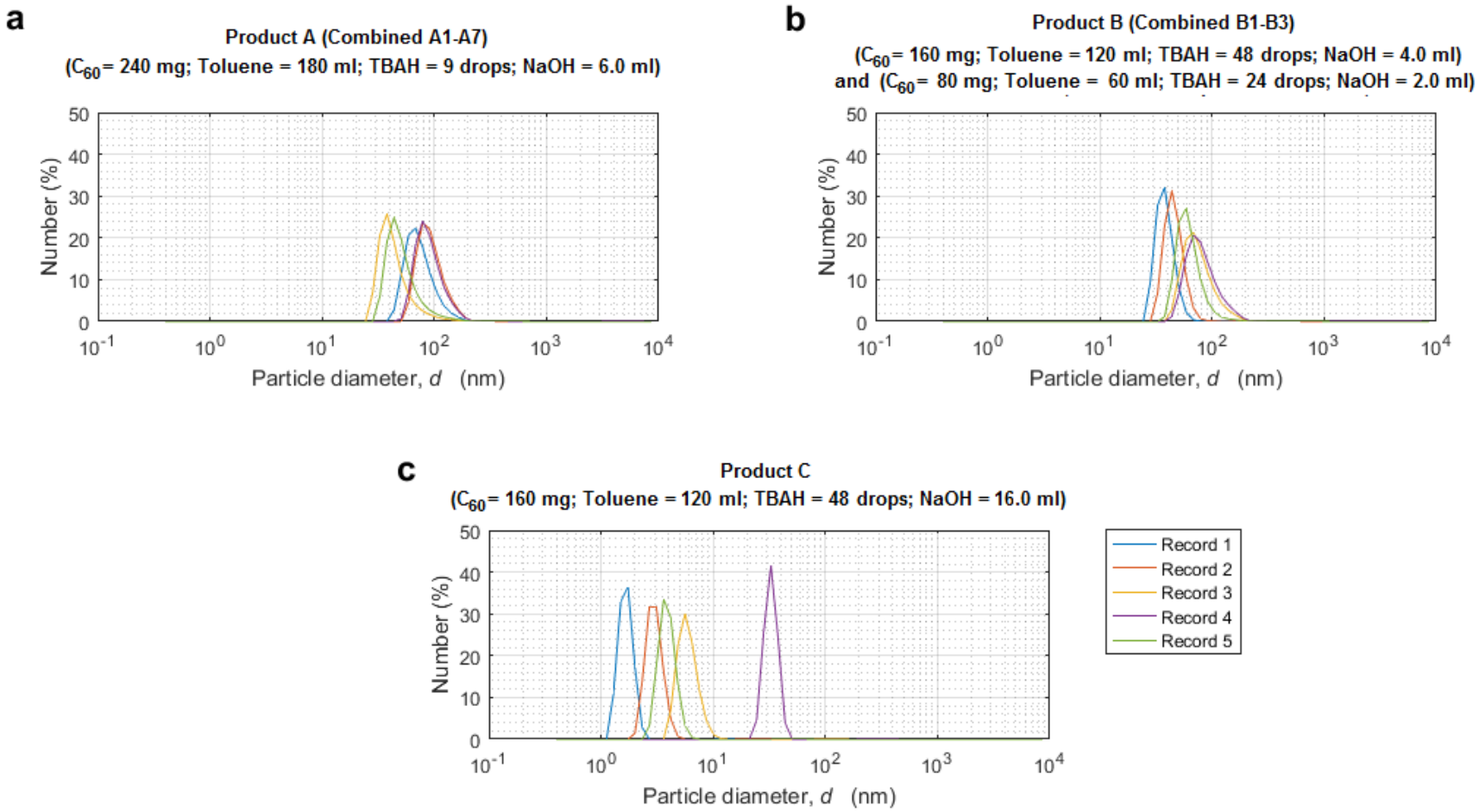

Figure 5-83 DLS results of Combined Product A (A1-A7), Combined Product B (B1-B3), and Product C from Scale-up Experiment. Amounts of reagents used for synthesis of corresponding product are shown in brackets above the plots.

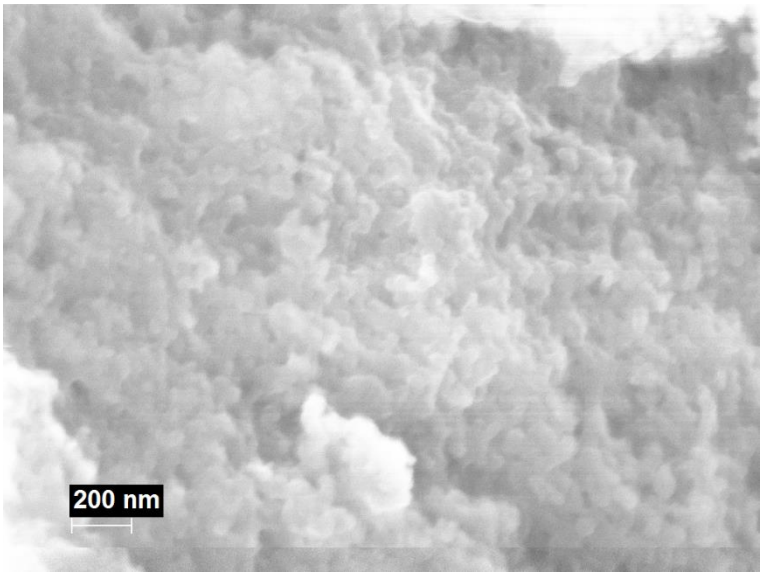

Figure 5-84 SEM micrograph (160kx) of Product A from Scale-up Experiment, using Protocol 1 (TBAH = 3 drops; NaOH = 2.0 ml) with scaling factor = 3 (Image produced by SEM/EDX facilities at National Physical Laboratory, London)

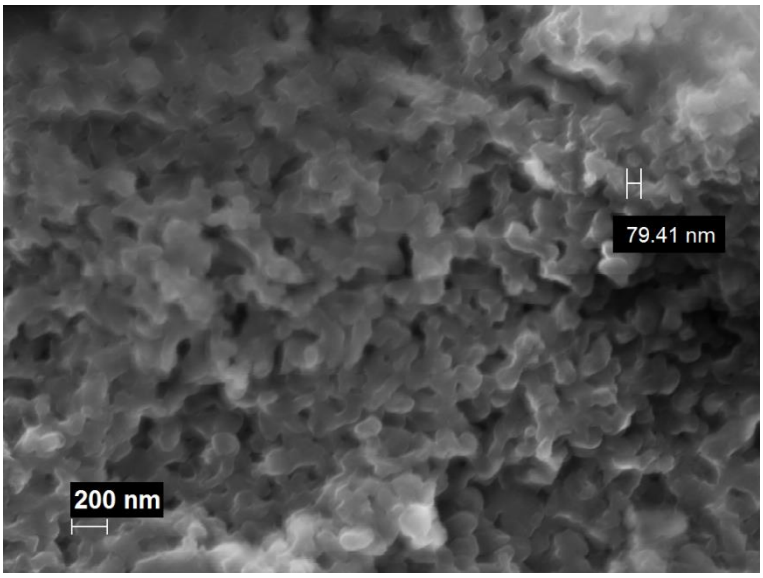

Figure 5-85 SEM micrograph (160kx) of Product B from Scale-up Experiment, using Protocol 2 (TBAH = 24 drops; NaOH = 2.0 ml) with normal scale and scaling factor = 2 (Image produced by SEM/EDX facilities at National Physical Laboratory, London)

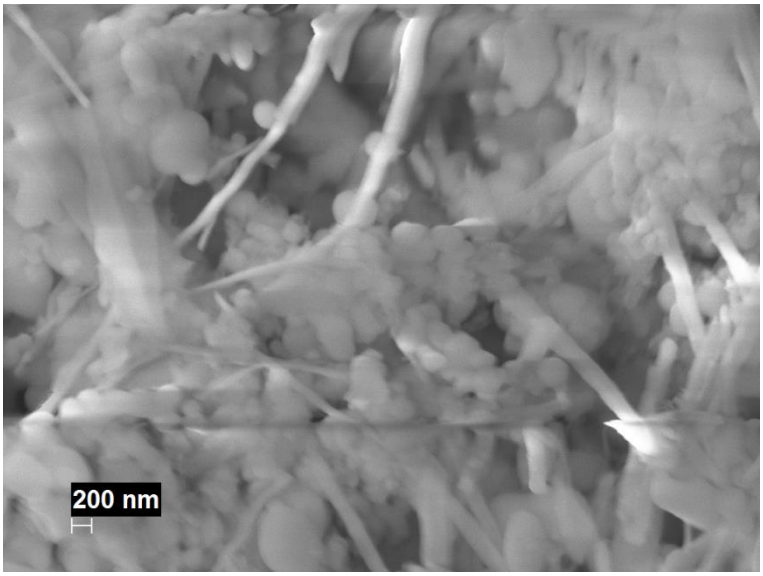

Figure 5-86 SEM micrograph (160kx) of Product C from Scale-up Experiment, using Protocol 3 (TBAH = 24 drops; NaOH = 8.0 ml) with scaling factor = 2 (Image produced by SEM/EDX facilities at National Physical Laboratory, London)

5.8.2 Estimation of level of hydroxylation

Due to the fact that weight loss associated with epoxide groups was present in thermograms of some products, 'TGA method' was not suitable for use in estimation of level of hydroxylation of the products, and the 'TGA-EDX method' developed in this research was applied to all products for estimations. Table 5-25 show calculation results with the assumption that all products consisted of only fullerene with hydroxyl groups and some physically bound water molecules. However, characterisation of the products showed that epoxide groups were present in most batches. Therefore, it was decided that the existence of epoxide groups within the products could not be neglected although it was not present in every single batch. Calculation results accounting for the presence of epoxide groups are shown in Table 5-26. Between the two estimations, $n_{(OH)}$ was the only parameter that changed when epoxide model was considered (reduced by 1 group in each product). Figure 5-87 illustrates differences between values of $n_{(OH)}$ from the two series of estimations. To arrive as close as possible to the real properties of the products, further uses of estimated $n_{(OH)}$ of Product A, B and C were based on Table 5-26.

Table 5-25 Calculation results using 'TGA-EDX method' for Product A-C showing determined product empirical formula and analysis on molecular and elemental compositions

Product	Calculation results							
	Product empirical formula	**%wt $C_{60}(OH)_n$**	**%wt H_2O**	**%wt Na_2CO_3**	**%C**	**%O**	**% Na**	**% H**
A	$C_{60}(OH)_{10}.16H_2O$ with $6Na_2CO_3$	49.06	15.88	35.06	43.66	38.81	15.22	2.32
B	$C_{60}(OH)_{14}.9H_2O$ with $6Na_2CO_3$	54.00	10.15	35.85	44.64	37.88	15.56	1.92
C	$C_{60}(OH)_{20}.20H_2O$ with $10Na_2CO_3$	42.74	14.52	42.74	33.87	45.16	18.55	2.42

Table 5-26 Calculation results using 'TGA-EDX method' for Product A-C showing determined product empirical formula and analysis on molecular and elemental compositions (with consideration for the presence of epoxide groups)

Product	Calculation results							
	Product empirical formula	**%wt $C_{60}O(OH)_n$**	**%wt H_2O**	**%wt Na_2CO_3**	**%C**	**%O**	**%Na**	**%H**
A	$C_{60}O(OH)_9.16H_2O$ with $6Na_2CO_3$	49.03	15.89	35.08	43.68	38.83	15.22	2.26
B	$C_{60}O(OH)_{13}.10H_2O$ with $6Na_2CO_3$	53.98	10.15	35.87	44.67	37.90	15.57	1.86
C	$C_{60}O(OH)_{19}.20H_2O$ with $10Na_2CO_3$	42.72	14.52	42.76	33.88	45.18	18.56	2.38

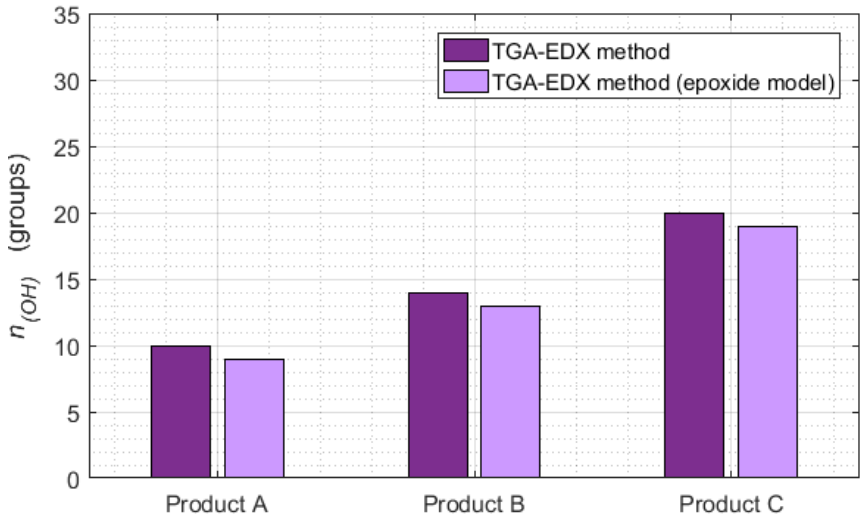

Figure 5-87 Bar chart illustrating $n_{(OH)}$ values of Product A, B and C estimated by 'TGA-EDX method' comparing between normal model(dark violet) and epoxide model (light violet)

The values of $n_{(OH)}$ of Product A ($n_{(OH)}$ = 9 groups) and B ($n_{(OH)}$ = 13 groups) are similar to their corresponding normal-scale products in previous experiments. For Product C ($n_{(OH)}$ = 19 groups), $n_{(OH)}$ is slightly higher than its normal-scale product in NaOH experiment ($n_{(OH)}$ = 15 groups) but still in the same range.

PPF mass ratios of individual batches in this experiment are plotted and shown in Figure 5-88. For Product A, it should be noted that a certain amount of isolated yield from Batch A2 to Batch A7 were accidentally lost at product collection step as the powder ‘flew away’ due to static electricity. The lost portion of each batch was estimated to equal the amount which brings PPF ratio to the value similar to that of Batch A1. In case of Batch A1, its isolated yield (which did not suffer from an accidental lost during product collection) is triple of the amount collectable the normal-scale product, while its PPF ratio remains similar to that of the normal-scale. This confirms that scaling up is practical.

It was suggested that the lower PPF mass ratios in Product B and C (compared to corresponding normal-scale values) could result from a certain amount of product still remained within the bulk of black solids and this portion was filter out together with water-insoluble solids. Duration for stirring the suspenstion (after toluene removal) for scale-up synthesis might need to be longer than 12

hours in order to dissolve as much as possible product into the aqueous phase. Unfortunately, this was not practical for the research due to limitations especially on working space and time.

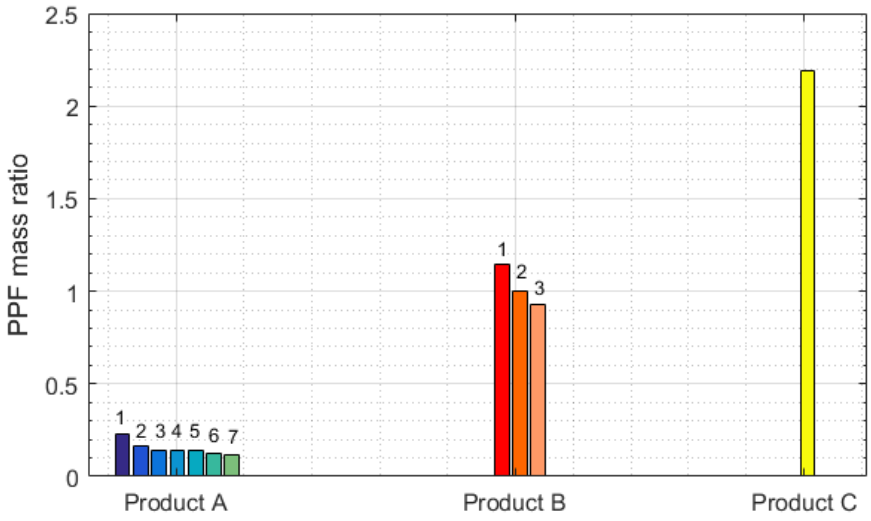

Figure 5-88 Bar chart illustrating PPF mass ratio from individual batches of Product A (Batch A1-A7, total of 7 batches), Product B (Batch B1-B3, total of 3 batches), and Product C (total of 1 batch)

Following the approach described in Appendix C, values of approximate percent yield from Scale-up Experiment were 6.1, 42.5 and 63.6 for Product A, B and C respectively – noticeably lower than their corresponding normal-scale values. Similar to PPF mass ratio, this was suggested to also associate with being unable to dissolve some portion of the desired product from the water-insoluble filter cake in each scale-up synthesis due to the limitations on available working space and time mentioned above.

5.9 Investigation on the effect of fullerenol as additives in activated carbon electrode for supercapacitor

This set of electrochemical experiments belongs to *Part Two* of the research, where different classes of fullerenol (Product A, B, and C), each containing a unique level of hydroxylation ($n_{(OH)}$), were investigated for their uses in supercapacitor application.

As fullerenol has not been explored in supercapacitor application before, this research chose to apply fullerenol as electrode additives. The decision was also supportive to the limited availability of experimental materials. Among the list of supercapacitor electrode materials (Section 2.7.2.1), activated carbon was selected as the active material for supercapacitors in this research based on a reason that both fullerenol and activated carbon belong to the carbon family. Symmetric electrode configuration was used throughout the investigation in order to avoid complications associated with asymmetric electrode contributions. Following this direction, the investigation focused on the effect of different electrode additives (different $n_{(OH)}$) on character and performance of symmetric activated carbon supercapacitor. Pristine C_{60} was also involved as fullerenol with zero hydroxylation. The results from additive-containing supercapacitors were analysed against that from a supercapacitor without any additives (i.e. 100% activated carbon as active material during electrode fabrication).

Five symmetric activated carbon supercapacitors were assembled using different compositions of active materials during electrode fabrication as summarised in Table 5-27. For ease of clarification, supercapacitors S1, S2, S3, S4, and S5 were denoted as ‘AC’, ‘AC+C_{60}’, ‘AC+A’, ‘AC+B’ and ‘AC+C’ respective in all figures throughout the investigation.

Table 5-27 Summary of active material compositions and denotations for different supercapacitors

Supercapacitor	Composition of electrode active material (%wt)		Denotation for figures
	Activated carbon	Additives	
S1	100	0	AC
S2	90	10 (C_{60})	AC+C_{60}
S3	90	10 (Product A)	AC+A
S4	90	10 (Product B)	AC+B
S5	90	10 (Product C)	AC+C

CV, GCD and EIS were performed on each assembled supercapacitor following the procedures described in Section 4.8. Since Product A, B and C were all produced from protocols based on the same synthesis route, analyses and comparison could be done without concerns associated with variations among different fullerenol synthesis routes.

It should be noted that the formulation of electrode slurry for electrode fabrication used in this research was a modification from the formulation optimised for activated carbon (Liu et al., 2014) which might not be optimal for fullerenol to exhibit its full capability and performance. It would have been ideal if the research could explore other formulations as well, but it was not possible to allocate more time and resources due to several limitations on working space, available time and budget.

5.9.1 Cyclic voltammetry (CV)

Figure 5-89 shows cyclic voltammograms obtained from the five supercapacitors. It was found that voltage windows of all supercapacitors were 0.85 V, which is typical for a system with an aqueous electrolyte (Stoller and Ruoff, 2010). From the voltammograms alone, apart from Product B, voltammogram loops of additive-containing supercapacitors are smaller than that of the additive-free one (control). A smaller loop might suggest for smaller

values of capacitance. The order of sizes of the voltammograms from large to small is AC, AC+B, AC+A and AC+C_{60}, followed by AC+C respectively. Nevertheless, cell capacitance is best estimated through GCD (Stoller and Ruoff, 2010).

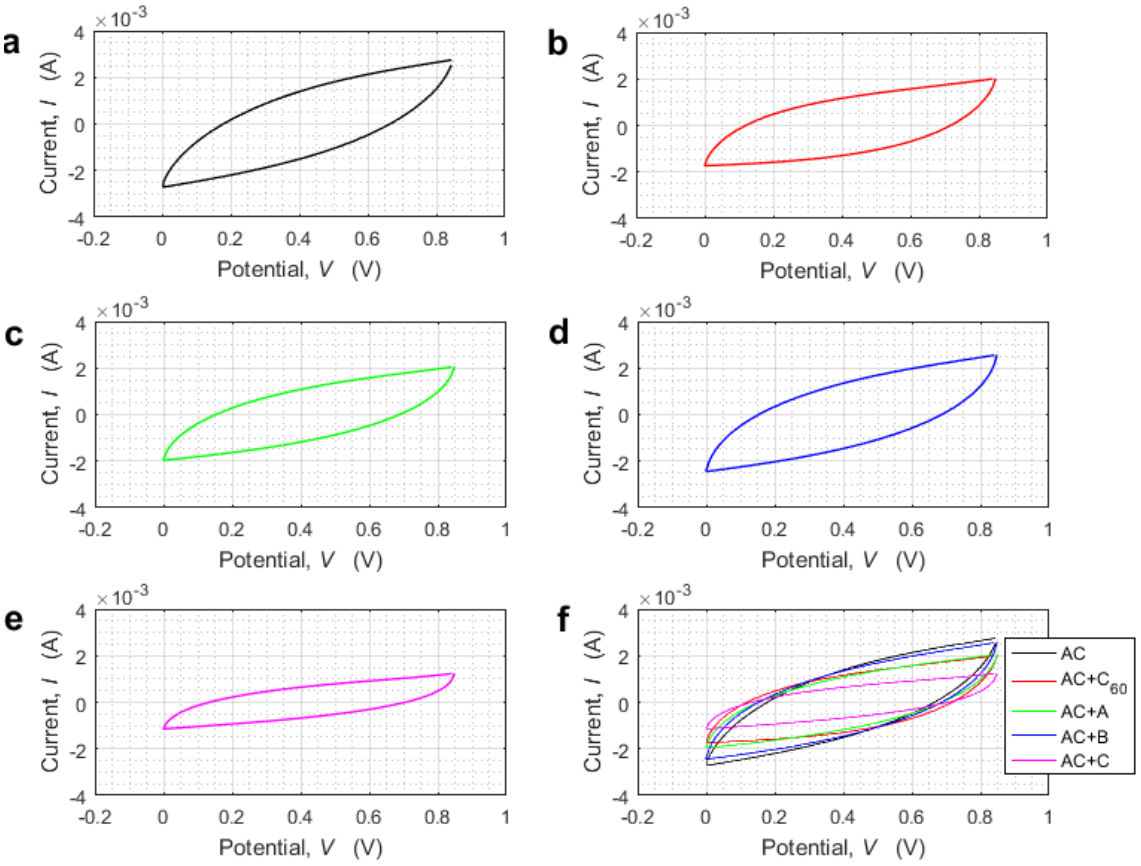

Figure 5-89 Cyclic voltammograms of symmetric supercapacitors S1-S5 (a-e respectively). Superimposed curves are shown in f.

5.9.2 Galvanostatic charge-discharge (GCD)

Figure 5-90 shows 20 GCD cycles of the five supercapacitors. It could be seen that apart from supercapacitor S3 (AC+A), the ranges of potential response observed in GCD curves of other additive-containing supercapacitors are wider than that of the control S1 (AC). The 20th GCD cycle of each supercapacitor is shown in Figure 5-91, which was used in conjunction with Equation (2-2) and Equation (2-5) to estimate specific capacitance ($C_{sp,cell}$) and ESR. The estimated values are shown in Table 5-28, which was further analysed and discussed in Section 5.9.4.

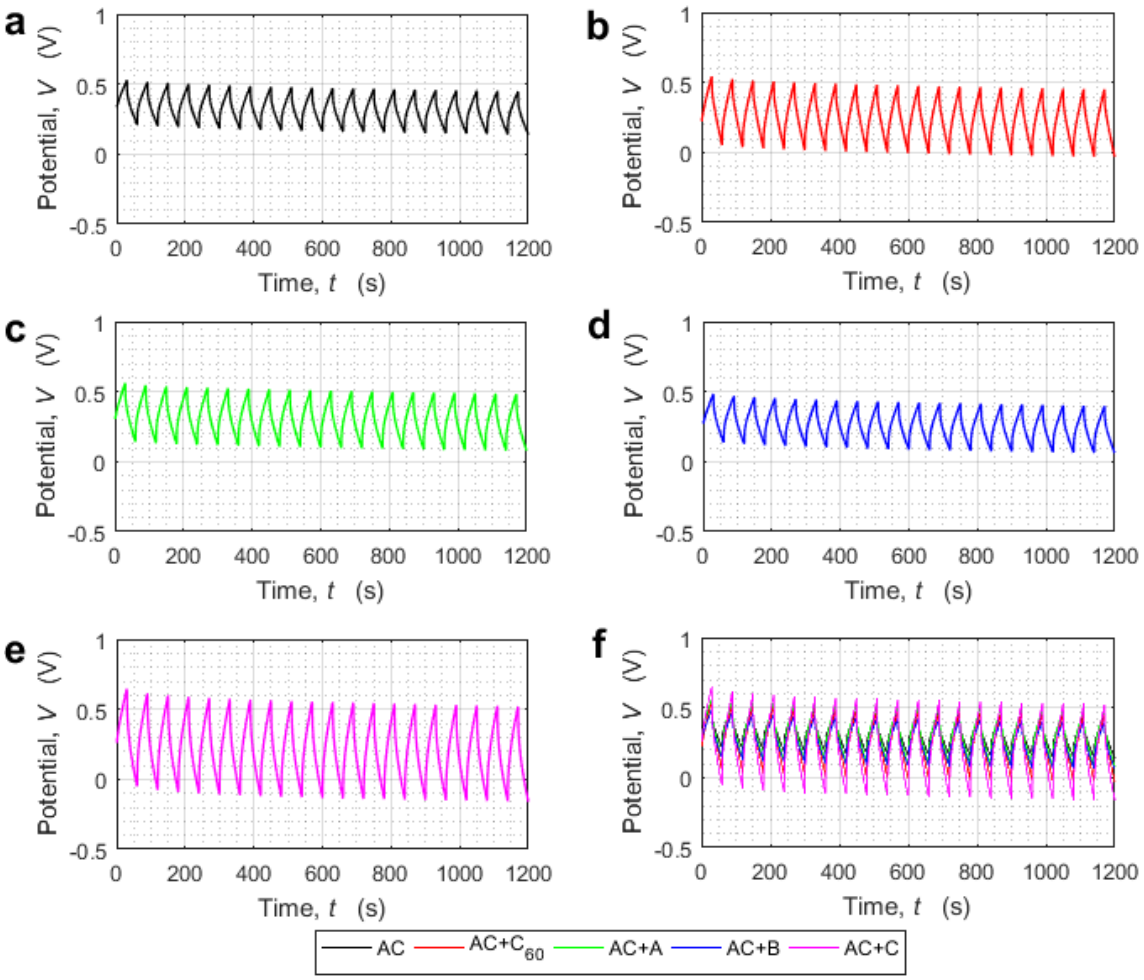

Figure 5-90 GCD curves showing 20 cycles from symmetric supercapacitors S1-S5 (a-e respectively). Superimposed curves are shown in f.

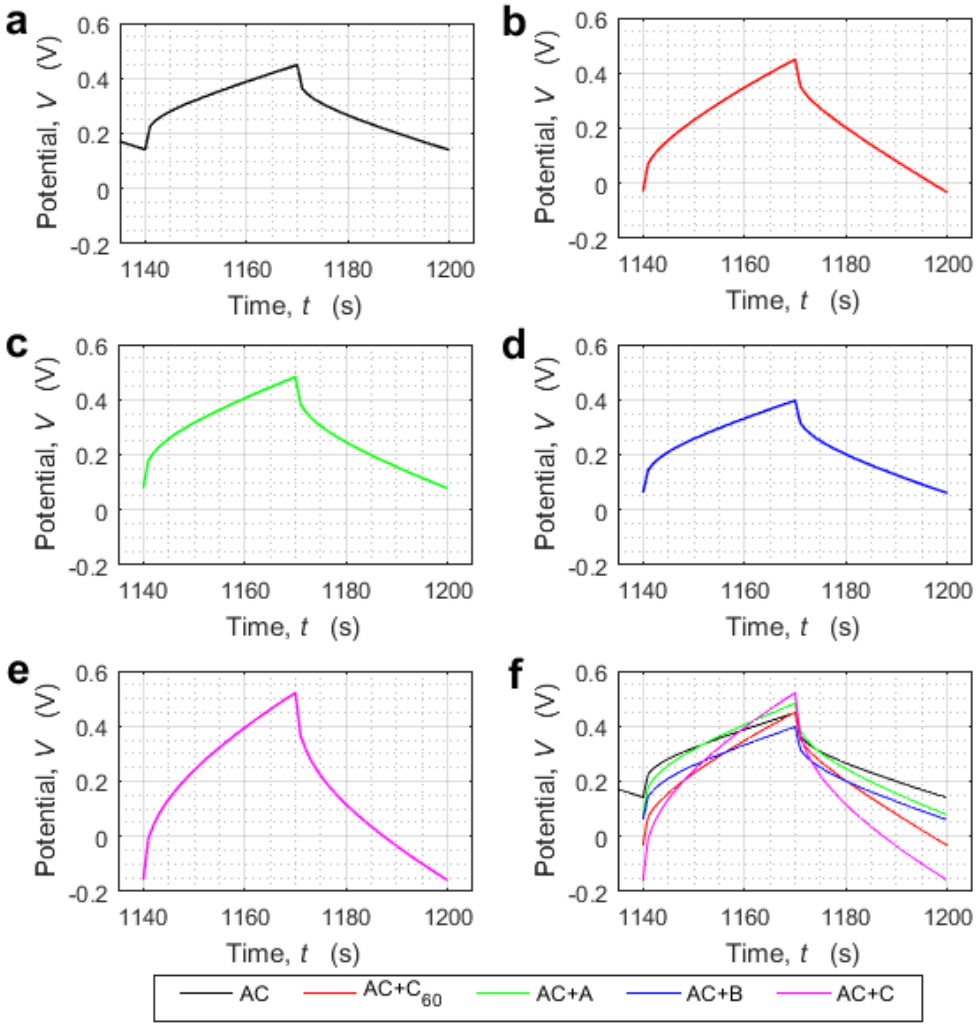

Figure 5-91 GCD curves of the 20th cycles from supercapacitor S1-S5 (a-e respectively). Superimposed curves are shown in f.

Table 5-28 Specific capacitance ($C_{sp,cell}$) and ESR of each assembled supercapacitor estimated from GCD curves

Electrode active material	$C_{sp,cell}$ (F/g)	ESR (Ω)
100%AC	22.2	43.0
AC+10%C_{60}	11.1	49.0
AC+10%A	13.8	49.7
AC+10%B	15.6	41.0
AC+10%C	7.7	78.0

5.9.3 Electrochemical impedance spectroscopy (EIS)

Figure 5-92 show Nyquist plots obtained from the five supercapacitors. From each plot, values of solution and charge-transfer resistance (R_{Ω} and R_{ct} respectively) were determined and shown in Table 5-29.

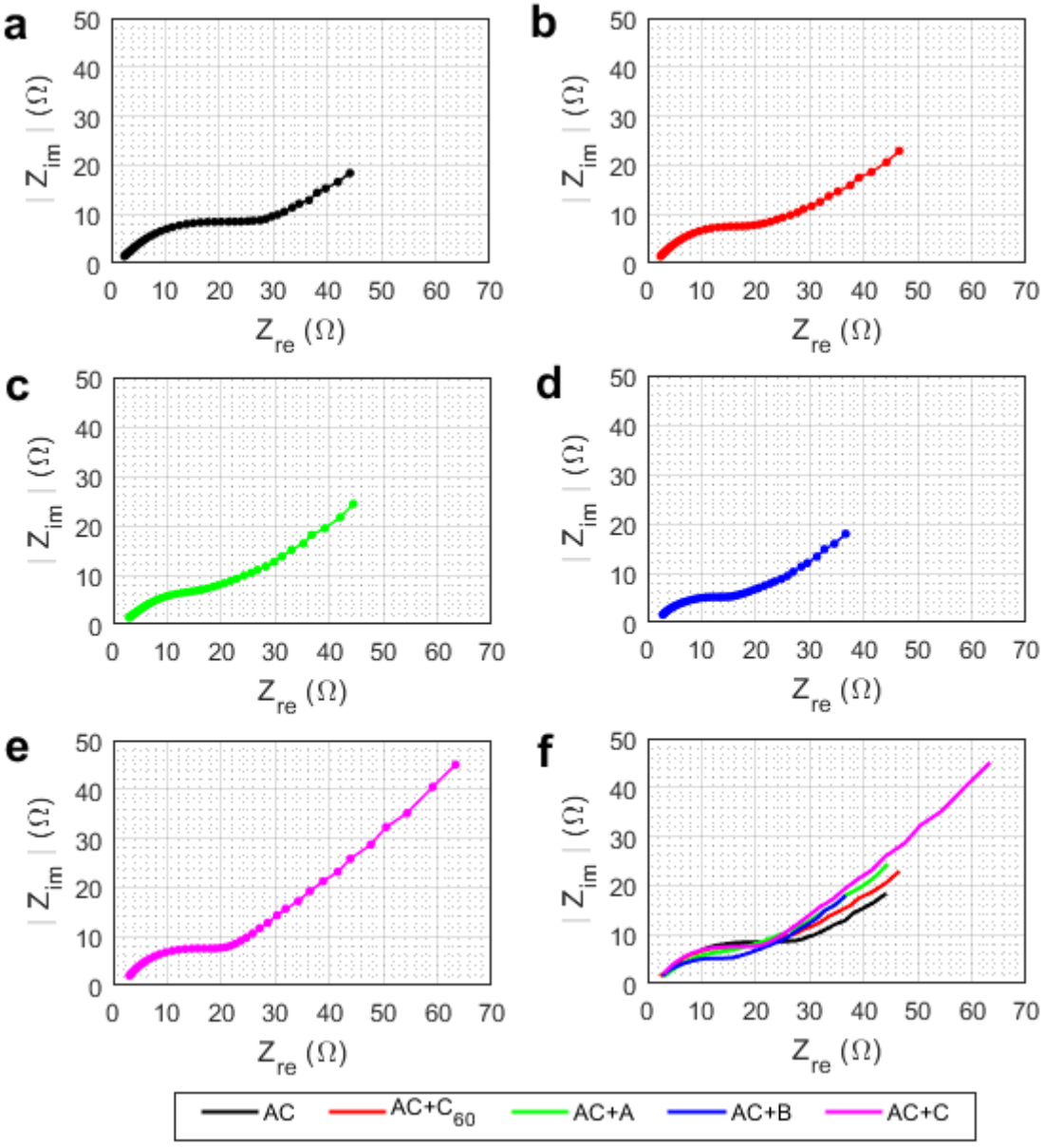

Figure 5-92 Nyquist plots of symmetric supercapacitors S1-S5 (a-e respectively). Superimposed curved are shown in f.

Table 5-29 Solution resistance (R_Ω) and charge-transfer resistance (R_{ct}) derived from Nyquist plot of each supercapacitor

Electrode active material	R_Ω (Ω)	R_{ct} (Ω)
100%AC	1.5	31.5
AC+10%C_{60}	1.0	27.0
AC+10%A	1.5	27.5
AC+10%B	1.0	21.0
AC+10%C	1.0	25.0

5.9.4 Effect of fullerenol as electrode additives on the performance of symmetric activated carbon supercapacitor

Values of estimated specific capacitance of each supercapacitor (from Table 5-28) was plotted against the corresponding level of hydroxylation ($n_{(OH)}$) in the additives present in its electrode, shown in Figure 5-93. Additive-containing supercapacitors S2-S5 have lower C_{sp} when compared to the control S1 (AC). However, other performance metrics, such as ESR, E, and P_{max} should also be considered for evaluation of overall performance.

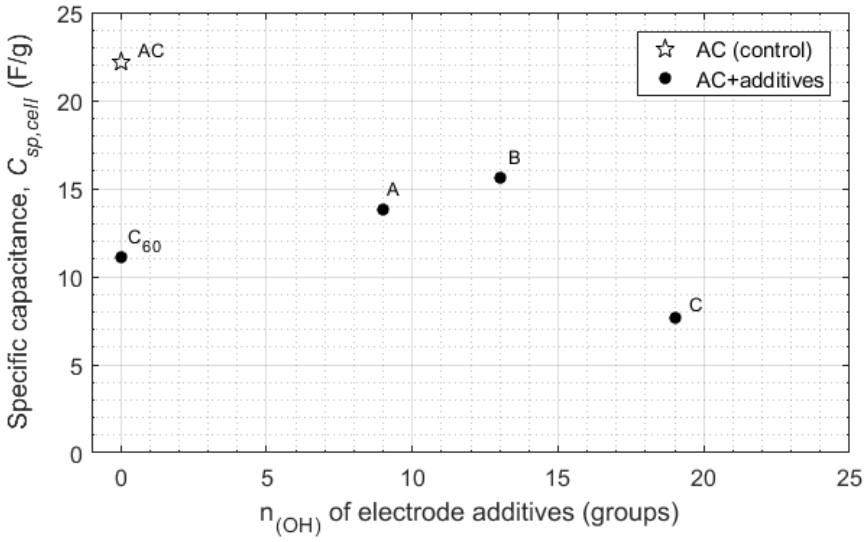

Figure 5-93 Plot of specific capacitance ($C_{sp,cell}$) against $n_{(OH)}$ of electrode additives

Resistance is another important performance parameter. Figure 5-94 plots ESR values derived from GCD curves against the corresponding $n_{(OH)}$ of the additives. ESR of almost all supercapacitors, apart from S4 (AC+B), are higher when compared to the control S1 (AC). The observed trend is, however, different from that of R_{ct} (of which values were determined from Nyquist plots), shown in Figure 5-95 together with R_{Ω}. Values of R_{Ω} remain constant among all five supercapacitors, indicating that there was no significant difference regarding solution resistance which was a good sign. Considering the trends of ESR and R_{ct}, it was suggested that there might be contributions from some other resistance components of the cell which resulted in ESR values of additive-containing supercapacitors S2-S4 being higher than that of the control.

Using Equation (2-3) together with values of estimated C_{sp} from Table 5-28, energy density (E) of each supercapacitor was estimated and plotted against the corresponding $n_{(OH)}$ of additives, shown in Figure 5-96. From Equation (2-3), E is directly proportional to C_{sp}. Despite this fact, the observed trend appeared in the opposite direction to most of the cells, but resembles the trend of ESR-$n_{(OH)}$ in Figure 5-94. The largest energy density was obtained from supercapacitor S5 (AC+C), and the lowest was from supercapacitor S4 (AC+B). All additive-containing supercapacitors offered higher energy densities than that of the control S1 (AC).

The final parameter to consider for evaluating performance of each supercapacitor in the investigation was maximum power (P_{max}). Using Equation (2-4) together with ESR and potential values from GCD curves, P_{max} of each supercapacitor was estimated and plotted against corresponding $n_{(OH)}$ in additives present in the electrodes. The observed trend in Figure 5-97 resembles both that of E and ESR.

All parameters from the five supercapacitors could now be considered together to determine the effect of $n_{(OH)}$ on supercapacitor performance when fullerenol is used as electrode additives in symmetric activated carbon supercapacitors.

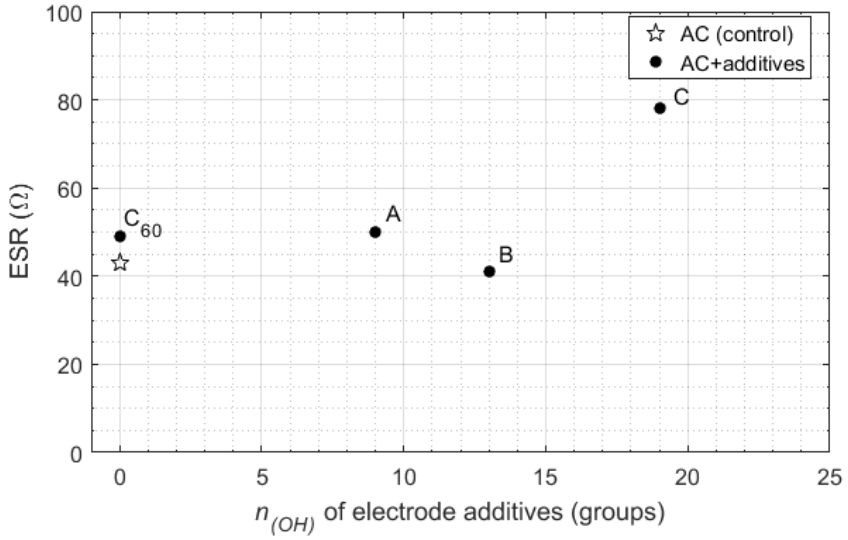

Figure 5-94 Plot of ESR against $n_{(OH)}$ of electrode additives

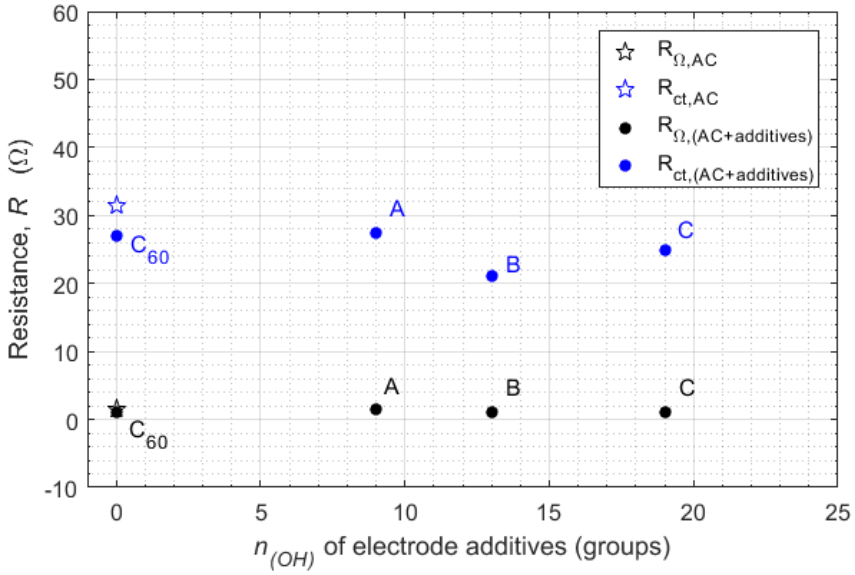

Figure 5-95 Plot of solution resistance (R_Ω) and charge-transfer resistance (determined from Nyquist plots) against $n_{(OH)}$ of electrode additives

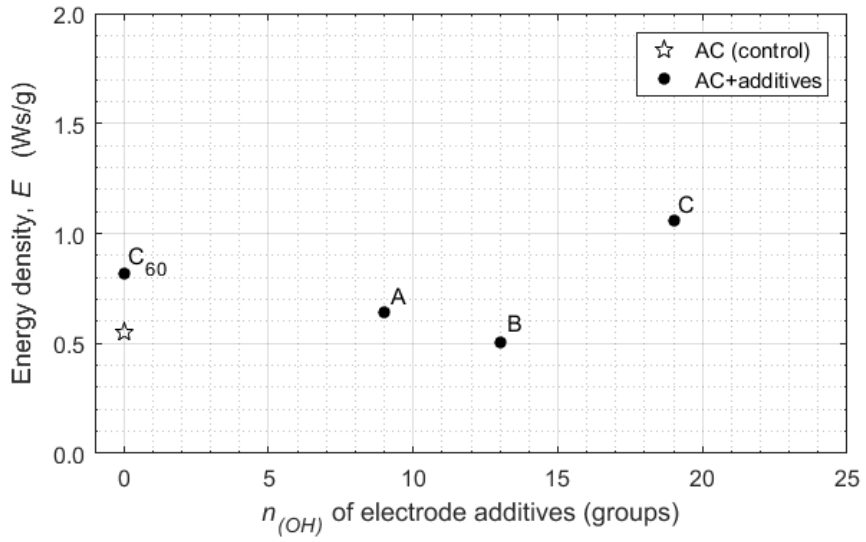

Figure 5-96 Plot of specific energy density against $n_{(OH)}$ of electrode additives

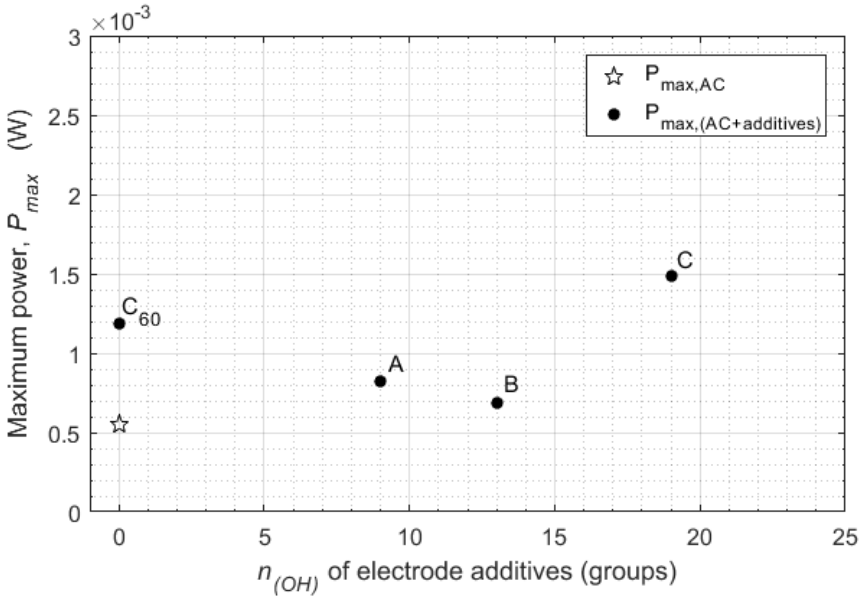

Figure 5-97 Plot of maximum power against $n_{(OH)}$ of electrode additives

The fullerene cage structure, which is present in both plain C_{60} and fullerenol, is known to be an excellent facilitator for electron transport (Hirsch, 2010; Cao et al., 2016). This leads to the smaller R_{ct} values from all additive-containing supercapacitors when compared to the control (additive-free), which are also in agreement with their higher values of slopes from discharge curves and higher values of P_{max}.

Based on the fact that R_{Ω} from all supercapacitors were roughly the same, and another fact that R_{ct} of additive-containing supercapacitors were higher than that of the control, it was proposed that there might be contributions from some other resistance components which ultimately resulted in higher values of ESR for additive-containing supercapacitors, for example, choice of binder or ratio between binder and additives for electrode slurry formulation might not be optimal for fullerene-based materials yet.

Another phenomenon in an opposite direction to the satisfying results (P_{max}, E and R_{ct}) for additive-containing supercapacitors is C_{sp}. It is proposed that charge transfer by fullerene cage structure (in both pristine C_{60} and fullerenol) might not be synchronous with activated carbon, resulting in a counter-action. There could be some factors, which were not yet understood, causing difference between the cage and activated carbon concerning speed of response to electrical change. It is believed that this phenomenon leads to a counter-current in the cyclic voltammetry experiments, which might be responsible for the narrower cyclic voltammograms, as well as the higher values of ESR, for supercapacitors with additives when compared to the control.

The relationship between $n_{(OH)}$ and each supercapacitor performance metric seemed to be non-linear. Supercapacitor S5 which contained Product C, (the highest $n_{(OH)}$) offered the best performance among the fullerenol-containing supercapacitors, also among all five supercapacitors, in terms of P_{max}, E and R_{ct}. Surprisingly, the lowest performance in terms of the mentioned parameters was from supercapacitor S4 containing Product B (medium-$n_{(OH)}$).

Based on the fact that all fullerenol-containing supercapacitors offered higher values of P_{max}, E and lower R_{ct} when compared to the control (additive-free), it was suggested that fullerenol could be used in supercapacitor applications. The current challenges are raising C_{sp} while reducing ESR which might be achievable through improvement and optimisation of electrode formulation and fabrication techniques to be optimal for fullerenol to show its full performance.

6 CONCLUSIONS

Fullerenol is an attractive water-soluble fullerene derivative which are being explored on its applications in many areas, with the largest proportions of existing publications on medical applications which would be greatly beneficial to human lives. However, it was realised that applications of fullerenol are being advanced on an unstable ground of synthesis as different research groups synthesised fullerenol for their uses from different routes. To avoid complications arising from variations between different synthesis routes including residual components and possible contaminations, this research sees that development of protocols to produce different fullerenol (i.e. different levels of hydroxylation) based on a single route is necessary. It was also realised that, with the current knowledge and synthesis capability within fullerenol research community, the producible fullerenol are still not suitable for medical applications which require material of superior grades and extremely narrow profiles. Until such capability is possible, fullerenol sector requires much more investment for research and development and therefore it is essential to find other fullerenol application which is both compatible with the currently producible grades of material and is in demand – energy storage applications.

Guided by this direction, the main aim of this research is to develop synthesis protocols capable of producing fullerenol with specified level of hydroxylation based on a single route (*Part One*). The complementary aim is to test the developed protocols and investigate the effects of the synthesised fullerenols as electrode additives in symmetric activated carbon supercapacitors for energy storage (*Part Two*).

The research started from selecting two candidates from available fullerenol synthesis routes and determining the most suitable route for the main aim and industrialisation. Considering several factors including efficiency as well as health and safety, the route for hydroxylation of C_{60} by sodium hydroxide in presence of phase-transfer catalyst (TBAH-NaOH route) was chosen. Consistency Evaluation Experiment was conducted where ANOVA was performed on values of estimated level of hydroxylation achieved in four

batches produced from the same process conditions. The analysis showed that, based on the available and accessible equipment and chemicals, the selected synthesis route offered a consistent production in terms of the achieved level of hydroxylation at significance level 0.025, with an average number of hydroxyl groups per fullerenol molecule of 19 groups. It is suggested that improvement on precision of synthesis equipment, control of working environment, as well as using quantitative analytical technique to confirm the amount of C_{60} molecules present in the C_{60}-toluene, could help satisfying consistency at higher significance levels.

The rest of the syntheses in this research were conducted in a laboratory different to Consistency Evaluation Experiment. All syntheses conducted in this location showed a common observation not previously present in Consistency Evaluation Experiment – a trace of white water-soluble solid. Also, TGA thermograms of some products deviated from normal fullerenol pattern. Through analysis of characterisation results, it was concluded that all products produced in this location contained sodium carbonate (as a result of reaction between sodium hydroxide solution and carbon dioxide in the atmosphere). Sodium carbonate was only existing as surroundings of the product particles within the bulk of isolated product. In addition, some products (Product 4, 10, 11 and 12) contained fullerene epoxide which resulted from the reaction between ambient ozone and C_{60} molecules in C_{60}-toluene solution. Once formed, individual fullerene epoxides could aggregate and form densely packed clusters of micron sizes, observed as black solids which did not dissolve in toluene. During the reaction, hydroxide ions and water molecules could not access the epoxide rings in the centre of these clusters but could still react with surfaces of the clusters, forming clusters which contained both hydroxyl groups and epoxide groups. Based on these analyses, the research has uncovered more critical requirements of the TBAH-NaOH route that the working environment must be free from carbon dioxide and ozone.

Due to the presence of sodium carbonate and fullerene epoxide in the isolated products, ‘TGA method’ could no longer be used to estimate $n_{(OH)}$ achieved in

each production. Based on a method to derive a hydrated empirical formula of fullerenol reported by a team of fullerenol researcher, this research has made some improvement and finally developed systematic mathematical calculations for determining empirical formula of fullerenol using information from TGA and EDX ('TGA-EDX method') which gives a finite solution in a single run without the need to guess the first value for iterative calculations as previously required by the original method. 'TGA EDX method' was used for estimation of level of hydroxylation in all products from experiments to study the effects of three selected process parameters on level of hydroxylation achieved, and the scale-up experiment. For products which show weight loss corresponding to decomposition of fullerene epoxide in TGA thermograms, estimation was based on a special model which included epoxide groups into product formula ($aC_{60}O(OH)_n \cdot bH_2O$ with cNa_2CO_3 as surroundings). For other products which did not show this variation, the normal model ($aC_{60}(OH)_n \cdot bH_2O$ with cNa_2CO_3 as surroundings) was used.

The TBAH experiment revealed a non-linear relationship between the amount of TBAH added for the reaction and $n_{(OH)}$ achieved. Within the range of 3 to 192 drops TBAH with two-fold incrementation, the capability of this parameter in controlling level of hydroxylation is 8-14 groups. The maximum level of 14 groups were obtained when 24 drops of TBAH were used, while the minimum level of 8 groups were obtained when 3 drops were used. The ratio between mass of isolated yield and mass of initial fullerene (PPF mass ratio) was defined by this research to analyse the effect of this parameter on production capacity (for use at the current stage where no stoichiometric information of the reaction was available). PPF mass ratios also followed the same trend as $n_{(OH)}$.

Through NaOH Experiment, this research has discovered that the relationship between volume of sodium hydroxide solution added for the reaction and $n_{(OH)}$ resembled Freundlich Adsorption Isotherm (with an extra term). This leads to one step closer to understanding of the reaction. From the results, this parameter seemed to have a greater effect on PPF mass ratio than on level of hydroxylation. When the lowest volume of 0.5 ml of sodium hydroxide solution

was used, $n_{(OH)}$ was 8 groups per molecule similar to when 3 drops of TBAH was used in TBAH Experiment but PPF mass ratio was even lower (very little amount of isolated product). As the added volume increases, $n_{(OH)}$ increases and levels off after volume equals to 4.0 ml. However, the trend of PPF mass ratio does not level off. Within the conducted range, maximum $n_{(OH)}$ (as well as maximum amount of isolated yield) was obtained when 8.0 ml of sodium hydroxide solution was used.

Results from Reaction Time Experiment might indicate that the reaction had reached saturation after 10 minutes and that the range of reaction time less than 10 minutes might hold critical information on the point where saturation started. Unfortunately, further confirmation in this region as well as the region above 30 minutes could not be done in this research due to certain limitations.

Combining analyses of experimental results, characterisation and the discovered requirements, the research finally developed Protocol 1-3 for producing three different classes of fullerenol, all based on TBAH-NaOH route. Protocol 1, 2, and 3 are for producing low-$n_{(OH)}$ ($<$10 groups, using 3 drops of TBAH and 2.0 ml sodium hydroxide solution), medium-$n_{(OH)}$ (10-14 groups, using 24 drops of TBAH and 2.0 ml sodium hydroxide solution) and high-$n_{(OH)}$ (15-20 groups, using 24 drops of TBAH and 8.0 ml sodium hydroxide solution) respectively. Scale-up Experiment confirmed scalability of the developed protocols. $n_{(OH)}$ values of Product A (Protocol 1), Product B (Protocol 2) and Product C (Protocol 3) were estimated at 9, 13 and 19 groups respectively. Product A, B and C were used as experimental material in supercapacitor experiments.

Supercapacitor experiments responded to the complementary aim (*Part Two*) of this research, using three different classes of fullerenol produced from the same route to study the effect of $n_{(OH)}$ on supercapacitor performance when fullerenol was used as electrode additives in symmetric activated carbon supercapacitor. Pristine C_{60} was also involved to represent zero level of hydroxylation, and activated carbon represented a control. Analysis and comparison could be done without concerns regarding variations from different synthesis routes. Analysis

of electrochemical results revealed that all assembled supercapacitors exhibited capacitive behaviour in the potential window 0.00-0.85 V, and that supercapacitors with electrodes containing fullerenol and fullerene additives gave higher values of P_{max}, higher E, and lower R_{ct} when compared to the supercapacitor without additives. This could be related to the fact that C_{60} cage is an excellent ability in electron transfer. Among different additives, supercapacitor with Product C addtives ($n_{(OH)}$ = 19 groups) had highest values of P_{max} and E, and lowest R_{ct}. Supercapacitors with Product A ($n_{(OH)}$ = 9 groups) and B ($n_{(OH)}$ = 13 groups) additives both have P_{max}, E, and R_{ct} lower than C_{60}. All parameters from the supercapacitor with Product B additives were the lowest among the additive-containing supercapacitors. However, additive-containing supercapacitors offered lower C_{sp}, with higher ESR, than that of the control. R_{Ω} of all cells were roughly the same. It was supposed that there were some other factors contributing to higher values of ESR and lower values of C_{sp} in the cells with additives (despite their low R_{ct}). This might include non-synchronous response to electrical changes between C_{60} cages and activate carbon, resulting in a counter-current, hence narrower voltammograms and smaller C_{sp}. It was suggested that improvement on formulation of electrode slurry, as well as fabrication technique, might raise the performance of fullerenol as electrode material for supercapacitor.

Through this research, both aims, and their related objectives, have been achieved. Three synthesis protocols have been developed for producing three different classes of fullerenol based on a single synthesis route within practical range. Discoveries of two additional important requirements of the TBAH-NaOH route on working conditions have been made. The obtained relationships between the selected process parameters and level of hydroxylation also facilitates better understanding of the behaviour of the reaction. Systematic mathematical calculations to determine level of hydroxylation for fullerenol ('TGA-EDX method') have been developed. The first investigation on application of fullerenol in supercapacitor has been made and showed that, with further development, the material should have its place in material for energy applications. This research wishes that the achievements would support the

fullerenol research community in approaching the time when the ultimate and ambitious benefits of fullerenol could finally be harvested.

7 FURTHER WORK

With regards to the studies of selected process parameters, the experiments were designed to cover as wide as possible ranges under certain limitations. As a result, large increments appeared in TBAH experiment and determining the relationship between TBAH and $n_{(OH)}$ in the missing range is important to confirm the overall behaviour. For NaOH Experiment, it may be useful to confirm if saturation is already reached by conducting syntheses using more than 8.0 ml of sodium hydroxide solution (although care should be taken when designing the experiment regarding the issue with total volume of the reaction). The range of reaction time below 10 minutes and above 30 minutes could not be involved in this research. However, experimental results from Reaction Time Experiment suggested that the range of less than 10 minutes might hold critical information, and that range above 30 minutes might also be interesting.

Expansion to investigating the effects of other process parameters on $n_{(OH)}$ achieved from the synthesis is also of interest.

The heart of this research, i.e. producing different fullerenol with specifiable $n_{(OH)}$ within practical range from a single route, could also be expanded and applied to other synthesis routes.

One very essential aspect which needs to be further investigated is quantitative determination of $n_{(OH)}$ achieved from a fullerenol synthesis. From this research, it can be seen that TGA method is convenient but cannot be used for its aimed purpose in certain circumstances where assistance from other technique such as EDX is required. However, so far, there has not been an official standard on how to determine this character yet. Analyses from more than two techniques might actually be required to make a more accurate conclusion on product formula and structure. Detailed studies on the list and the number of techniques required for estimation of $n_{(OH)}$ are therefore of great interest.

Considering the fact that the symmetric activated carbon supercapacitors with fullerenol as additives possess higher maximum powers compared to when no additive was used, it may be possible to step further. However, improvement on

formulation of electrode slurry and fabrication techniques which allows better performance of fullerenol are essential. Investigation on the choice of electrolyte for fullerenol-containing systems would also be beneficial.

REFERENCES

Addicoat, M.A., Page, A.J., Brain, Z.E., Flack, L., Morokuma, K. and Irle, S. (2012) 'Optimization of a genetic algorithm for the functionalization of fullerenes', *Journal of Chemical Theory and Computation*, 8(5), pp. 1841–1851. Available at: DOI:10.1021/ct300190u.

Aikawa, S., Yoshida, Y., Hatae, S., Nishiyama, S. and Kumar, D.S. (2007) 'Synthesis and characterization of a fullerene derivatives', *Molecular Crystals and Liquid Crystals*, 463(1), pp. 237/[519]-244/[526]. Available at: DOI:10.1080/15421400601028005.

Alves, G.C., Ladeira, L.O., Righi, A., Krambrock, K., Calado, H.D., Pereira de Freitas Gil, R. and Pinheiro, M.V.B. (2006) 'Synthesis of $C_{60}(OH)_{18-20}$ in aqueous alkaline solution under O_2-atmosphere', *Journal of Brazilian Chemical Society*, 17(6), pp. 1186-1190.

Anderson, S.A., Lee, K.K. and Frank, J.A. (2006) 'Gadolinium-fullerenol as a paramagnetic contrast agent for cellular imaging', *Investigative Radiology*, 41(3): 332–338. Available at: DOI:10.1097/01.rli.0000192420.94038.9e.

Arrais, A. and Diana, E. (2003) 'Highly water-soluble C_{60} derivatives: A new synthesis', *Fullerenes, Nanotubes, and Carbon Nanostructures*, 11(1), pp. 35-46.

Bai, L., Chen, Y., Bai, Y., Chen, Y., Zhou, J. and Huang, A. (2017) 'Fullerene-doped polyaniline as new redox nanoprobe and catalyst in electrochemical aptasensor for ultrasensitive detection of Mycobacterium tuberculosis MPT64 antigen in human serum', *Biomaterials*, 133, pp. 11–19. Available at: DOI:10.1016/j.biomaterials.2017.04.010.

Bard, A.J. and Faulkner, L.R. (2001) *Electrochemical Methods: Fundamentals and Applications*. 2nd edn. USA: John Wiley & Sons Inc.

Bednarikova, Z., Huy, P.D.Q., Mocanu, M., Fedunova, D., Li, M.S., Gazova, Z. (2016) 'Fullerenol $C_{60}(OH)_{16}$ prevents amyloid fibrillization of $A\beta_{40}$ – in vitro and

in silico approach', *Physical Chemistry Chemical Physics*, 18(28), pp. 18855–18867. Available at: DOI:10.1039/C6CP00901H.

Bobylev, A.G., Marsagishvili, L.G. and Podlubnaya, Z.A. (2010) 'Fluorescence analysis of the action of soluble derivatives of fullerene C_{60} on amyloid fibrils of the brain peptide Aβ(1–42)', *Biophysics*, 55(5), pp. 699–702. Available at: DOI:10.1134/S0006350910050027.

Brenson, M.L., Levine, D.M. and Krehbiel, T.C. (2012) *Basic Business Statistics: Concepts and Applications*. 12th edn. Prentice Hall.

Bourlinos, A.B., Georgakilas, V., Mouselimis, V., Kouloumpis, A., Mouzourakis, E., Koutsioukis, A., Antoniou, M., Gournis, D., Karakassides, M.A., Deligiannakis, Y., Urbanova, V., Cepe. K., Bakandritsos, A. and Zboril, R. (2017) 'Fullerol–graphene nanobuds: Novel water dispersible and highly conductive nanocarbon for electrochemical sensing', *Applied Materials Today*, 9, pp. 71–76. Available at: DOI:10.1016/j.apmt.2017.05.006.

Budde, M.D. and Frank, J.A. (2009) 'Magnetic tagging of therapeutic cells for MRI', Journal of Nuclear Medicine, 50(2), pp. 171–174. Available at: DOI:10.2967/jnumed.108.053546

Cai, X., Jia, H., Liu, Z., Hou, B., Luo, C., Feng, Z., Li, W. and Liu, J. (2008) 'Polyhydroxylated fullerene derivative $C_{60}(OH)_{24}$ prevents mitochondrial dysfunction and oxidative damage in an MPP+-induced cellular model of Parkinson's disease', Journal of Neuroscience Research, 86(16), pp. 3622–3634. Available at: DOI:10.1002/jnr.21805.

California FACE Program (2010) *09CA004: A Chemist Dies from Burns Caused by Mixing Chemicals*. Richmond, CA: California FACE Program.

Cao, T., Wang, Z., Xia, Y., Song, B., Zhai, Y., Chen, N. and Li, Y. (2016) 'Facilitating electron transportation in Perovskite solar cells via water-soluble fullerenol interlayers', *ACS Applied Materials & Interfaces*, 8, pp. 18284-18291.

Cataldo, F. (2002) ‘A Study on the thermal stability to 1000°C of various carbon allotropes and carbonaceous matter both under nitrogen and in air’, *Fullerenes, Nanotubes, and Carbon Nanostructures*, 10(4), pp. 293-311.

Centers for Disease Control and Prevention (2015) *CDC – SODIUM HYDROXIDE – International Chemical Safety Cards – NIOSH*. Available at: https://www.cdc.gov/niosh/ipcsneng/neng0360.html (Accessed: 27 November 2017).

Chandra, A. (2012) ‘Supercapacitors: An alternate technology for energy storage’, *Proceedings of the National Academy of Sciences India Section A - Physical Sciences*, 82(1): pp. 79–90. Available at: DOI:10.1007/s40010-012-0009-9.

Chang, R. and Goldsby, K.A. (2016) *Chemistry*. 12th edn. USA : McGraw-Hill Education.

Chen, Y., Cai, R., Chen, S. and Huang, Z. (2001) ‘Synthesis and characterization of fullerol derived from $C_{60}n-$ precursors’, *Journal of Physics and Chemistry of Solids*, 62(5), pp. 999–1001. Available at: DOI:10.1016/S0022-3697(00)00242-0.

Chen, Y.W. and Lai, Y.L. (2002) ‘Fullerene derivative protects against oxidative stress in raw 264.7 cells and ischemia-reperfused (IR) lungs’, *Free Radical Biology and Medicine*, 33(1), pp. S167–S168.

Chen, Z., Ma, L., Liu, Y. and Chen, C. (2012) ‘Applications of functionalized fullerenes in tumor theranostics’, *Theranostics*, 2(3), pp. 238–250. Available at: DOI:10.7150/thno.3509.

Chiang, L.Y., Bhonsle, J.B., Wang, L., Shu, S.F. and Chang, T.M (1996) ‘Efficient one-flask synthesis of water-soluble [60] fullerenols’, *Tetrahedron*,52(14), pp. 4963–4972. Available at: DOI:10.1016/0040-4020(96)00104-4.

Chiang, L.Y., Swirczewski, J.W., Hsu, C.S., Chowdhury, S.K., Cameron, S. and Creegan, K. (1992) ‘Multi-hydroxy additions onto C_{60} fullerene molecules’,

Journal of the Chemical Society, Chemical Communications, 62(24), pp. 1791. Available at: DOI:10.1039/c39920001791.

Chiang, L.Y., Upasani, R.B. and Swirczewski. J.W. (1992) 'Versatile Nitronium Chemistry for C_{60} Fullerene Functionalization', *Journal of American Chemical Society*, 114, pp.10154-10157.

Chiang, L.Y., Wang, L., Swirczewski. J.W., Soled, S. and Cameron, S. (1994) 'Efficient synthesis of polyhydroxylated fullerene derivatives via hydrolysis of polycyclosulfated precursors', *Journal of Organic Chemistry*, 59(14), pp. 3960–3968. Available at: DOI: 10.1021/jo00093a030.

Chibante, L.P.F. and Heymann, D. (1993) 'On the geochemistry of fullerenes: Stability of C_{60} in ambient air and the role of ozone', *Geochimica et Cosmochimica Acta*, 57(8), pp. 1879-1881.

Choi, H. and Yoon, H. (2015) 'Nanostructured electrode materials for electrochemical capacitor applications', *Nanomaterials*, 5, pp. 209-936.

Cong, W., Wang, P., Qu, Y., Tang, J., Bai, R., Zhao, Y., Chen, C. and Bi, X. (2015) 'Evaluation of the influence of fullerenol on aging and stress resistance using Caenorhabditis elegans', *Biomaterials*, 42, pp. 78–86. Available at: DOI:10.1016/j.biomaterials.2014.11.048.

Coro, J., Suárez, M., Silva, L.S.R., Eguiluz, K.I.B. and Salazar-Banda, G.R. (2016) 'Fullerene applications in fuel cells: A review', *International Journal of Hydrogen Energy*, 41(40), pp. 17944–17959. Available at: DOI:10.1016/j.ijhydene.2016.08.043.

Creegan, K.M., Robbins, J.L., Robbins, W.K., Millar, J.M., Sherwood, R.D., Tindall, P.J. and Cox, D.M. (1992) 'Synthesis and characterization of $C_{60}O$, the first fullerene epoxide', *Journal of American Chemical Society*, 114, pp. 1103-1105.

Darabi, S. and Mohammadi, MT. (2017) 'Fullerol potentiates the brain antioxidant defense system and decreases γ-glutamyl transpeptidase (GGT) mRNA during cerebral ischemia/reperfusion injury', *Journal of Mazadaran*

University of Medical Sciences, 9(1), pp. 25–32. Available at: DOI:10.1515/ejnm-2016-0024.

Dattani, R., Gibson, K.F., Few, S., Borg, A.J., DiMaggio, P.A., Kazarian, S.G. and Cabral, J.T. (2015) 'Fullerene oxidation and clustering in solution induced by light', *Journal of Colloid and Interface Science*, 446, pp. 24-30.

Davies, A. and Yu, A. (2011) 'Material advancements in supercapacitors: From activated carbon to carbon nanotube and graphene', *Canadian Journal of Chemical Engineering*, 89(6), pp. 1342–1357. Available at: DOI:10.1002/cjce.20586.

Djordjevic, A. (2000) *Synthesis of Water-Soluble Derivatives of Fullerene C_{60}* PhD thesis. University of Novi Sad.

Dobashi, R., Matsunaga, K. and Tajima, M. (2014) 'Effects of fullerene derivatives on the gas permeability of thermoplastic polyurethane elastomers', *Journal of Applied Polymer Science*, 131(6), pp. 1–6. Available at: DOI:10.1002/app.39986.

El-Nagar, D.M., Ahmed, H.M., Aldahmash, B.A. and Ibrahim, K.E. (2016) 'Toxic effects of oral administration doses of hydroxylated C_{60} fullerene on liver in swiss albino mice', *Nanoscience and Nanotechnology Letters*, 8(12), pp. 1040–1046. Available at: DOI:10.1166/nnl.2016.2244.

Evtushenko, Y.M., Ivanov, V.M. and Zaitsev, B.E. (2003) 'Determination of epoxide and hydroxyl groups in epoxide resins by IR spectrometry', *Journal of Analytical Chemistry*, 58(4), pp.347-350.

Faraji, S. and Ani, F.N. (2014) 'Microwave-assisted synthesis of metal oxide/hydroxide composite electrodes for high power supercapacitors – A review', *Power Sources*, 263, pp. 338-360. Available at: DOI:10.1016/j.powsour.2014.03.144.

Fluri, F., Grünstein, D., Cam, E., Ungethuem, U., Hatz, F., Schäfer, J., Samnick, S., Israel, I., Kleinschnitz, C., Orts-Gil, G., Moch, H., Zeis, T., Schaeren-Wiemers, N. and Seeberger, P. (2015) 'Fullerenols and glucosamine fullerenes

reduce infarct volume and cerebral inflammation after ischemic stroke in normotensive and hypertensive rats', *Experimental Neurology*, 265, pp. 142–151. Available at: DOI:10.1016/j.expneurol.2015.01.005.

Gamry (2017) *Basics of EIS: Electrochemical Research-Impedance*. Available at: https://www.gamry.com/application-notes/EIS/basics-of-electrochemical-impedance-spectroscopy/ (Accessed: 30 June 2017).

Gonzalez, M.G., Cabanelas, J.C. and Baselga, J. (2012) 'Applications of FTIR on Epoxy Resins – Identification, Monitoring the Curing Process, Phase Separation and Water Uptake', in Theophile, T. (ed.) *Infrared Spectroscopy – Material Science, Engineering and Technology*. InTech. Available at: http://www.intechopen.com/books/infrared-spectroscopy-materials-science-engineering-and-technoloy/applications-of-ftir-on-epoxy-resins-identification-monitoring-the-curing-process-phase-separatio (Accessed: 3 August 2017).

González, A., Goikolea, E., Barrena, J.A. and Mysyk, R. (2016) 'Review on supercapacitors: Technologies and materials', *Renewable and Sustainable Energy Reviews*, 58, pp. 1189–1206. Available at: DOI:10.1016/j.rser.2015.12.249.

Goswami, T.H., Singh, R., Alam, S. and Mathur, G.N. (2004) 'Thermal analysis: a unique method to estimate the number of substituents in fullerene derivatives', *Thermochimica Acta*, 419, pp. 97-104.

Grebowski, J., Kazmierska, P. and Krokosz, A. (2013) 'Fullerenols as a new therapeutic approach in nanomedicine', *BioMed Research International*, Available at: DOI:10.1007/978-1-62703-475-3_5.

Grebowski, J., Krokosz, A. and Puchala, M. (2013) 'Fullerenol C60(OH)36 could associate to band 3 protein of human erythrocyte membranes', *Biochimica et Biophysica Acta (BBA) – Biomembranes*, 1828(9), pp. 2007–2014. Available at: DOI:10.1016/j.bbamem.2013.05.009.

Grobmyer, S.R. and Krishna, V. (2012) 'Minimally invasive cancer therapy using polyhydroxy fullerenes', *European Journal of Radiology*, 81(S1), pp. S51–S53. Available at: DOI:10.1016/S0720-048X(12)70019-0.

Hart, P.W., Houtman, C. and Hirth, K. (2013) 'Hydrogen peroxide and caustic soda: Dancing with a dragon while bleaching', *Tappi Journal*, 12(7), pp. 59-65.

He, H., Zheng, L., Jin, P. and Yang, M. (2011) 'The structural stability of polyhydroxylated C60(OH)24: Density functional theory characterizations', *Computational and Theoretical Chemistry*, 974(1–3), pp. 16–20. Available at: DOI:10.1016/j.comptc.2011.07.005.

Heckl, S. (2007) 'Future contrast agents for molecular imaging in stroke', *Current Medicinal Chemistry*, 14(16), pp. 1713–1728. Available at: DOI:10.2174/092986707781058896.

Heymann, D., Bachilo, S.M., Weisman, R.B., Cataldo, F., Fokkens, R.H., Nibbering, N.M.M., Vis, R.D. and Chibante, L.P.F. (2000) '$C_{60}O_3$, a fullerene ozonide: Synthesis and dissociation in to $C_{60}O$ and O_2', *Journal of American Chemical Society*, 122, pp. 11473-11479.

Heymann, D. and Cataldo, F. (2001) 'Unstable products from the ozonation of C_{60} in solvents', *Fullerene Science and Technology*, 9(1), pp. 71-76. Available at: DOI: 10.1081/FST-100000166.

Heymann, D. and Chibante, L.P.F. (1993a) 'Reaction of C_{60} and C_{70} with ozone at different temperatures', *Recueil des Travaux Chimiques des Pays-Bas*, 112, pp. 531-534. Available at: DOI: 10.1002/recl/19931121004.

Heymann, D. and Chibante, L.P.F. (1993b) 'Reaction of C_{60}, C_{70}, C_{76}, C_{78} and C_{84} with ozone at 23.5°C', *Recueil des Travaux Chimiques des Pays-Bas*, 112(12), pp. 639-642. Available at: DOI: 10.1002/recl.19931121206.

Hirsch, A. (2010) 'The era of carbon allotropes', *Nature Materials*, 9, pp. 868–871. Available at: DOI:10.1038/nmat2885.

Hirsch, A. and Brettreich, M. (2004) *Fullerenes: Chemistry and Reactions*. Weinheim, FRG: Wiley. Available at: DOI:10.1002/3527603492 (Accessed: 22 June 2017).

Huang, C.K. and Kerr. P.F. (1960) 'Infrared study of the carbonate minerals', *The American Mineralogist*, 45, pp. 311-324.

Hulliwell, B. and Gutteridge, J.M.C. (2015) *Free Radicals in Biology and Medicine*. 5th edn. Oxford: Oxford University Press.

Husen, A. and Siddiqi, K. (2014) 'Carbon and fullerene nanomaterials in plant system', *Journal of Nanobiotechnology*, 12(1), pp. 16. Available at: DOI:10.1186/1477-3155-12-16.

Iijima, S. (1991) 'Helical microtubules of graphitic carbon', *Nature*, 354, pp. 56–58. Available at: DOI:10.1038/354056a0.

Injac, R., Perse, M., Cerne, M., Potocnik, N., Radic, N., Govedarica, B., Djordjevic, A., Cerar, A. and Strukelj, B. (2009) 'Protective effects of fullerenol $C_{60}(OH)_{24}$ against doxorubicin-induced cardiotoxicity and hepatotoxicity in rats with colorectal cancer', *Biomaterials*, 30(6), pp. 1184–1196. Available at: DOI:10.1016/j.biomaterials.2008.10.060.

Injac, R., Prijatelj, M. and Strukelj, B. (2013) 'Fullerenol Nanoparticles: Toxicity and Antioxidant Activity' in Armstrong, D. and Bharali, D.J. (eds.) *Oxidative Stress and Nanotechnology: Methods and Protocols*. New York: Springer, pp. 75–100. Available at: DOI:10.1007/978-1-62703-475-3.

Jacevic, V., Djordjevic, A., Srdjenovic, B., Milic-Tores, V., Segrt, Z., Dragojevic-Simic, V. and Kuca, K. (2017) 'Fullerenol nanoparticles prevents doxorubicin-induced acute hepatotoxicity in rats', *Experimental and Molecular Pathology*, 102(2), pp. 360–369. Available at: DOI:10.1016/j.yexmp.2017.03.005.

Jiang, J., Li, Y., Liu, J., Huang, X., Yuan, C. and Lou, X.W.D. (2012) 'Recent advances in metal oxide-based electrode architecture design for electrochemical energy storage', *Advanced Materials*, 24(38), pp. 5166–5180. Available at: DOI:10.1002/adma.201202146.

Jiao, F., Liu, Y., Qu, Y., Li, W., Zhou, G., Ge, C., Li, Y., Sun, B. and Chen, C. (2010) 'Studies on anti-tumor and antimetastatic activities of fullerenol in a mouse breast cancer model', *Carbon*, 48(8), pp. 2231–2243. Available at: DOI:10.1016/j.carbon.2010.02.032.

Jin, H., Chen, W.Q., Tang, X.W., Chiang, L.Y., Yang, C.Y., Schloss, J.V., Wu, J.Y. (2000) 'Polyhydroxylated C60, fullerenols, as glutamate receptor antagonists and neuroprotective agents', *Journal of Neuroscience Research*, 62(4), pp. 600–607. Available at: DOI:10.1002/1097-4547(20001115)62:4<600::AID-JNR15>3.0.CO;2-F.

Jin, J., Dong, Y., Wang, Y., Xia, L., Gu, W., Bai, X., Chang, Y., Zhang, M., Chen, K., Li, J., Zhao, L. and Xing, G. (2016) 'Fullerenol nanoparticles with structural activity induce variable intracellular actin filament morphologies', *Journal of Biomedical Nanotechnology*, 12(6), pp. 1234–1244. Available at: DOI:10.1166/jbn.2016.2251.

Jović, D.S., Seke, M.N., Djordjevic, A.N., Mrđanović, J.Ž., Aleksić, L.D., Bogdanović, G.M., Pavic, A.B. and Plavec, J. (2016) 'Fullerenol nanoparticles as a new delivery system for doxorubicin', *RSC Advances*, 6(45), pp. 38563–38578. Available at: DOI:10.1039/C6RA03879D.

Kampouris, .DK., Ji, X., Randviir, E.P. and Banks, C.E. (2015) 'A new approach for the improved interpretation of capacitance measurements for materials utilised in energy storage', *RSC Advances,* 5, pp. 12782–12791. Available at: DOI:10.1039/c4ra17132b .

Kano, K., Hayashi, T., Takaya, Y. and Kokubo, K. (2010) 'Verification of generation and removal process of surface brittle film, in polishing process using water soluble fullerenol, *10th International Symposium on Measurement and Quality Control 2010, ISMQC 2010*. Osaka, Japan. pp. 555–558.

Kausar, A. (2017) 'Advances in Polymer/Fullerene Nanocomposite: A Review on Essential Features and Applications', *Polymer-Plastics Technology and Engineering*, 56(6), pp. 594–605. Available at: DOI:10.1080/03602559.2016.1233278.

Kim, J. and Lee, H. (2001) ‘Thermal and Carbothermic Decomposition of Na2CO3 and Li2CO3’, *Metallurgical and Materials Transactions B*, 32B, pp. 17-24.

Knezevic, N., Milenkovic, S., Jovic, D., Lazarevic, S., Mrdjanovic, J. and Djordjevic, A. (2015) ‘Fullerenol-capped porous silica nanoparticles for pH-responsive drug delivery’, *Advances in Materials Science and Engineering*. 2015: Article ID 567350. Available at: DOI:10.1155/2015/567350.

Kokubo, K., Matsubayashi, K., Tategaki, H., Takada, H. and Oshima, T. (2008) ‘Facile synthesis of highly water-soluble fullerenes more than half-covered by hydroxyl groups’, *ACS Nano*, 2(2), pp. 327–333. Available at: DOI:10.1021/nn700151z.

Kokubo, K., Shirakawa, S., Kobayashi, N., Aoshima, H. and Oshima, T. (2011) ‘Facile and scalable synthesis of a highly hydroxylated water-soluble fullerenol as a single nanoparticle’, *Nano Research*, 4(2), pp. 204–215. Available at: DOI:10.1007/s12274-010-0071-z.

Kokubo, K. (2012) ‘Water-Soluble Single-Nano Carbon Particles: Fullerenol and Its Derivatives’ in Hashim, A.A. (ed.) *The Delivery of Nanoparticles*. InTech. Available at: DOI:10.5772/36352.

Kong, L., Tedrow, O., Chan, Y.F., Zepp, R.G. (2009) ‘Light-initiated transformations of fullerenol in aqueous media’, *Environmental Science & Technology*, 43(24), pp. 9155–9160. Available at: DOI:10.1021/es901839q.

Krishna, V., Singh, A., Sharma, P., Iwakuma, N., Wang, Q., Zhang, Q., Knapik, J., Jiang, H., Grobmyer, S.R., Koopman, B. and Moudgil, B. (2010) ‘Polyhydroxy fullerenes for non-invasive cancer imaging and therapy’, *Small*, 6(20), pp. 2236–2241. Available at: DOI:10.1002/smll.201000847.

Kroto, H.W., Heath, J.R., O’Brien, S.C., Curl, R.F. and Smalley, R.E. (1985) ‘C_{60}: Buckminsterfullerene’, *Nature*, 318(6042), pp. 162–163. Available at: DOI:10.1038/318162a0.

Kumar, R., Kumar, P., Naqvi, S., Gupta, N., Saxena, N., Gaur, J., Maurya, J.K. and Chand, S. (2014) 'Stable graphite exfoliation by fullerenol intercalation via aqueous route', *New Journal of Chemistry*, 38(10), pp. 4922–4930. Available at: DOI:10.1039/c4nj00907j.

Kyokane, J., Tsujimoto, K., Yanagisawa, Y., Ueda, T. and Fukuma, M. (2004) 'Actuator using electrostriction effect of fullerenol-doped polyurethane elastomer (PUE) films', *IEICE TRANSACTIONS on Electronics*, E87–C(2), pp. 136–141.

Li, J., Takeuchi, A., Ozawa, M., Li, X., Saigo, K. and Kitazawa, K. (1993) 'C60 fullerol formation catalysed by quaternary ammonium hydroxides', *Journal of the Chemical Society, Chemical Communications*, pp.1784. Available at: DOI:10.1039/c39930001784.

Liu, D., Chen, L., Liu, T., Fan, T., Tsou, E. and Tiu, C. (2014) 'An effective mixing for lithium ion battery slurries', *Advances in Chemical Engineering and Sciences*, 4, pp.515-528.

Liu, J.M., Gao, F., Yang, T.L., Lai, J.H. and Li, Z.M. (2008) 'Catalytic solid substrate-room temperature phosphorimetry for the determination of trace As(V) based on oxidising reaction between hydrogen peroxide and fullerenol using tween-80 as sensitizer', *International Journal of Environmental Analytical Chemistry*, 88(9), pp. 613–624. Available at: DOI:10.1080/03067310801930493.

Liu, Y.H., Liu, P.X., Che, L., Shu, C.Y. and Lu, X.C. (2012) 'Tunable tribological properties in water-based lubrication of water-soluble fullerene derivatives via varying terminal groups', *Chinese Science Bulletin*, 57(35), pp. 4641–4645. Available at: DOI:10.1007/s11434-012-5515-2.

Liu, Y., Wang, Z. and Wang, X. (2015) 'AFM-based study of fullerenol ($C_{60}(OH)_{24}$)-induced changes of elasticity in living SMCC-7721 cells', *Journal of the Mechanical Behavior of Biomedical Materials*, 45, pp. 65–74. Available at: DOI:10.1016/j.jmbbm.2014.12.011.

Liu, Y., Wang, Z., Wang, X. and Huang, Y (2015) ‘Quantitative analysis of dynamic adhesion properties in human hepatocellular carcinoma cells with fullerenol’, *Micron*, 79, pp. 74–83. Available at: DOI:10.1016/j.micron.2015.08.005.

Mabbott, G.A. (1983) ‘An introduction to cyclic voltammetry’, *Journal of Chemical Education*, 60(9), pp. 697-702. Available at: DOI:10.1021/ed060p697.

MathWorks (2016) ‘Evaluating Goodness of Fit’, *MATLAB Documentation*, MathWorks.

Max-Planck-Institut für Festkörperforschung (2017) *Fullerenes (MPI-FKF)*. Available at: https://www2.fkf.mpg.de/andersen/fullerene/intro.html (Accessed: 22 June 2017).

Mirkov, S.M., Djordjevic, A.N., Andric, N.L., Andric, S.A., Kostic, T.S., Bogdanovic, G.M., Vojinovic-Miloradov, M.B., Kovacevic, R.Z. (2004) ‘Nitric oxide-scavenging activity of polyhydroxylated fullerenol, C60(OH)24’, *Nitric Oxide*, 11, pp. 201–207. Available at: DOI:10.1016/j.niox.2004.08.003.

Miyamoto, A., Okimoto, H., Shinohara, H. and Shibamoto, Y. (2006) ‘Development of water-soluble metallofullerenes as X-ray contrast media’, *European Radiology*, 16(5), pp. 1050–1053. Available at: DOI:10.1007/s00330-005-0064-6.

Mohan, H., Palit, D.K., Mittal, J.P., Chiang, L.Y., Asmus, K.D. and Guldi, D.M. (1998) ‘Excited states and electron transfer reactions of $C_{60}(OH)_{18}$ in aqueous solution’, *Journal of the Chemical Society, Faraday Transactions*, 94(3): 359–363.

Montgomery, D. (2009) *Design and Analysis of Experiments*. 7th edn. John Wiley & Sons Inc.

Mousavi, S.Z., Nafisi, S. and Maibach, H.I. (2017) ‘Fullerene nanoparticle in dermatological and cosmetic applications’, *Nanomedicine: Nanotechnology, Biology, and Medicine*, 13(3), pp. 1071–1087. Available at: DOI:10.1016/j.nano.2016.10.002.

Murai, R., Takaya, Y., Hayashi, T. and Michihata, M. (2014) 'Study on chemical interaction analysis of reactive fullerenol molecules in Cu-CMP using high-sensitive raman spectroscopy', *Key Engineering Materials*, 625, pp. 332–338. Available at: DOI:10.4028/www.scientific.net/KEM.625.332.

Murdianti, B.S., Damron, J.T., Hilburn, M.E., Maples, R.D., Koralege, R.S.H., Kuriyavar, S.I. and Ausman, K.D. (2012) 'C_{60} oxide as a key component of aqueous C_{60} colloidal suspensions', *Environmental Science & Technology*, 46, pp. 7446-7453. Available at: DOI: 10.1021/es20366521.

Niu, F., Wu, J., Zhang, L., Li, P., Zhu, J., Wu, Z., Wang, C. and Song, W. (2011) 'Hydroxyl group rich C_{60} fullerenol: An excellent hydrogen bond catalyst with superb activity, selectivity, and stability', *ACS Catalysis*, 1(10), pp. 1158–1161. Available at: DOI:10.1021/cs200317d.

Novoselov, K.S., Geim, A.K., Morozov, S.V., Jiang, D., Zhang, Y., Dubonos, S.V., Grigorieva, I.V. and Firsov, A.A. (2004) 'Electric field effect in atomically thin carbon films', *Science*, 306(5696). Available at: http://science.sciencemag.org/content/306/5696/666/tab-pdf (Accessed: 22 June 2017).

Okumura, M., Mikawa, M., Yokawa, T., Kanazawa, Y., Kato, H. and Shinohara, H. (2002) 'Evaluation of water-soluble metallofullerenes as MRI contrast agents', Academic Radiology, 9(Suppl 2), pp. S495-497, Available at: DOI:10.1016/S1076-6332(03)80274-X.

Panova, G.G., Ktitorova, I.N., Skobeleva, O.V., Sinjavina, N.G., Charykov, N.A. and Semenov, K.N. (2016) 'Impact of polyhydroxy fullerene (fullerol or fullerenol) on growth and biophysical characteristics of barley seedlings in favourable and stressful conditions', *Plant Growth Regulation*, 79(3), pp. 309–317. Available at: DOI:10.1007/s10725-015-0135-x.

Pavia, D.L., Lampman, G.M. and Kriz, G.S. (2001) *Introduction to Spectroscopy*. 3rd edn. USA: Thomson Learning.

Penkova, A.V., Acquah, S.F.A., Dmitrenko, M.E., Chen, B., Semenov, K.N., Kroto, H.W. (2014) 'Transport properties of cross-linked fullerenol-PVA membranes', *Carbon*, 76, pp. 446–450. Available at: DOI:10.1016/j.carbon.2014.04.053.

Penkova, A.V., Acquah, S.F.A., Dmitrenko, M.E., Sokolova, M.P., Mikhailova, M.Y., Polyakov, E.S., Ermakov, S.S., Markelov, D.A. and Roizard, D. (2016) 'Improvement of pervaporation PVA membranes by the controlled incorporation of fullerenol nanoparticles', *Materials and Design*, 96, pp. 416–423. Available at: DOI:10.1016/j.matdes.2016.02.046.

Penkova, A.V., Dmitrenko, M.E., Ermakov, S.S., Toikka, A.M. and Roizard, D. (2017) 'Novel green PVA-fullerenol mixed matrix supported membranes for separating water-THF mixtures by pervaporation', *Environmental Science and Pollution Research*, Available at: DOI:10.1007/s11356-017-9063-9.

Petrie, E.M. (2013) *Addressing Silicone Contamination Issue*. SpecialChem. Available at: https://www.techsil.co.uk/media/wysiwyg/pdf/Addressing_Silicone_Contamination_Issues.pdf (Accessed: 10 June 2015).

Pinteala, M., Dascalu, A. and Ungurenasu, C. (2009) 'Binding fullerenol $C_{(60)}(OH)_{(24)}$ to dsDNA', *International Journal of Nanomedicine*, 4, pp. 193–199.

Prekodravac, J.R., Jovanović, S.P., Holclajtner-Antunović, I.D., Peruško, D.B., Pavlović, V.B., Tošić, D.D., Todorovic-Markovic, B.M. and Markovic, Z.M. (2014) 'Monolayer graphene films through nickel catalyzed transformation of fullerol and graphene quantum dots: A Raman spectroscopy study', *Physica Scripta*, 2014(T612): 014030. Available at: DOI:10.1088/0031-8949/2014/T162/014030.

Pushkarchuk, A.L., Potkin, V.I., Kilin, S.J., Nizovtsev, A.P., Soldatov, A.G., Kuten S.A., Pushkarchuk, V.A. (2016) 'Structure and magnetic properties of Saturn-shaped fullerenol complexes with ferrocene and nickelocene dicarboxylic acids: DFT simulation', *Structural Chemistry*, 27(1), pp. 281–284. Available at: DOI:10.1007/s11224-015-0718-1.

Qi, Z., Huang, S., Younis, A., Chu, D. and Li, S. (2016) 'Nanostructured Metal Oxides-Based Electrode in Supercapacitor Applications', in Stevic, Z. (ed.), *Supercapacitor Design and Applications*, InTech. Available at: DOI:10.5772/65155 (Accessed: 30 June 2017).

Rade, I., Natasa, R., Biljana, G., Aleksandar, D. and Borut, S. (2008) 'Bioapplication and activity of fullerenol $C_{60}(OH)_{24}$', *African Journal of Biotechnology*, 7(25), pp. 4940–4950.

Ratnikova, O.V., Melenevskaya, E.Y., Amsharov, K.Y., Vlasova, E.N., Volchek, B.Z., Gribanov, A.V., Shibaev, L.A. and Zgonnik, V.N. (2005) 'The new method for the synthesis of fullerols based on radical reaction', *Fullerenes, Nanotubes and Carbon Nanostructures*, 12(1–2), pp. 155–158. Available at: DOI:10.1081/FST-120027149.

Richardson, J.F., Harker, J.H. and Backhurst, J.R. (2002) *Particle Technology and Separation Processes*. 5th edn. Great Britain: Butterworth-Heimann, pp. 970-1021 (Coulson and Richardson's Chemical Engineering Series, 2).

Roldán, S., Barreda, D., Granda, M., Menéndez, R., Santamaría, R. and Blanco, C. (2015) 'An approach to classification and capacitance expressions in electrochemical capacitors technology', *Physical Chemistry Chemical Physics*, 17, pp. 1084–1092. Available at: DOI:10.1039/c4cp05124f.

Rokitskaya, T.I. and Antonenko, Y.N. (2016) 'Fullerenol C60(OH)24 increases ion permeability of lipid membranes in a pH-dependent manner', *Biochimica et Biophysica Acta – Biomembranes*, 1858(6), pp. 1165–1174. Available at: DOI:10.1016/j.bbamem.2016.02.009.

Saitoh, Y., Xiao, L., Mizuno, H., Kato, S., Aoshima, H., Taira, H., Kokubo, K. and Miwa, N. (2010) 'Novel polyhydroxylated fullerene suppresses intracellular oxidative stress together with repression of intracellular lipid accumulation during the differentiation of OP9 preadipocytes into adipocytes', *Free Radical Research*, 44(9), pp. 1072–1081. Available at: DOI:10.3109/10715762.2010.499905.

Saotome, T., Kokubo, K., Shirakawa, S., Oshima, T. and Hahn, H.T. (2011) 'Polymer nanocomposites reinforced with C_{60} fullerene: effect of hydroxylation', *Journal of Composite Materials*, 45(25), pp. 2595–2601. Available at: DOI:10.1177/0021998311416682.

Satoh, M. and Takayanagi, I. (2006) 'Review pharmacological studies on fullerene (C_{60}), a novel carbon allotrope, and its derivatives', *Journal of Pharmacological Sciences*, 100, pp. 513–518. Available at: DOI:10.1254/jphs.CPJ06002X.

Schneider, N.S., Darwish, A.D., Kroto, H.W., Taylor, R. and Walton, D.R.M. (1994) 'Formation of fullerols', *Journal of the Chemical Society, Chemical Communications*, pp.463-464.

Semenov, K.N., Charykov, N.A., Letenko, D.G., Nikitin, V.A., Namazbaev, V.I., Keskinov, V.A. and Pukharenko, Y.V. (2012) 'Synthesis and protection effect of fullerenol-d. II. Modification of water-soluble priming enamel with fullerenol-d', *Protection of Metals and Physical Chemistry of Surfaces*, 48(3), pp. 334–339. Available at: DOI:10.1134/S2070205112030161.

Semenov, K.N., Charykov, N.A., Postnov, V.N., Sharoyko, V.V., Vorotyntsev, I.V., Galagudza, M.M., Murin, I.V. (2016) 'Fullerenols: Physicochemical properties and applications', *Progress in Solid State Chemistry*, 44(2): 59–74. Available at: DOI:10.1016/j.progsolidstchem.2016.04.002.

Semenov, K.N., Kanterman, I.G., Charykov, N.A., Murin, I.V. and Kritchenkov, A.S. (2014) 'Solid-liquid phase equilibria in the fullerenol-d-$CuCl_2$-H_2O system at 25°C', *Russian Journal of Physical Chemistry A*, 88(6), pp. 1073–1075. Available at: DOI:10.1134/S0036024414060272.

Semenov, K.N., Letenko, D.G., Charykov, N.A., Nikitin ,V.A., Matuzenko, M,Y., Keskinov, V.A., Postnov, V.N. and Kopyrin, A.A. (2011) 'Electrochemical properties of aqueous solutions of fullerenol-d', *Russian Journal of Applied Chemistry*, 84(1), pp. 79–83. Available at: DOI:10.1134/S1070427211010137.

Semenov, K.N., Letenko, D.G., Charykov, N.A., Nikitin, V.A., Matuzenko, M.Y., Keskinov, V.A., Postnov, V.N. and Kopyrin, A.A. (2010) 'Synthesis and identification of fullerenol prepared by the direct oxidation route', *Russian Journal of Applied Chemistry*, 83(12), pp. 2076–2080. Available at: DOI:10.1134/S1070427210120025.

Sharma, P. and Bhatti, T.S. (2010) 'A review on electrochemcial double-layer capacitors', *Energy Conversion and Management*, 52, pp. 2901-2912.

Silva, G.A. (2010) 'Nanotechnology applications and approaches for neuroregeneration and drug delivery to the central nervous system', *Annals of the New York Academy of Sciences*, 1199, pp. 221–230. Available at: DOI:10.1111/j.1749-6632.2009.05361.x.

Singh, R. and Goswami, T. (2011) 'Photophysical and optical limiting properties of multifunctional hemi-ortho ester derivatives of fullerenol: Effects of TBAH doping, fullerenol concentration and solvent polarity', *Synthetic Metals*, 161(9–10), pp. 670–679. Available at: DOI:10.1016/j.synthmet.2011.01.012.

Singh, R. and Goswami, T. (2008) 'Synthesis and evaluation of thermal, photophysical and magnetic properties of novel starlike fullerene-organosilane macromolecules', *Journal of Organometallic Chemistry*, 693(11), pp. 2021–2032. Available at: DOI:10.1016/j.jorganchem.2008.03.006.

Sinnott, R.K. (2005) *Chemical Engineering Design*. Butterworth-Heimann (Coulson and Richardson's Chemical Engineering Series, 6).

Srdjenovic, B., Milic-Torres, V., Grujic, N., Stankov, K., Djordjevic, A. and Vasovic, V. (2010) 'Antioxidant properties of fullerenol $C_{60}(OH)_{24}$ in rat kidneys, testes, and lungs treated with doxorubicin', *Toxicology Mechanisms and Method,* 20(6), pp. 298–305. Available at: DOI:10.3109/15376516.2010.485622.

Sriramoju, B., Kanwar, R.K. and Kanwar, J.R. (2015) 'Neurobehavioral burden of multiple sclerosis with nanotheranostics', *Neuropsychiatric Disease and Treatment*, 11, pp. 2675–2689. Available at: DOI:10.2147/NDT.S82768.

Stasheuski, A.S., Galievsky, V.A., Stupak, A.P., Dzhagarov, B.M., Choi, J.M., Chung, B.H. and Jeong, J.Y. (2014) 'Photophysical properties and singlet oxygen generation efficiencies of water-soluble fullerene nanoparticles', *Photochemistry and Photobiology*, 90, pp. 997-1003.

Stoller, M.D. and Ruoff, R.S. (2010) 'Best practice methods for determining an electrode material's performance for ultracapacitors', *Energy & Environmental Science*, 3(9), pp. 1294-1301. Available at: DOI:10.1039/c0ee00074d.

Sun, Y., Cao, C., Yang, S., Huang, P., Wang, C. and Song, W. (2014) 'C_{60} fullerenol as an active and stable catalyst for the synthesis of cyclic carbonates from CO_2 and epoxides', *Chemical* Communications, 50(71), pp. 10307. Available at: DOI:10.1039/C4CC04891A.

Tachika, H., Takaya, Y., Hayash,i T., Tanada, H., Kokubo, K. and Suzuki, K. (2009) 'Study on the copper-chemical mechanical polishing method using water-soluble fullerenol slurry - investigation of polishing performance', *Journal of the Japan Society for Precision Engineering*, 75(4), pp. 489–495.

Tachikawa, H., Iyama, T. and Abe, S. (2011) 'DFT study on the interaction of Fullerene (C_{60}) with hydroxyl radical (OH)', *Physics Procedia*, 14, pp. 139–142. Available at: DOI:10.1016/j.phpro.2011.05.027.

Takaya, Y., Tachika, H., Hayashi, T., Kokubo, K. and Suzuki, K (2009) 'Performance of water-soluble fullerenol as novel functional molecular abrasive grain for polishing nanosurfaces', *CIRP Annals - Manufacturing Technology*, 58(1), pp. 495–498. Available at: DOI:10.1016/j.cirp.2009.03.118.

Torres, V.M., Srdjenovic, B., Jacevic, V., Simic, V.D., Djordjevic, A. and Simplício, A.L. (2010) 'Fullerenol $C_{60}(OH)_{24}$ prevents doxorubicin-induced acute cardiotoxicity in rats', *Pharmacological Reports*, 62(4), pp. 707–718.

Troshin, P.A., Astakhova, A.S. and Lyubovskaya, A.N. (2005) 'Synthesis of fullerenols from halofullerenes', *Fullerenes, Nanotubes, and Carbon Nanostructures*, 13, pp. 331-343.

Vangari, M., Pryor, T. and Jiang, L. (2013) ‘Supercapacitors: Review of materials and fabrication methods’, *Journal of Energy Engineering*, pp. 72-79.

Vesna, J., Danica, J., Kamil, K., Viktorija, D.S., Silva, D., Sanja, T., Ivana, B., Zoran, S., Zoran, M., Dubravko, B. and Aleksandar, D. (2016) ‘Effects of fullerenol nanoparticles and amifostine on radiation-induced tissue damages: Histopathological analysis’, *Journal of Applied Biomedicine*, 14(4), pp. 285–297. Available at: DOI:10.1016/j.jab.2016.05.004.

Vileno, B., Sienkiewicz, A., Lekka, M., Marcoux, P.R. and Forró, L. (2007) ‘Photo-oxidative stress in the presence of a water-soluble derivative of C_{60}: ESR and AFM assays’, in Pifat-Mrzlijak G (ed.) *Supramolecular Structure and Function 9*, pp. 153–180. Available at: DOI:10.1007/978-1-4020-6466-1_9.

Wade, L.G. (2014) *Organic Chemistry*. 8th edn. USA: Pearson.

Wang, Y., Guo, J., Wang, T., Shao, J., Wang, D. and Yang, Y. (2015) ‘Mesoporous transition metal oxides for supercapacitors’, *Nanomaterials*, 5, pp. 1667-1689.

Wang, S., He, P., Zhang, J., Jiang, H. and Zhu, S. (2005a) ‘Novel and efficient synthesis of water-soluble [60]fullerenol by solvent-free reaction’, *Synthetic Communications*, 35(13), pp. 1803–1808. Available at: DOI:10.1081/SCC-200063958.

Wang, N., Sun, L., Zhang, X., Bao, X., Zheng, W. and Yang, R.(2014) ‘Easily-accessible fullerenol as a cathode buffer layer for inverted organic photovoltaic devices’, *RSC Advances*, 4(49), pp. 25886. Available at: DOI:10.1039/c4ra03045a.

Wang, Z., Wang, S., Lu, Z. and Gao, X. (2015b) ‘Syntheses, structures and antioxidant activities of fullerenols: Knowledge learned at the atomistic level’, *Journal of Cluster Science*, 26(2), pp. 375–388. Available at: DOI:10.1007/s10876-015-0855-0.

Wang, F.F., Wang, C., Liu, R.Q., Tian, D. and Li, N. (2012) ‘Experimental study on the preparation of Ag nanoparticle doped fullerenol for lithium ion battery application’, *The Journal of Physical Chemistry C,* 116, pp. 10461–10467.

Weber, L. (2009) *Preparations, Characteristics, and Applications of Carbon-based Nanomaterials*. PhD thesis. Technische Universität Ilmenau.

Winter, M. and Brodd, R.J. (2004) ‘What are batteries, fuel cells, and supercapacitors ?’, *Chemical Reviews*, 104, pp. 4245–4270. Available at: DOI:10.1021/cr020730k.

Withers, J.C., Loutfy, R.O. and Lowe, T.P. (1997) ‘Fullerene commercial vision’, *Fullerene Science and Technology*, 5(1), pp. 1-31 . Available at: DOI:10.1080/15363839708011971.

Wohlers, M., Bauer, A., Belz, T., Ruhle, T., Schedel-Niedrig, T. and Schlogl, R. (1996) ‘The mechanism of oxidation of fullerenes with molecular oxygen’, *Preprints of Papers, Americal Chemical Society, Division of Fuel Chemistry*, 41(1). Available at: https://web.anl.gov/PCS/acsfuel/preprint%20archive/Files/41_1_NEWORLEANS_03-96-0108.pdf (Accessed: 2 August 2017).

Yang, X. (2014) ‘Fullerene – biomolecule conjugates and their biomedicinal applications’, *International Journal of Nanomedicine*, 9, pp. 77–92.

Yang, L.Y., Gao, J.L., Gao, T., Dong, P., Ma, L., Jiang, F.L. and Liu, Y. (2016) ‘Toxicity of polyhydroxylated fullerene to mitochondria’, *Journal of Hazardous Materials*, 301, pp. 119–126. Available at: DOI:10.1016/j.jhazmat.2015.08.046.

Yang, P. and Mai, W. (2014) ‘Flexible solid-state electrochemical supercapacitors’, *Nano Energy*, 8, pp. 274–290. Available at: DOI:10.1016/j.nanoen.2014.05.022.

Yang, S.T., Wang. H., Guo, L., Gao, Y., Liu, Y. and Cao, A. (2008) ‘Interaction of fullerenol with lysozyme investigated by experimental and computational approaches’, *Nanotechnology*, 19(39). Available at: DOI:10.1088/0957-4484/19/39/395101.

Yao, L., Kang, F., Peng, Q. and Yang, X. (2010) ‘An improved method for fullerol preparation based on dialysis’, *Chinese Journal of Chemical Engineering*, 18(5), pp. 876–879. Available at: DOI:10.1016/S1004-9541(09)60142-7.

Ye, S., Zhou, T., Pan, D., Lai, Y., Yang, P., Chen, M., Wang, Y., Hou, Z., Ren, L. and Jiang, Y. (2006) ‘Fullerene C_{60} derivatives attenuated microglia-mediated prion peptide neurotoxicity’, *Journal of Biomedical* Nanotechnology, 14, pp. 1820–1833. Available at: DOI:10.1166/jbn.2016.2281.

Zhang, G., Liu, Y., Liang, D., Gan, L. and Li, Y. (2010) ‘Facile synthesis of isomerically pure fullerenols and formation of spherical aggregates from $C_{60}(OH)_8$’, *Angewandte Chemie International Edition*, 49(31), pp. 5293–5295. Available at: DOI:10.1002/anie.201001280.

Zhang, P., Pan, H., Liu, D., Guo, Z., Zhang, F. and Zhu, D. (2003) ‘Effective mechanochemical synthesis of [60]fullerols’, *Synthetic Communications*, 33(14), pp. 2469-2474.

Zhang, Z., Wei, L., Qin, X. and Li, Y. (2015) ‘Carbon nanomaterials for photovoltaic process’, *Nano Energy*, 15, pp. 490–522. Available at: DOI:10.1016/j.nanoen.2015.04.003.

Zhang, L.L. and Zhao, X.S. (2009) ‘Carbon-based materials as supercapacitor electrodes’, *Chemical Society Reviews*, 38, pp. 2520-2531.

Zhu, Y.S., Sun, D.Y., Liu, G.Z., Liu, Z.Y., Zhan, R.Y. and Liu, S.Y. (1996) ‘An ESR study on˙OH-radical scavenging activity of water-soluble fullerenols’, International Journal of Electrochemical Science, 17(7), pp. 8270-8279.

Zhu, X., Zhang, N., Wang, Z. and Liu, X. (2016) ‘Investigation of work of adhesion of biological cell (human hepatocellular carcinoma) by AFM nanoindentation’, *Journal of Micro-Bio Robotics*, 11(1–4), pp. 47–55. Available at: DOI:10.1007/s12213-016-0089-8.

APPENDICES

Appendix A List of symbols

A	Ampere (unit of electrical current)
C_{60}	C_{60} fullerene
C_{sp}	Specific capacitance (units, F/g)
E	Energy density of a supercapacitor (units, J/g)
F	Farad (unit of electrical capacitance); F-distribution test statistic
F_{crit}	Critical value of F-distribution test statistic
g	Gram (unit of mass)
Hz	Hertz (unit of frequency)
H_0	Null hypothesis
H_1	Alternative hypothesis
I	Electrical current (unit, A)
m	Mass of both electrodes of a supercapacitor (unit, g)
$n_{(OH)}$	Number of hydroxyl groups per fullerene cage (level of hydroxylation) (unit, groups)
P_{max}	Maximum power of supercapacitor (unit, Watt)
R_{ct}	Charge-transfer resistance (unit, Ω)
R_{Ω}	Solution resistance (unit, Ω)
S	Cyclic voltammetry scan rate (units, V/s)
s	Second (unit of time)
t	Time (unit, s)
V	Volt (unit of potential difference)
V_{drop}	Potential drop at the beginning of discharge curve in a GCD cycle
x	Percentage weight loss of TGA specimen from temperature of 150°C to 570°C
y	Percentage weight of TGA specimen from 570°C onwards
μ	Arithmetic mean
μ_i	Arithmetic mean of $n_{(OH)}$ values from fullerenol batch i

Appendix B References for Figure 2-8 in Section 2.6

An, H. and Jin, B. (2012) 'Impact of fullerene particle interaction on biochemical activities in fermenting *Zymomonas mobilis*', *Environmental Toxicology and Chemistry*, 31(4), PP. 712-716.

Arifa, R.D.N., Prosperi de Paula, T., Madeira, M.F.M., Lima, R.L., Garcia, Z.M., Avila, T.V., Pinho, V., Barcelos, L.S., Pinheiro, M.V.B., Ladeira, L.O., Krambrock, K., Teixeira, M.M. and Souza, D.G. (2016) 'The reduction of oxidative stress by nanocomposite fullerol decreases mucositis severity and reverts leukopenia induced by irinotecan', *Pharmacological Research*, 107, pp. 102-110.

Astefanei, A., Nunez, O., Galceran, M.F., Kok, W.T. and Schoenmakers, P.J. (2015) 'Aggregation behavior of fullerenes in aqueous solutions: a capillary electrophoresis and asymmetric flow field-flow fractionation study', *Analytical and Bioanalytical Chemistry*, 407, pp. 8035-8045.

Awan, F., Bulger, E., Berry, R.M. and Tam, K.C. (2016) 'Enhanced radical scavenging activity of polyhydroxylated C_{60} functionalized cellulose nanocrystals', *Cellulose*, 23, pp. 3589-3599.

Bednarikova, Z., Huy, P.D.Q., Mocanu, M., Fedunova, D., Li, M.S., Gazova, Z. (2016) 'Fullerenol $C_{60}(OH)_{16}$ prevents amyloid fibrillization of $A\beta_{40}$ – in vitro and in silico approach', *Physical Chemistry Chemical Physics*, 18(28), pp. 18855–18867. Available at: DOI:10.1039/C6CP00901H.

Cai, X., Jia, H., Liu, Z., Hou, B., Luo, C., Feng, Z., Li, W. and Liu, J. (2008) 'Polyhydroxylated fullerene derivative $C_{60}(OH)_{24}$ prevents mitochondrial dysfunction and oxidative damage in an MPP+-induced cellular model of Parkinson's disease', Journal of Neuroscience Research, 86(16), pp. 3622–3634. Available at: DOI:10.1002/jnr.21805.

Cao, T., Wang, Z., Xia, Y., Song, B., Zhai, Y., Chen, N. and Li, Y. (2016) 'Facilitating electron transportation in Perovskite solar cells via water-soluble fullerenol interlayers', *ACS Applied Materials & Interfaces*, 8, pp. 18284-18291.

Chen, Y., Hwang, K., Yen, C. and Cai, Y. (2004) ‘Fullerene derivatives protect against oxidative stress in RAW264.7 cells and ischemia-reperfused lungs’, *American Journal of Physiology Regulatory, Integrational Comparative Physiology*, 287, pp. R21-R26.

Chen, Z., Wu, W., Zhang, W. and Deng, S. (2011) ‘Thermodynamics of the interaction of sweeteners and lactisole with fullerenols as an artificial sweet taste receptor Model’, *Food Chemistry*, 128, pp. 134-144.

Dobashi, R., Matsunaga, K. and Tajima, M. (2014) ‘Effects of fullerene derivatives on the gas permeability of thermoplastic polyurethane elastomers’, *Journal of Applied Polymer Science*, 131(6), pp. 1–6. Available at: DOI:10.1002/app.39986.

Goswami, T.H., Nandan, B., Alam, S. and Mathur, G.N. (2003) ‘A selective reaction of polyhydroxy fullerene with cycloaliphatic epoxy resion in designing ether connected epoxy star utilising fullerene as a molecular core’, *Polymer*, 44, pp. 3209-3214.

Hinokuma, K. and Ata, M. (2001) ‘Fullerene proton conductors’, *Chemical Physics Letters*, 341, pp. 442-446.

Hirai, T., Yoshioka, Y., Udaka, A., Uemura, E., Ohe, T., Aoshima, H., Gao, J., Kokubo, K., Oshima, T., Nagano, K., Higashisaka, K., Mashino, T. and Tsutsumi, Y. (2016) ‘Potential suppressive effects of two C_{60} fullerene derivatives on acquired immunity’, *Nanoscale Research Letters*, 11(449). Available at: DOI: 10.1186/s11671-016-1663-7.

Injac, R., Boskovic, J., Perse, M., Koprivec-Furlan, E., Cerar, A., Djordjevic, A. and Strukelj, B. (2008) ‘Acute doxorubicin nephrotoxicity in rats with malignant neoplasm can be successfully treated with fullerenol $C_{60}(OH)_{24}$ via suppression of oxidative stress’, *Pharmacological Reports*, 60, pp. 742-749.

Jacevic, V., Djordjevic, A., Srdjenovic, B., Milic-Tores, V., Segrt, Z., Dragojevic-Simic, V. and Kuca, K. (2017) ‘Fullerenol nanoparticles prevents doxorubicin-

induced acute hepatotoxicity in rats', *Experimental and Molecular Pathology*, 102(2), pp. 360–369. Available at: DOI:10.1016/j.yexmp.2017.03.005.

Ji, Z.Q., Sun, H., Wang, H., Xie, Q., Liu, Y. and Wang, Z. (2006) 'Biodistribution and tumor uptake of $C_{60}(OH)_x$ in mice', *Journal of Nanoparticle Research*, 8, pp. 53-63.

Jiao, F., Liu, Y., Qu, Y., Li, W., Zhou, G., Ge, C., Li, Y., Sun, B. and Chen, C. (2010) 'Studies on anti-tumor and antimetastatic activities of fullerenol in a mouse breast cancer model', *Carbon*, 48(8), pp. 2231–2243. Available at: DOI:10.1016/j.carbon.2010.02.032.

Jin, H., Chen, W.Q., Tang, X.W., Chiang, L.Y., Yang, C.Y., Schloss, J.V., Wu, J.Y. (2000) 'Polyhydroxylated C_{60}, fullerenols, as glutamate receptor antagonists and neuroprotective agents', *Journal of Neuroscience Research*, 62(4), pp. 600–607. Available at: DOI:10.1002/1097-4547(20001115)62:4<600::AID-JNR15>3.0.CO;2-F.

Kamat, J.P., Devasagayam, T.P.A., Priyadarsini, K.I. and Mohan, H. (2000) 'Reactive oxygen species mediated membrane damage induced by fullerene derivatives and its possible biological implications', *Toxicology*, 155, pp. 55-61.

Krokosz, A., Grebowski, J., Rodacka, A., Pasternak, B. and Puchala, M. (2014) 'The effect of fullerenol $C_{60}(OH)_{\sim 30}$ on the alcohol dehydrogenase activity irradiated with x-rays', *Radiation Physics and Chemistry*, 97, pp. 102-106.

Kudryasheva, N.S., Kovel, E.S., Sachkova, A.S., Vorobeva, A.A., Isakova, V.G. and Churikov, G.N. (2017) 'Bioluminescent enzymatic assay as a tool for studying antioxidant activity and toxicity of bioactive compounds', *Photochemistry and Photobiology*, 93, pp. 536-540.

Kumar, R., Kumar, P., Naqvi, S., Gupta, N., Saxena, N., Gaur, J., Maurya, J.K. and Chand, S. (2014) 'Stable graphite exfoliation by fullerenol intercalation via aqueous route', *New Journal of Chemistry*, 38, pp. 4922-4930.

Lao, F., Li, W., Han, D., Qu, Y., Liu, Y., Zhao, Y. and Chen, L. (2009) 'Fullerene derivatives protect endothelial cells against NO-induced damage', *Nanotechnology*, 20. Available at: DOI: 10.1088/0957-4484/20/22/225103.

Monteiro-Riviere, N.A., Linder, K.E., Inman, A.O., Saathoff, J.G., Xia, X. and Riviere, J.E. (2012) 'Lack of hydroxylated fullerene toxicity after intravenous administration to female Sprague-Dawley rats', *Journal of Toxicology and Environmental Health, Part A*, 75, pp. 367-373.

Najafi, A. (2017) 'An investigation on dispersion and stability of water-soluble fullerenol ($C_{60}OH$) in water via UV-Visible spectroscopy', *Chemical Physics Letters*, 669, pp. 115-118.

Navarro, D.A., Kookana, R.S., McLaughlin, M.J. and Kirby, J.K. (2015) 'Fullerol as a potential pathway for mineralization of fullerene nanoparticles in biosolid-amended soils', *Environmental Science & Technology Letters*, 3, pp. 7-12.

Panova, G.G., Ktitorova, I.N., Skobeleva, O.V., Sinjavina, N.G., Charykov, N.A. and Semenov, K.N. (2016) 'Impact of polyhydroxy fullerene (fullerol or fullerenol) on growth and biophysical characteristics of barley seedlings in favourable and stressful conditions', *Plant Growth Regulation*, 79(3), pp. 309–317. Available at: DOI:10.1007/s10725-015-0135-x.

Penkova, A.V., Acquah, S.F.A., Sokolova, M.P. Dmitrenko, M.P. and Toikka, A.M. (2015) 'Polyvinyl alcohol membranes modified by low-hydroxylated fullerenol $C_{60}(OH)_{12}$', *Journal of Membrane Science*, 491, pp. 22-27.

Prekodravac, J.R., Markovic, Z.M., Jovanovic, S.P., Holdajtner-Antunovic, I.D., Kepic, D.P., Budimir, M.D. and Todorovic-Markovic, B.M. (2017) 'Graphene quantum dots and fullerenol as new carbon sources for single-layer and bi-layer graphene synthesis by rapid thermal annealing method', *Material Research Bulletin*, 88, pp. 114-120.

Sachkova, A.S., Kovel, E.S., Churikov, G.N., Guseynov, O.A., Bondar, A.A., Dubinina, I.A. and Kudryasheva, N.S. (2017) 'On mechanism of antioxidant effect of fullerenols', *Biochemistry and Biophysics Reports*, 9, pp. 1-8.

Semenov, K.N., Charykov, N.A., Keskinov, V.A., Letenko, D.G., Nikitrin, V.A. and Namazbaev, V.I. (2011) 'The synthesis and identification of mixed fullerenol prepared by the direct one-stage oxidation of fullerene black', *Russian Journal of Chemistry A*, 85(6), pp. 1009-1015.

Semenov, K.N., Kanterman, I.G., Charykov, N.A., Keskinov, V.A. and Kusenova, K.A. (2014) 'Solubility in the ternary system fullerenol-d-uranyl sulfate-water at 25°C', *Radiochemistry*, 56(5), pp. 493-495.

Singh, R. and Goswami, T. (2011) 'Photophysical and optical limiting properties of multifunctional hemi-ortho ester derivatives of fullerenol: Effects of TBAH doping, fullerenol concentration and solvent polarity', *Synthetic Metals*, 161(9–10), pp. 670–679. Available at: DOI:10.1016/j.synthmet.2011.01.012.

Slavic, M., Djordjevic, A., Radojicic, R., Milovanovic, S., Orescanin-Dusic, Z., Rakocevic, Z., Spasic, M.P. and Blagojevic, D. (2013) 'Fullerenol $C_{60}(OH)_{24}$ nanoparticles decrease relaxing effects of dimethyl sulfoxide on rat uterus spontaneous contraction', *Journal of Nanoparticle Research*, 15. Available at: DOI: 10.1007/s11051-013-1650-1.

Ueno, H., Nakamura, Y., Ikuma, N. and Kokubo, K. (2012) 'Synthesos of lithium-encapsulated fullerenol and the effects of the internal lithium cation on its aggragation behavior', *Nano Research*, 5(8), pp. 558-564.

Vesna, J., Danica, J., Kamil, K., Viktorija, D.S., Silva, D., Sanja, T., Ivana, B., Zoran, S., Zoran, M., Dubravko, B. and Aleksandar, D. (2016) 'Effects of fullerenol nanoparticles and amifostine on radiation-induced tissue damages: Histopathological analysis', *Journal of Applied Biomedicine*, 14(4), pp. 285–297. Available at: DOI:10.1016/j.jab.2016.05.004.

Vileno, M., Marcoux, P.R., Lekka, M., Sienkiewicz, A., Feher, T. and Forro, L. (2006) 'Spectroscopic and photophysical properties of a highly derivatized C_{60} fullerol', *Advanced Functional Materials*, 16, pp. 120-128.

Vileno, B., Sienkiewicz, A., Lekka, M., Kulik, A.J. and Forro, L. (2004) 'In vitro assay of singlet-oxygen generation in the presence of water-soluble derivatives of C_{60}', *Carbon*, 42, pp. 1195-1198.

Wang, C., Zhang, H., Ruan, L., Chen, L., Li, H., Chang, X., Zhang, X. and Yang, S. (2016) 'Bioaccumulation of ^{13}C-fullerenol nanomaterials in wheat', *Environmental Science Nano*, 3, pp. 799-805.

Xu, T., Zhu, R., Liu, J., Zhou, Q., Zhu, J., Liang, X., Xi, L. and He, H. (2016) 'Fullerol modification ferrihydrite for the degradation of acid red 18 under simulated sunlight radiation', *Journal of Molecular Catalysis A: Chemical*, 424, pp. 393-401.

Yao, L., Kang, F., Peng, Q. and Yang, X. (2010) 'An improved method for fullerol preparation based on dialysis', *Chinese Journal of Chemical Engineering*, 18(5), pp. 876–879. Available at: DOI:10.1016/S1004-9541(09)60142-7.

Ye, S., Chen, M., Jiang, Y., Chen, M., Zhou, T., Wang, Y., Hou, Z. and Ren, L. (2014) 'Polyhydroxylated fullerene attenuates oxidative stress-induced apoptosis via a fortifying Nrf2-regulated cellular antioxidant defence system', *International Journal of Nanomedicine*, 9, pp. 2073-2087.

Yur'ev, G.O., Keskinov, V.A., Semenov, K.N. and Charykov, N.A. (2017) 'Phase equilibria in a ternary fullerenol-d($C_{60}(OH)_{22-24}$) — $SmCl_3$ — H_2O System at 25°C', *Russian Journal of Physical Chemistry A*, 91(5) pp. 797-799.

Zhang, M., Xu, Z., Ge, Y., Jiang, F. and Liu, Y. (2012) 'Binding of fullerol to human serum albumin: Spectroscopic and electrochemical approach', *Journal of Photochemistry and Photobiology B: Biology*, 108, pp. 34-43.

Zhu, J., Ji, Z., Wang, J., Sun, R., Zhang, X., Gao, Y., Sun, H., Liu, Y., Wang, Z., Li, A., Ma, J., Wang, T., Jia, G. and Gu, Y. (2008) 'Tumor-inhibitory effect of immunomodulatory activity of fullerol $C_{60}(OH)_x$', *Small*, 4(8), pp. 1168-1175.

Appendix C Approximation of theoretical yield and percent yield of fullerenol synthesis

Percent yield of a chemical reaction is defined as (Chang and Goldsby, 2016):

$$\text{Percent yield} = \frac{\text{Actual yield}}{\text{Theoretical yield}} \times 100 \quad \textbf{(C-1)}$$

where 'actual yield' refers to the actual amount of product collected from the reaction, and 'theoretical yield' refers to the maximum achievable yield according to the balanced chemical equation of the reaction (Chang and Goldsby, 2016).

C.1 Original TBAH-NaOH route reported by Li and colleagues (1993)

Starting with 80 mg of C_{60} fullerene, Li and colleagues (1993) reported that 115 mg of fullerenol was collected, and that their product contained 26 hydroxyl groups per fullerenol molecule (based on results from elemental analysis).

- Molar mass of product with estimated formula $C_{60}(OH)_{26}$ = 1162
- $\frac{\text{Molar mass of product}}{\text{Molar mass of } C_{60}} = \frac{1162}{720} = 1.62$
- Expected mass of product based on molar mass ratio = 80×1.62 = 130 mg (This may be considered as an approximation of the theoretical yield of the reaction)
- Therefore, $\text{Percent yield} = \frac{115}{130} \times 100 = 88.5$

C.2 Modified TBAH-NaOH route used in this research

C.2.1 Contamination-free fullerenol (products from Consistency Evaluation Experiment)

Starting with 80 mg C_{60} fullerene (molar mass = 720), the average mass of product (Batch 1-3) collected from this experiment was 104 mg. The product was estimated to contain 19 hydroxyl groups per molecule, i.e. $C_{60}(OH)_{19}$ (Section 5.2.3).

- Molar mass of product with estimated formula $C_{60}(OH)_{19}$ = 1043
- $\frac{\text{Molar mass of product}}{\text{Molar mass of } C_{60}} = \frac{1043}{720} = 1.45$
- Expected mass of product based on molar mass ratio = 80×1.45 = 116 mg (theoretical yield of the reaction)
- Therefore, $\text{Percent yield} = \frac{104}{116} \times 100 = 89.7$

C.2.2 Fullerenol contaminated with sodium carbonate only

Products which belong to this calculation approach are those with the estimated empirical formula in the form of **$C_{60}(OH)_n .xH_2O$ with yNa_2CO_3.**

The following calculation demonstration was based on the information from Product 1 (TBAH = 3 drops; TBAH Experiment).

Starting with 80 mg C_{60} fullerene (molar mass = 720), the mass of product collected from this experiment was 16 mg. The estimated empirial formula of the product was $C_{60}(OH)_9 .17H_2O$ with $6Na_2CO_3$, and fullerenol part in the product was determined to be 48.10 %wt (Section 5.3.2).

- Molar mass of fullerenol part in the product with estimated formula $C_{60}(OH)_9$ = 873
- $\frac{\text{Molar mass of fullerenol part in the product}}{\text{Molar mass of } C_{60}} = \frac{873}{720} = 1.21$
- Expected mass of achievable fullerenol based on molar mass ratio = 80×1.21 = 96.8 mg (theoretical yield of the reaction for Product 1)
- Actual mass of fullerenol in the collected product = 0.4810×16 = 7.696 mg
- Therefore, $\text{Percent yield} = \frac{7.696}{96.8} \times 100 \approx 8.0$

C.2.3 Fullerenol with epoxide group and sodium carbonate contamination

Products which belong to this calculation approach are those with the estimated empirical formula in the form of **$C_{60}O(OH)_n .xH_2O$ with yNa_2CO_3.**

The following calculation demonstration was based on the information from Product 10 (NaOH = 2.0 ml; NaOH Experiment).

Starting with 83.5 mg C_{60} fullerene (molar mass = 720), the mass of product collected from this experiment was 174.9 mg. The estimated empirial formula of the product was $C_{60}O(OH)_{13}$.$19H_2O$ with $10Na_2CO_3$, and fullerenol part (epoxide-containing fullerenol) in the product was determined to be 40.57%wt (Section 5.4.2).

- Molar mass of fullerenol part in the product with estimated formula $C_{60}O(OH)_{13}$ = 957
- $\frac{\text{Molar mass of fullerenol part in the product}}{\text{Molar mass of } C_{60}} = \frac{957}{720} = 1.33$
- Expected mass of achievable fullerenol based on molar mass ratio = 83.5×1.33 = 111.06 mg (theoretical yield of the reaction for Product 10)
- Actual mass of fullerenol in the collected product = 0.4057×174.9 = 70.96 mg
- Therefore, $\text{Percent yield} = \frac{70.96}{111.06} \times 100 = 63.9$

Appendix D Thermal decomposition and thermogravimetric analysis of pure sodium carbonate and sodium carbonate-carbon black mixture

All information and figures in this section were referred from the work done by Kim and Lee (2001) on thermal and carbothermic decomposition of sodium carbonate (Na_2CO_3) and lithium carbonate (Li_2CO_3) using both thermogravimetric analysis (TGA) and differential scanning calorimetry (DSC) up to 1200°C. For this research in which evidences suggesting the existence of sodium carbonate in the products was found (without the use of DSC), only the information related to TGA of sodium carbonate and sodium carbonate-carbon black mixture from their work was considered. (Nevertheless, some results from their DSC and lithium carbonate experiments were incorporated in some original figures from the literature, but were not involved in this research.) Similar to the operating conditions for TGA in this research, their TGA measurements were performed under inert atmosphere, at the same heating rate of 10 K/min.

This section summarises information, as well as important figures, from the original literature (Kim and Lee, 2001) that are related to and used to assist analyses of TGA thermograms of the products in this research. The literature is already included in the list of references.

There are two chemical reactions involved in thermal decomposition of pure sodium carbonate:

$$\mathrm{Na_2CO_{3(l)}} \rightarrow \mathrm{Na_2O_{(s)}} + \mathrm{CO_{2(g)}} \quad \textbf{(D-1)}$$

$$\mathrm{Na_2O_{(l)}} \rightarrow 2\mathrm{Na_{(g)}} + \frac{1}{2}\mathrm{O_{2(g)}} \quad \textbf{(D-2)}$$

The first reaction (D-) progresses at a very slow rate, and controls the overall decomposition. TGA thermogram related to thermal decomposition of pure sodium carbonate can be found in Figure D-1 from the curve indicated with ‘TG (Na_2CO_3)’. The weight of pure sodium carbonate sample remained constant

until the temperature passed its melting point at 850°C. After it had melted, loss of sample weight, hence thermal decomposition, then began at such a very slow rate that decomposition was still incomplete at 1200°C and sample weight loss was only 26%.

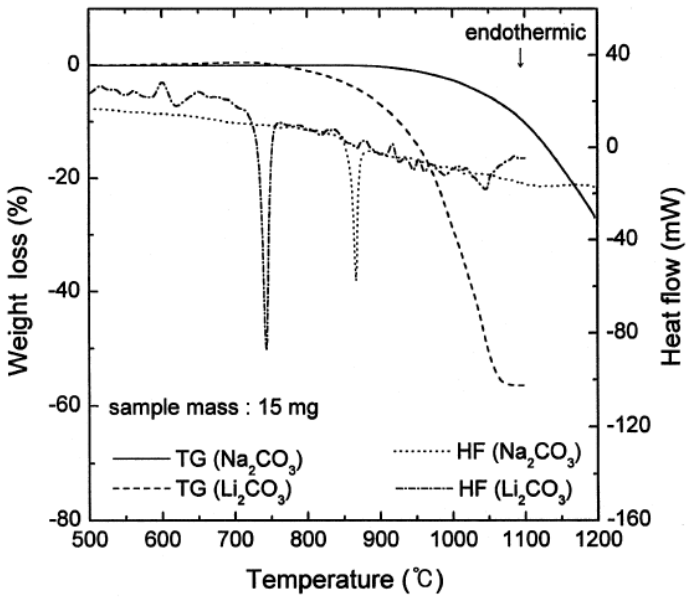

Figure D-1 TGA and DSC thermograms of pure Na_2CO_3 and Li_2CO_3 (image from Kim and Lee (2001)). TGA curves are denoted with 'TG', and DSC curves are denoted with 'HF'.

Kim and Lee (2001) also studied thermal decomposition behaviour of sodium carbonate-carbon black mixture. Due to the fact that both carbon black and fullerene belong to all-carbon materials, while no information on thermal behaviour of fullerenol- or fullerene-sodium carbonate mixture was available at the time this research was being conducted, results from Kim and Lee's work on sodium carbonate-carbon black mixture might be used as the most related reference available.

By adding carbon black (20%wt) to sodium carbonate (80%wt), the rate of thermal decomposition of the mixture was noticeably greater than that of pure sodium carbonate, as can be seen from 'TG (Na_2CO_3 + C.B.)' curve in Figure D-2. Sample weight loss had already reached approximately 90% at 1000°C.

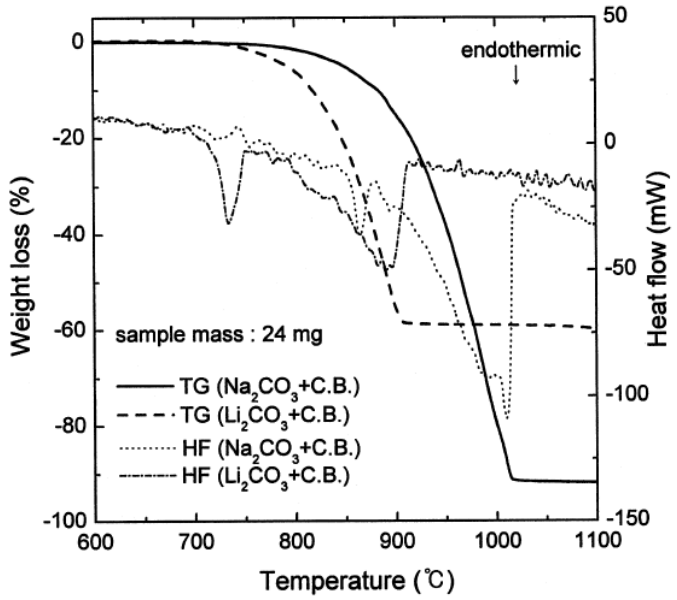

Figure D-2 TGA and DSC thermograms of Na_2CO_3 mixed with carbon black, and Li_2CO_3 mixed with carbon black (image from Kim and Lee (2001)). TGA curves are denoted with 'TG', and DSC curves are denoted with 'HF'. 'C.B. refers to carbon black.

The chemical reaction involved in thermal decomposition of the mixture is different from that of the pure sodium carbonate, and is expressed as:

$$\mathrm{Na_2CO_{3(l)}} + 2\mathrm{C_{(s)}} \rightarrow 2\mathrm{Na_{(g)}} + 3\mathrm{CO_{(g)}} \qquad \textbf{(D-3)}$$

Kim and Lee (2001) also reported that decomposition rate of sodium carbonate-carbon black mixture increased as carbon black proportion increased, and that weight loss of the mixture could be divided into two types. The first type shows continuous rapid weight loss ending with a constant weight, while the second type features Continuous rapid weight loss followed by further weight loss (Figure D-3).

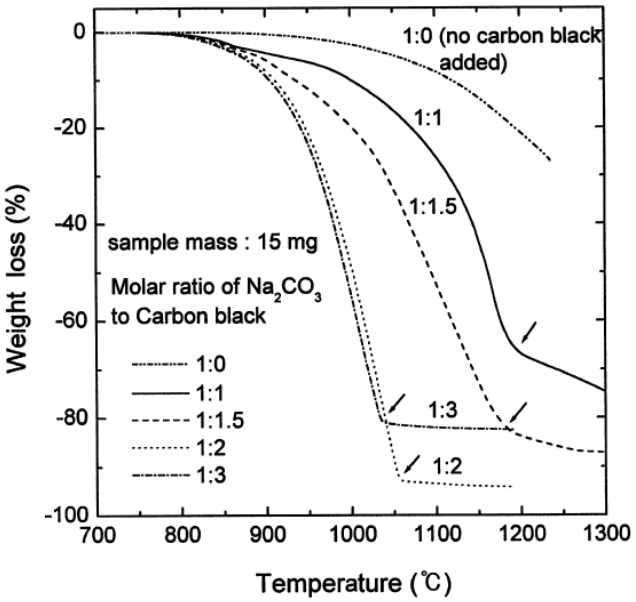

Figure D-3 TGA thermograms of Na_2CO_3 mixed with carbon black at different molar ratios (image from Kim and Lee (2001)). Arrows indicate points where continuous rapid loss of sample mass end.